INFORMATION TO USERS

This manuscript has been reproduced from the microfilm master. UMI films the text directly from the original or copy submitted. Thus, some thesis and dissertation copies are in typewriter face, while others may be from any type of computer printer.

The quality of this reproduction is dependent upon the quality of the copy submitted. Broken or indistinct print, colored or poor quality illustrations and photographs, print bleedthrough, substandard margins, and improper alignment can adversely affect reproduction.

In the unlikely event that the author did not send UMI a complete manuscript and there are missing pages, these will be noted. Also, if unauthorized copyright material had to be removed, a note will indicate the deletion.

Oversize materials (e.g., maps, drawings, charts) are reproduced by sectioning the original, beginning at the upper left-hand corner and continuing from left to right in equal sections with small overlaps.

Photographs included in the original manuscript have been reproduced xerographically in this copy. Higher quality 6" x 9" black and white photographic prints are available for any photographs or illustrations appearing in this copy for an additional charge. Contact UMI directly to order.

UMI®

University of Alberta

A Fundamental Understanding of the Electrochemical Noise

Related to Pitting Corrosion of Carbon Steel

by

Yufeng Cheng ©

A thesis submitted to the Faculty of Graduate Studies and Research in partial fulfillment
of the requirements for the degree of Doctor of Philosophy.

in

Materials Engineering

Department of Chemical and Materials Engineering

Edmonton, Alberta

Spring 2000

0-612-59942-6

Canada

University of Alberta

Library Release Form

Name of Author: Yufeng Cheng

Title of Thesis: A Fundamental Understanding of the Electrochemical
Noise Related to Pitting Corrosion of Carbon Steel

Degree: Doctor of Philosophy

Year this Degree Granted: 2000

Permission is hereby granted to the University of Alberta Library to reproduce single copies of this thesis and to lend or sell such copies for private, scholarly, or scientific research purpose only.

The author reserves all other publication and other rights in association with the copyright in the thesis, and except as hereinbefore provided, neither the thesis nor any substantial portion thereof may be printed or otherwise reproduced in any material form whatever without the author's prior written permission.

Yufeng Cheng
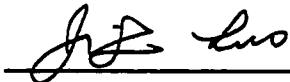
2928-16 Street N.E.
NOVA Research and Technology Centre
Calgary, Alberta
Canada T2E 7K7

Date: Nov. 19, 1999

University of Alberta

Faculty of Graduate Studies and Research
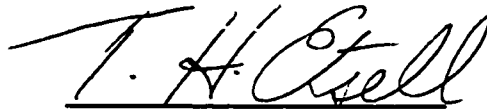
The undersigned certify that they have read, and recommend to the Faculty of Graduate Studies and Research for acceptance, a thesis entitled **A Fundamental Understanding of the Electrochemical Noise Related to Pitting Corrosion of Carbon Steel** submitted by **Yufeng Cheng** in partial fulfillment of the requirements for the degree of **Doctor of Philosophy** in **Materials Engineering**.

Dr. J.L. Luo, Supervisor

Dr. D.D. Macdonald

Dr. T.H. Etsell

Dr. R.L. Eadie

Dr. M.L. Wayman

Dr. J.A. Plambeck

Date: _Nov. 19, 1999_

To my beloved wife, Jianshu

ABSTRACT

The pitting behavior of carbon steel in chloride-containing solutions was studied by the electrochemical noise technique. The semiconducting nature of the passive film formed on carbon steel was revealed as well. The initiation of metastable pits is generally indicated by a typical current and potential transient with the shape of a quick current rise and potential drop followed by a slow recovery. The potential fluctuations mainly come from the response of the electrode capacitance to pit growth charge. Only the current transients directly reflect the metastable pitting 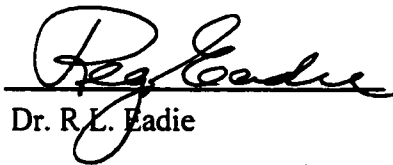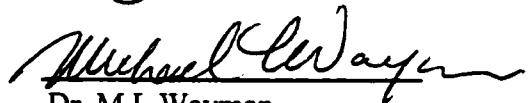process. The potential dependence of the pit initiation rate is well illustrated by the point defect model, which assumes that pitting initiation is due to the anion-catalyzed cation vacancy condensation at the film/metal interface. Pit growth kinetics are controlled by the ohmic potential drop across the cover over the pits. The repassivation time of metastable pits is affected by the potential drop across the pit cover. A pit stabilization criterion of the ratio of peak pit current to pit radius indicates that the critical condition to maintain the stable pit growth must exceed 2 × 10^{-2} A cm^{-1} to avoid repassivation. The main role of chloride ions in pitting is to increase the chance of the breakdown of a passive film, rather than to inhibit surface repassivation. The initiation of a metastable pit will have a certain influence on subsequent pitting events in the case of high pitting activity. When the pitting activity decreases, the metastable pitting events will follow the Poisson distribution.

Spectral analysis of noise data indicates that any transient having a sudden birth or a sudden death generates f^{-2} noise, while that without sudden change shows f^{-4} behavior. The roll-off frequency reflects the repassivation or growth rate of metastable pits.

The noise resistance coincides with the polarization resistance only in passivity or general corrosion. For pitting, the noise resistance cannot track quantitatively the change of the corrosivity of the system.

The passive film on carbon steel is a highly disordered n-type semiconductor. There are two donor levels in the space charge layer of the passive film. The divalent iron cation vacancies caused by the ionization of deep donor levels and then the complexity of iron cation with chloride ions are mainly responsible for pitting. The diffusivity of oxygen vacancies within the passive film is estimated to be in the range of $10^{-16} - 10^{-15}$ $cm^2 s^{-1}$.

ACKNOWLEDGEMENTS

CONTENTS

LIST OF TABLES

LIST OF FIGURES

LIST OF SYMBOLS

a	current rise rate in current transient
A	average magnitude of current transients
b	pit repassivation rate
C	electrode capacitance
C_a	concentration of aggressive ions
C_d	double-layer capacitance
C_i	concentration of inhibitive ions
C_O	concentration of oxygen vacancies
C_{sc}	capacitance of the space-charge layer
D_O	diffusivity of oxygen vacancies
E	energy
E_c	energy level of conductor band
E_{D1}	shallow energy level in the space charge layer
E_{D2}	deep energy level in the space charge layer
E_F	Fermi energy
E_v	energy level of valence band
f	frequency
f_c	roll-off frequency
f_i	frequency at the maximum imaginary impedance
F	Faraday's constant
$F(\omega)$	Fourier transfer
I	current
I_{org}	original passive current
I_{peak}	peak pitting current
I_{pit}	peak pit current
$I_{PSD}(f)$	PSD of current noise

I_{mean}	mean noise current
i	current density
i_c	cathodic current density
i_{corr}	corrosion current density
i_{pit}	pitting current density
J_O	flux of oxygen vacancies
k	Boltzmann constant
k_i	rate constant of the ith reaction during passivity
L	thickness
L_{film}	thickness of the passive film
m	metal atom
M	metal cation
N	number of samples in each run of noise records
N_A	acceptor density
N_D	donor density
N_{D1}	donor density at the shallow donor level
N_{D2}	donor density at the deep donor level
N_{mean}	average number of metastable pitting events
q	charge
Q_{cath}	faradaic cathodic charge
Q_{pit}	pit growth charge
$r_{a\,or\,i}$	Temkin parameters
r_{pit}	pit radius
R	Plank constant
R_e	electrolyte resistance
R_n	noise resistance
R_p	polarization resistance
R_{pit}	resistance of the pitting site
R_{sn}^0	spectral noise resistance
$R_{sn}(f)$	spectral noise impedance
R_t	charge-transfer resistance

S	electrode area
t	time
t_c	pit growth time
T	infinite period of time
t_i	time point to initiate pits
t_f	time point when the peak current is reached
U	potential
U_c	critical potential to ionize two donor levels of space charge layer
U_{corr}	corrosion potential
U_{fb}	flat-band potential
U_{peak}	peak potential
U_{pit}	pitting potential
$U_{PSD}(f)$	PSD of potential noise
U_{tr}	transitional potential
V_M^x	cation vacancy
$V_{\ddot{O}}$	anion (oxygen) vacancy
W	atomic weight
W_{sc}	thickness of the space charge layer
x	variable along the direction of thickness
z	chemical valence
z_a	charge number of aggressive ions
z_i	charge number of inhibitive ions
Z_a	impedance of localized pitting site
Z_c	impedance of passive surface
α	exponent of noise spectrum, that is, the value of roll-off slope
α_i	transfer coefficient of the ith reaction during passivity
$\alpha_{i/n}$	transfer coefficient of the reaction at the inner layer/outer layer interface
ε	dielectric constant
ε_0	permittivity of the free space
ε_L	electrical strength of the passive film

σ	standard deviation
σI	standard deviation of the current
σU	standard deviation of the potential
ΔU	potential drop
$<U_{peak}>$	average peak potential
$\phi_{f/s}$	potential difference across the film/solution interface
$\Delta\phi_{SC}$	potential difference across the space charge layer
Δt	sampling interval
λ	pit initiation rate
λ_t	the mean length of noise peak
τ	time constant of exponential function during pit growth or repassivation
θ_a	coverage of aggressive ions
θ_{crit}	critical coverage of ions on electrode surface
θ_i	coverage of aggressive ions
ρ	density
ω	angle frequency

ABBREVIATIONS

ACF	autocorrelation function
AES	Auger electron spectroscopy
CE	counter electrode
ECN	electrochemical current noise
EIS	electrochemical impedance spectroscopy
EN	electrochemical noise
EPN	electrochemical potential noise
FFT	fast Fourier transform
LPR	linear polarization resistance
MEM	maximum entropy method
PDM	point defect model
PI	pitting index
PSD	power spectral density
RE	reference electrode
r.m.s	root mean square
SCC	stress corrosion cracking
SEM	scanning electron microscopy
SIMS	secondary ion mass spectroscopy
SPD	stochastic process detector
WE	working electrode
XPS	x-ray photo-electron spectroscopy
ZRA	zero-resistance ammeter

Chapter 1 Introduction

Localized corrosion of passivated metals generally includes various types of corrosion phenomena, such as pitting, crevice corrosion and stress corrosion cracking. Compared with uniform corrosion, localized corrosion is more dangerous and destructive due to its latent incubation and quick propagation.[1] Among the different forms of localized corrosion, pitting is encountered most frequently in metallic materials of technological significance. Carbon steels, low alloy and stainless steels, nickel base alloys, aluminum, titanium, copper, and many other metals and alloys may suffer severe pitting in different environments, especially in those containing chloride ions.[2,3]

Due to its widespread occurrence and damaging effects, pitting has been a matter of great concern for over 40 years.[4] Extensive studies have been undertaken and continued with the aim of determining conditions that lead to pitting, understanding the basic mechanisms of the processes involved, and developing the most effective methods of protection. While much experimental data was gathered and major progress was made in both the understanding of the principal causes of pitting and the prevention or control of pit initiation and growth, many issues remain unsolved and some important knowledge is still lacking; for example, the nucleation mechanism of pits and the early growth stage.[5]

Even for the nature of pitting process, there also bears the opposite understandings. Many people believe that the initiation of a pit is an unpredictable event.[1,6] The intrinsic unpredictability and random nature associated with the pitting process make it extremely difficult to identify the mechanisms controlling the pitting and to understand their interaction by classic electrochemical techniques, such as steady-state polarization plots and A.C. impedance.[7,8] However, Macdonald's work[9] shows that once the properties of the passive film at the breakdown sites are known, the breakdown potential and the induction time are quite predictable and the resulting accumulated damage can be calculated with considerable accuracy. Therefore, the pitting is definitely a deterministic process.

1

With respect to the complexity of the studies of pitting corrosion, the electrochemical noise technique has unparalleled advantages compared with other electrochemical techniques. Spontaneous fluctuations of the corrosion potential and/or current generated by corrosion reactions are known as electrochemical noise (EN).[8,10,11] The time and frequency processing techniques devised for random signals can be applied for EN data. In the case where the elementary transients are not too numerous and are discernible, a statistical counting can be done on the time series to evaluate a mean appearance rate. However, in the case where many events occur at the same time and their transients overlap, a spectral analysis of the random signal in the frequency domain will allow the characteristic parameters of the process to be attained.

The EN technique has proven to be a valid approach to study pitting processes.[10,12,13] It has been shown that EN signals generated during pitting result from the breakdown and repair of the passive film and directly reflect the change of surface states of metals. Noise analysis can provide fundamental information about the initiation, propagation and repassivation of metastable pits, and thus, reveal the pit initiation mechanisms and reaction kinetics of the pitting processes. In addition, the EN technique is especially effective for monitoring applications.[12,14,15]

This work is aimed at investigating the metastable pitting phenomena occurring on carbon steel by electrochemical noise analysis and providing fundamental information about carbon steel pitting. Some basic viewpoints in pitting studies and the physical significance of the noise parameters are clarified. In addition, the semiconducting nature of the passive film on carbon steel is studied and the relationship between the electronic structure of the passive film and the pitting susceptibility is determined.

In order to present the above-mentioned work clearly and systematically, this thesis is divided into eight chapters. Chapter 2 is a comprehensive review of the EN technique, including the EN source and nature, measurements, analysis and its application to corrosion studies. In addition, the basic theories describing the formation and breakdown of the passive film are also reviewed.

The preparation of electrode and solution, the establishment of experiments and the main approach methods employed in this work are introduced in Chapter 3.

Chapter 4 presents the statistical analysis of EN signals in the time series generated during carbon steel pitting. The results contain the analysis of the role of electrode capacitance in potential fluctuations, the potential dependence of the initiation, growth and repassivation processes of metastable pits and their transition toward stability, the cooperative pitting behavior, the role of chloride ions in pitting processes, and some design factors worth considering during EN measurements.

The spectral analysis of noise data is illustrated in Chapter 5, where the physical significance of the noise spectrum and spectral parameters are clarified.

According to the statistical and spectral analysis results of EN signals, noise resistance is theoretically explained and its application to carbon steel corrosion is evaluated in Chapter 6.

Chapter 7 discusses the semiconducting nature of the passive film and the relationship between electronic structure and pitting susceptibility of the passivated carbon steel. An investigation of the relationship between donor density and film formation potential is performed and the diffusivity of oxygen vacancies within the passive film on carbon steel is calculated.

In the final chapter, the main conclusions and the significance of the present work are summarized, as well as some general recommendations for future work.

References

1. D.A. Jones, in *Principles and Prevention of Corrosion*, p. 11, Macmillan Publishing Company, New York, USA (1992).

2. Z. Szklarska-Smialowska, in *Pitting Corrosion of Metals*, p. 1, NACE, Houston, USA (1986).

3. Z. Szklarska-Smialowska, in *Corrosion of Metals and Hydrogen-Related Phenomena*, J. Flis, Editor, p. 9, Elsevier Science Publishing Co., New York, USA (1991).

4. Z. Szklarska-Smialowska, in *Advances in Localized Corrosion*, H. Isaacs, U. Bertocci, J. Kruger and S. Smialowska, Editors, p. 41, NACE, Houston, USA (1987).

5. H. Bohni, *Materials Science Forum* **111-112**, 401 (1992).

6. S.M. Sharland, C.M. Bishop, P.H. Balkwill and J. Stewart, in *Advances in Localized Corrosion*, H. Isaacs, U. Bertocci, J. Kruger and S. Smialowska, Editors, p. 109, NACE, Houston, USA (1987).

7. C. Gabrielli and M. Keddam, *Corrosion* **48**, 794 (1992).

8. C. Gabrielli, F. Huet and M. Keddam, in *Electrochemical and Optical Techniques for the Study and Monitoring of Metallic Corrosion*, M.G.S. Ferreira and C.A. Melendres, Editors, p. 135, Kluwer Academic Publishers, Netherlands (1991).

9. D.D. Macdonald, *J. Electrochem. Soc.* **139**, 3434 (1992).

10. J.L. Dawson, in *Electrochemical Noise Measurement for Corrosion Applications*, J.R. Kearns, J.R. Scully, P.R. Roberge, D.L. Reichert and J.L. Dawson, Editors, p. 3, ASTM STP 1277, West Conshohocken, PA (1996).

11. D.A. Eden and A.N. Rothwell, in *Corrosion '92*, paper no. 292, NACE, Houston, USA (1992).

12. C. Gabrielli, F. Huet, M. Keddam and R. Oltra, *Corrosion* **46**, 266 (1990).

13. M. Hashimoto, S. Miyajima and T. Murata, *Corros. Sci.* **33**, 685, 905, 917 (1992).

14. A. Legat and V. Dolecek, *Corrosion* **51**, 295 (1995).

15. H.J. Debruyn, K. Lawson and E.E. Heaver, in *Electrochemical Noise Measurement for Corrosion Applications*, J.R. Kearns, J.R. Scully, P.R. Roberge, D.L. Reichert and J.L. Dawson, Editors, p. 214, ASTM STP 1277, West Conshohocken, PA (1996).

4

Chapter 2 Literature Review

2.1 Noise Sources in Electrochemical Systems

2.1.1 Thermal noise

The lowest magnitude or intensity of electrical noise generated in electrochemical systems is the thermal or Johnson noise as a result of the random motion of the electrons and charge carriers in thermal equilibrium with their surroundings.[1] This vibration occurs at temperatures above absolute zero.

Thermal noise determines the absolute minimum that can be expected because the signal generators are internal to the system. In some studies involving low levels of EN, thermal noise must be minimized. One widely used approach is to use computational means to remove this instrument noise. A certain amount of interest has been directed to the possibility of assessing whether thermal noise can be used to obtain information on the electrochemical behavior of the system under study.[2,3] However, the applicability of thermal fluctuations on electrochemical systems is open to question.[4]

2.1.2 Shot noise

Shot noise in an electrical circuit is due to the quantitative nature of the electronic charge and is typically associated with low levels of current flow in electronic devices, as during electrodeposition,[5,6] and is several orders of magnitude greater than that caused by thermal noise. In these cases, the source of power driving the fluctuations must be other than thermal motion and must be found in the free energy available for the reaction. The fluctuations observed in electrochemical systems are often due to current bursts, at levels much higher than a single charge, taking place at the electrodes.

The noise generated by current fluctuations can be described as largely similar to that observed first in vacuum tubes and is generally called shot noise.[7] The noise is related to the finite size of the charge carriers; in a vacuum tube, each electron transports a charge

5

(q) in a very short time, causing a current spike.

In the case of interest to electrochemistry, q is much larger than the electron charge. In the classic experiments of electrocrystallization on quasi-perfect Ag single crystals,[8] where the charge corresponds exactly to a monolayer of metal, the electrochemical properties are then revealed.

2.1.3 Flicker noise

Flicker noise, also called $1/f$ noise, is noise whose amplitude is inversely proportional to the frequency (f). It may be more correct to write $1/f^{\alpha}$ noise, but the exponent α is often close to 1.[9] This kind of noise is observed in a great variety of systems, and while several different explanations for its origin have been proposed, none seems to have sufficient generality to explain its nearly universal presence.[10,11] Many spectra of noise measured on electrochemical systems tend to show some inverse proportionality with frequency in the range measured (usually from 10^3 Hz to 10^{-2} Hz), and the slope at the lower frequencies is often close to $1/f$. However, there is no theoretical treatment that would suggest that electrochemical systems will exhibit flicker noise.

Flicker noise occurs in the instrument, therefore limiting its sensitivity. Flicker noise appears to be one of the major limitations, together with the drift of the signals, in the measurement of electrochemical noise.

2.2 Noise Sources in Corrosion Systems

The major sources of noise observed in corrosion systems can be ascribed to macroscopic random (stochastic) phenomena, which have been shown to be widely varied. They include:

* Pit initiation, metastable pitting, and stable pit growth;[12,13,14,15]

* Hydrogen evolution involving bubble nucleation, growth, and detachment;[16,17] changes in solution resistance and diffusion of anion into propagating microcracks;[15] and discharge on freshly exposed metal at propagating cracks;[18]

* Propagating stress corrosion cracking (SCC) involving metal dissolution or water discharge;[18,19,20,21,22]

6

* Crevice corrosion;[23,24,25]
* Mechanical impingement and abrasion;[26]
* Underfilm corrosion;[26,27]
* Passive systems;[28,29]
* High-temperature processes;[30,31]
* Microbial-induced corrosion;[32,33]
* Uniform corrosion.[34,35]

In all cases, noise data from corrosion studies only indicate possible types of stochastic processes.[36] The data must then be interpreted to provide corrosion information and/or an understanding in terms of models and corrosion principles.

2.3   Nature of Electrochemical Noise

All physical processes are divided into deterministic or non-deterministic (the latter being random or stochastic) categories. Deterministic processes may be periodic or non-periodic (transient); they are described by time-varying functions, such as those produced by sinusoidal perturbations used in electrochemical impedance studies. In conventional electrochemical studies, the deterministic input is typically controlled by an external potentiostatic or galvanostatic perturbation.

The nature of EN phenomena is determined by the noise sources. The thermal noise generated during electron vibration, due to the temperature difference, belongs to the general category of non-deterministic processes. The EN during pitting is, according to Macdonald, is a deterministic phenomenon. He argues that passivity breakdown and pitting initiation occur for good mechanistic reasons that render the process and the then generated noise deterministic in nature. However, some people attribute the EN during pitting to the general random category.[36] The stochastic processes are described either by probability density function equations or in statistical terms. Non-stationary random processes have time-varying functions that are determined by obtaining instantaneous averages over the ensemble of time records forming the process. One of the most comprehensive studies of such ensembles was made by the Williams group on current noise transients produced during pitting.[37,38,39] The data sets were generated by a method

7

in which a potentiostatic sweep was terminated at a constant potential.

2.4   Measurements of Electrochemical Noise

Electrochemical noise data can be obtained in a conventional manner using potentiostatic and galvanostatic techniques.[38,39,40] The current or potential time records are then analyzed to provide information on the corrosion processes. Such measurements can be useful in research investigations since only one measured parameter varies with time. However, the apparatus used for modulating potential or current in the galvanic cell will introduce unwanted noise into the system, and may not always provide a true representation of an actual corrosion situation.[41]

An alternative approach is to allow the natural corrosion process to occur on the electrode and then to record the potential changes of the freely corroding metal on a sensitive digital voltmeter.[42,43] A preferred variation is to combine the corrosion potential measurement with a current measurement by coupling two freely corroding electrodes together through a sensitive zero-resistance ammeter (ZRA).[44,45] The two meters provide simultaneous time records of the spontaneous changes in coupling current and corrosion potential. Analysis of such data can be used in either research studies or practical corrosion monitoring applications.

2.4.1   Potentiostatic and galvanostatic measurements

The use of potentiostatic/galvanostatic measurements has been a preferred method in many research studies. This technique is particularly useful for investigations of passivity and its breakdown leading to pitting. Of major concern in early investigations of EN in corrosion was the development and use of low-noise potentiostats and galvanostats.[46] Initial experiments also favored the use of a two-channel cross-correlation method and two reference electrodes, all contained within a faradaic cage.[47] This approach was abandoned when it was recognized that in corrosion studies most noise signals are significantly in excess of the instrumentation noise. Obviously, in all studies, it is necessary to use well-designed instrumentation with a low instrument noise output to achieve minimum interference from the measurement equipment. Examples of the use of

8

potentiostatic and galvanostatic measurements are given below.

The relationships between the electrochemical behavior of the passive film on stainless steel under potentiodynamic conditions and the current noise in the pre-pitting range have been evaluated by Keddam et al.[48] Pit nucleation was described by a Poisson process. The amplitude and frequency of the current noise decreased drastically with aging of the passive film.

In contrast to the large number of papers using potentiostatic measurements, there are few reports of the use of noise measurements obtained galvanostatically. Of particular interest has been the work by Gabrielli and Keddam[49] on noise generated by iron dissolution and simultaneous hydrogen generation. The data were analyzed to demonstrate that the fluctuations were due to the formation and release of hydrogen bubbles. This analysis is an extension of the original postulates by Baker[50] that electrochemical noise may be due to hydrogen bubble formation.

2.4.2 Electrochemical potential noise (EPN) measurement in freely corroding metals

Many of the early observations of EN were made by monitoring the corrosion potential of freely corroding electrodes.[12,23] When used in combination with more conventional techniques, such as linear polarization and electrochemical impedance, EPN monitoring is able to discriminate between periods of uniform corrosion and localized corrosion in situ and in a range of operating plants and test apparatus.[51,52] Other researchers have also suggested subsequently that EPN measurements may be used to quantify corrosion rates of steel in concrete[53] and active dissolution of iron.[49,54]

2.4.3 Electrochemical current noise (ECN) measurements from coupled electrodes

The use of coupled electrodes where the coupling current flow is monitored with a ZRA provides a method of monitoring current noise on freely corroding specimens.[44] In most cases, nominally identical electrodes are used. In principle, there should be no net current flow between the electrodes; however, in practice, the statistical variation in corrosion rates across surfaces means that current flow and electrochemical noise are observed. This process can be considered as the experimental verification of the original Evans' concept of mobile anodic and cathodic areas on a uniformly corroding surface.[36]

9

Changes in corrosion potential of the coupled electrode assembly are measured with a third electrode, either a reference electrode in the case of laboratory studies or a piece of metal of similar composition as the electrode assembly. The three-electrode arrangement enables changes in current noise that produce changes in corrosion potential to be followed as the environmental conditions change.

The simultaneous monitoring of current and potential noise signals was first used in 1984 by Eden[44] using simple analog instrumentation. The combined monitoring of corrosion potential and coupling current has been particularly useful in research studies of localized corrosion, materials testing and in-situ corrosion monitoring. In the case of localized corrosion, one of the electrodes may generate a pit, and hence, the net current transient is observed. It is also possible to use specially designed electrode assemblies in which one electrode is stressed; this may be used to evaluate SCC. Crevice corrosion can be assessed with an electrode covered by a crevice with the second electrode acting as the external cathodic area.

2.5   Analysis of Electrochemical Noise

Analysis of the EN data may be undertaken using a variety of methods. Two principal techniques have been extensively used.[55] The first method involves the digital acquisition of raw data as a time record series and subsequent analysis using statistical techniques, frequency domain transforms and transient analysis, providing kinetic and mechanistic information. This technique is suited to do research and development studies where the aim is to characterize the response of specific systems. The second method involves the processing of the signals using electronic filters and amplifiers and the production of an output voltage proportional to the root mean square (r.m.s.) of the noise signals. These data are subsequently recorded by a data logging system and analyzed to provide an indication of corrosion rate and mechanism. The latter technique has been proven to be more useful in long-term, on-line monitoring situations, where correlation of corrosion-related information with processing operations is important.

10

2.5.1 Digital techniques

The digital techniques involve the measurements and analysis of raw time record data, containing simultaneous recordings of current and potential signals. The noise data collected during corrosion can be analyzed either in the time domain or in the frequency domain depending on whether the transients are discernible or not, i. e., the amplitude of the nucleation rate of the transients. In the case of the growing stable pits, a statistical counting can only be performed since spectral analysis requires a relatively stationary corrosion stage. In the case of the random current transients related to the birth and death of the pit nuclei (pre-pitting stage), a time recording and a spectral analysis of the random transients could be carried out if the pits are not too numerous. If there are too many pits only a spectral analysis can be performed.

2.5.1.1 Time recording

Examination of the raw digitized data recorded in the time series can often give valuable insight into the processes occurring on the specimens. However, it is difficult to assess values of corrosion rate without further analysis.

The EN generated by uniform corrosion consists of spontaneous low-frequency fluctuations of potential and current, with an amplitude typically of the order of tens or hundreds of microvolts and from picoamps/cm^2 to microamps/cm^2, respectively.[40,56]

In contrast, when localized corrosion takes place, the raw data traces typically show evidence of transients, which give an indication of the amplitude and frequency of the localized events, and may be used to identify the mechanistic processes associated with the corrosion type.[55] For example, Gabrielli et al.[57,58] analyzed the time records published in the literature and indicated that two types of current transients were always reported. The type I transient is distinguished by a slow current growth followed by a sudden drop. It seems to be characteristic of metastable pitting of iron,[59] iron-chromium alloy[60] and stainless steels.[61,62,63] The type II transient is characterized by a sudden birth that is followed by a slow recovery, which is typical of metastable pitting of aluminum and aluminum alloys[64,65] and non-chemical initiation of the corrosion, such as abrasion,[66,67] scratching,[68] and laser illumination.[69]

11

2.5.1.2 Statistical analysis

Statistical analysis provides a simple and rapid method for the interpretation of the EN data. It can reduce the large number of measurements in a noise recording to a single figure. Various statistical measurements have been proposed to identify certain features of the corrosion process, including:

* <u>Standard deviation of the current or potential (σI or σU)</u>

The standard deviation of the current or potential is calculated using the relationship:

$$\sigma = \sqrt{\frac{\sum_{i=1}^{n} X_i^2 - (\sum_{i=1}^{n} X_i)^2 / n}{n-1}} \qquad (2\text{-}1)$$

where X_i is the measured value, and n is the number of points in the recording.

As discussed,[70] σI is expected to increase with the increasing corrosion rate (the electrode size is kept constant). However, the establishment of a quantitative relationship between σI and the corrosion rate depends on the corrosion type.[71] σI is either proportional to the corrosion current density (i_{corr}) or to $(i_{corr})^{1/2}$, depending upon whether the current transients are superimposed or temporally separated. For localized corrosion processes where the duration of transients generally is short compared with the average inter-transient time, the square-root relationship is more likely. Proportionality is expected for general corrosion and passivity where the superimposed transients are apparent. Therefore, although the corrosion rate normally is expressed as a current density, which is independent of electrode size, no such simple relationship is available for σI in the case of localized corrosion.

* <u>Pitting index (PI)</u>

The pitting index is calculated as shown according to Kelly et al.:[72]

$$PI = \frac{\sigma I}{I_{r.m.s.}} \qquad (2\text{-}2)$$

12

where $I_{r.m.s.}$ is the root mean square of the noise current. Because the ECN may vary with time, these quantities should be calculated over the same time period.

Table 2-1. *Correlation between the pitting index (PI) and type of corrosion expected*[75]

Pitting Index Value Range	Type of Corrosion Expected
0.001 < PI < 0.01	Uniform corrosion
0.01 < PI < 0.1	Mixed corrosion
0.1 < PI < 1	Pitting corrosion

The pitting index may have a value between 0 and 1. Eden et al.[73] reported the classification for the pitting index shown in Table 2-1. The reason behind the formulation of the PI is that pitting occurs on initially passive electrodes, which exhibit small background current. The initiation of localized attack can be detected by the relatively large current transients, which lead to a large standard deviation in the current. Values near zero indicate general corrosion. The root mean square of the current signal is used instead of the mean current to account for all current, independent of its direction.

* Noise resistance (R_n)

Noise resistance is defined as the ratio of the standard deviation of potential to the standard deviation of current:[44,74,75]

$$R_n = \frac{\sigma U}{\sigma I}$$

(2-3)

In the same way that polarization resistance is inversely proportional to corrosion current density by the Stern-Geary equation,[76] noise resistance is taken to be a direct measure of the change of corrosion rate, especially the general corrosion rate.[77] In addition, theoretical analysis[78] has proven that the potential and current noise are related by the impedance of the metal/solution interface. Noise resistance is a function of the electrochemical behavior of the material under study and, thus, some important

13

electrochemical parameters, for example, the electrode impedance,[55] can be derived from the noise resistance.

While more sophisticated statistical measures (e.g., quantification of the extent to which the distribution deviates from a normal distribution) might be of use, they have not widely been applied to EN measurements and analysis, and are not considered here.

2.5.1.3 Spectral analysis

Standard methods of analysis are typically used to show noise data as spectra, which are representations of the time record as "averages" in the frequency domain display. This technique is used mainly to examine whether the noise occurs at specific frequencies,[79] and to compare the recorded signal with the intrinsic noise of the recording system to decide whether recordings contain useful information or are swamped by system noise. The transformation into the frequency domain may also be used to calculate the low frequency impedance spectra from the potential and current noise data.

Two common mathematical procedures used to convert time domain records into frequency domain spectra are the fast Fourier transform (FFT) and the maximum entropy method (MEM). The FFT method[80] is widely used in many branches of engineering and science; it produces somewhat "noisy" spectra and is appropriate for repetitive signals and data sets with a reasonable number of sample points, and in the case of EN analysis, may be used to evaluate periodic signals. MEM was developed by Burg[81] to analyze a limited number of sample points in geophysical studies and uses filter coefficients to describe the data. Details of the computational procedures for MEM are available.[82] MEM is considered to produce smoother spectral representations of data, from which two important spectral parameters, roll-off slope and roll-off frequency, can be easily evaluated.[83] Results have indicated[83,84] that FFT and MEM produce identical spectra from EN data, except for low ECN buried in the parasitic noise generated by the measurement system. In this case, the FFT technique is more appropriate than the MEM, which gives qualitative results only. Therefore, selection of the transformation method (FFT or MEM) of noise data would appear to be a personal choice.

Noise spectra are presented as either power spectral density (PSD) or amplitude (dB)

plots. In both cases, either the logarithm of spectral power density (V^2/Hz or A^2/Hz) or the amplitude (dB), that is, logarithm of power spectral amplitude ($V/Hz^{1/2}$ or $A/Hz^{1/2}$) is plotted against the logarithm of frequency (Hz). The noise amplitude is the square root of noise power. The spectral analysis provides valid information in the following frequency range:

$$f_{min} = \frac{1}{N\Delta t}$$

$$f_{max} = \frac{1}{2\Delta t} \qquad\qquad (2\text{-}4)$$

where N and Δt are the number of samples in each run and the sampling interval, respectively.

Although PSD is an effective expression for the study of EN, much useful information is lost when the real time data are converted into frequency data since the calculation of PSD includes an averaging procedure. Therefore, the noise data should be analyzed as time series data, especially when one studies the fundamental steps of the random fluctuation of signals and how this fluctuation is related to the kinetics of cathodic and anodic reactions.[85] Once the stochastic and deterministic nature of EN in the real time domain is analyzed, it will be an easy task to convert the real time data into frequency data, and observe how the electrochemical reactions affect the shape of the PSD curve.

2.5.2 Analogue techniques

The analogue techniques involve processing of the potential and current signals in real time using electronic amplifiers and filters, typically providing an output proportional to the r.m.s. value of the low frequency noise signals. The output is usually a signal in the 0 to 10 volt range corresponding to low frequency potential noise signals in the 1 to 10 microvolt range and the current noise signals which may vary from microamps to milliamps (usually over a four-decade dynamic range). This type of signal processing is particularly useful in continuous on-line monitoring applications where it is

15

important to evaluate both steady state corrosion conditions and also to identify transitions between corrosion modes.

2.5.3 Other techniques

Considering the complex and difficult work involved in EN analysis, many other techniques have also been attempted. Some typical examples are listed.

* Stochastic process detector (SPD)

The SPD technique was designed to quantify the stochasticity of EN records as a function of frequency.[86] The main idea behind SPD is that specific corrosion modes, such as pitting or other forms of localized corrosion, will potentially generate EN containing deterministic features. It is hoped that by focusing on the stochasticity of EN recordings, the technique will be highly sensitive to any feature falling outside such category and reveal some information not detectable by any other technique. The SPD technique consists of two levels of EN transformation. First, EN records are transformed into a series of singular events, that is, each point of a time series is examined for its appurtenance to either positive or negative noise peaks. The distribution of peak lengths $h(t)$ is then examined and compared with the theoretical exponential first-order decay distribution, represented by

$$h(t) = \lambda_t e^{-\lambda t} \tag{2-5}$$

where λ_t and t are the mean value and the time length of the noise peak. The goodness-of-fit of real data by the exponential function is calculated to serve as a measure of stochasticity of the time records. Roberge et al.[86,87] used the SPD technique to analyze the voltage fluctuations during the corrosion of aluminum. The analysis result was confirmed to be reasonable by microscopic examination of the specimen and EIS measurements.

* Chaos data analyzer

Over the last twenty years in nonlinear dynamic theory, some new mathematical parameters have been developed to characterize nonperiodic and chaotic systems,[88] such as the reconstruction of attractor, factual dimensions and Lyapunov exponents.[56] Various chaotic parameters of current oscillations have been used to describe the initiation of

16

localized corrosion.[89] as well as to simulate the evolution of pits on silver.[90]

It was established[91] that the power law $(1/f^\alpha)$ of the power spectrum might indicate the chaotic nature of a time series, where the exponent α is considered to be an index of its irregularity. The results of the spectral analysis of measured EN usually indicate the continuous broadband nature of fluctuations. Whereas this type of spectrum is characteristic for random and chaotic signals, rescaled range analysis has been used to extend the statistical approach of EPN.[86,92] Fractal dimensions of EPN and ECN measured on stainless steel have been calculated to estimate the dimensionality of the phase space of different types of corrosion.[93]

2.6 Application of EN Technique to Electrochemical Systems

Initial studies of noise in electrochemical systems by Tyagai,[94,95,96] Baker[16,97,98] and Fleischmann and Oldham[99] have been reviewed by Seralathan and Rangarajan.[100,101] They have presented detailed mathematical models for assessing fundamental processes. For example, the Rangarajan models consider EN as a process involving faradaic shot noise; their methodology provides a fundamental treatment of the previous studies of basic electrochemical reactions, but no corrosion. The method involves consideration of primary noise sources, which are fundamental, but invariably uncorrelated assessment of macroscopic phenomena. The treatment includes equations for conversion of the current into power spectra. The macro-variables include partial faradaic currents, electron transfer and chemical kinetics, but these are described as discrete Poisson processes.

These earlier studies highlight two major drawbacks for the use of EN in studies of redox systems: (1) the noise signal is relatively small, and (2) there is no particular advantage of noise measurements compared with deterministic methods, such as impedance, for these systems.[16]

2.7 Application of EN Technique to Corrosion Systems

EN in corrosion was first reported in the early 1960s.[12,102] It is only since the corrosion publications of the late 1970s and early 1980s[5,6,41,42,47,103] that there has been an

17

increasing interest in this subject. This is partly because the availability of digital equipment makes the measurement and recording of noise data a relatively easy task. Equally important is the recognition that EN interpretation provides scientific answers in corrosion research and solves practical problems in corrosion engineering.

2.7.1 Uniform corrosion

Active dissolution of iron and steel in acidic solutions is controlled by the hydrogen evolution process. The noise signals obtained under galvanostatic and potentiostatic control have been interpreted in terms of a stochastic process determined by bubble formation, growth and detachment.[16,17]

Monitoring measurements made on mild steel in dilute sulfuric acid at the corrosion potential indicate that noise resistance, charge-transfer resistance (R_t) from impedance measurements, and weight-loss data provide similar results.[18,70] In other systems, for example, in carbon dioxide-containing brines and aerated sodium chloride solutions, the corrosion rates, indicated by R_n, R_t and polarization resistance (R_p) from linear polarization measurements, decrease with time as corrosion product films develop. Some organizations now recommend EN measurements for determining general corrosion rates.[104]

2.7.2 Localized corrosion

2.7.2.1 Pitting corrosion

Pitting is a stochastic process, and noise analysis has provided greater understanding of the initiation and propagation stages. In particular, analysis of individual noise transients is a useful research method for the study of fundamental corrosion mechanisms. Similar information can be obtained from potentiostatic and free corrosion data.

Initiation events are observed as short-lived transients. In some cases, transients may continue and give rise to metastable pits, which have only a limited life and repassivate within a few seconds.[15,62,105] Only a small number of initiation events continue to form stable pits. Even stable pits have a finite life. Therefore, there are probabilities associated

with birth and death of the initiating transients and the metastable and stable pits.

The noise trace from a stable growth pit is typically that of an actively corroding metal surface. Analysis of the current and potential relationship shows that in the free corrosion situation, the pit is not driven by an IR effect, as with potentiostatic experiments,[64] but by the retained local environment. For example, Frankel et al.[106] observed the presence of a preexisting passive film across a pit mouth. Burstein and Pistorius[62,105,107] further demonstrated that the transients are consistent with the absence or presence of the original passive film. The partial covering of a pit mouth will appear to play an important part in controlling the diffusion processes in the incipient pit environment. This local environment in turn determines the pit life and the type of noise transient observed.

Dawson[29] thought that initiation transients are due to local film rupture events, and pitting noise is mechanically triggered. The overall mechanism involves adsorption of negatively charged chloride ions, and this adsorption increases as the electrode potential rises towards the pitting potential. The change in adsorption affects the film surface tension, which in turn changes the pressure within the film. A film rupture event that occurs at an area of high chloride adsorption has a greater probability of continuing to metastable or stable pits.

EN measurements on pitting, either by analysis of individual transients or a series of transients, is able to provide detailed information on the fundamental processes involved. The actual stochastic processes are influenced by factors such as age and thickness of the passive film, composition of the environment, electrode potential, diffusion restriction as a result of pit geometry, and flow enhancement in turbulent environment.

2.7.2.2 Crevice corrosion

Crevice corrosion on stainless steel is typically observed as pitting, but with the anodic dissolution assisted by restricted diffusion produced by the crevice geometry. Initial film rupture or breakdown occurs within the crevice, and then, provided the corrosion potential is sufficiently anodic, the metal dissolution will continue as a large current transient.[52,108,109] This noise transient is similar to that produced by a stable pit but

19

with an extended life that continues over a number of hours.

In the case of iron and carbon steels, which have a less protective film, regular potential oscillations may be observed.[23] These appear to be characteristic of diffusion control, but are more likely to be due to the formation and dissolution of unstable films in the restricted crevice environment. Similar oscillations have been observed with stress-assisted intergranular corrosion[18] and unstable film formation and dissolution.[110]

2.7.2.3 Stress corrosion cracking (SCC)

EN measurements during SCC have been reported for both potentiostatic-controlled experiments[21,22] and corrosion monitoring at the free corrosion potential.[18,19,20]

Anodic transients are the result of metal dissolution at the crack tip and are, therefore, similar to pit initiation. In many cases, there could be difficulty in the ability to discriminate between anodic SCC, pitting and crevice corrosion. Extensive active corrosion outside the crack can mask the cracking transients.[20,111]

Cathodic transients can be observed in some SCC systems.[18] These result from the hydrogen generation reaction that occurs on the newly fractured metal surface of a propagating crack. This freshly exposed surface is highly catalytic and, hence, conversion of adsorbed water to atomic hydrogen occurs rapidly at the base of the crack. The fast cathodic reaction consumes electrons that are generated from the film dissolution and the electrochemical double layer present on the metal surface, both external to the crack and on the crack walls. The electrochemical interface is then recharged by subsequent metal dissolution. The observed potential and current transients, therefore, both increase in a negative direction during the propagation step. Rapid branched cracking and slowly propagating single cracks have been observed with EN.

2.7.3 Other aspects

2.7.3.1 Coating evaluation

One of the most significant ongoing developments of the EN technique over the past ten years has been the use of noise analysis in coating evaluation.[112] Particularly noteworthy is the work by Skerry et al.[113,114,115,116] that has demonstrated that noise can be

20

considered as a standard test procedure. In addition, Mansfeld and co-workers[45,75,112] performed many work in the relevant aspects and obtained many valuable results.

The main advantages of EN measurements and analysis in evaluating coatings are ease of application and production of quantifiable data which, unlike impedance measurements, are also easy to interpret. Typical data can be presented as a change of noise resistance with time of exposure. In general, through-coating corrosion is a relatively slow process with good systems, and measured parameters do not change rapidly during the test exposure period. EN is, however, very sensitive to any change, and hence, trends of noise resistance with exposure time are ideal for coating evaluations. The data are more amenable to simple analysis involving water uptake, increasing corrosion of the substrate, than that provided by electrochemical impedance.

2.7.3.2 Inhibition mechanism

The EN technique has been used in inhibitor studies and evaluations.[117,118,119,120] The corrosion rate data and indications of pitting are typical examples of these applications.

The dependence of noise resistance on exposure time in inhibitive solutions and the comparison of R_n with polarization resistance or charge-transfer resistance provide the base for EN analysis as a convenient method of continuous corrosion rate monitoring. The changes of potential and current noise data strongly suggest that EN is a practical technique in the monitoring of inhibitor film performance and in the evaluation of inhibitor film persistency.

The analysis of noise data in the frequency domain can provide a useful means of characterization of the corrosion attack and of the inhibition mechanisms. For example, Monticelli et al.[121] found that an organic inhibitor, mercaptopyimidine, inhibits localized corrosion by surface adsorption. As a consequence, the noise spectra appear to be depressed, particularly in the low-frequency region and at short immersion times. Nitrate and molybdate act mainly by reinforcing the surface passive film. The $1/f^\alpha$ trend shown by their noise spectra, with α close to 20 dB/decade, appears to be a consequence of their film-forming activity.

21

2.8 Industrial Application of EN Technique – Corrosion Monitoring

The goal of industrial corrosion monitoring is to provide a clear picture of the conditions in an operating plant that lead to corrosion damage in order to avoid unscheduled downtime. The advantages of EN for corrosion monitoring applications have been demonstrated in numerous publications.[18,52,58,108,122,123]

Evaluations have been made of acid dew point corrosion in flue gas exhaust equipment and ductwork,[52,124] flue gas de-sulphurizing systems,[125,126] boiler plant,[127] cooling water systems,[128] oil and gas production,[129] reinforced concrete,[53,122,130] and the nuclear power industry.[131]

The main emphasis has been troubleshooting, assessment of process control, effects of environmental changes, and inhibitor evaluations. Measurement of corrosion rates, identification of the onset of localized corrosion and trend monitoring are typical of most studies.

2.9 Passivation and Localized Corrosion

The studies of localized corrosion is one of the main applications of the EN technique in the corrosion field. In general, the occurrence of localized corrosion is subject to the existence of a protective film on the electrode surface.[132] Some fundamental aspects of the passivation of metals and the breakdown of passive film are reviewed.

2.9.1 Passivation

The passivity of metals and alloys is one of the most important phenomenon responsible for our metal-based civilization. Most structural metals are viable in an engineering sense only because of the existence of a surface oxide film whose thickness may be less than a few nanometers. Although the phenomenon of passivity has been known for more than 150 years, a satisfactory description of the passive state still eludes us.[133] This state of affairs is due, in part, to the experimental difficulties in probing surface films whose thickness may not exceed a few nanometers, and also to the conceptual difficulty in using bulk phase concepts in formulating theoretical descriptions.

22

The first attempt to explain the phenomenon was made by Faraday,[134] more than one century ago, and since then numerous studies have been carried out leading to several theories.[135] For many years there has been great opposition between two models: the adsorption model, which describes the passive state based on the adsorption of a layer of oxygen or oxygen-containing species on the metal surface, and the oxide film model, which is based on the formation of a protective oxide film.

Recently, the advent of spectroscopic techniques, such as Auger electron spectroscopy (AES) and X-ray photo-electron spectroscopy (XPS), which provide information on the composition of small thickness of matter, has been in favor of the oxide film theory. Consequently, the discussions have become centered on other factors, such as the degree of crystallinity of the passive film and its composition.

2.9.1.1 Models of passivation

Although at present it is accepted that passivation is a consequence of the presence of oxides on the surface, a large variety of theories have been proposed involving different structures and compositions.

* <u>Crystalline oxide model</u>

This model explains the passivation based on the formation of a crystalline oxide on the metallic surface. In the case of iron the films are composed of either $\gamma-Fe_2O_3$ or $Fe_2O_3 \bullet nH_2O$ or Fe_3O_4 and $\gamma-Fe_2O_3$.

The crystalline oxide is assumed in many cases to have a spinel structure that supports ionic transport. The presence of water in the films formed in aqueous medium is interpreted as being due either to H_2O adsorption at the film/solution interface[136] or to a process of stabilization of $\gamma-Fe_2O_3$ by hydrogen in the outer layer of the film.[137] Thus, the passive film usually contains hydrogen in addition to metal ions and oxygen, hydrogen being present in the form of protons, OH⁻ or water.

Concerning its composition in depth the film can be considered as homogeneous[138] or having a stoichiometry continuously changing with thickness[139] or even a sandwich type of structure.[137]

23

* Sandwich structure

This model is based on the fact that the ferric oxide constituting the passive film is thermodynamically unstable when in direct contact with metallic iron.[135] The sandwich oxide structure appears by analogy with the oxidation in the air at high temperatures where the film is composed of an outer layer of α–Fe_2O_3 and an inner layer of Fe_3O_4 and was initially proposed by Nagayama and Cohen.[140] Several studies, however, indicate that for passive iron, the outer layer may be of γ–Fe_2O_3.[138]

* Polymeric hydrated oxide model

According to this model, the water has a key role in passivation, acting as a binder between polymeric oxide chains, in an essentially amorphous structure. According to Okamoto,[141] the film shows a gel-type of structure (Fig. 2-1).

In the region where the film is not present, the production of the metal ions takes place with formation of MOH^+ species. This species is then captured by the involving water and precipitates as a solid film with a high degree of hydration. Anodic polarization or aging of the film leads to a loss of protons (Fig. 2-1a).

Okamoto postulates the existence of three kinds of bridges between metal ions: H_2O-M-OH_2, -HO-M-OH- and -O-M-O-. The H_2O-M-OH_2 structure, corresponding to a higher degree of hydration, is the more reactive.

Okamoto's model was originally proposed for stainless steel, but has also been applied to iron.[142,143]

2.9.1.2 Passivation of stainless steel

The passive films formed on stainless steel are thinner than those formed on pure iron, show a more complex composition, and in addition, cannot be reduced cathodically,[135] which makes their study quite difficult.

Although it is universally accepted that the films formed on stainless steel are enriched in chromium, many doubts still persist concerning the film composition and structure, as well as the role of the alloying elements.[144]

Concerning the film structure, there are various studies pointing towards a "duplex" or sandwich type of oxide with an inner layer enriched in chromium and an outer layer

24
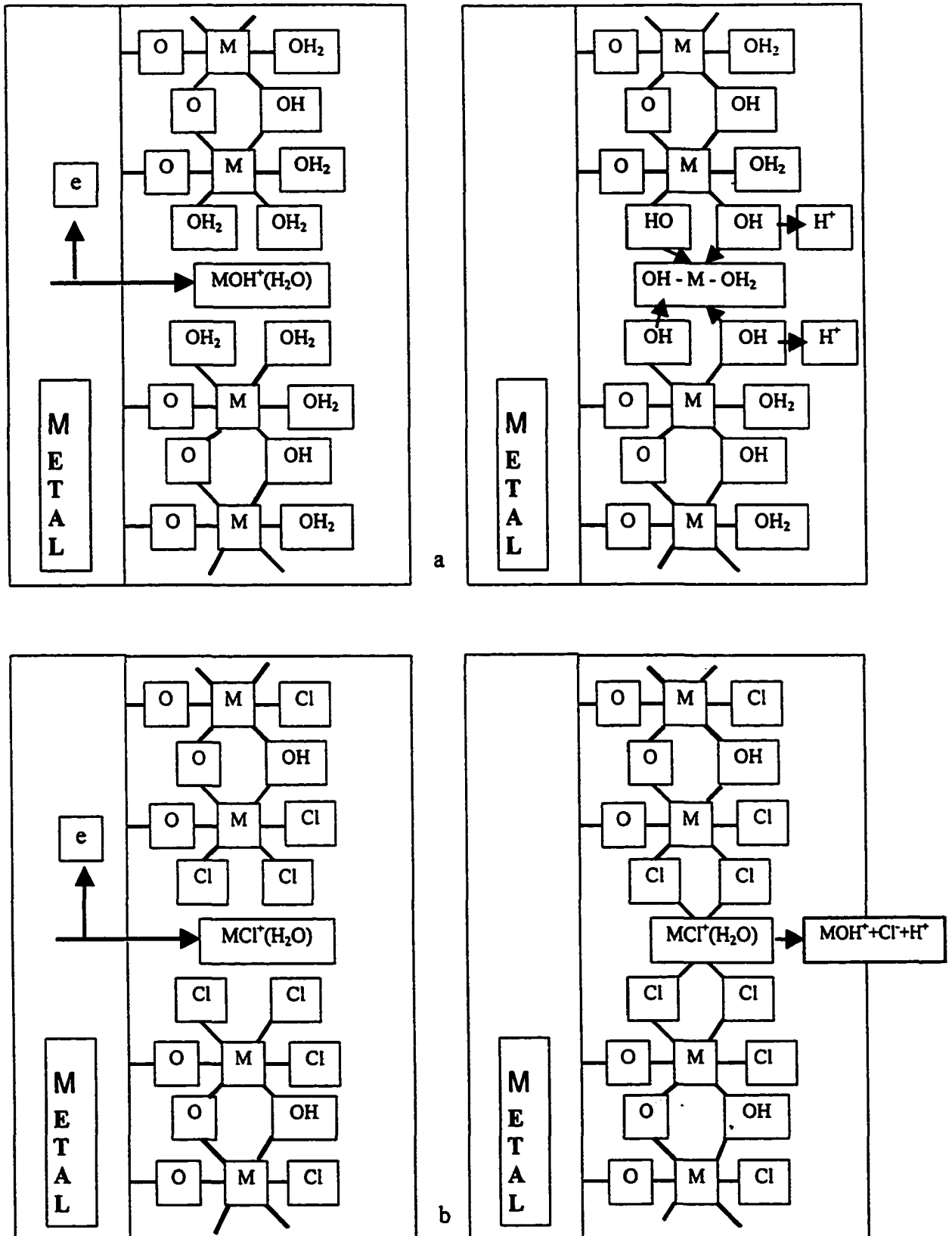
Fig. 2-1 Polymeric oxide model (a) Dissolution of metallic ions leading to film formation; (b) Chloride ions replace water molecules causing breakdown of the film.[141]

25

enriched in iron.[145,146] However, XPS measurements on passive ferritic stainless steel at the corrosion potential revealed a maximum chromium content in the outer layer.[147] There is also an indication that an increase of chromium in the alloy decreases the thickness of the film and is responsible for a certain amorphous character.[135]

In spite of the great confusion existing in the studies performed with stainless steel, the bipolar model[142,146] describing the passivation of stainless steel is worth further consideration. This model describes a passive film as a bipolar ionic rectifier constituted of a Cr-rich inner layer and a Fe-rich outer layer, which is shown in Fig. 2-2. The inner layer, resulting from the direct reaction of Cr with H_2O, is formed of Cr_2O_3 and $Cr(OH)_3$ and is anion selective. The outer layer, rich in iron, incorporates SO_4^{2-} ions, which makes it cation selective. Immediately below the iron layer, CrO_4^{2-} is present, resulting from the dehydration of $Cr(OH)_3$.

When an anodic potential is imposed, a de-protonation reaction takes place in the internal layer near the interface of the duplex film, resulting in the loss of protons to the solution through the external layer. Since the inner layer is anion selective, the exit of metal cations from the substrate is difficult. As a consequence, the O^{2-} ions originating from the deprotonation reaction accumulate at the interface, then migrate towards the metal surface, and form a dehydrated oxide.

2.9.1.3 Remarks on passivation

Investigations of the composition, structure and properties of the passive films have been carried out on various metals and alloys. However, a considerable amount of disagreement still exists concerning the results. This is due to several factors: different experimental conditions, surface preparations and limitations of the techniques.

At present there are many promising techniques used for the characterization of surfaces (SEM, XPS, AES, SIMS, Raman spectroscopy, EIS, ...). However, while techniques like AES and XPS are fairly good for analysis, their detection levels are much higher than that of SIMS, which can detect species in extremely low concentrations, but which in turn is an essentially qualitative technique.

Electrochemical techniques like EIS, Mott-Schottky plots and photoelectrochemical
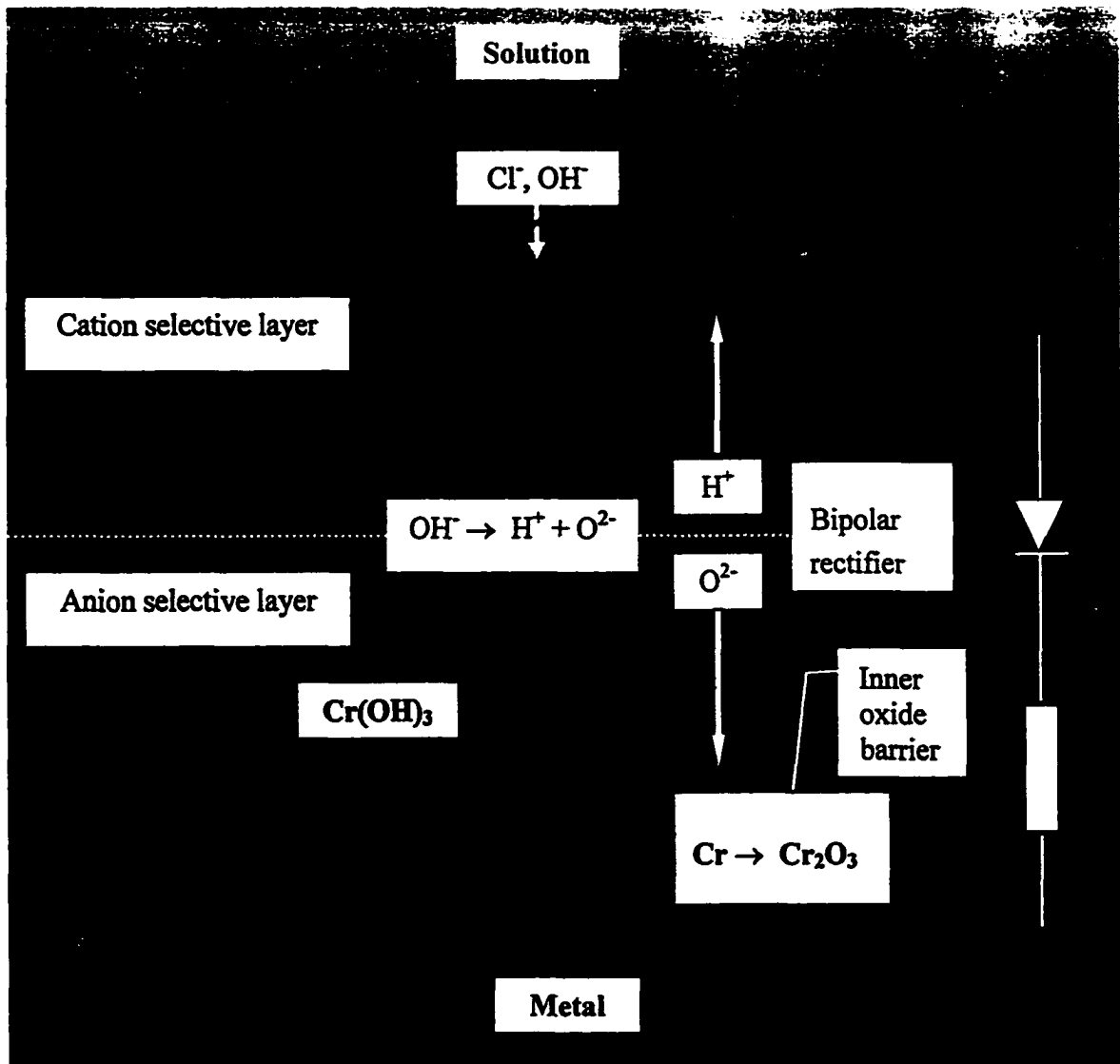
Fig. 2-2 The bipolar model describing the passivation of stainless steels.

measurements are "in-situ" techniques, which have become quite popular during the past decade for the study of the behavior of passive films and also for their characterization from the point of view of their semiconducting properties.

In spite of all efforts and developments achieved, many points still remain to be clarified, the questions being such as: Are passive films amorphous or crystalline? Are the semiconducting properties of the films related or not to their stability and if they are, in what way? What is the relation between composition and behavior?

27

2.9.2 Breakdown of passivation

The breakdown of the passive film in a situation of localized corrosion, such as pitting or crevice corrosion, is commonly accepted as being developed in two stages:

* initiation, in which local corrosion sites are formed on the surface, and

* propagation, in which those microscopic sites develop into larger or deeper corrosion sites, often leading to severe attack.

A third phenomenon, consisting of repassivation of already activated sites, can also occur under favorable conditions.

Although there is a general agreement concerning the mechanisms of the propagation stage, many doubts still remain on the processes leading to the nucleation of corrosion sites on the surface of the passive film. The most relevant theories concerning the initiation stage are presented as follows.

2.9.2.1 Anion penetration/migration model

Under the influence of the electric field existing across the film, the aggressive anion (in general Cl^-) will penetrate and reach the metal/film interface. The way by which the anion moves through the oxide can be either by diffusion through pre-existing micro-pores,[148] by ion exchange with the O^{2-} ions of the lattice[149] or by a process involving the formation of cation vacancies.[150]

Irrespective of the diffusion mechanisms, film breakdown occurs when the aggressive anion reaches the metal.

Another version of this model has been proposed by Okamoto,[141] in the light of the hydrated polymeric oxide model for the passive film. The water molecules adsorbed on the surface are substituted by chloride ions, which then migrate into the oxide, where they meet OH^-. Because chloride ions are stronger Lewis bases, they tend to substitute for the OH^- ions, with the formation of iron chlorocomplexes, which afterwards diffuse into the electrolyte.

28
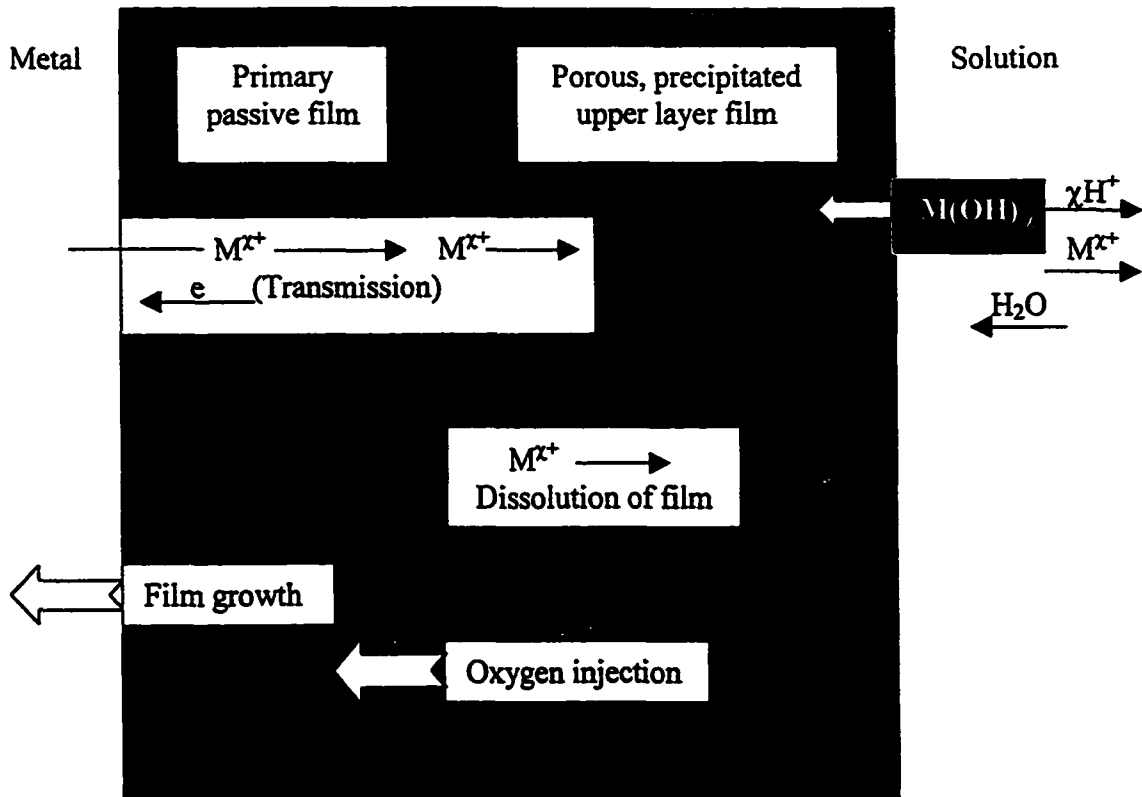
Fig. 2-3 Schematic of processes that lead to the formation of bilayer passive films on metal surfaces.

2.9.2.2 The chemico-mechanical model

According to Hoar,[151] aggressive anions are adsorbed on the oxide film, substituting for water molecules. The repulsive forces among adsorbed anions lower the interfacial tension, leading to the formation of cracks in the oxide.

Sato[152] has suggested that the mechanical stress can become critical as the result of an electrostrictive pressure (dielectric deformation resulting from the generation of opposite charges by the electric field).

2.9.2.3 Point defect model

Passive films generally form as bilayers, with a highly disordered "barrier" layer

29
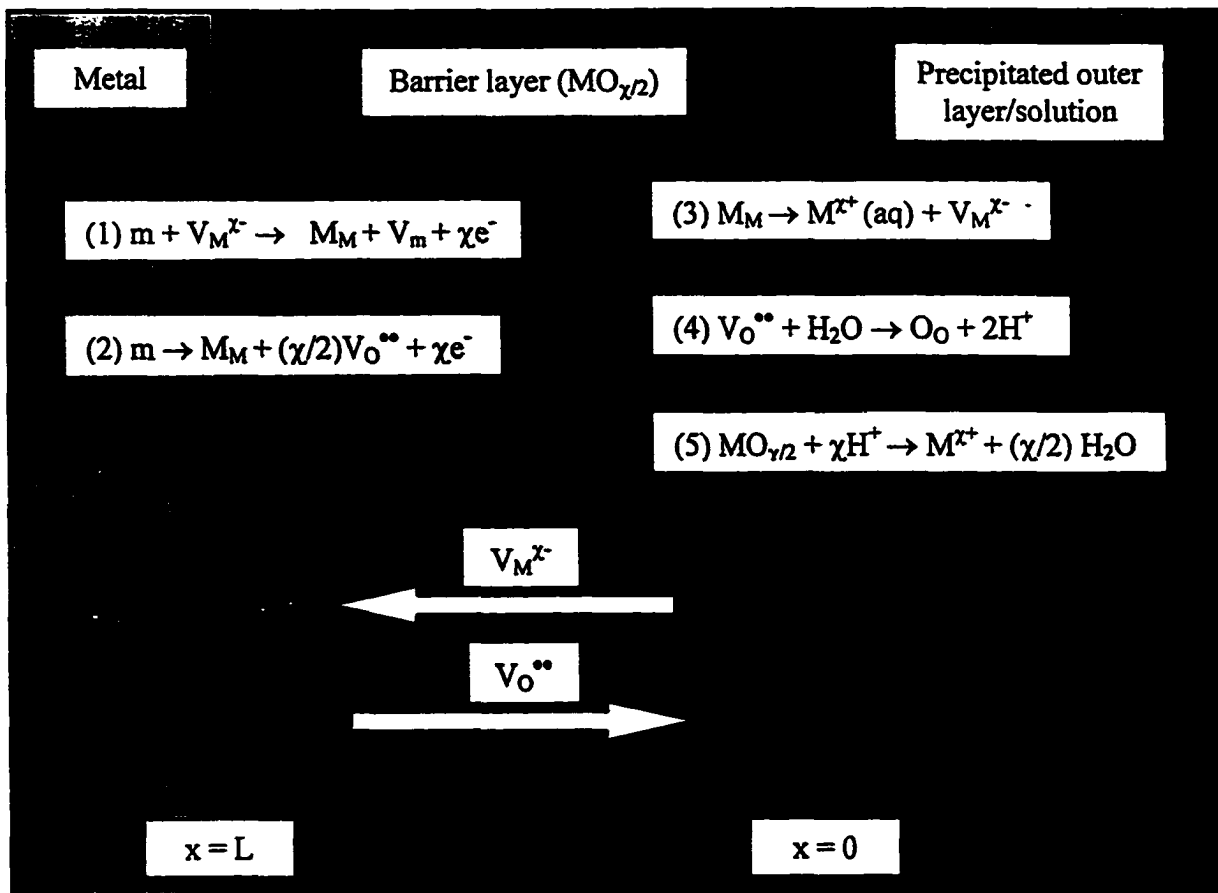
Fig. 2-4 Schematic of physicochemical processes occurring within a passive film according to the point defect model. During film growth, cation vacancies are produced at the film/solution interface, but are consumed at the metal/film interface. Likewise, anion vacancies are formed at the metal/film interface, but are consumed at the film/solution interface.

adjacent to the metal and an outer film comprised of a precipitated phase that may incorporate anions and/or cations from the solution (Fig. 2-3). Because passivity is sometimes observed in the absence of the outer film, e.g., in highly acidic or basic solutions where precipitation may not occur, the passivity is generally attributed to the barrier layer.

Assuming that the transmission of ions through the barrier layer occurs by vacancy motion, due to the preponderance of Schottky defects, the reactions that occur at the metal/film and film/solution interfaces are those depicted in Fig. 2-4. The reactions

30

shown are not assumed, but are the only possible elementary reactions for vacancy generation and annihilation. These reactions differ fundamentally in terms of whether they conserve the film boundary with respect to some fixed reference point in space. Reactions 1, 3 and 4 conserve the film, because they involve the movement of ions across the boundaries. Reaction 2 results in the generation of new film $[M_M + (\chi/2)V_O^{\bullet\bullet}]$ by a fluctuation in electron density around an atom in the metal at the metal/film interface. The metal atom (m) does not move substantially, but some movements of the ions within the film must occur to create the oxygen vacancy. Likewise, reaction 5 results in the destruction of the film by dissolution, which may or may not be an electrochemical process, and hence, is also non-conservative. Therefore, according to PDM, the principal entities involved in film growth are point defects, notably cation $(V_M^{\chi'})$ and anion $(V_O^{\bullet\bullet})$ vacancies, in a disordered barrier layer of nominal stoichiometry $MO_{\chi/2}$.
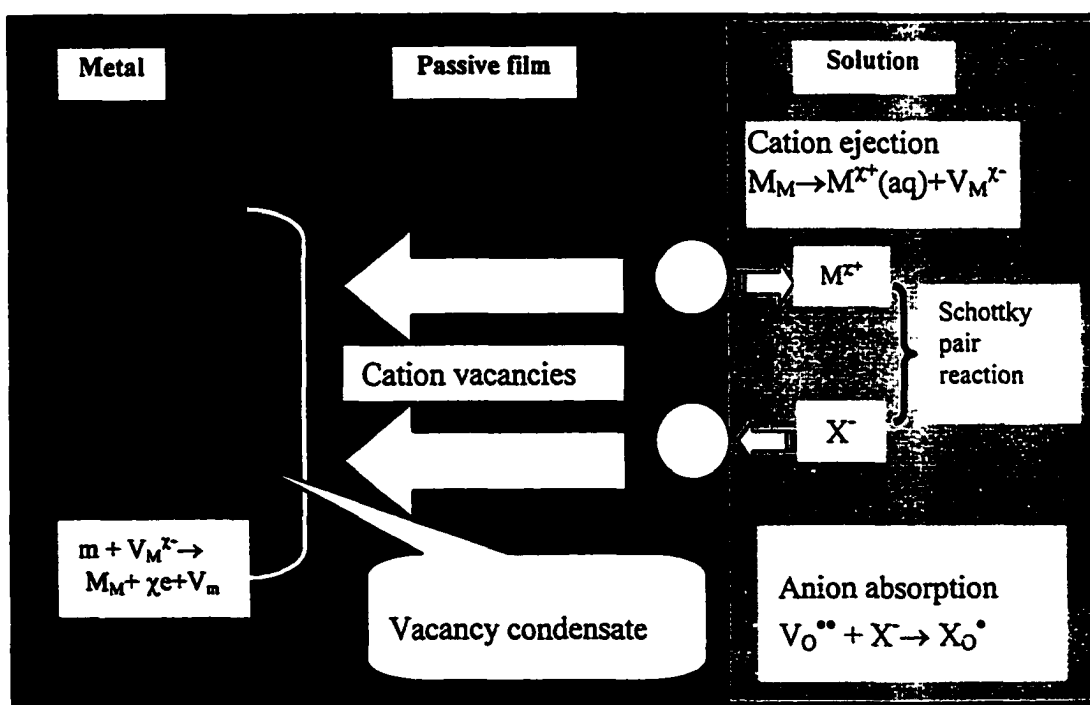
Fig. 2-5 The process leading to the breakdown of passive films according to PDM.

31

According to PDM, passive film breakdown and pitting initiation in an aggressive solution is due to the anion-catalyzed cation vacancy condensation at the film/metal interface.[153,154,155] Fig. 2-5 shows the process leading to the breakdown of the passive film based on PDM. The initial reaction that occurs at the film/solution interface is the absorption of an aggressive anion (Cl⁻) into a surface oxygen vacancy and then a Schottky-pair type reaction. Therefore, anion absorption causes the generation of cation vacancies at the film/solution interface, and hence, leads to the flux of cation vacancies across the passive film to the film/metal interface. If the cation vacancy flux is so high that the cation vacancies cannot be annihilated at the metal/film interface by reaction (1), a cation vacancy condensate will be formed, causing the thinning of the film or local detachment from the metal. Once the condensate has grown to a critical size, the film ruptures and a rapid local attack then occurs, either due to complete dissolution or the stress in the film induces a mechanical or structural instability.

A condensate of cation vacancies can grow if the diffusion flux of cations towards the solution exceeds that of vacancies towards the metal. When this condensate reaches a critical size, a local collapse of the film takes place. The role of aggressive ions consists of occupying anion vacancies in the outer layers of the film, generating a Schottky pair type of reaction and, therefore, increasing the cation vacancy concentration at the surface and the migration of the charged cation vacancies towards the metal/film interface.

2.9.2.4 Theory of chemical dissolution

Initially proposed by Hoar and Jacobs,[156] this theory illustrates that three or four halide ions are adsorbed on the film surface, around a cation of the lattice, preferably near an anion vacancy. The complex thus formed can immediately separate from the oxide, and in this way the dissolution of cations is accelerated when compared with the aquo-complexes. The thickness of the film is therefore reduced in that area, which will increase the electric field. Consequently, the migration of metal ions through the film is enhanced, as well as the local dissolution rate. In the limit, the film becomes locally destroyed and the underlying metal becomes exposed to the electrolyte.

32
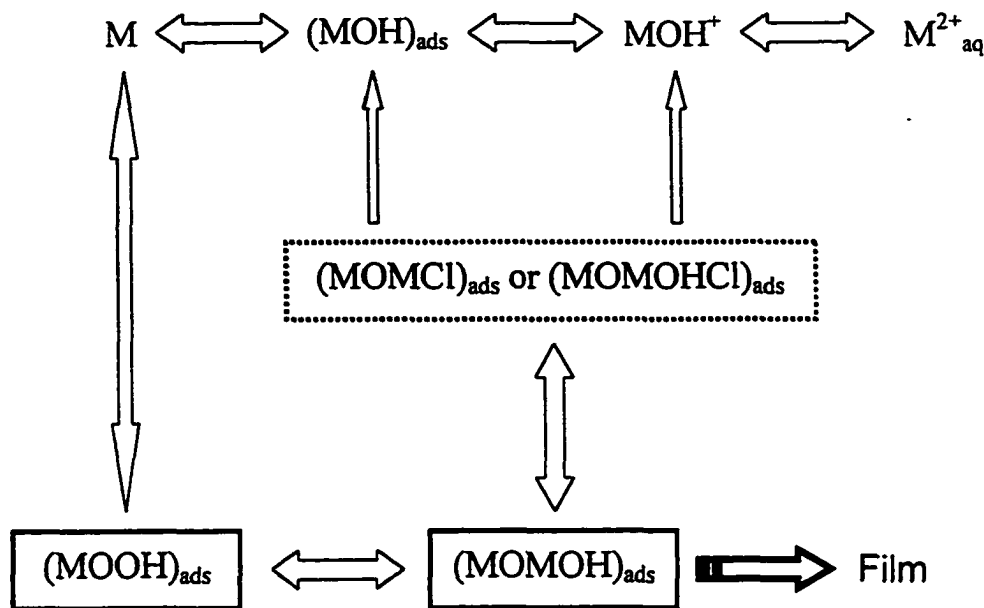
Fig. 2-6 Scheme for the dissolution/passivation of austenitic stainless steel. The species in solid blocks are passivating species, while those in the dotted blocks are non-passivating species.

2.9.2.5 Theory of depassivation-repassivation

The passive film is envisaged as a dynamic system in which a competition takes place between metal dissolution and film formation, i.e., between breakdown and repassivation.[157] Repassivation is hindered either by the presence of aggressive anions[158] or by anodic potential.[159]

Recently, based upon a number of reaction paths appearing in the literature, a scheme of competition among the processes of film formation, anodic dissolution, film breakdown and repassivation (Fig. 2-6) has been proposed.[160]

2.9.2.6 Theory of local acidification

Essentially developed by Galvele,[161] it assumes the existence of "micro-pits" on the

33

surface, even below the critical potential for pitting corrosion. Inside those micro-pits there is dissolution and hydrolysis of metal ions, with the formation of free protons. The corrosion products diffuse towards the electrolyte.

The local acidification theory has been the object of some criticism, because it does not explain effects such as the specific action of the aggressive anion or the increase of the induction time with film thickness.[135,162]

Initially built to explain the initiation of pitting corrosion, the theory seems to be more adapted to the propagation stage, since the acidification inside the pits seems to be decisive for its growth.

From the above exposition, it is seen that a good number of attempts have been made in order to explain both passivation and localized corrosion. However, a great deal of work is still needed before a final model can be created. As far as the models for passivation are concerned, considerable developments have been registered in the past few years, especially due to the development of electrochemical, surface observation and microanalysis techniques. Due to these techniques, it is at present known that passive films constitute a phase different both from the metallic matrix and the environment, which excludes the hypothesis of the simple oxygen adsorption being responsible for passivation. Of various models and theories describing the breakdown of the passive film and the initiation of pits, the point defect model should be borne special attention. The PDM exploits the term of passivity from an atomic scale and quantitatively describes the growth, breakdown and repassivation kinetics with the consideration of environmental conditions and affecting factors.

Electrochemical techniques have been of importance not only for fundamental studies in the laboratory but also for corrosion monitoring in industry. More and more instrumentation in the laboratory is becoming adapted to a wider use in field tests, and in the future great developments are to be expected in this area.

2.10   Summaries

The above review has outlined the major parameters and factors to be considered in

performing passivity and pitting studies and undertaking EN measurements and analysis. EN has been proven to be useful in fundamental research studies; for testing of materials, coatings, and inhibitors; for online corrosion monitoring both for process control and surveillance; and for the investigation of plant corrosion problems. An appreciation of the likely sources of noise and their measurement is essential to recognize the advantages and limitations of the technique.

Noise analysis of time recordings for research purposes is not necessarily a trivial task. It may require detailed analysis of individual transients to provide information on the fundamental processes that underlie the corrosion mechanisms. In cases where a series of transients are evaluated, a modeling exercise is often used. The modeled data, which describe the noise transients in fundamental terms, are then compared with experimental data to propose viable mechanisms.

In practical situations, the shapes of the random noise transients can be used to discriminate between uniform corrosion and various forms of localized corrosion. A simple statistical interpretation of the EN data can also provide information on uniform corrosion rates, and can be related to noise resistance and the degree of localized activity, such as pitting index.

The question of whether "electrochemical noise is the definitive corrosion technique" will only be fully answered in the long term as further scientific information becomes available. However, the literature presented demonstrates that EN measurements provide some of the most fundamental information on the basic stochastic processes involved in electrochemical corrosion reactions. EN information has also been used in practice and, particularly, adopted as a standard method for coatings and corrosion rate determination.

2.11   Shortcomings of the current knowledge and objectives of the present work

Although the EN technique has been used in pitting studies more than 30 years, there is still no complete and clear understanding in some fundamental aspects. In addition, previous research work mainly focused on various stainless steels, pure iron, aluminum and aluminum alloys. Few studies have been reported in which carbon steels are used as the test material. Therefore, some basic results about the EN during the pitting of carbon

35

steel are lacking. For example, there are no systematic studies about the potential dependence of the initiation, growth and repassivation processes of metastable pits on carbon steel. Similarly, the transition criterion of metastable pits developing towards stable pits on carbon steel is lacking. It cannot be certain under what conditions the metastable pitting events follow the cooperative distribution or Poisson behavior. The understandings about the physical significance of the noise spectrum and spectral parameters are vague. There are no systematic studies about the influences of the semiconducting properties of passive films on pitting behavior. No fundamental relationship between the electronic structure of a passive film and the pitting susceptibility is established at this stage. Even for the usual testing materials, there still exist quite different or even contradictory viewpoints in many aspects, such as the reasons responsible for the potential fluctuations and the role of chloride ions in pitting.

In this work, some fundamental research has been performed with the following objectives:

* Fundamental understanding about the metastable pitting processes on carbon steel, including initiation, growth, repassivation and the transition towards stabilization, and the features of electrochemical noise generated during pitting;

* Role of chloride ions in carbon steel pitting;

* Distribution law of metastable pitting events on carbon steel;

* The physical significance of the noise spectrum and spectral parameters;

* Application of noise resistance in carbon steel corrosion;

* The semiconducting properties of the passive film on carbon steel and the relationship between the electronic structure of the passive film and its pitting susceptibility.

References

1. H. Nyquist, *Phys. Rev.* 29, 614 (1927); 32, 110 (1928).
2. M.J. Stephen, *J. Phys. C.* 11, L965 (1978).
3. B. Fourcade and A.M.S. Tremblay, *Phys. Rev.* B.34, 7802 (1986).

4. G. Giraud, J.P. Clerc, B. Orsal and J.M. Laugier, *Europhys. Lett.* **3**, 935 (1987).

5. C. Gabrielli, M. Ksouri and R. Wiart, *J. Electroanal. Chem.* **86**, 233 (1978).

6. G. Blanc, C. Gabrielli, M. Ksouri and R. Wiart, *Electrochim. Acta* **23**, 337 (1978).

7. W. Schottky, *Ann. Phys.* **4F, 57**, 541 (1918).

8. E. Budewski, W. Bostanov, T. Vitanov, Z. Stoinov and A. Kotzeva, *Electrochim. Acta* **11**, 1697 (1966).

9. U. Bertocci and F. Huet, *Corrosion* **51**, 131 (1995).

10. W.H. Press, *Comm. Astrophys.* **7**, 103 (1978).

11. P. Dutta and P.M. Horn, *Rev. Modern Phys.* **53**, 497 (1981).

12. T. Hagyard and J.R. Williams, *Transactions of the Faraday Society* **57**, 2288 (1961).

13. U. Bertocci, J.L. Mullen and Y.X. Ye, in *Proceedings of the 5th International Symposium on Passivity and Metallic Semiconductors*, M. Froment, Editor, p. 244, Elsevier, New York (1986).

14. K. Nachstedt and K.E. Heusler, *Electrochim. Acta* **33**, 311 (1988).

15. S.P. Mattin and G.T. Burstein, in *Proceedings of the 10th European Corrosion Congress*, Vol. 2, p. 1109, London (1993).

16. G.C. Barker, *J. Electroanal. Chem.* **21**, 127 (1969).

17. U. Bertocci and J. Krugger, *Surf. Sci.* **101**, 608 (1980).

18. D.A. Eden, A.N. Rothwell and J.L. Dawson, in *Corrosion'91*, paper no. 444, NACE, Houston (1991).

19. R.A. Cottis and C.A. Loto, *Materials Science Forum* **8**, 201 (1986).

20. C.A. Loto and R.A. Cottis, *Corrosion* **45**, 136 (1989).

21. J. Stewart, P.M. Scott, D.E. Williams and D.B. Wells, *Corros. Sci.* **33**, 73 (1992).

22. D.B. Wells, J. Stewart, R. Davidson, P.M. Scott and D.E. Williams, *Corros. Sci.* **33**, 13 (1992).

23. K. Hladky and J.L. Dawson, *Corros. Sci.* **21**, 317 (1981).

24. A.M.P. Simoes and M.G.S. Ferreira, *Br. Corros. J.* **27**, 21 (1987).

25. A.M.P. Simoes and M.G.S. Ferreira, in *Proceedings of the 10th International Congress on Metal Corrosion*, Vol. IV, Key Engineering Material, Vols. 20-28, p. 3125 (1988).

26. D.A. Eden, M. Hoffman and B.S. Skerry, in *Polymeric Materials for Corrosion Control, ACS Symposium Series 322*, R.A. Dicke and F.L. Floyd, Editors, American Chemical Society (1986).

27. C.T. Chen and B.S. Skerry, *Corrosion* **47**, 598 (1991).

37

28. K. Tachibana and G. Okamoto, *Reviews on Coatings and Corrosion* 3, 229 (1981).

29. J.L. Dawson and M.G.S. Ferreira, *Corros. Sci.* 26, 1009 (1986).

30. P.D.W. Bottomley. J.S. Gill and J.L. Dawson, *Materials Science Forum* 8, 509 (1986).

31. G. Gao, F.H. Stott, J.L. Dawson and D.M. Farrell, *Oxidized Metal* 33, 79 (1990).

32. W.P. Iverson and L.F. Heverly, in *Corrosion Monitoring in Industrial Plants Using Nondestructive Testing and Electrochemical Methods*, ASTM STP 908, p. 459, ASTM, West Conshohocken, PA (1986).

33. S.C. Dexter, D.J. Duquette, O.W. Siebert and H.A. Videla, *Corrosion* 47, 303 (1991).

34. S. Webster, L. Nathanson, A.G. Green and B.V. Johnson, in *Proceedings of the 12th International Corrosion Congress*, NACE, Houston (1993).

35. I. Al-Zanki, J.S. Gill and J.L. Dawson, *Materials Science Forum* 8, 463 (1986).

36. J.L. Dawson, in *Electrochemical Noise Measurement for Corrosion Applications*, J.R. Kearns, J.R. Scully, P.R. Roberge, D.L. Reichert and J.L. Dawson, Editors, p. 3, ASTM STP 1277, West Conshohocken, PA (1996).

37. D.E. Williams, C. Westcott and M. Fleischmann, *J. Electrochem. Soc.* 132, 1796 (1985).

38. D.E. Williams, C. Westcott and M. Fleischmann, *J. Electroanal. Chem.* 180, 549 (1984).

39. D.E. Williams, C. Westcott and M. Fleischmann, *J. Electrochem. Soc.* 132, 2804 (1985).

40. C. Gabrielli, F. Huet and M. Keddam, *J. Appl. Electrochemistry* 15, 503 (1985).

41. I. Epelboin, C. Gabrielli, M. Keddam and L. Raillon, *J. Electroanal. Chem.* 93, 155 (1978).

42. K. Hladky and J.L. Dawson, *Corros. Sci.* 22, 231 (1982).

43. D.E. Williams, in *Electrochemical Corrosion Testing*, Vol. 101, p. 253, Dechema, Monograph (1986).

44. D.E. Eden, K. Hladky, D.G. John and J.L. Dawson, in *Corrosion '86*, paper no. 274, NACE, Houston (1986).

45. F. Mansfeld and H. Xiao, *J. Electrochem. Soc.* 140, 2205 (1993).

46. I. Epelboin, C. Grabrielli, M. Keddam and R. Wiart, *J. Electroanal. Chem.* 105, 389 (1979).

47. G. Blanc, C. Gabrielli and M. Keddam, *Electrochim. Acta* 23, 687 (1975).

48. M. Keddam, M. Krarti and C. Pallotta, *Corrosion* 43, 454 (1987).

49. C. Gabrielli and M. Keddam, *Corrosion* 48, 794 (1992).

50. G.C. Baker, *J. Electroanal. Chem.* 21, 127 (1969).

51. J.L. Dawson, in *Proceedings of the International Conference on Corrosion of Reinforcement in Concrete Construction*, p. 175, Ellis Horwood, London (1983).

52. W.M. Cox, D. Gearey and J.L. Dawson, in *Proceedings of the Kuwait Corrosion*

Conference, p. 83, Pergamon Press, Oxford (1987).

53. R.G. Harden, P. Lambert and C.L. Page, *Br. Corros. J.* **23**, 225 (1988).

54. F. Carassiti, R. Cigna, G.K. Gusmano and R. Goolamallee, *Materials Science Forum* **44-45**, 271 (1989).

55. D.A. Eden and A.N. Rothwell, in *Corrosion '92*, paper no. 292, NACE, Houston (1992).

56. A. Legat and V. Dolecek, *Corrosion* **51**, 295 (1995).

57. C. Gabrielli, F. Huet, M. Keddam and R. Oltra, *Corrosion* **46**, 266 (1990).

58. C. Gabrielli, F. Huet and M. Keddam, in *Electrochemical and Optical Techniques for the Study and Monitoring of Metallic Corrosion*, M.G.S. Ferreira and C.A. Melendres, Editors, p. 135, Kluwer Academic Publishers, Netherlands (1991).

59. C. Gabrielli, F. Huet, M. Keddam, R. Oltra and C. Pallotta, in *Passivity of Metals and Semiconductor*, M. Froment, Editor, p. 293, Elsevier, Amsterdam, Netherlands (1983).

60. U. Bertocci and Y.X. Ye, *J. Electrochem. Soc.* **131**, 1011 (1984).

61. D.E. Williams, M. Fleischmann, J. Stewart and T. Brooks, *Materials Science Forum* **8**, 151 (1986).

62. P.C. Pistorius and G.T. Burstein, *Phil. Trans. Royal Soc. Lond.* **A341**, 531 (1992).

63. L. Stockert and H. Bohni, in *Proc. 8th Europern Corrosion Congress*, Vol. 2, p. 22, Paris, France (1985).

64. S.T. Pride, J.R. Scully and J.L. Hudson, *J. Electrochem. Soc.* **141**, 3028 (1994).

65. R. Holliger and H. Bohni, in *Computer Aided Acquisition and Analysis of Corrosion Data*, M.W. Kendig, U. Bertocci and J.E. Strutt, Editors, Vol. 85-3, p. 200, The Electrochemical Society, Pennington, NJ (1985).

66. R. Oltra, C. Gabrielli, F. Huet and M. Keddam, *Electrochimica Acta* **31**, 1501 (1986).

67. C. Gabrielli, F. Huet, M. Keddam, R. Oltra and J.C. Colson, *Materials Science Forum* **8**, 491 (1986).

68. J. Pattinson and G.T. Burstein, in *Computer Aided Acquisition and Analysis of Corrosion Data*, M.W. Kendig, U. Bertocci and J.E. Strutt, Editors, Vol. 85-3, p. 108, The Electrochemical Society, Pennington, NJ (1985).

69. K. Sieradski and R.C. Newman, *Philosophical Mag.* **A51**, 95 (1985).

70. J.L. Dawson, D.M. Farrell, P.J. Aylott and K. Hladky, in *Corrosion '89*, paper no. 31, NACE, Houston (1989).

71. P.C. Pistorius, *Corrosion* **53**, 273 (1997).

72. R.G. Kelly, M.E. Inman and J.L. Hudson, in *Electrochemical Noise Measurement for*

Corrosion Applications, J.R. Kearns, J.R. Scully, P.R. Roberge, D.L. Reichert and J.L. Dawson, Editors, p. 101, ASTM STP 1277, West Conshohocken, PA (1996).

73. D.A. Eden, D.G. John and J.L. Dawson, Interational Patent WO 87/07022, World Intellectual Property Organization (1987).

74. A.N. Rothwell and D.A. Eden, in *Corrosion '92*, Paper no. 223, NACE, Houston (1992).

75. F. Mansfeld and H. Xiao, in *Electrochemical Noise Measurement for Corrosion Applications*, J.R. Kearns, J.R. Scully, P.R. Roberge, D.L. Reichert and J.L. Dawson, Editors, p. 59, ASTM STP 1277, West Conshohocken, PA (1996).

76. M. Stern and A.L. Geary, *J. Electrochem. Soc.* **104**, 56 (1957).

77. D.L. Reichert, in *Electrochemical Noise Measurement for Corrosion Applications*, J.R. Kearns, J.R. Scully, P.R. Roberge, D.L. Reichert and J.L. Dawson, Editors, p. 79, ASTM STP 1277, West Conshohocken, PA (1996).

78. R. A. Cottis and S. Turgoose, *Materials Science Forum* **192-4**, 663 (1995).

79. W.H. Press, B.P. Flannery, S.A. Teukolsky and W.T. Vetterling, in *Numerical Recipes in Pascal*, p. 217, Cambridge University Press, Cambridge, UK (1989).

80. J.W. Cooly and J.W. Tukey, *Mathematics of Computation* **19**, 297 (1965).

81. J.P. Burg, Maximum Entropy Spectral Analysis, in *Proceedings of the 37th International Meeting of the Society of Exploration Geophysicists*, Oklahoma City, Oct. 1967.

82. S. Haykin, in *Adaptive Filter Theory*, 2nd edition, p. 798, Prentice Hall, Englewood Cliffs, NJ (1991).

83. L. Beaunier, J. Frydman, C. Gabrielli, F. Huet and M. Keddam, in *Electrochemical Noise Measurement for Corrosion Applications*, J.R. Kearns, J.R. Scully, P.R. Roberge, D.L. Reichert and J.L. Dawson, Editors, p. 114, ASTM STP 1277, West Conshohocken, PA (1996).

84. P.C. Searson and J.L. Dawson, *J. Electrochem. Soc.* **135**, 1908 (1988).

85. M. Hashimoto, S. Miyajima and T. Murata, *Corros. Sci.* **33**, 885 (1992).

86. P.R. Roberge, *Corrosion* **50**, 502 (1994).

87. P.R. Roberge, D. Lenard, J.G. Moores and E. Halliop, *Corros. Sci.* **35**, 213 (1993).

88. A.A. Tsonis, in *Chaos—From Theory to Applications*, Plenum, New York (1992).

89. S.M. Sharland, C.M. Bishop, P.H. Balkwill and J. Stewart, in *Advances in Localized Corrosion*, H.S. Isaacs, U. Bertocci, J. Kruger and S. Smialovska, Editors, p. 109, NACE, Orlando (1987).

90. S. Corcoran and K. Sieradzki, *J. Electrochem. Soc.* **139**, 1568 (1992).

91. B. Mandelbrot and J.W. van Ness. *SIAM Review* **10**, 422 (1968).

92. P.R. Roberge, *J. Appl. Electrochemistry* **23**, 1223 (1993).

93. A. Legat and E. Govekar, *Fractals* **2**, 241 (1994).

94. V.A. Tyagai, *Elektrokhimiya* **3**, 1331 (1967).

95. V.A. Tyagai, *Elektrokhimiya* **10**, 1 (1974).

96. V.A. Tyagai, *Electrochimica Acta* **16**, 1674 (1971).

97. G.C. Baker, *J. Electroanal. Chem.* **39**, 484 (1972).

98. G.C. Baker, *J. Electroanal. Chem.* **82**, 145 (1977).

99. M. Fleischmann and J.W. Oldham, *J. Electroanal. Chem.* **27**, 207 (1970).

100. M. Seralathan and S.K. Rangarajan, *J. Electroanal. Chem.* **208**, 13 (1986).

101. M. Seralathan and S.K. Rangarajan, *J. Electroanal. Chem.* **208**, 29 (1986).

102. W.P. Iverson, J. *Electrochem. Soc.* **115**, 617 (1968).

103. M. Fleischmann, M. Labram, C. Gabrielli and A. Sattar, *Surf. Sci.* **101**, 583 (1980).

104. S. Webster, L. Nathanson, A.G. Green and B.V. Johnson, in *Proceedings of the 12th International Corrosion Congress*, NACE, Houston (1993).

105. G.T. Burstein, P.C. Pistorius and S.P. Mattin, *Corros. Sci.* **35**, 57 (1993).

106. G.S. Frenkel, L. Stockert, F. Hunkeler and H. Bohni, *Corrosion* **43**, 429 (1987).

107. P.C. Pistorius and G.T. Burstein, *Materials Science Forum* **111-112**, 429 (1992).

108. K. Hladky, D.G. John, S.E. Worthington and D. Herbert, in *UK Corrosion/85*, p. 295, London (1985).

109. M.G.S. Ferreira and A.M.P. Simoes, *Materials Science Forum* **8**, 373 (1986).

110. W. Li, K. Nobe and J. Pearlstein, *Corros. Sci.* **31**, 615 (1990).

111. C.A. Loto and R.A. Cottis, *Bulletin of the Electrochemical Society* **4**, 1001 (1988).

112. H. Xiao and F. Mansfeld, *J. Electrochem. Soc.* **141**, 2332 (1994).

113. M. Moon and B.S. Skerry, *Polymer Preprints* **35**, 303 (1994).

114. C.T. Chen and B.S. Skerry, *Corrosion* **47**, 598 (1991).

115. D.A. Eden, M. Hoffman and B.S. Skerry, *Polymer Material Science and Engineering* **53**, 388 (1985).

116. B.S. Skerry, *Progress in Organic Coatings* **15**, 269 (1987).

117. J.L. Dawson, A.N. Rothwell, T.G. Walsh, K. Lawson and J.W. Palmer, in *Corrosion'93*, NACE, Houston (1993).

118. P.R. Roberge, V.S. Sastri and W. Revie, in *Proceedings of the 7th European Symposium on Corrosion Inhibitors*, Vol. 1, p. 1003, Ferrara, Italy (1990).

41

119. C. Monticelli, G. Brunoro, A. Frignani and G. Trabanelli, *J. Electrochem. Soc.* 139, 706 (1992).

120. Y.J. Tan, S. Bailey and B. Kinsella, *Corros. Sci.* 38, 1681 (1996).

121. C. Monticelli, G. Brunoro, A. Frignanai and G. Trabanelli, *J. Electrochem. Soc.* 139, 693 (1992).

122. J.L. Dawson, D.G. John, M.I. Jafar, K. Hladky and L. Sherwood, in *Corrosion of Reinforcement in Concrete*, p. 358, Elsevier Applied Science, London (1990).

123. A.M. Brennenstuhl and T.S. Gendron, in *Microbiologically Influenced Corrosion Testing*, ASTM STP 1232, West Conshohocken, PA (1994).

124. J.L. Dawson, D. Gearey and W.M. Cox, in *UK Corrosion/82*, p. 99, London (1982).

125. D.M. Farrell, W.M. Cox, B.A. Wrobel and B.C. Syrett, in *Proceedings of the Symposium on Corrosion in Power Utilities*, NACE, Houston (1987).

126. D.M. Farrell, W.M. Cox, B.C. Syrett and R.J. Keeth, in *Proceedings of the 1ˢᵗ Combined Flue Gas Desulfurization and Dry SO₂ Control Symposium*, EPRI GS-6307 (1989).

127. D.H. Roarty, W.T. Bogard, W.M. Cox, D.C.A. Moore and G.P. Quirk, in *Corrosion'93*, paper no. 392, NACE, Houston (1993).

128. M.A. Winters, P.S.N. Stokes, P.O. Zuniga and D.J. Schlottenmeier, in *Corrosion'93*, paper no. 393, NACE, Houston (1993).

129. H.J. Debruyn, K. Lawson and E.E. Heaver, in *Electrochemical Noise Measurement for Corrosion Applications*, J.R. Kearns, J.R. Scully, P.R. Roberge, D.L. Reichert and J.L. Dawson, Editors, p. 214, ASTM STP 1277, West Conshohocken, PA (1996).

130. J.L. Dawson, in *Proceedings of the International Conference on Corrosion of Reinforcement in Concrete Construction*, p. 175, Ellis Horwood, London (1983).

131. J.I. Mickalonis, R.J. Jacko, G.P. Quicrk and D.A. Eden, in *Electrochemical Noise Measurement for Corrosion Applications*, J.R. Kearns, J.R. Scully, P.R. Roberge, D.L. Reichert and J.L. Dawson, Editors, p. 201, ASTM STP 1277, West Conshohocken, PA (1996).

132. G. Bianchi, A. Cerquetti, F. Mazza and S. Torchio, *Localized Corrosion* 3, 399 (1974).

133. D.D. Macdonald, *J. Electrochem. Soc.* 139, 3434 (1992).

134. M. Faraday, "Experimental Research in Electricity", Vol. II, University of London (1844).

135. Z. Szklarska-Smialowska, in *Pitting Corrosion of Metals*, p. 7, NACE, Houston (1986).

136. S.C. Tjong and E. Yeager, *J. Electrochem. Soc.* 128, 2251 (1981).

137. M.C. Bloom and L. Goldenberg, *Corros. Sci.* 5, 623 (1965).

42

138. C. Foley, J. Kruger and C. Bechtoldt, *J. Electrochem. Soc.* **114**, 994 (1967).

139. C. Wagner, *Ber. Phys. Chem.* **77**, 1090 (1973).

140. M. Nagayama and M. Cohen, *J. Electrochem. Soc.* **109**, 781 (1962).

141. G. Okamoto, *Corros. Sci.* **13**, 471 (1973).

142. M. Sakashita and N. Sato, in *Passivation of Metals*, R.P. Frankental and J. Kruger, Editors, p. 479, The Electrochemical Society, Corrosion Monograph Series, Princeton (1978).

143. M. Sakashita and N. Sata, *Corrosion* **35**, 351 (1979).

144. M.G.S. Ferreira and A.M.P. Simoes, in *Electrochemical and Optical Techniques for the Study and Monitoring of Metallic Corrosion*, M.G.S. Ferreira and C.A. Melendres, Editors, p. 485, Kluwer Academic Publishers, Netherlands (1991).

145. V. Mitrovic-Scepanovic, B. MacDougalls and M.J. Graham, *Corros. Sci.* **24**, 479 (1984).

146. A.R. Brooks, C.R. Clayton, K. Doss and Y.C. Lu, *J. Electrochem. Soc.* **133**, 2459 (1986).

147. C. Hultquist, C. Leygraf and D. Brune, *J. Electrochem. Soc.* **131**, 1773 (1984).

148. R. Nishimura and K. Kudo, In *Proc. 8th ICMC*, 1, p. 6, Mainz (1981).

149. I.L. Rozenfeld and I.K. Marshakov, *Corrosion* **20**, 115 (1964).

150. M.A. Heine, D.S. Keir and M.S. Pryor, *J. Electrochem. Soc.* **112**, 24 (1965).

151. T.P. Hoar, *Corros. Sci.* **7**, 335 (1967).

152. N. Sato, *Electrochim. Acta* **16**, 1683 (1971).

153. A. Goossens, M. Vazquez and D.D. Macdonald, *Electrochimica Acta* **41**, 35 (1996).

154. E. Sikora, J. Sikora and D.D. Macdonald, *Electrochimica Acta* **41**, 783 (1996).

155. C.B. Breslin, D.D. Macdonald, J. Sikora and E. Sikora, *Electrochimica Acta* **42**, 127 (1997).

156. T.P. Hoar and W.R. Jacob, *Nature* **216**, 1209 (1967).

157. J.A. Richardson and G.C. Wood, *Corros. Sci.* **10**, 313 (1970).

158. B. Macdonald, *J. Electrochem. Soc.* **126**, 919 (1979).

159. M. Barbosa and J.C. Scully, *Corros. Sci.* **22**, 1025 (1982).

160. J.L. Dawson and M.G.S. Ferreira, *Corros. Sci.* **26**, 1009 (1986).

161. J.R. Galvele, *J. Electrochem. Soc.* **123**, 464 (1986).

162. M. Janik-Czachor, *Werkstoffe Korros.* **30**, 255 (1979).

Chapter 3 Experimental Procedure

3.1 Electrodes and solutions

Electrodes were made of a sheet of A516-70 carbon steel (ASTM), an extensively used pressure vessel plate in the sweet oil and gas fields, with the chemical composition (%, wt): C 0.31, Mn 1.0, P 0.035, S 0.04 and Si 0.25. Each sample was cut to 6 mm × 7 mm × 5 mm and ground to 600 grit on all faces. The unexposed edges were coated with a masking paint (alkyd enamel, ANDARR) to prevent crevice corrosion between the epoxy mount and the electrode. The specimens were embedded in Epofix resin manufactured by LECO resulting in an exposed steel area of 0.4 cm^2. The working surface of the specimen was ground to 600$^\#$ emery paper and then 1000$^\#$ SiC paper. The sample was cleaned with distilled water and methanol.

All the solutions were made from analytical grade reagents and distilled water. In order to pre-passivate the carbon steel electrode, 0.5 M sodium bicarbonate ($NaHCO_3$) was always used as the base solution. The reason for using bicarbonate solutions is that the water phase in sweet oil wells has properties nearly identical to distilled water with dissolved carbon dioxide (CO_2) and thus contains bicarbonate in various concentrations.[1] Although much research has been carried out to elucidate the corrosion and stress corrosion cracking behavior of pipeline steel in bicarbonate solutions, less work has focused on corrosion problems of carbon steel in bicarbonate solutions in the presence of Cl$^-$.[2,3] The investigation of electrochemical behavior of A516-70 carbon steel in bicarbonate solutions can further improve the understanding of sweet corrosion of carbon steel pipeline.

In order to initiate the pits on passivated carbon steel specimens, sodium chloride (NaCl) was added to the base solution according to the pre-designed volume. Prior to various electrochemical measurements, the solution was stirred immediately upon the

44

addition of NaCl to keep the solution mix uniformly. The stirring process was completed within 5 seconds.

All tests were carried out at ambient temperature and the solutions were open to air. This design is aimed at simulating the practical situation.

3.2 Measurements of electrochemical noise

3.2.1 Electrodes in a freely corroding condition

During the measurements of current and potential noise, a pair of nominally identical A516-70 carbon steel electrodes was used as working electrodes (WE). A Ag/AgCl electrode was employed as a reference electrode (RE). The measurement circuit is shown in Fig. 3-1. The noise data, i.e., the galvanic current flowing between two WEs and the potential difference between the coupled WEs and the RE, were recorded using an ACM AutoZRA measurement system with various sampling rates.
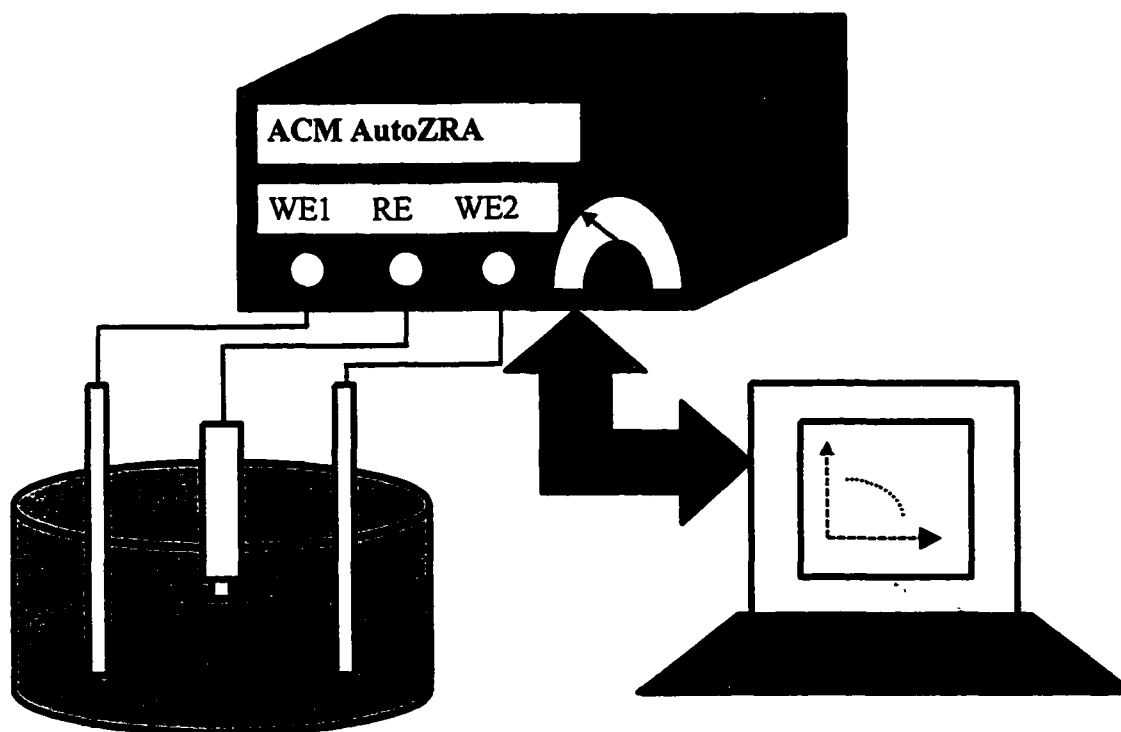
Fig. 3-1 The schematic setup of potential and current noise measurements under free corrosion conditions.

3.2.2 Electrodes under potentiostatic control

The A516-70 carbon steel WE was immersed vertically in a conventional three-electrode electrochemical cell. A Ag/AgCl RE was connected to the cell through a Luggin capillary. A platinum plate was used as the counter electrode (CE). The experimental setup is schematically shown in Fig. 3-2. The potential of the WE, which was relative to Ag/AgCl electrode, was controlled by a Gamry CMS 100/105 corrosion measurement system. Prior to the measurements of current signals, the specimen was immersed in the solution for two hours and then potentiostatically controlled at the required potential values, while the anodic current was recorded simultaneously at a specific sampling rate.
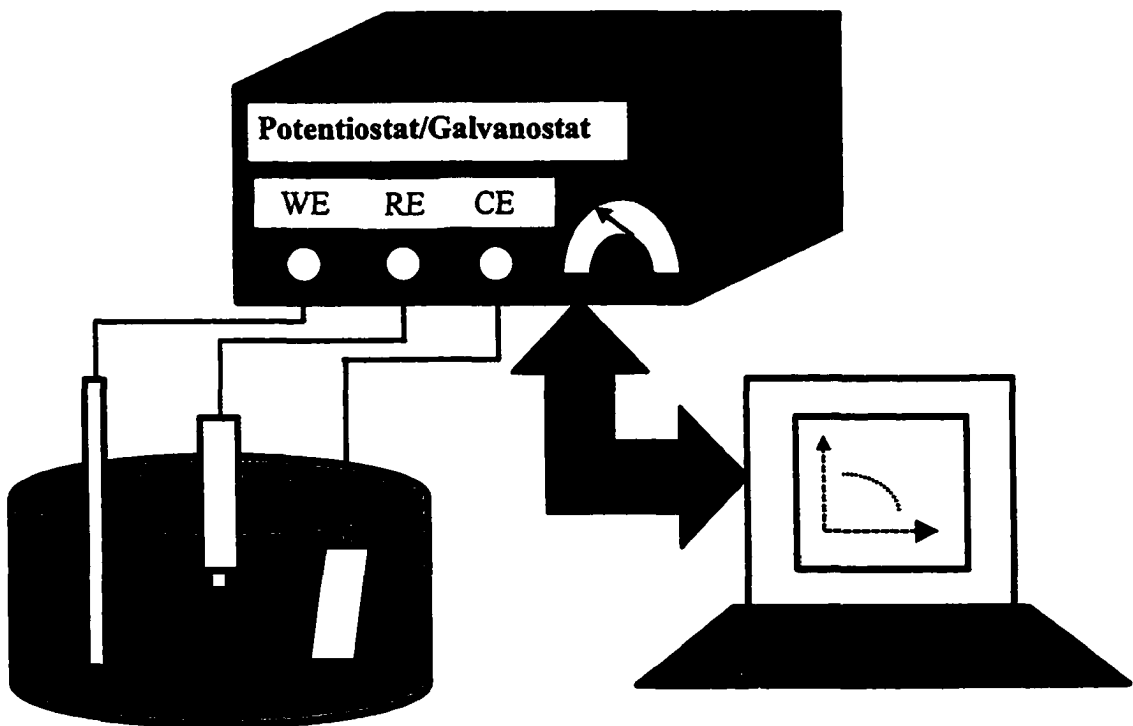
Fig. 3-2 The schematic setup of potential and current noise measurements under potentiostatic or galvanostatic control.

3.3 Other electrochemical measurements

A conventional three-electrode cell was employed in this work for other electrochemical measurements, as shown in Fig. 3-2.

3.3.1 Polarization curves

After 2 hours of immersion in the solution, the electrode was believed to reach a steady state, indicated by a stable value of corrosion potential. The potentiodynamic polarization curves were then measured by sweeping the potential positively from −50 mV relative to the corrosion potential at a rate of 0.2 mV/s.

There is a certain influence of the potential scan rate on the polarization behavior of the electrode. In the case of a large scan rate, some information related to the electrode process may be missed because some steps cannot change fast enough to reach a steady state. If the potential scan rate is too slow, it will take much longer time to measure a polarization curve. An optimum scan rate is always determined based on the preliminary tests. A potential scan rate of 0.2 mV/s was appropriate for the given system and used in the measurements of polarization curve.

3.3.2 Electrochemical impedance spectroscopy (EIS)

EIS measurements were performed on the specimen after 2 hours of immersion in the solutions. A Gamry 100/300 system was used. The impedance data were obtained within the frequencies ranging from 5,000 Hz to 0.005 Hz, and with perturbation potential signal amplitude of 10 mV (peak-to-peak).

3.3.3 Capacitance measurements

The specimens were pre-passivated at various film formation potentials for 2 hours in a 0.5 M $NaHCO_3$ solution. The capacitance of the electrode was then determined with the Gamry 100/300 corrosion system by performing a potential scan in the anodic direction. Macdonald[4] thinks that the passive film thickness cannot remain constant when the

47

potential is positively increased and, therefore, a potential sweep in the negative direction is recommended so as to "freeze" the vacancy structure and hence allow the system to conform more closely to the conditions assumed in the derivation of the Mott-Schottky equation. In the present work, it is approximately assumed that the thickness of the passive film does not change very much during the potential sweep in the anodic direction considering a pre-reached stable passive state and a fast potential scan rate of 50 mV/s. During the recording of the capacitance-potential profiles, the excitation potential was 10 mV (peak-to-peak), and the measurement frequency was 1000 Hz unless specified otherwise.

Reference

1.   K. Videm and A.M. Koren, *Corrosion* **49**, 746 (1993).
2.   R.N. Parkins and P.M. Singh, *Corrosion* **46**, 485 (1990).
3.   R.W. Revie and R.R. Ramsingh, *Can. Metall. Q.* **22**, 235 (1983).
4.   A.Goossens, M. Vazquez and D.D. Macdonald, *Electrochim. Acta* **41**, 35 (1996).

Chapter 4 Statistical Analysis of Electrochemical Noise in the Time Domain

4.1 Introduction

It has been proven that the statistical analysis of EN signals can provide fundamental information about metastable pitting processes.[1,2,3] The potential and current noise during metastable pitting is generally attributed to the breakdown and repair of the passive film.[4,5] The current transients directly reflect the initiation, growth and repassivation processes of metastable pits.[6,7,8]

As stated in the literature review in Chapter 2, previous pitting research by EN techniques mainly used various stainless steels, pure iron, aluminum and aluminum alloys as the test materials. Fewer studies have been reported on carbon steels. The fundamental results about EN generated during pitting of carbon steel are lacking. For example, there are no systematic studies of the potential dependence of the initiation, growth, repassivation processes of metastable pits and the transition towards stabilization. Even for the usual testing materials, there still exist different or even contradictory standpoints in many aspects, such as the reasons for the potential fluctuations and the role of chloride ions in pitting.

In the present chapter, the potential and current noise generated during metastable pitting of A516-70 carbon steel in chloride-containing solutions is statistically analyzed in the time domain. It is aimed at obtaining the fundamental information about the metastable pitting occurring on carbon steel. Simultaneously, some debated opinions are clarified through noise analysis.

49

4.2 Analysis of the role of electrode capacitance in the initiation and growth of metastable pits

Although it has been acknowledged that current transients reflect the metastable pitting processes: initiation, growth and repassivation, the reason for the potential fluctuations is still controversial. For example, Hashimoto et al.[9] found that the potential fluctuations generated during metastable pitting of pure iron follow a pattern of a quick potential drop followed by a slow recovery. They suggested that the drop in potential is due to the nucleation and growth of a metastable pit and the following slow rise is caused by the repassivation of the pitted area. Many others[10,11,12,13,14] have also attempted to use potential noise to monitor the onset of events characterizing metastable pitting.

Pistorius[15], Isaacs[16] and Pride et al.[17] found that the current transients recorded during metastable pitting correlate in time with a quick drop in potential. However, a slower recovery in potential to the original value than current was observed in these studies. It was suggested that the current fluctuations resulted from the breakdown and repassivation of the passive film, while the potential fluctuations reflected the recharging and discharging processes of the capacitance of the passive film. Electrode capacitance plays a major role in the fluctuations of potential. Therefore, electrochemical potential noise does not directly reflect the pitting processes.

In order to illustrate the electrode process responsible for the potential noise during carbon steel pitting, the role of the electrode capacitance in potential fluctuations is analyzed quantitatively based on the experimental results in this section. The passive behavior of carbon steel in bicarbonate solution is also discussed.

4.2.1 Polarization behavior of carbon steel in bicarbonate solution

The polarization curves of A516-70 carbon steel in 0.5 M NaHCO$_3$ solutions without and with the addition of 0.1 M NaCl are shown in Fig. 4-1. It can be seen that A516-70 carbon steel was passivated in 0.5 M NaHCO$_3$ solution over a large potential region, ranging from -100 mV to 950 mV (Ag/AgCl). Chloride ions have a dramatically negative effect on carbon steel passivity. When the inhibitive solution contained 0.1 M Cl$^-$, the

50

passive potential range decreased to about 150 mV and the passive current density increased remarkably.
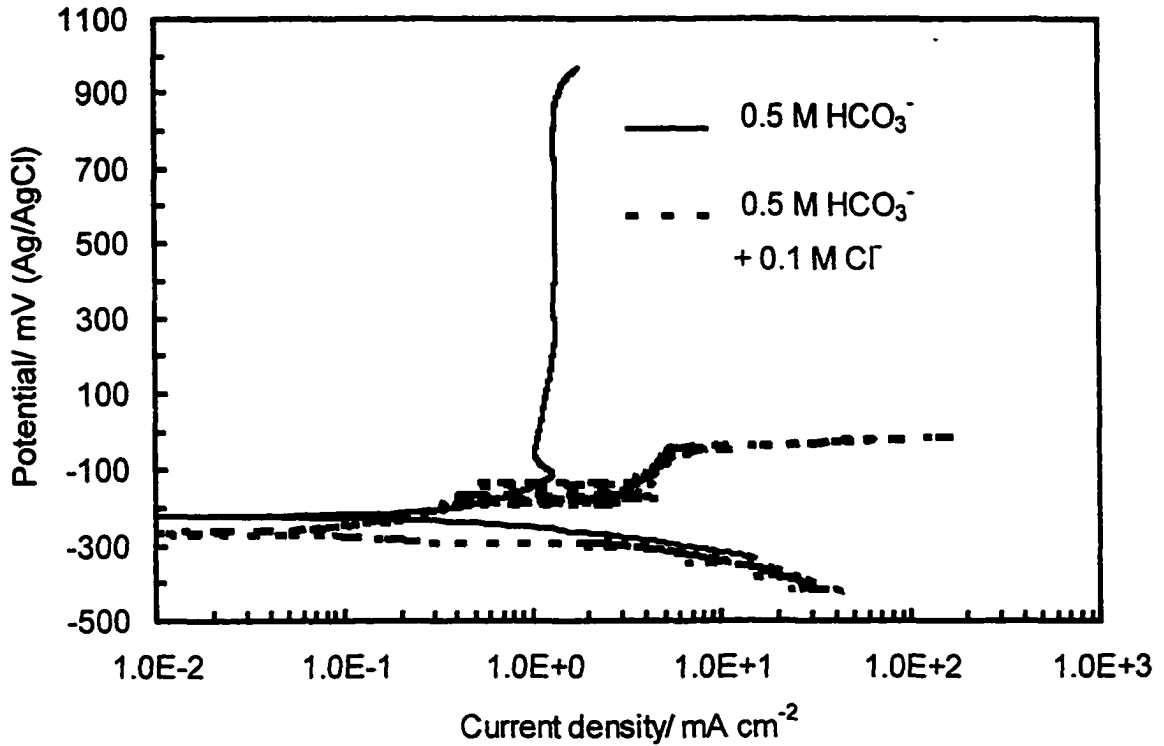
Fig. 4-1 The polarization curves of A516-70 carbon steel in 0.5 M NaHCO₃ solution without and with 0.1 M NaCl.

It has been accepted[18,19,20] that the anodic behavior of Fe in a bicarbonate solution is generally subject to the formation of a precipitated layer of hydrous ferrous hydroxide firstly, which is produced through a complex pathway formally written as follows:[21]

$$Fe + H_2O \rightarrow Fe(OH)_{ads} + H^+ + e \tag{4-1}$$

$$Fe(OH)_{ads} \rightarrow Fe(OH)^+ + e \tag{4-2}$$

$$Fe(OH)^+ + OH^- \rightarrow Fe(OH)_2 \tag{4-3}$$

51

Simultaneously, the growth of the precipitated layer is accompanied with the chemical dissolution due to the presence of HCO_3^- according to the reaction (4-4):

$$Fe(OH)_2 + HCO_3^- \rightarrow CO_3^{2-} + OH^- + Fe^{2+} + H_2O \qquad (4\text{-}4)$$
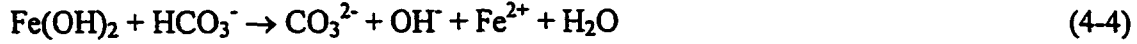
When the local saturation of ferrous species at the electrode/solution interface is reached, bicarbonate ions should favor the precipitation of $FeCO_3$ in the outer layer:[22]

$$Fe^{2+} + HCO_3^- \rightarrow FeCO_3 + H^+ \qquad (4\text{-}5)$$

The $Fe(OH)_2/FeCO_3$-containing outer layer precipitating on the Fe surface undergoes oxidation at a more positive potential.[20] Simultaneously, a barrier layer is formed towards the metal substrate based on the oxidation of metal itself. The structure of a stable passive film formed on Fe surface may be a composite of Fe_2O_3/Fe_3O_4:

$$3Fe(OH)_2 + 2OH^- \rightarrow Fe_3O_4 + 4H_2O + 2e^- \qquad (4\text{-}6)$$

$$2FeCO_3 + 3H_2O \rightarrow Fe_2O_3 + 2CO_3^{2-} + 6H^+ + 2e \qquad (4\text{-}7)$$

$$2Fe(OH)_2 + 1/2O_2 \rightarrow Fe_2O_3 + 2H_2O \qquad (4\text{-}8)$$
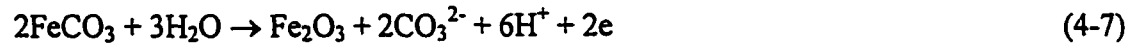
4.2.2 Features of EN generated at different pitting stages

Prior to the measurements of EN in the corrosion medium, instrumental noise in both the potential and current channels was determined. The background noise, which is shown in Fig. 4-2, consist of very frequent and stochastic potential and current fluctuations with amplitudes less than 0.2 mV and 1 nA, respectively.

After 2 hours of immersion of the carbon steel specimen in 0.5 M $NaHCO_3$ solution, a stable passive state was reached. The recorded potential and current fluctuations are shown in Fig. 4-3. It is seen that the noise pattern is similar to that of background noise, that is, stochastic potential and current fluctuations with high frequency and a small amplitude of approximately 0.8 mV and 2 nA, respectively. No sharp potential and

52
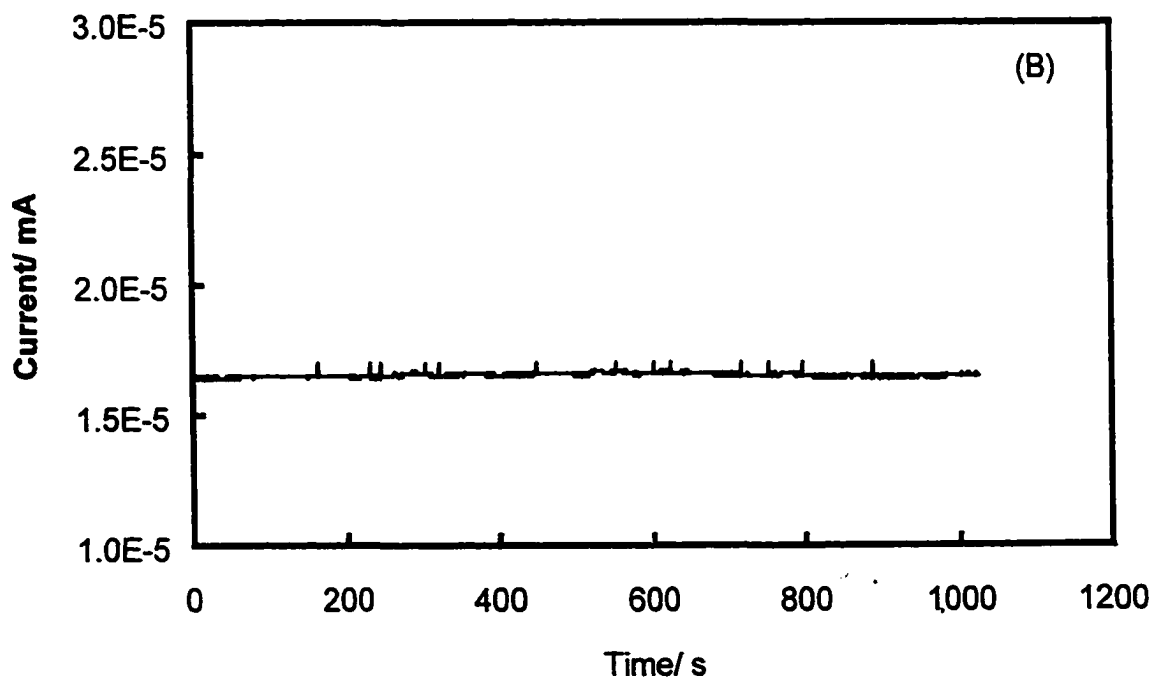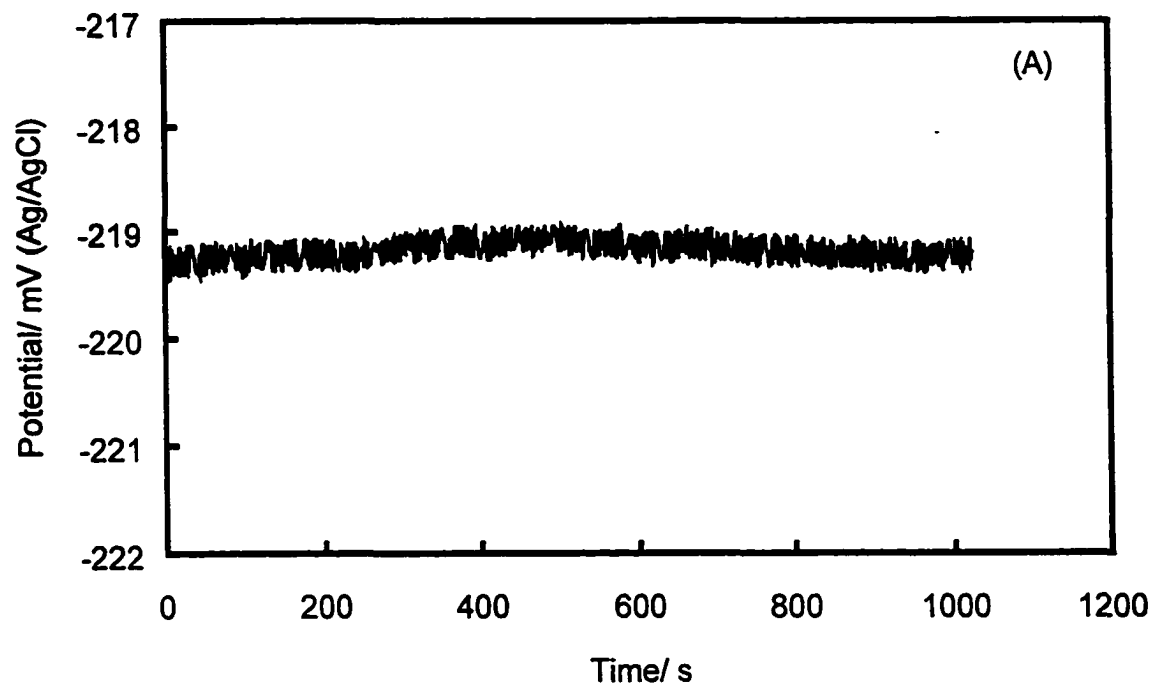
Fig. 4-2 Background potential (A) and current (B) noise recordings.
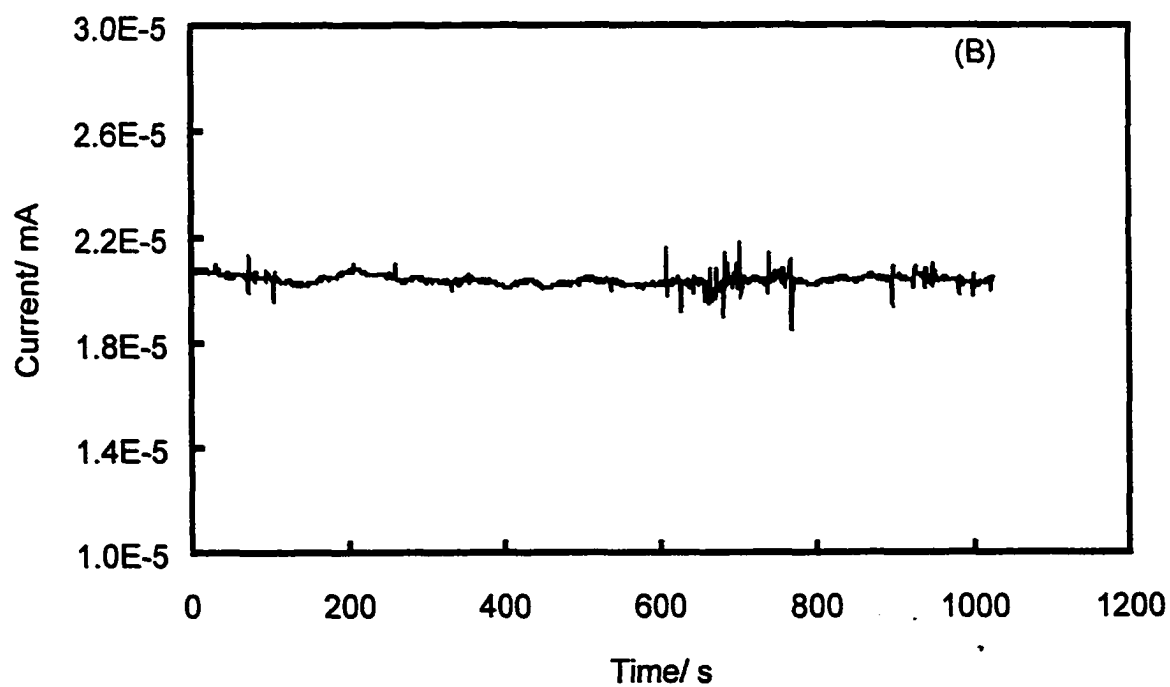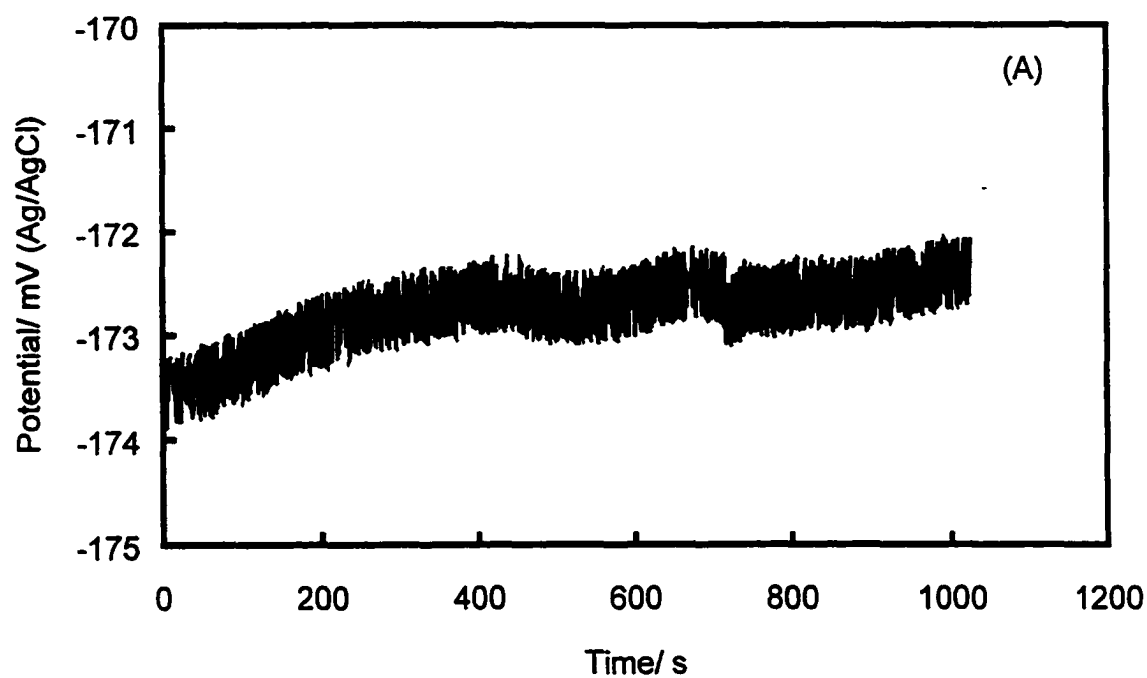
Fig. 4-3 Time-recordings of potential (A) and current (B) fluctuations of A516-70 carbon steel in 0.5 M NaHCO₃ solution.

current transients were observed. This is the typical noise pattern observed in the passive system.

In order to study the pitting susceptibility of passivated carbon steel, chloride ions were added to the bicarbonate solution. On addition of sodium chloride to the solution, the electrode potential decreased and the current increased immediately. The potential and the current fluctuated in a very regular pattern, that is, they traced the changes each other. Both transients produced and died at the same time, as shown in Fig. 4-4. This kind of regular fluctuation lasted about 4 hours, typical potential and current transients were then observed (Fig. 4-5). A common feature of this type of potential and current transient is a quick potential drop and current rise followed by a slow recovery. Additionally, the current recovery took a shorter time than the potential recovery.

Carbon steel in the passive state will maintain a stable potential and current. When Cl^- is added, the specific adsorption of chloride ions on some "active spots" of the electrode surface can lead to local thinning of the passive film through a series of reactions.[23] When the local electrochemical environment is not too aggressive, the dissolution and repair of the local passive film will remain in a steady state. The potential and current fluctuations at this stage reflect the active dissolution of the passive film. Their high regularity and the identical fluctuation rhythm express the common characteristics for stable passivity. The fluctuation in the potential keeps that in the current, indicating that the faradaic current now plays a major role in the potential and current fluctuations.

After 4 hours of immersion of the specimen in a chloride-containing solution, the regular noise pattern with the same fluctuation rhythm was replaced by a sharp and typical pattern of potential and current fluctuations. It is recognized[7] that each transient indicates the initiation of a metastable pit. According to Shibata,[24] the incubation time of pitting corrosion equals the period between the addition of aggressive ions (e.g., Cl^-) to the electrolyte and the initiation of the first metastable pit accompanied by a sharp fluctuation of the corrosion potential and/or current. Therefore, the incubation time of the pitting of A516-70 carbon steel in the present system is approximately determined as 4 hours.
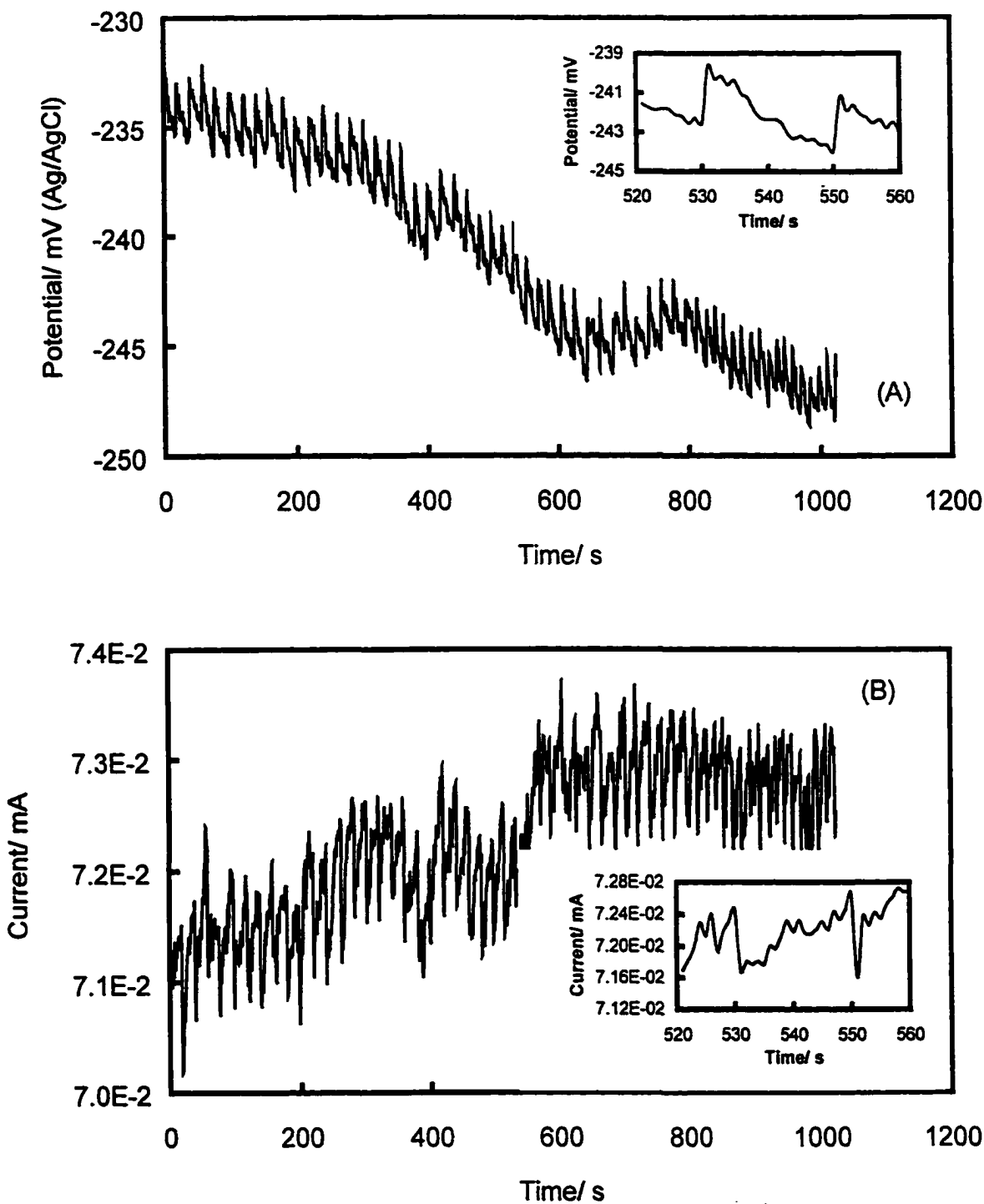
Fig. 4-4 Time-recordings of potential (A) and current (B) fluctuations after 2 hours of immersion of A516-70 carbon steel in 0.5 M NaHCO$_3$ + 0.1 M NaCl solution.
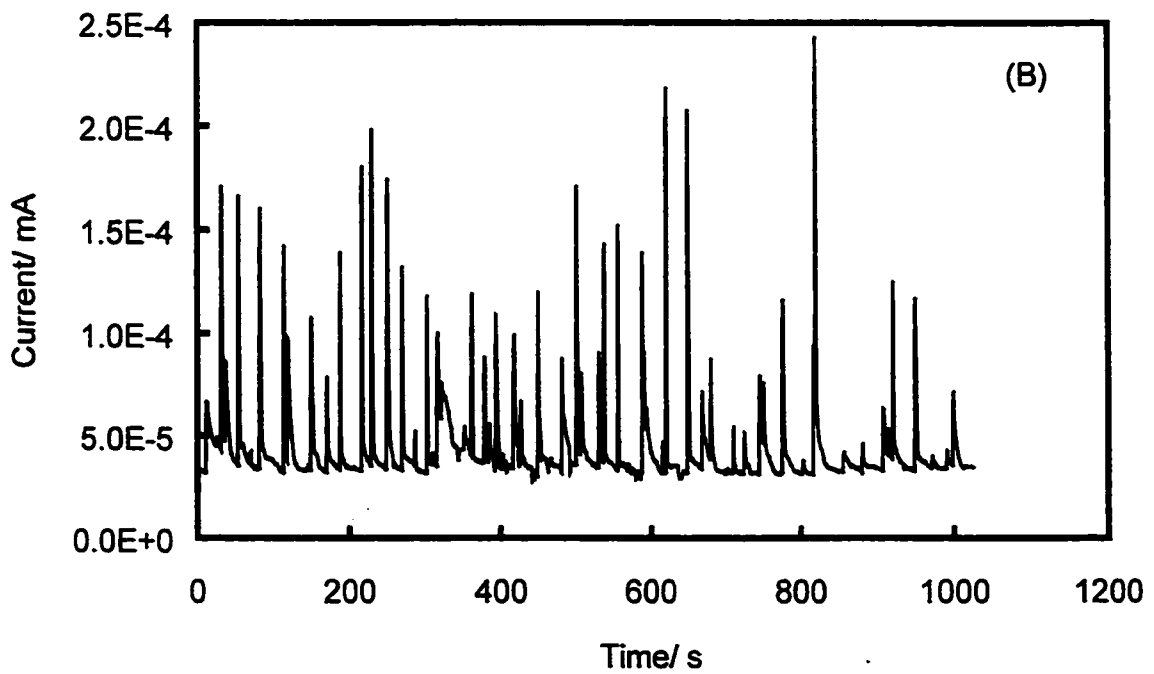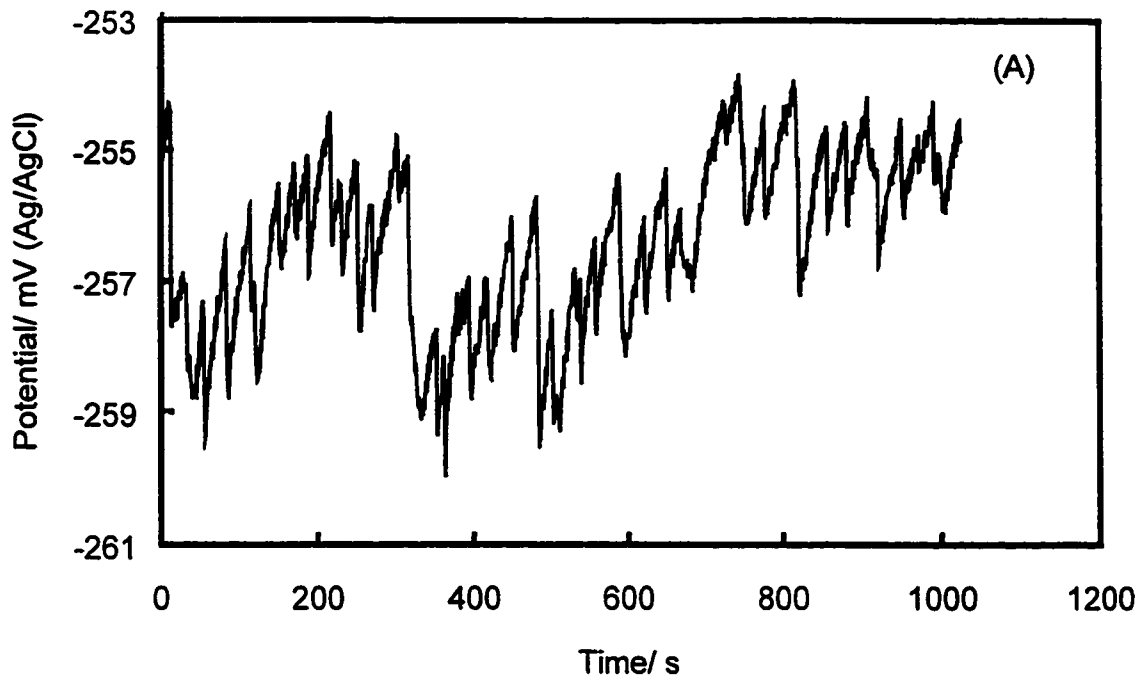
Fig. 4-5 Time-recordings of potential (A) and current (B) fluctuations after 4 hours of immersion of A516-70 carbon steel in 0.5 M NaHCO₃ + 0.1 M NaCl solution.

57

4.2.3 Analysis of EN generated in pitting initiation stage

Fig. 4-6 shows two typical potential and current transients generated in pitting initiation. It can be seen that current and potential transients have different times during their recovery stages. The time for the rise in potential occurs for periods that always exceed the time for decay of current to its baseline although their transients occur simultaneously.

It has been shown[15,17] that the sharp rise in current and the drop in potential indicate a local breakdown of the passive film. Only the current transients directly reflect the nature of the events occurring on the electrode surface. The rapid rise in current is attributed to the breakdown of passive film and the initiation of a metastable pit, while the slow recovery of current comes from the repair of local passive film and the repassivation of the pitted area.

It is evident that the minimum value in every potential transient corresponds to the beginning point of repassivation of metastable pits; however, the slow recovery of the potential does not appear to result from the repassivation process. No current flows to the pitted carbon steel surface during the later stage of potential recovery. This behavior should result from the dominant role of the electrode capacitance. The cathodic reaction in the present system is oxygen reduction. During pit growth, the anodic current rises quickly. The oxygen reduction is not fast enough to consume all the electrons released from anodic reaction within the pit. Since the total anodic current must be balanced by the total cathodic current, a major part of the charge produced by pit growth will be used to recharge the capacitance of the passive film on carbon steel. Therefore, the pit growth charge (Q_{pit}) is balanced by the sum of capacitive charge, which is used to recharge the capacitance of passive film, and the faradaic cathodic charge (Q_{cath}), which is consumed by the cathodic reaction (oxygen reduction). That is,

$$Q_{pit} = C\Delta U + Q_{cath} \tag{4-9}$$

where ΔU is the potential drop. The recovery of the potential is controlled by the slow
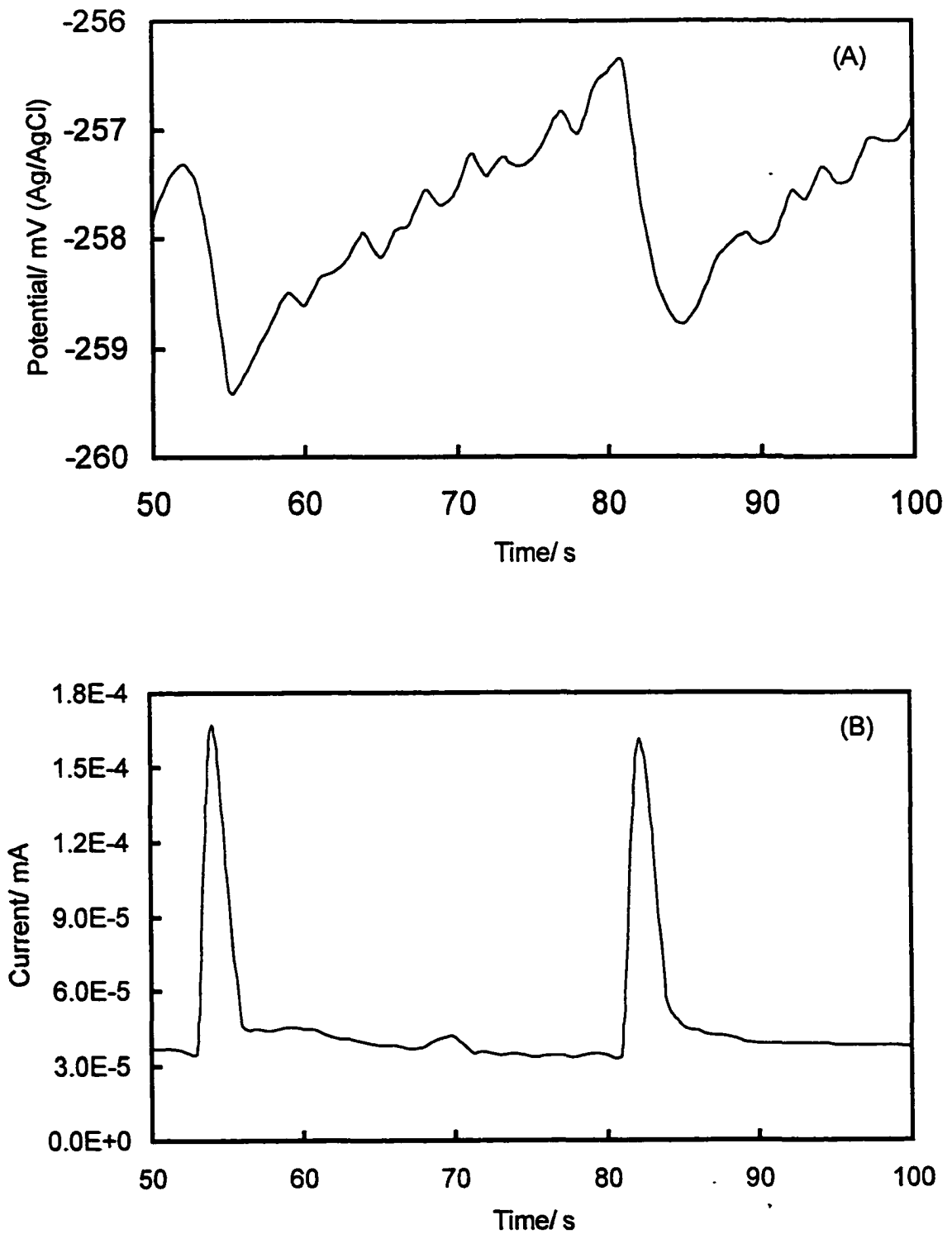
Fig. 4-6 Two typical potential (A) and current (B) transients generated during metastable pitting of carbon steel.

discharging of the electrode capacitance.

4.2.4 Statistical analysis of the role of electrode capacitance in potential fluctuations

The pit growth charge is consumed both by the capacitance of the passive film on carbon steel and the faradaic cathodic reaction. To determine the fraction of the pit charge consumed by the capacitance, the amplitude of the potential drop was compared with the pit growth charge. The potential and current noise of A516-70 carbon steel within 1024 seconds after 4 hours of immersion in 0.5 M $NaHCO_3$ + 0.1 M NaCl solution (Fig. 4-5) were chosen for this purpose. The amplitude of the potential drop, ΔU, was measured from the local maximum in the potential-time curve (at the start of metastable pit growth) to the local minimum value, which corresponded to pit repassivation. The corresponding pit growth charge was obtained by integration of the current-time transient.

Fig. 4-7 shows the relationship between the potential drop and the pit growth charge (small square points). If the complete pit growth charge is used to recharge the capacitance, one expects the potential drop to be proportional to the pit charge if the capacitance is constant. The broken line in the figure shows this assumed behavior. The reciprocal of the slope of the broken line is the constant capacitance value of 80.8 μF, which is measured by the EIS method. The Nyquist diagram based on impedance measurements is shown in Fig. 4-8. Because of the pattern of the semicircle in the Nyquist diagram, the electrochemical equivalent circuit of the electrode system can be described as the parallel connection of the charge-transfer resistance (R_t) and the electrode capacitance (C), which is then in series connection with the solution resistance. The diameter of the semicircle in the Nyquist diagram is determined as the charge-transfer resistance. The value of C is estimated from the measured R_t and the frequency at the maximum imaginary impedance (f_i):

$$C = \frac{1}{2\pi f_i R_t} = \frac{1}{2\pi \times 1.9905 \times 999.6}$$
$$= 8.08 \times 10^{-5} F \tag{4-10}$$
$$= 80.8 \mu F$$

60
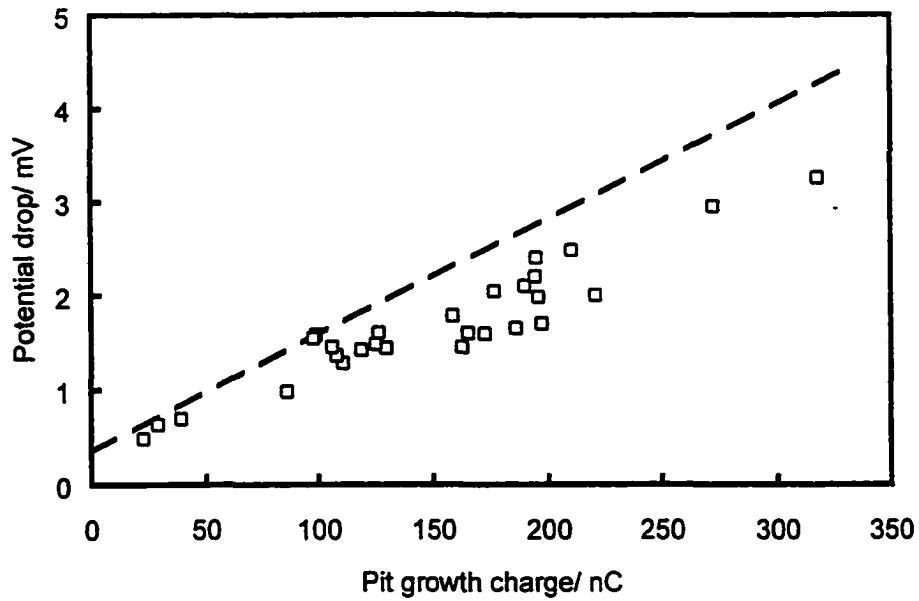
Fig. 4-7 Relationship between the pit growth charge and the potential drop obtained during metastable pitting of carbon steel.
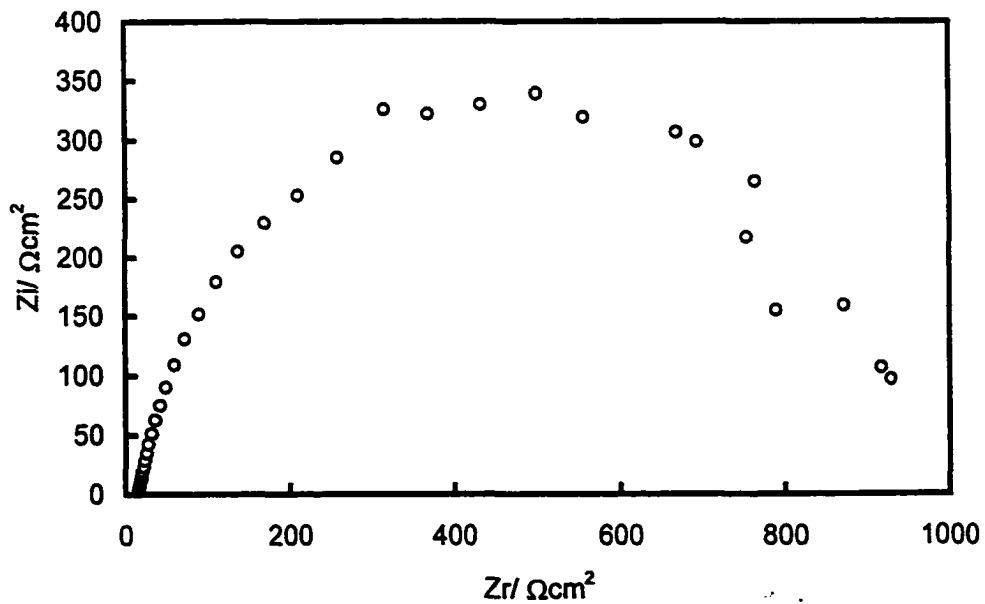
Fig. 4-8 EIS of A516-70 carbon steel immersed in 0.5 M NaHCO₃ + 0.1 M NaCl solution.

Fig. 4-7 illustrates that the actual square points lie slightly to the right of the broken line, indicating that the actual pit charge is larger than the assumed value, that is, the charge consumed by the capacitance. A statistical analysis shows that approximate 75%-80% pit growth charge is used by electrode capacitance. Only a small part of the charge is consumed by the faradaic cathodic reaction.

According to the statistical analysis of the noise data, it is seen that some part of the charge during pit growth is indeed consumed by the faradaic cathodic reaction, however, the capacitance of the passive film consumes the majority of the charge. The capacitance does play a significant role in potential fluctuations during pitting of carbon steel. This is similar to the observations made with stainless steels.[15,16,25]

4.2.5 Analysis of the role of the electrode capacitance in potential fluctuations by electrochemical equivalent circuit

The analysis of the behavior of the passive surface with a localized pitting site has been carried out by considering the electrical analogue of the electrode/solution interface shown in Fig. 4-9 (a). Z_a represents the localized pitting site and Z_c is the passive surface.

The impedance of a passive surface has been attributed to the dielectric, resistive and space-charge properties of the oxide[26] or to the presence of adsorbed species on the surface.[27] Neither of these models has been unequivocally demonstrated, and an equivalent circuit based on either model will be controversial. In view of this, an analogue for the convenience of analysis of the response of the system rather than attempting to conform to a particular model is chosen. The analysis of the potential response is in terms of a capacitor (C) with a parallel resistor (R_t) and offers sufficient accuracy for the present result. The equivalent circuit of the pitting site has been proven to be reasonably simulated as a resistor (R_{pit}).[16] The above consideration leads to an equivalent circuit shown in Fig. 4-9 (b) to describe the electrode/solution interface.

It becomes clear from the equivalent circuit that the capacitance of the passive surface is a component of major importance when pitting is initiated. The equivalent resistance of the passive surface plays a minor role due to its high value. During the initiation of pits, the potential decrease, and the passive surface can be represented by a single capacitor, which is shown in Fig. 4-9 (c). Prior to pit initiation, the value of R_{pit} is infinite. On
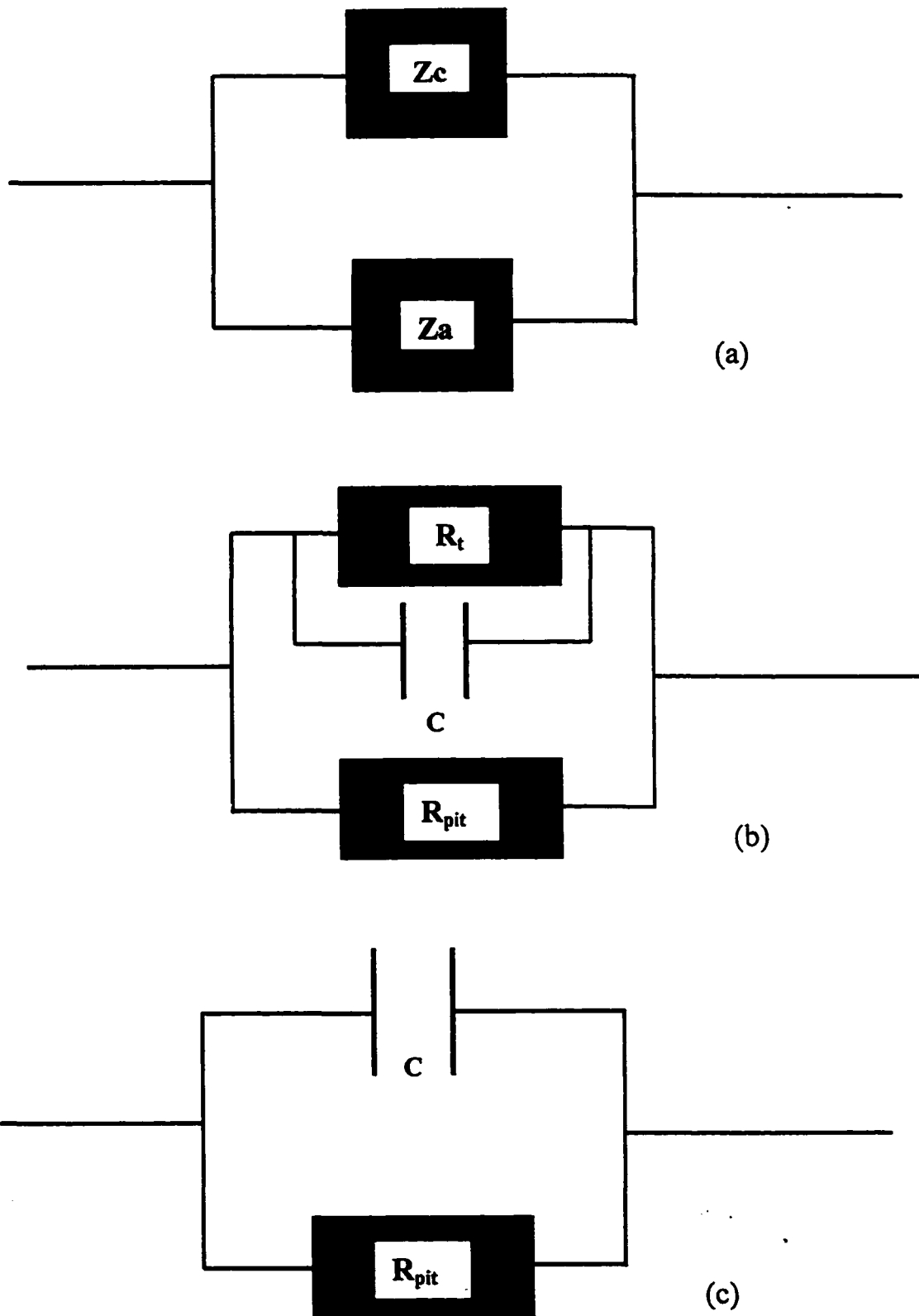
Fig. 4-9 Electrochemical equivalent circuit showing the impedance of the passive surface with initiated pits.

63

initiation of pitting, the presence of R_{pit} leads to the recharging of the capacitance. Following the repassivation of the pits, the value of R_{pit} is again infinite and the potential changes are then controlled by the slow discharging of the capacitance via the high parallel resistance.

4.3 Metastable pitting of carbon steel under potentiostatic control

Metastable pitting, which can be observed as stochastic current fluctuations, is believed to correspond to passive film breakdown and repair occurring either below the pitting potential (U_{pit}) or during the induction time prior to onset of the stable pits under potentiostatic polarization above U_{pit}.[7,8,25,28,29,30,31,32] Metastable pits themselves cause no great damage to the material, since their diameter is typically only a few micrometers.[6] However, the early development of the stable pits appears to be identical to that of the metastable pits,[33] and the probability of stable pitting is directly linked to the occurrence and intensity of metastable pitting.[34] A better understanding of the pit initiation, stabilization and growth may be gained from a thorough investigation of the metastable pitting phenomena.

The statistical analysis of the current noise generated during metastable pitting in the time domain is a valid approach to study the initiation, growth and repassivation of a microscopic pit. Previous work[6,29,31,35,36,37,38] has demonstrated that the growth of corrosion pits occurs in two consecutive stages, characterized by metastable growth in the early period, followed by stable growth. The metastable pit growth may be terminated at any time, in which case the pit surface repassivates and the current drops sharply. The chances of achieving stability for the metastable pits increase as the potential is raised. Pistorius and Burstein[6,35,36,37] studied 304 stainless steel in a chloride solution and suggested that pits grow under diffusion control. In the stage of stable growth, the diffusion barrier is provided by the depth of the pit itself. In the early metastable state, however, the barrier comes from a perforated cover, a remnant of the passive film, over the pit mouth. Bohni and co-workers[29,39] also found that metastable pits are covered during growth and exhibit a constant current density. Rupture of the cover during metastable growth leads to the repassivation of the pit. They concluded that both

metastable and stable pit growth rates are ohmically controlled. Only at very positive applied potentials is pit growth controlled by the mass-transport step. Pride and Scully[7] studied the current transients associated with pitting on high-purity aluminum over a range of potentiostatically applied potentials and received the same result.

Fundamental studies of metastable pitting process occurring on carbon steel are still lacking. In this section, the current noise generated during metastable pitting of A516-70 carbon steel under potentiostatic control in bicarbonate/chloride solutions is statistically analyzed. The relationship between the current transient pattern and pit cover is discussed. The potential dependence of the initiation, growth and repassivation processes of metastable pits was studied. Finally, the pit sizes calculated from the current noise data and those measured under microscopy are compared to prove the correlation between current transients and metastable pitting events.

4.3.1 Current transients generated during metastable pitting of carbon steel

The current transients generated during metastable pitting of carbon steel can be recorded by adding chloride ions of an appropriate concentration to the base solution and controlling the applied potential. Fig. 4-10 shows the time series that corresponds to the applied potentials of -200 mV, -100 mV and -50 mV (Ag/AgCl) for A516-70 carbon steel in a 0.5 M NaHCO$_3$ + 0.01 M NaCl solution. One typical transient is enlarged in Fig. 4-11. The transient displays the typical shape characterizing metastable pitting of carbon steel, that is, a quick rise in current followed by a slow drop.[40,41] In addition, the drop of the current from the maximum to its baseline is not smooth. It is initiated by a fast decay to an intermediate value, then falls to the original value with a number of fluctuations.

4.3.2 Potential dependence of the initiation of metastable pits

The influence of potential on metastable pitting is shown in Fig. 4-10. When the applied potential was at -200 mV, the current recordings were similar to those measured in a bicarbonate solution (Fig. 4-3) and no typical current transient was observed. For the potential at -100 mV, lots of typical current transients, indicating metastable pitting events,[7] appeared after an incubation period of approximately 500 seconds. The comparison of current noise recorded at -100 mV and -50 mV indicates clearly that

65
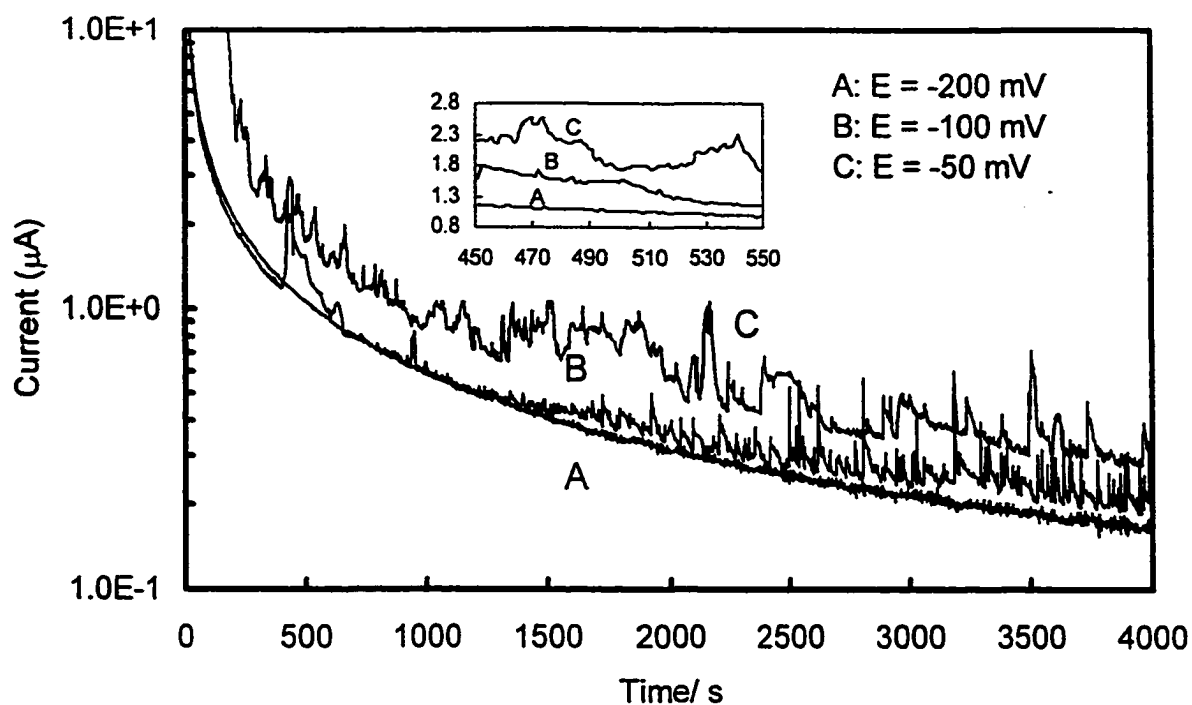
Fig. 4-10 Current noise recordings of A516-70 carbon steel at -200 mV (A), -100 mV (B) and -50 mV (C) in 0.5 M NaHCO₃ + 0.1 M NaCl solution.
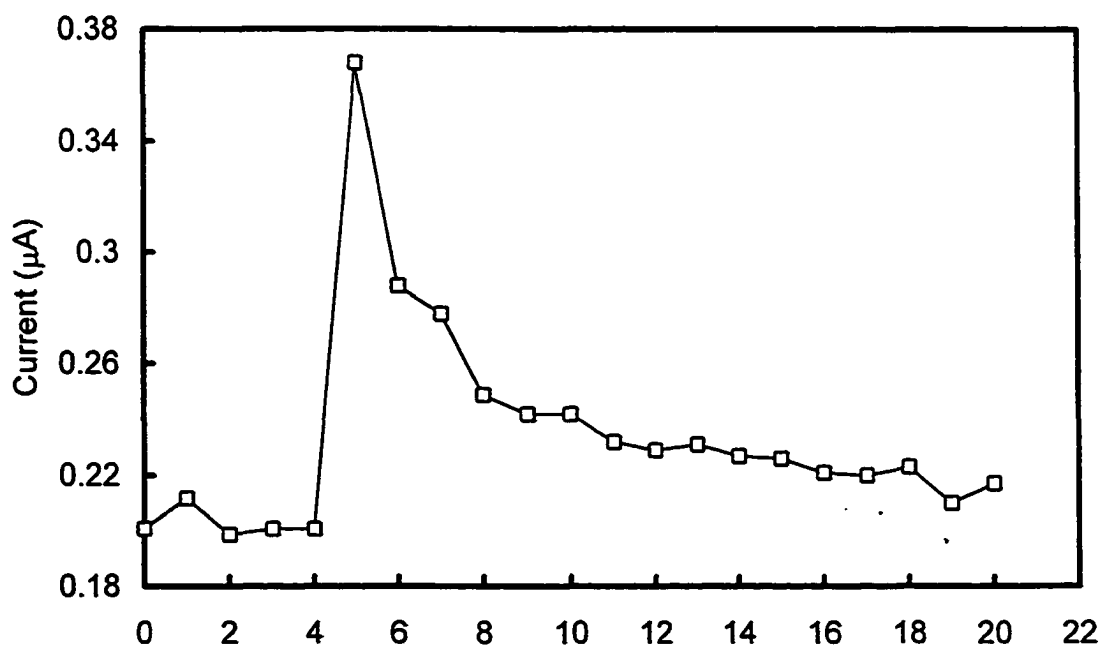
Fig. 4-11 The details of the current transient.

the peak values and the occurrence frequency of current transients increase with increasing potential. However, when the potential reached 0 mV, the anodic current rose quickly to a very high value, which is associated with the continuous growth of stable pits since the potential was applied. No fluctuation is apparent in such a case due to the large DC current shift. In addition, the pitting incubation time strongly depends on the applied potential. It decreases with an increase in the applied potential. The incubation times are approximately 500 seconds and 240 seconds when the applied potentials are -100 mV and -50 mV, respectively.

4.3.3 Observation of pit morphology

Optical microscopic examination of the sample surface after tests revealed the presence of pits on the surface of carbon steel specimens. The mouths of all pits were approximately circular. These pits varied in diameter, but were mainly less than 3 μm, while only a few larger pits reached 9 μm in diameter. It was also found that both the pits and other regions of the electrode surface were always covered by the detached barrier layer or the outer precipitated layer, which can be cleaned up after ultrasonic cleaning. Fig. 4-12 shows the sample surface photographed microscopically with a magnification of 1,000 times before and after ultrasonic cleaning. It can be seen that a layer of deposited product was present over the pit mouth and other regions of the electrode surface.

4.3.4 Analysis of current transients during metastable pitting of carbon steel

The initiation of metastable pits on carbon steel is indicated by typical current transients, characterized as a quick current rise followed by a slow drop. Examination of the pits grown on the electrode surface revealed the presence of a deposited cover as shown in Fig. 4-12. It has been established[42] that significant disruption of the pit cover leads to repassivation of the metastable pits although the cover over a pit must certainly contain flaws or defects for an ionic current to pass between the pit anolyte and the bulk solution. The deposit is probably the passive film covering the electrode surface and most likely some corrosion products as well.

The deposited cover is so porous that it is easily weakened. Openings in the film are produced at some susceptible sites due to the attack of chloride ions. At ruptures in
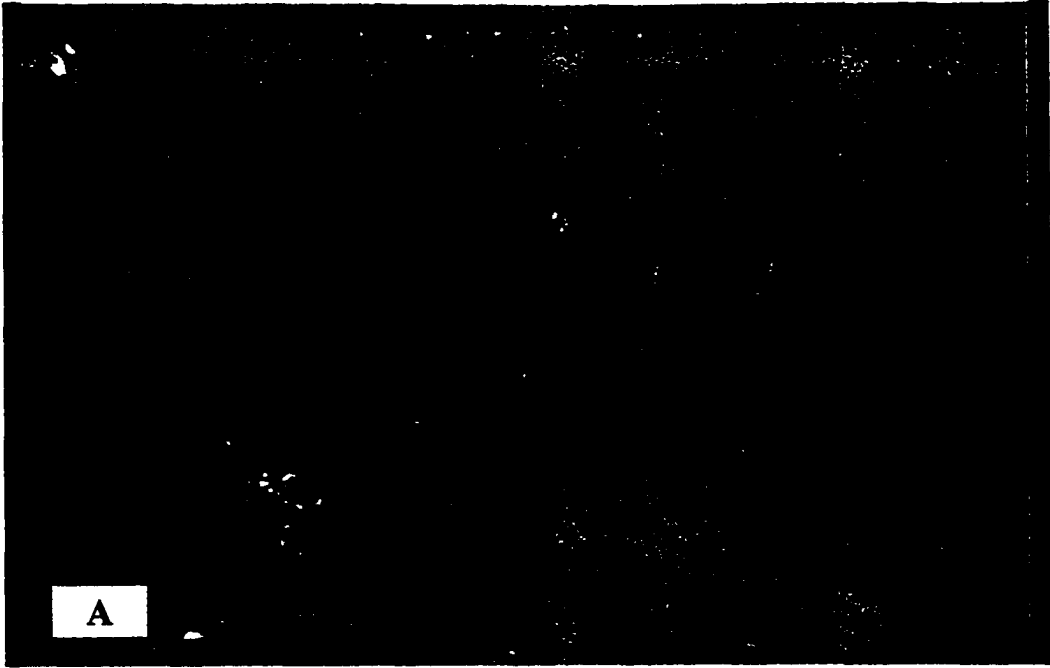
Fig. 4-12 The microscopical photographs of the sample surface before (A) and after (B) ultrasonic cleaning.

68

the deposited layer, metastable pits are initiated. The metastable pitting is indicated by a sharp rise in current, which always takes one or two seconds to reach the peak value. Pit growth is due to an increase in local acidity within the pit, as well as a concentration difference between the pit anolyte and the electrolyte outside the pit. These two results lead to the dissolution of the deposit layer over the pit and, consequently, further enlargement of the openings in the cover. Further expansion and rupture of the pit cover will cause the dilution of the solution inside the pit to below a critical aggressive concentration and then result in repassivation. The quick drop of current from the maximum to an intermediate value comes from repassivation of the internal surface within the pit. The following fluctuations during current decay may be associated with a new deposit over the pit mouth.

It is clear that the deposited layer over the metastable pits plays an important role in sustaining pit growth (small holes present on the cover) and causing repassivation (large rupture of the cover), and, consequently, producing the typical current transients.

4.3.5 Initiation of metastable pits

In general, all pits are metastable when they first start growing. Therefore, the mechanism of pit initiation is the same for both stable and metastable pits.[32] In a chloride solution, the occurrence frequency of current transients is directly associated with the initiation rate of metastable pits. Fig. 4-13 shows the potential dependence of the pit initiation rate, which is defined as the ratio of the number of metastable pits during a certain period to the time, of A516-70 carbon steel during 4,000 seconds of immersion in a 0.5 M $NaHCO_3$ + 0.01 M NaCl solution. Since the current fluctuation range is about 2 nA when A516-70 carbon steel is in a stable passive state (Fig. 4-3), it is reasonable to assume that the upper limit of background noise does not exceed this value. Therefore, each data point in Fig. 4-13 results from a count of the numbers of metastable pits giving current transients with an amplitude greater than 2 nA. No current transient was observed below the potential of -200 mV. The transient numbers became greater with increasing potential and reached a maximum at about -70 mV. The behavior above -70 mV showed a negative dependence of the pitting events on applied potential. This result is similar to others' studies on stainless steels in chloride solutions.[28,31,36]

.
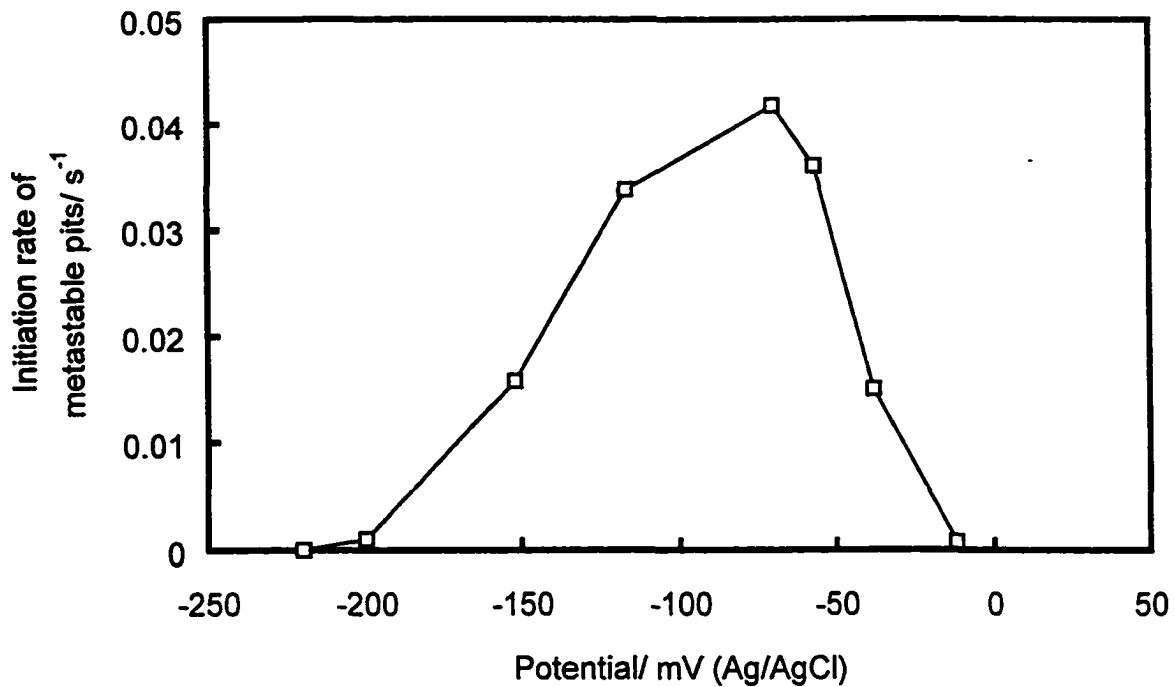
Fig. 4-13 Potential dependence of the pit initiation rate of A516-70 carbon steel in 0.5 M NaHCO₃ + 0.1 M NaCl solution.
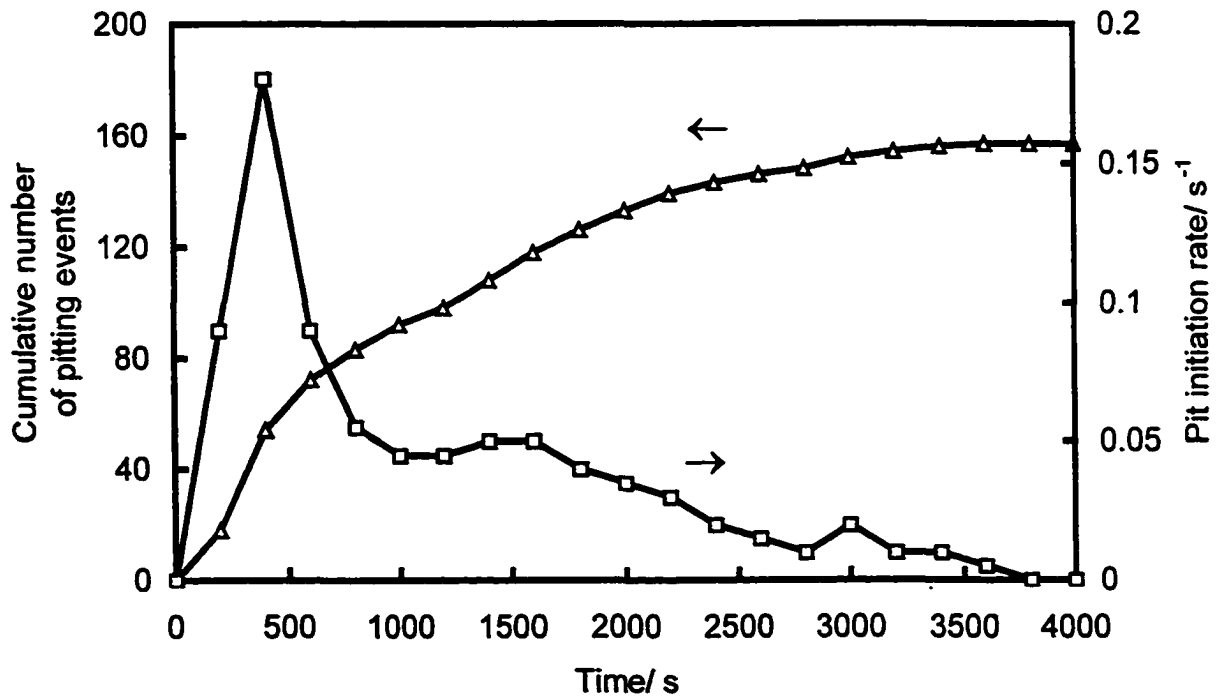
Fig. 4-14 Time dependence of the cumulative number of pitting events and the pit initiation rate for carbon steel specimen at -100 mV.

The effect of applied potential on the occurrence frequency of metastable pits shows that there is a transitional potential (U_{tr}), below which the pitting initiation increases with the potential. Above U_{tr}, there is a negative role of potential in the rate of pit occurrence. The time dependencies of the cumulative numbers of metastable pitting events and the pit initiation rate for A516-70 carbon steel at -100 mV (below U_{tr}) are shown in Fig. 4-14. The cumulative number of pitting events reached a constant value after a certain time. An initial linear increase in the pit initiation rate was followed by an exponential decay. Holliger and Bohni also found an exponential decay relationship for the nucleation frequency of the metastable pits in aluminum.[43]

The breakdown of the passive film and the pitting initiation can be well illustrated by the point defect model (PDM) of a passive film developed by Macdonald.[23,44] According to the PDM, the passive film breakdown and pitting initiation in an aggressive solution are due to the anion-catalyzed cation vacancy condensation at the film/metal interface.[45,46,47] Below the pitting onset potential (-200 mV in this work), the cation vacancy diffusivity in the "weak spots" is not high enough to nucleate pits. When the potential increases positively from pitting onset potential, more "weak spots", characterized by high cation vacancy diffusivity, will be activated and become the potential pit nucleation sites. Therefore, the pit initiation rate increases with increasing potential. In addition, it has been reported that the pit induction time also decreases.[48] When the applied potential is increased to reach a critical value, i.e., the transitional potential of -70 mV in this work, the pit initiation rate is found to decrease with increasing applied potential. Under this potential, the electronic structure of the space charge layer of the passive film changes, and leads to the alteration of the types of cation vacancies involved in the passive film growth and dissolution. The exact mechanism will be discussed in Chapter 7. Once the applied potential reaches the pitting potential, which is about -20 mV, the condensation of cation vacancies at the metal/film interface causes a macroscopic decohesion of the passive film from the metal. When the breakdown of a passive film has occurred over a macroscope scale, the high dissolution rate of the substrate will inhibit the re-formation of the film. Accordingly, the system does not passivate and the initiation rate of the metastable pits drops to zero quickly.

71

There is indeed a maximum potential sites to initiate pits on the electrode surface for a given system. After repassivation of a metastable pit, that site will become unavailable for the subsequent pitting events because the repassivated site is more noble to other sites and, hence, a galvanic cell ensures the repassivated film does not break. The observed decrease in the pit initiation rate with time is due to a dwindling population of susceptible sites.

4.3.6 Growth of metastable pits

The growth of metastable pits has been well documented in the literature. For example, Pistorius and Burstein found that each metastable pit grew under diffusion control for 304 stainless steel,[36,37] while Frankel's work showed the ohmic resistance control of the porous pit cover for 302 stainless steel.[8] Pride et al.[7] suggested that both metastable and stable pit growth rates on high-purity Al were ohmically controlled in chloride solutions at potentials both at and below E_{pit}. At very positive potentials the pit growth was mass-transport controlled. Bohni et al.[28,29,38] also got identical results.

Fig. 4-15 shows the relationship between the applied potential and the average pitting current density at peak pit current for all metastable pits for A516-70 carbon steel during 4,000 seconds of immersion in 0.5 M $NaHCO_3$ + 0.01 M NaCl solution. It is assumed[49] that the generation of current transients is caused by pitting initiation, while the increase in current indicates the growth of the metastable pits. When the peak current is reached, the pit growth terminates and the pit begins to repassivate. Therefore, the total pit growth charge can be calculated by integrating the current-time curve over the time period between the pit initiation point (current rise) and the termination point of the pit growth (current maximum). The pitting current density is then obtained for each metastable pit from the peak pit current and the pit size by use of Eq. 4-11 with the assumption of hemispherical geometry.

$$R_{pit} = [(\frac{3W}{2\pi Fz\rho}) \int_{t_i}^{t_f} (I_{peak} - I_{org}) dt]^{\frac{1}{3}}$$

(4-11)

72
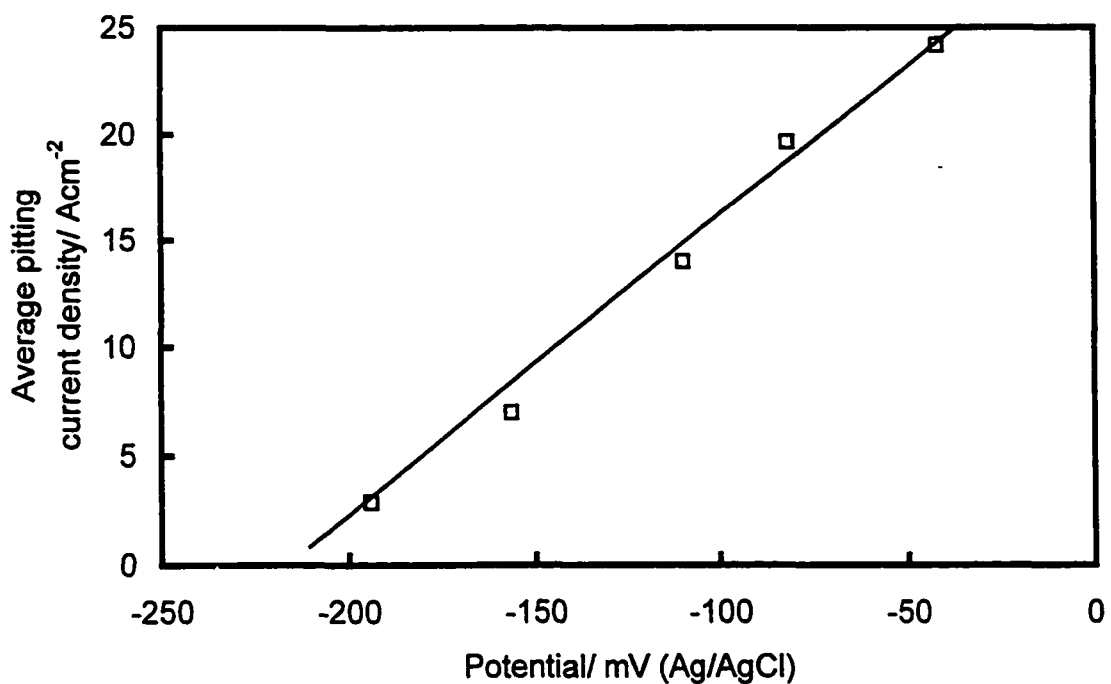
Fig. 4-15 Relationship between the applied potential and the average pitting current density at peak pit current for all metastable pitting events.
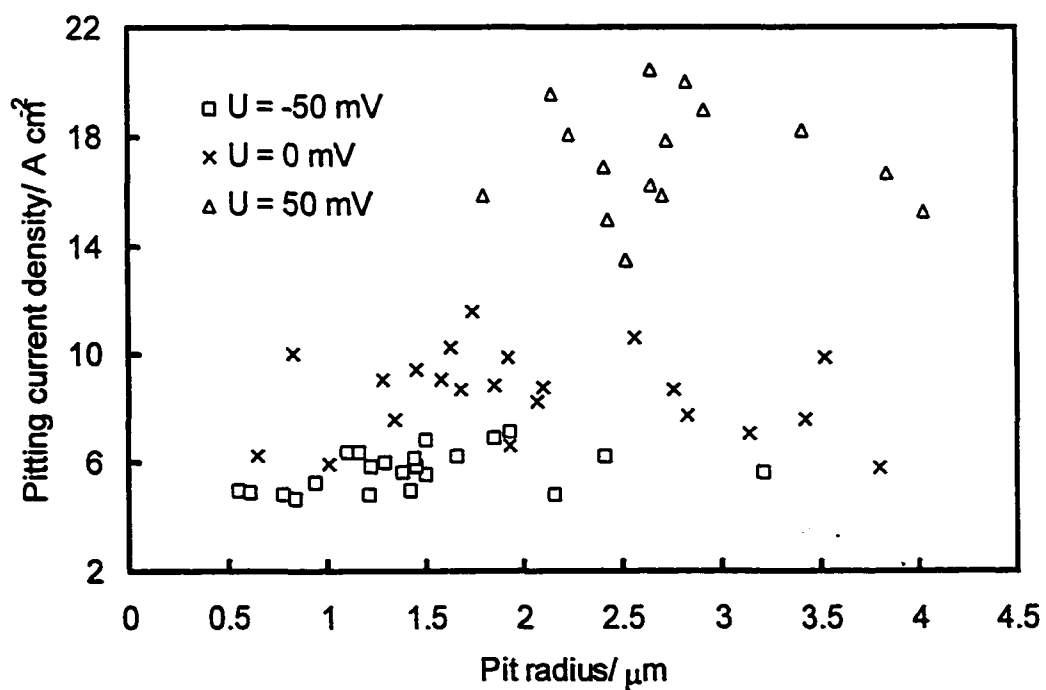
Fig. 4-16 The pit size dependence of the pitting current density for A516-70 carbon steel at three potentials.

73

where r_{pit} is the pit radius, W is the atomic weight, z is the chemical valence, F is Faraday's constant, ρ is the density of the electrode material, t_i is the time point to initiate pits, t_f is the time point when the peak current is reached, I_{peak} and I_{org} are the peak pit current and the original current, respectively.

It was evident from Fig. 4-15 that the pitting current density linearly depended on the potential with a slope of 47.6 $\Omega^{-1}cm^{-2}$ between -200 mV and -50 mV. Above -50 mV, no typical current transient was observed and the current increased to a high value in a short time. Below -200 mV, there was no typical transient, either.

In the intermediate potential range, the pit growth is not under diffusion control since the current density is potential dependent. It is also clear that the pit growth does not follow a simple activation-controlled kinetics because the Tafel-type relation[50] between current density and potential is not observed. The results presented suggest that the growth process of the metastable pits is ohmically controlled at potentials between -200 mV and -50 mV. This result is based on the following calculation. The corrosion potential of A516-70 carbon steel in the given solution is -260 mV. If the applied potential is assumed to be 0 mV, the total overpotential is 260 mV. The average pitting current density corresponding to an applied potential of 0 mV is about 10.7 A/cm^2 from Fig. 4-15. The product of a 10.7 A/cm^2 pitting current density and 0.021 Ω cm^2 resistance (reciprocal of the slope) yields a potential of 225 mV, which is a large fraction (about 86.5%) of the total overpotential. Therefore, the effective ohmic resistance dominates the relationship between the applied potential and the pitting current density, while the activation and concentration overpotentials are minor contributors.

The ohmic overpotential during the metastable pit growth may come from three aspects: the anolyte within the pits, the cover over the pit mouth and the bulk electrolyte. It has been shown that ohmic potential drops within small pits are insignificant due to high acidity and aggressive local environment inside pits.[51] In order to estimate the fractions of potential drop across the pit cover and that contributed by the bulk electrolyte, the pit size dependence of the pitting current density was measured. The results are shown in Fig. 4-16. If the potential drop in the bulk electrolyte plays a major role in the total potential drop, the current is mainly determined by the bulk solution resistance, which is almost constant for a given electrolyte. The pitting current density is,

therefore, equal to the approximately constant current divided by the pit area. So the pitting current density will depend on the pit radius. However, it was found from Fig. 4-16 that the pitting current density was independent of the pit radius at different applied potentials although an increase in potential caused an increase in pitting current density. Therefore, it is clear that the exact nature of the deposited cover over the pits is important in determining the resistance and thus controlling pit growth. Consequently, the current density-potential curve shown in Fig. 4-15 result mainly from the influence of an applied potential on the pit cover.

4.3.7 Repassivation of metastable pits

It has been analyzed in the above sections that the dissolution of the deposited cover over the pit mouth by the large concentration difference within and outside the pit may cause rupture of the pit cover. Immediately after the cover ruptures to form a large opening, the pit solution and the bulk electrolyte mix and the pit repassivates.

The current decay during repassivation in this work approximately followed an exponential law. The repassivation time, defined as the period between the maximum value of current and its recovery to its original value, is an appropriate parameter describing the repassivation process kinetics. Fig. 4-17 shows the potential dependence of the mean repassivation time calculated over all the metastable pitting events for A516-70 carbon steel during 4,000 seconds of immersion in 0.5 M NaHCO$_3$ + 0.01 M NaCl solution. The results indicate that the repassivation time is potential dependent. An increase in potential causes a decrease in mean repassivation time. Since a porous cover over the pits is mainly responsible for pit repassivation, it is reasonable to assume that the deposit of pit cover depends on the applied potential. From the current transient pattern shown in Fig. 4-11, the repassivation process is divided into two stages: the quick drop of current to an intermediate value and then a slow decay to the original value with a number of fluctuations. Comparing the current drop processes at different applied potentials, it is found that the times during the quick current drop are almost identical. The decreased repassivation time with increasing potential is mainly due to the decrease in the duration of the second repassivation stage, that is, the fluctuating current drop stage. However, the exact reason that potential affects the cover deposit is still not clear
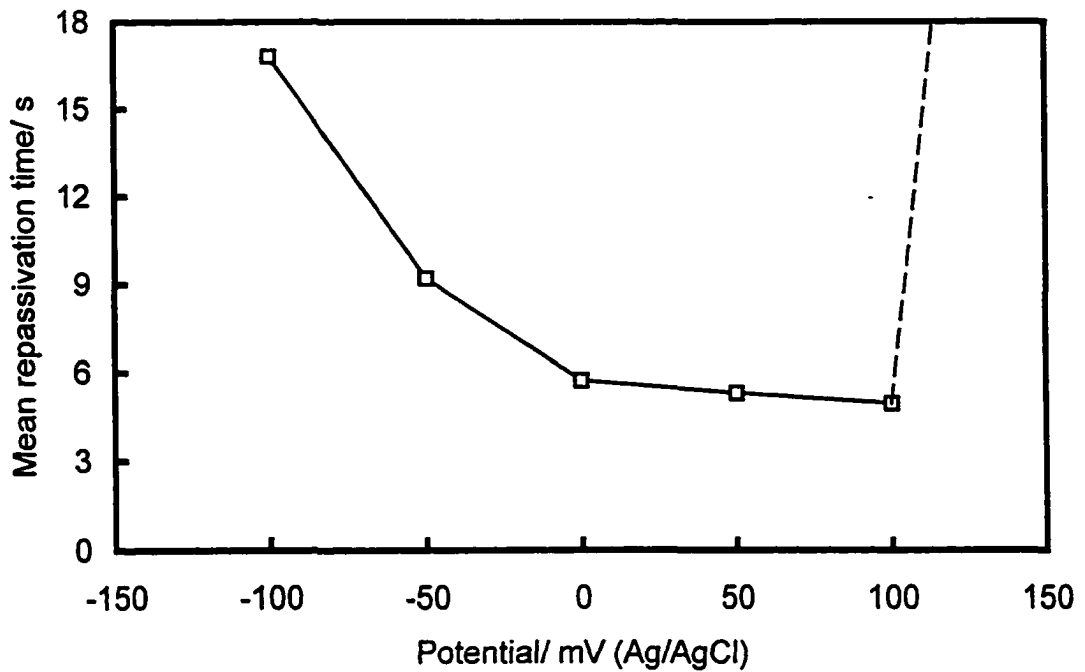
Fig. 4-17 The mean repassivation time as a function of the applied potential.
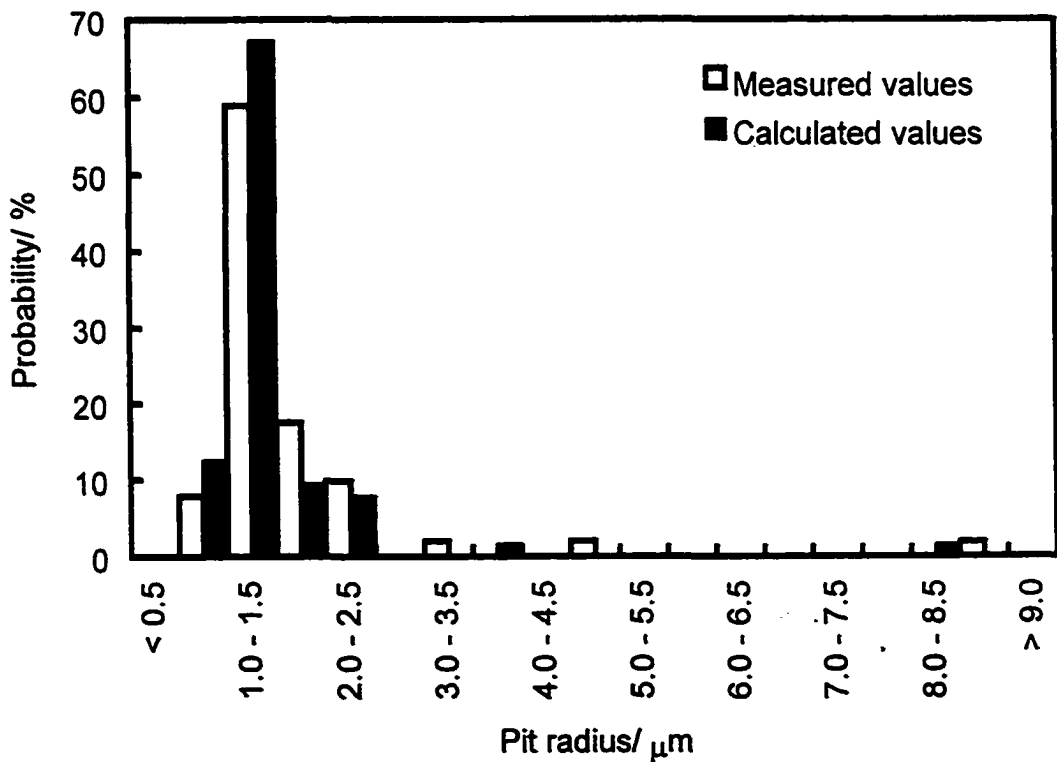
Fig. 4-18 Comparison of the pit radius calculated from the current noise data and that measured under an optical microscopy for carbon steel controlled at -100 mV.

76

at this stage. The potential dependence of the repassivation time is valid only within the passive potential range. When the potential continues to increase and exceeds the pitting potential, repassivation becomes impossible. Therefore, the repassivation time goes to infinity when $U > U_{pit}$.
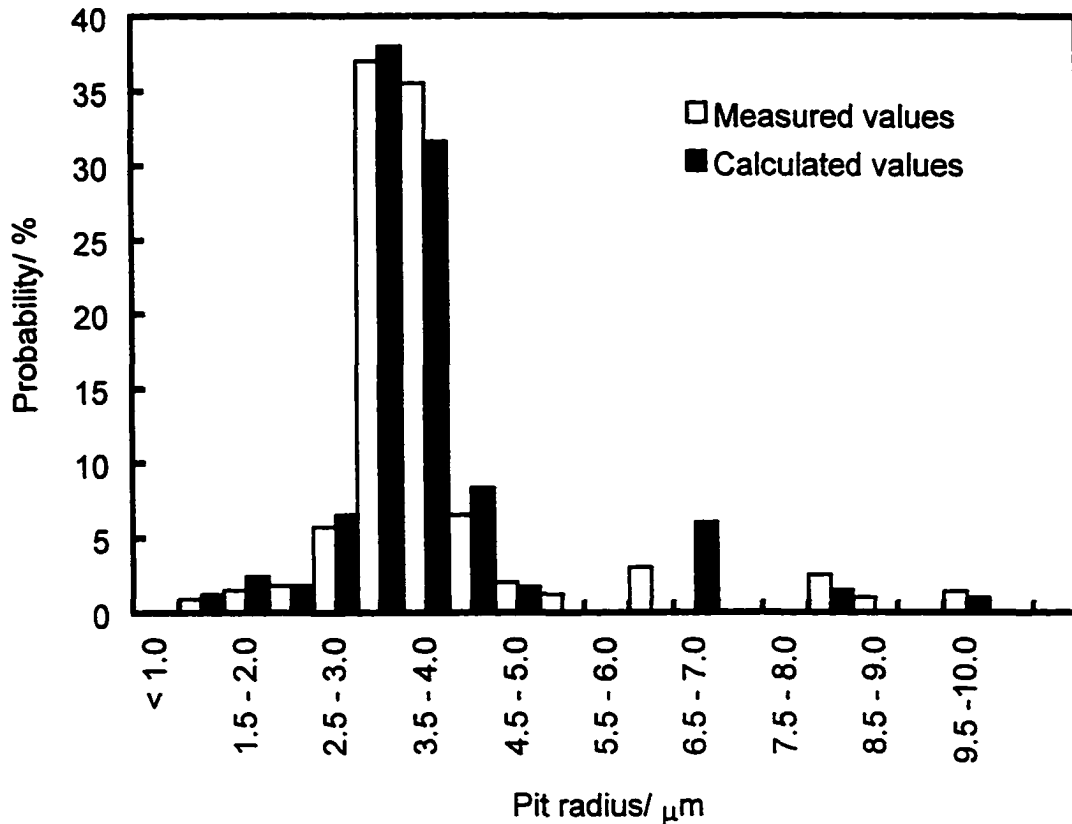
Fig. 4-19 Comparison of the probability distribution of pit radius calculated from the current noise data and that measured under an optical microscopy for A516-70 carbon steel at -50 mV.

4.3.8 Distribution of pit size

In general, the diameter of a metastable pit is only of the order of a few micrometers.[6] Integration of the current-time recordings from the initiation point of the metastable pits to the peak pitting current can give the charge passed during pit growth. From the charge for each pitting event, the metastable pit sizes at peak current can be calculated from the Faraday relationship (Eq. 4-11) assuming a hemispherical pit geometry.

The average radius of each pit can also be determined through optical microphotography by measurment of the diameter across the pit mouth. The measured pit radii are compared with the calculated values from the current noise data in Fig. 4-18. It is clear that they are very close. Therefore, it can be concluded that Eq. 4-9 gives a good approximation of the pit sizes for the present system. It can also be seen from Fig. 4-18 that about 80% of the calculated pit radii are less than 2 μm, and the distribution of actual pit sizes is slightly larger than the distribution of pit sizes calculated from the noise data for the larger pits. The likely explanation for this discrepancy is that the large pits are slightly dish-shaped, with a depth smaller than the radius of the pit mouth although the effect of this distinction has been shown to be small.

In order to prove the validity of the above comparison, the radii of the pits on the specimens at -50 mV have been calculated from the current transients and measured by microscopy. The results are shown in Fig. 4-19. It is seen that the distribution of the calculated pit sizes is close to that of the measured values. The radii of more than 70% of the metastable pits are about 3 - 4 μm. Therefore, it is reasonable to assume that the pits are hemispherical in geometry for calculation of the pit radii for this system.

4.4 The Transition of the Metastable Pitting towards Stability and the Determination of Transition Criterion

The electrochemical noise generated during metastable pitting has been analyzed statistically and spectrally to provide information about the early development of stable pits.[6,7,8,9,28,34,39,52] The transition from metastable to stable pits and the criteria for pit stabilization have been defined.[17,37] Some research work related to the pit stabilization are summarized here.

Pistorius and Burstein[6,37] developed a diffusion-based criterion for the stable growth of an open hemispherical pit on 304 stainless steel in a chloride solution. They assumed that the metal cation concentration on the surface of a growing pit is determined by the balance between the production of cations by the metal dissolution and the transport of cations away from the dissolving surface. The entire anodic dissolution current is carried by the diffusion of metal cations out of the pit. If the metal cation concentration in the

78

bulk solution is zero, the concentration difference between the pit interior surface and the bulk solution away from the pit must be greater than 3 M to sustain pit growth,[53] which determines the lower limit of the pit stabilization. The upper limit is defined by the solubility of the metal salt, which requires that the above concentration difference must be smaller than 4 M.[54] Therefore, the requirement for stable pit growth is $0.3 Am^{-1} \leq i_{pit} r_{pit} \leq 0.6 Am^{-1}$, where i_{pit} is pitting current density and r_{pit} is radius of the pit. The product $i_{pit} \cdot r_{pit}$ is called the pit stability product. The stable growth of pits requires the pit stability product to exceed $0.3\ Am^{-1}$, or else the pit will be repassivated.

The pit stabilization criterion derived by Williams et al.[34] is that the ratio of peak pit current to pit radius, I_{pit}/r_{pit}, must exceed a value of approximately $4 \times 10^{-2}\ A\ cm^{-1}$. Galvele[55] also determined that the stable pit growth occurred at $i_{pit} r_{pit} \geq 10^{-2}\ A\ cm^{-1}$. This relationship stems from the need to maintain a critically concentrated aluminum chloride pit chemistry to keep an active pit. Pride et al.[17] studied the EN generated during pitting in aluminum, aged Al-2% Cu and AA 2024-T3 Al alloys and concluded that the pit stabilization occurs when individual pits exceed a threshold value of $I_{pit}/r_{pit} > 10^{-2}\ A\ cm^{-1}$ at all times during pit growth.

In this section, the transition of the metastable pits to stable pits on A516-70 carbon steel is investigated by the single-event approach and statistical analysis of multiple pitting events. In the case of single-event analysis, the pit size, pit growth charge and pitting current density have been determined from an individual pitting event, i.e., one typical current transient obtained potentiostatically. The results have then been compared with the criterion for pit stabilization. In the case of the statistical method, a large number of metastable pitting events generated by galvanically coupled electrodes over a certain time period have been analyzed to gain insight into the pit stabilization process.

4.4.1 Analysis methods

4.4.1.1 Calculation of pit size and analysis of single pit events

The typical current transients generated during metastable pitting reflect the initiation, propagation and repassivation of the pits. The pit size, directly related to the dissolution rate inside the pits, can be calculated from the current noise data.

The pit growth charge passed over time from the pit initiation point to the peak pit current is determined for each current transient. From the pit growth charge, the radius of the metastable pit is calculated from Eq. 4-11. The pitting current density at the peak pit current is then obtained by dividing the peak pit current by the area of the metastable pit.

The ratio of the peak pit current to the pit radius, I_{pit}/r_{pit}, is generally used as the pit stabilization criterion based on the analysis of single pitting events.[17]

4.4.1.2 Statistical analysis of multiply pitting events

A statistical method can be applied to analyze the current noise data generated from galvanically coupled electrodes. The following equation[17] is used as a pit stabilization factor (PSF) for a time record containing multiply pitting events:

$$PSF = \frac{\sqrt{\dfrac{\sum_{i}^{n}(I - I_{org})_i^2}{n-1}}}{[(\dfrac{3W}{2\pi Fz\rho})\int(I - I_{org})dt]^{\frac{1}{3}}} = \frac{I_{r.m.s.}}{r_{total}}$$ (4-12)

where n is the number of data in the time record, I is the galvanic current measured with the ZRA, and $I_{r.m.s.}$ is the r.m.s. value of the galvanic current. This equation is similar to I_{pit}/r_{pit} used for a single pit, but includes all current data, not just the peak pit current.

Another statistical parameter is the pitting index (PI), which is defined as the standard deviation of current divided by its root mean square value in Eq. (2-2). PI values far less than 1 have been taken to indicate general corrosion, whereas numbers greater than or equal to 1 may indicate a localized corrosion process.[56]

4.4.2 Results and Discussion

4.4.2.1 Analysis of single pitting events (potentiostatic control)

Metastable pitting events were generated for A516-70 carbon steel at combinations of potential and Cl⁻ concentration. Fig. 4-20 shows the influences of chloride ion

80
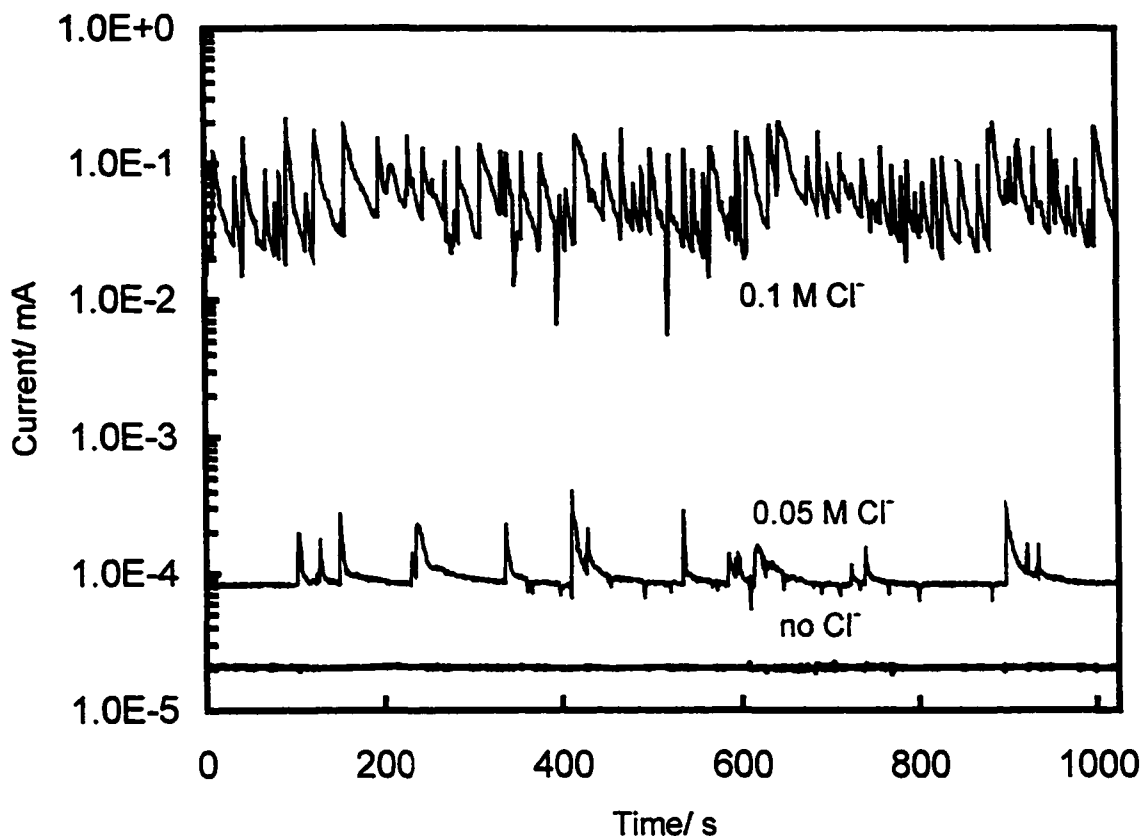
Fig. 4-20 Current noise recordings of A516-70 carbon steel at –50 mV when immersed in 0.5 M NaHCO₃ solution containing different amounts of Cl⁻.

concentration (at a constant $U = -50$ mV) on metastable pitting. The effect of applied potential on pitting has been shown in Fig. 4-10. From these two figures, it can be seen that an increase in Cl⁻ concentration or applied potential is correlated with increasing number and magnitude of the current transients. Stable pits were sometimes observed at more positive potentials in high Cl⁻ concentration.

The electrochemical criterion for pit stabilization always maintains[17,34,55] that the ratio of I_{pit}/r_{pit} must exceed a critical value to maintain the active pit. A large population of individual pitting transients generated at different applied potentials in 0.5 M NaHCO₃ + 0.01 M NaCl solution has been statistically analyzed. The relationship between peak pit

81
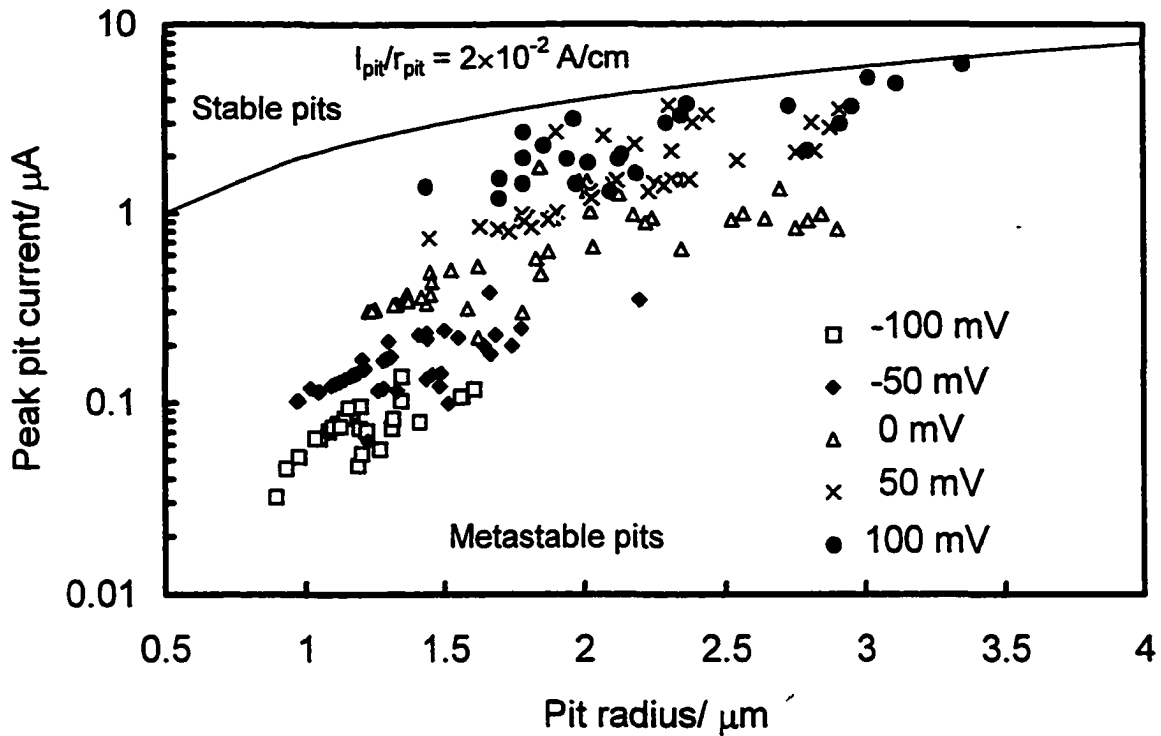
Fig. 4-21 Relationship between the peak pit current and the pit radius for A516-70 carbon steel at different potentials in 0.5 M NaHCO₃ + 0.01 M NaCl solution.
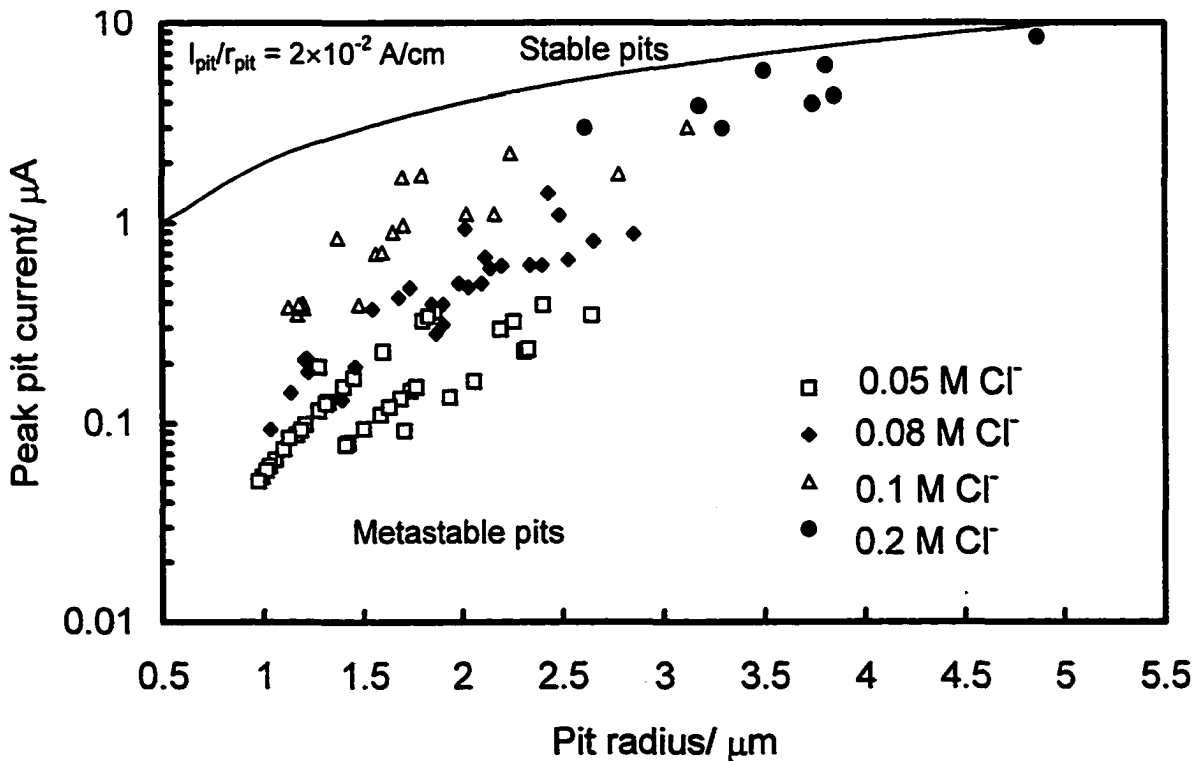
Fig. 4-22 Relationship between the peak pit current and the pit radius for A516-70 carbon steel at −50 mV in 0.5 M NaHCO₃ solution containing different amount of Cl⁻.

82

current and pit radius calculated from pit charge (Eq. 4-11) is shown in Fig. 4-21. A threshold value for the transition from metastable to stable pitting is revealed. As potential increases, both the peak pit current and the pit radius increase toward the I_{pit}/r_{pit} = 2 × 10^{-2} A cm^{-1} line. Pits below this line will repassivate because the 2×10^{-2} A cm^{-1} criterion is not met. In such a case the pit solution soon becomes too diluted to maintain an active pit. Above the potential of 100 mV, the stable pits will develop, which is indicated by the quick increase of current when the potential is applied immediately. Therefore, no typical current transient is observed.

The local corrosivity inside the pit can also be altered by changing Cl$^-$ concentration in the testing solution. Fig. 4-22 shows the relationship between the peak pit current and the pit radius for A516-70 carbon steel potentiostatically controlled at -50 mV in 0.5 M NaHCO$_3$ solution containing different amounts of chloride ions. The pit stabilization criterion of I_{pit}/r_{pit} = 2 × 10^{-2} A cm^{-1} is clearly indicated. Below 0.2 M Cl$^-$ concentration, the ratio of the peak pit current to the size of metastable pits does not reach this criterion and the metastable pits can be repassivated. When Cl$^-$ concentration reaches 0.3 M, stable pits form and the current increases very quickly when the potential is applied.

According to the statistical analysis of single current noise transients generated during metastable pitting of carbon steel, it is concluded that a criterion can be established to indicate the transition from metastable to stable pitting. The ratio of the single peak pit current to the pit radius must exceed 2 × 10^{-2} A cm^{-1} during stable growth of pits to avoid repassivation.

4.4.2.2 Statistical analysis of multiple pitting events (galvanic coupling)

The current noise of galvanically coupled A516-70 carbon steel specimens has been monitored in 0.5 M NaHCO$_3$ solution with chloride ions ranging from 0.01 to 0.5 M. Table 4-1 presents the statistical analysis results of some parameters as a function of Cl$^-$ concentration. The *PI* statistically calculated in the solution containing 0.01 M Cl$^-$ approached zero, indicating uniform dissolution of the passive film. When Cl$^-$ concentrations were above 0.05 M, *PI* increased towards one, indicating pitting. However, *PI* changed irregularly when Cl$^-$ concentration increased continuously.

Table 4-1. Statistical analysis of multiple metastable pitting events for A516-70 carbon steel during 1,024 seconds of immersion in 0.5 M NaHCO$_3$ solution containing different concentrations of chloride ions

Solutions	I_{rms} (μA)	σI (μA)	r_{total} (μm)	PSF (A/cm)	PI
0.01 M Cl⁻	1.09E-4	7.20E-6	0	∞	0.07
0.05 M Cl⁻	2.58E-4	2.55E-3	4.29	6.02E-6	0.98
0.1 M Cl⁻	2.37E-4	2.16E-2	32.45	7.31E-6	0.91
0.3 M Cl⁻	5.32E-4	4.99E-2	61.32	8.68E-6	0.94
0.5 M Cl⁻	9.77E-4	8.55E-2	101.39	9.63E-6	0.88

The statistical parameter of $I_{r.m.s}/r_{total}$ provides some indication of an increasing likelihood of pitting with an increase in Cl⁻ concentration, especially in comparison with 0.01 M Cl⁻-containing solution, in which the pit stabilization factor approaches infinity and shows no metastable pitting. However, the results presented in Table 4-1 are still unsatisfactory because the total pit radii and r.m.s. current are used. Their ratio with the order of magnitude of 10⁻⁶ A cm⁻¹ is much smaller than 2×10⁻² A cm⁻¹, a critical ratio established from potentiostatic experiments to indicate the transition from metastable to stable pitting. The r.m.s. current is smaller than the peak pit current, and the total pit radius representing the sum of all pit radii is larger than the mean pit radius from a number of pitting events. Therefore, the modification of this parameter, the mean of the ratio of peak pit current to pit radius, is expected to provide a better indication of pitting severity. Table 4-2 shows the mean of this ratio for all current transients and the maximum value of this ratio in 0.5 M NaHCO$_3$ solution containing different amounts of chloride ions (data in 0.01 M Cl⁻-solution were omitted because no current transient was observed). Both the mean and maximum ratios increase with increasing Cl⁻ concentration. This result qualitatively indicates the increasing trend towards stable

84

pitting when the Cl⁻ concentration increases. Although these ratios are larger than the statistical results of I_{rms}/r_{total}, they are still significantly below the 2×10^{-2} A cm⁻¹ criterion.

Table 4-2. Statistical analysis of the mean and maximum values of I_{pit}/r_{pit} obtained from the noise data in Table 4-1

Solutions	Mean I_{pit}/r_{pit} (A/cm)	Maximum I_{pit}/r_{pit} (A/cm)
0.05 M Cl⁻	2.96E-4	4.12E-4
0.1 M Cl⁻	8.53E-4	1.25E-3
0.3 M Cl⁻	1.54E-3	1.97E-3
0.5 M Cl⁻	2.18E-3	3.12E-3

Pride et al.[17] analyzed this underestimation and thought that the discrepancy was caused by the fact that only a portion of the anodic current required by the pit site on the first electrode during its growth period is actually measured by the ZRA. The measured ZRA coupling current from the second electrode during a pitting event is given by

$$I_{couple} = (I_{ax} + I_{ca} + A_2 C \frac{dU}{dt})$$ (4-13)

whereas the true anodic current at the pit is

$$I_{pit} = (I_{couple} - I_{ax}) + (I_{H_2} + I_{ca} + A_1 C \frac{dU}{dt})$$ (4-14)

where I_{ox} is the galvanic current between two passive electrodes, I_{ca} is the faradic cathodic current on the passive surfaces, C is the passive electrode interfacial capacitance, $A_{1,2}$ is the area participating in capacitance discharge, I_{H2} is the current

associated with hydrogen evolution in the pit, and dU/dt is the potential transient when a pit forms and the potential is shifted negatively.

The error introduced from the CdU/dt term may be lessened in the potentiostatic case because the potentiostat attempts to keep a constant applied potential. However, in the galvanic case, if the CdU/dt term on the first electrode is larger than the galvanic current from the second, then a large discrepancy may be observed between potentiostatic and the galvanic results even for the same testing conditions. Anyway, the statistical pit stabilization factors given by the ratio of I_{rms}/r_{total} and the mean of $(I_{peak} - I_{org})/r_{pit}$ can be used to track the development of metastable pitting with increasing Cl⁻ concentration more effectively than the pit index (PI).

4.4.2.3 Physical meaning of the pit stabilization factor -- I_{pit}/r_{pit}

In order to understand the physical meaning of the pit stabilization criterion of I_{pit}/r_{pit} mentioned in this paper and others'work,[17,34] it is helpful to consider the conditions inside a growing pit. The aggressiveness of the anolyte developed within a propagating pit results from a low pH and a high chloride concentration. The concentration of metal cations within the anolyte is a useful measure of the aggressiveness, since it is this concentration that produces the change in electrolyte composition.[57,58] It has been established that the steady-state diffusion rate from an open hemispherical pit is given by:

$$\frac{dm}{dt} = kr_{pit}D\Delta C \qquad (4\text{-}15)$$

where dm/dt is the corrosion rate, k is a constant, D is the diffusion coefficient, and ΔC is the concentration difference of cations between the bulk solution and the pit anolyte. Considering $dm/dt = I_{pit}/zF$, it is evident that the concentration difference is linearly related to the ratio of pit current to pit radius:

$$\Delta C = \frac{1}{zFkD} \bullet \frac{I_{pit}}{r_{pit}} \qquad (4\text{-}16)$$

86

It has been shown[6] that the metal cation concentration produced by dissolution must be greater than a certain value of saturation to sustain rapid dissolution inside the pit. This value of the saturation provides the lower limit on the metal cation concentration in the growing pit. From Eq. 4-14, I_{pit}/r_{pit} can give a critical value, below which the pit anolyte is not aggressive enough to maintain pit growth and repassivation is inevitable, and above which the requirement for stable pit growth is met. In the present system, the pit stabilization criterion for A516-70 carbon steel in chloride-containing solutions is determined as $I_{pit}/r_{pit} = 2 \times 10^{-2}$ A cm^{-1}.

4.5 The role of chloride ions in pitting of carbon steel

The pitting corrosion of metals has been commonly considered as being developed in two stages: initiation and propagation. Although there is a general agreement concerning the mechanisms of the propagation stage, doubts still remain about the process leading to the initiation of pits on the surface of a passive film.[59] Many theories have been developed to understand pitting initiation, such as local acidification theory,[55,60] depassivation-repassivation theory,[61,62] chemical dissolution theory,[63] point defect model,[64,65] chemical-mechanical models,[66,67] and anion penetration/migration models.[68,69,70] Of the various theories, there is a common requirement for the initiation of pits: the adsorption of aggressive ions, such as chloride ions. However, the role of chloride ions in pitting processes, especially the initiation stage, is controversial. Newman thought that Cl$^-$ increases the conductivity of electrolyte and then the dissolution rate to support activation of the pit sites.[71] Galvele's results showed that maintaining a sufficient transport of Cl$^-$ from the bulk electrolyte to the pits is the necessary condition to sustain the propagation of metastable pits.[60] Others thought that the main role of Cl$^-$ lies in increasing the initiation process itself by increasing the number of susceptible sites[35] or decreasing pitting potential.[72,73]

Analysis of EN signals during metastable pitting can provide useful information about the influences of chloride ions on pitting. For example, Bertocci and Ye[74] compared the current fluctuations of stainless steel in the absence and presence of Cl$^-$ and

concluded that the most important effect of Cl⁻ lied in increasing the chance of local breakdown of the passive film. Uruchurtu and Dawson[75] monitored the potential of pure aluminum in distilled water and Cl⁻-containing solutions and found that the potential fluctuations were also observed in the absence of chloride ions. They suggested that a dynamic cracking/healing process occurred at defect sites in the pure aluminum oxide film. Cl⁻ was largely responsible for preventing repassivation rather than promoting breakdown. Hashimoto et al.[49] statistically analyzed the potential noise generated during pitting of pure iron and concluded that the reaction order of the chloride attack was approximately 2. They also showed that the concentration of chloride ions affected not only the transition from metastable to stable pits, but the spatial distribution of pits.

The corrosion of carbon steels in aqueous carbon dioxide (CO_2) solutions has been given much attention because of the extensive use of such material in sweet oil and gas fields.[76] Sweet wells deliver formation water, which contains chloride ions (Cl⁻) and bicarbonate ions (HCO_3^-) in various concentrations.[77] Although much research has been carried out to elucidate the corrosion and stress corrosion cracking behavior of pipeline steel in bicarbonate solutions, less work has focused on corrosion problems of carbon steel in bicarbonate solutions in the presence of Cl⁻.[78,79]

This section investigates the fundamental role of Cl⁻ in pitting of carbon steel in a bicarbonate solution. The effects of Cl⁻ on pitting process have been studied by statistical analysis of the potential and current noise generated during metastable pitting of galvanically coupled A516-70 carbon steel specimens.

4.5.1 Polarization characteristics of carbon steel and competitive adsorption model

The polarization curves of A516-70 carbon steel in 0.5M $NaHCO_3$ solution without and with various concentrations of chloride ion are shown in Fig. 4-23. It is seen that carbon steel passivates in a 0.5M $NaHCO_3$ solution with the passive potential ranging from -100mV to 950mV. The anodic polarization behavior of carbon steel is remarkably affected by the addition of chloride ions. The passive range and the pitting potential decrease with increasing Cl⁻ concentration. When the amount of chloride ions reaches 0.5 M, the passivity of carbon steel cannot be maintained. It is clear that chloride ions

88
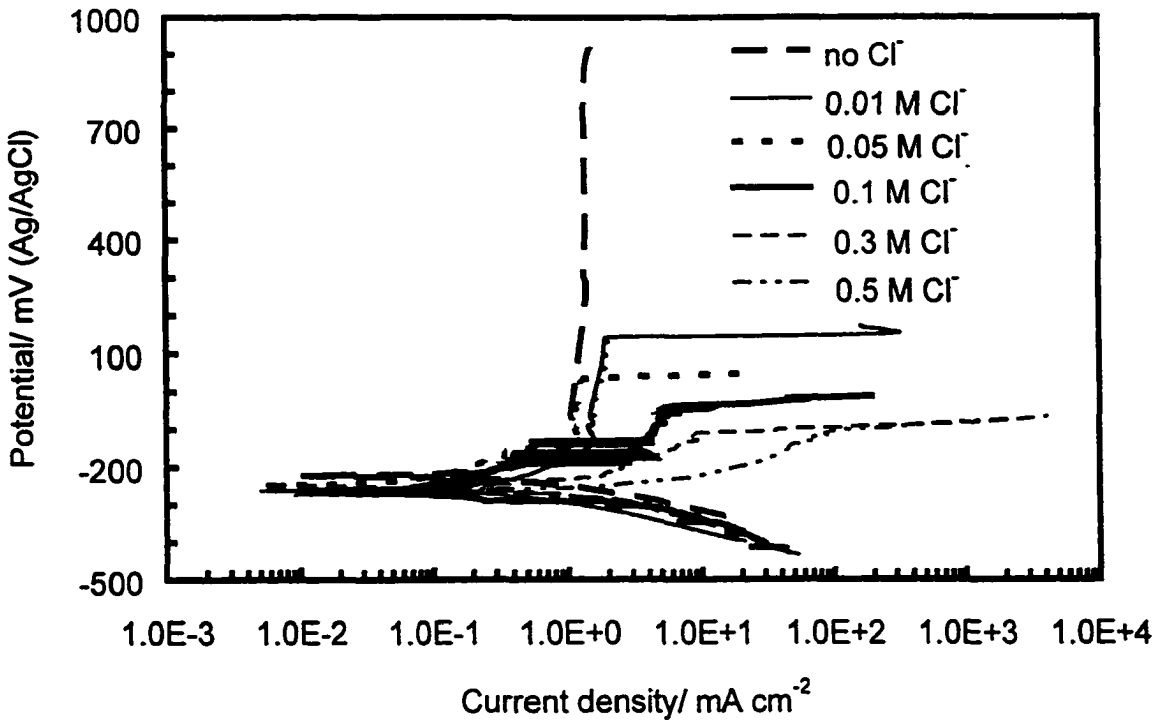
Fig. 4-23 Polarization curves of A516-70 carbon steel in 0.5 M NaHCO$_3$ solution containing different amount of chloride ions.
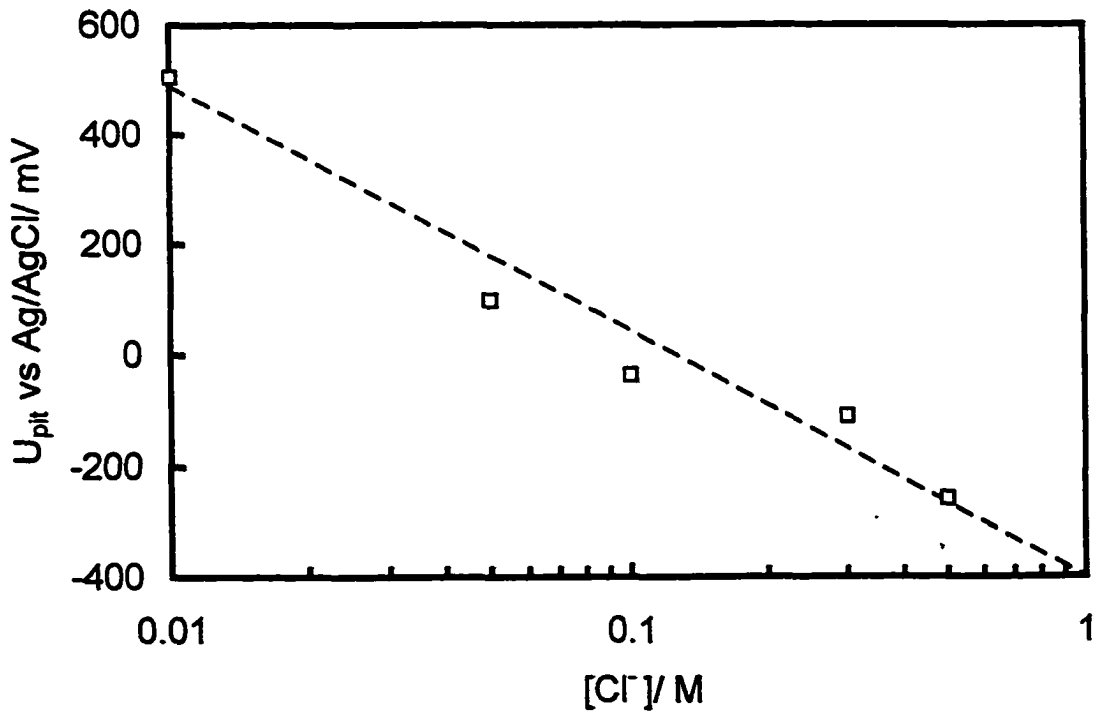
Fig. 4-24 Pitting potential of A516-70 carbon steel as a function of Cl$^-$ concentration.

are responsible for the degradation of carbon steel passivation in bicarbonate solution.

U_{pit} decreases linearly with the logarithm of Cl^- concentration, as shown in Fig. 4-24.

$$\left(\frac{\partial U_{pit}}{\partial \log C_{Cl^-}}\right)_{[HCO_3^-]} = \text{constant} \tag{4-17}$$

This result is exactly consistent with the prediction given by the point defect model.[23,48] According to PDM, the expression for the critical breakdown potential for a single breakdown site is derived as

$$U_{pit} = \frac{4.606RT}{\chi F \alpha_{1/o}} \log\left(\frac{J_M}{J^0 \mu^{-\chi/2}}\right) - \frac{2.303RT}{\alpha_{1/o}F} \log(C_{Cl^-}) \tag{4-18}$$

where χ is the barrier layer stoichiometry ($MO_{\chi/2}$), $\alpha_{1/o}$ is the transfer coefficient for the reaction occurring at the interface between the inner barrier layer and the outer precipitated layer, and J_M is the flux of the cations. Other parameters are as defined as normal.

Considering the slope of the linear relationship between U_{pit} and $\log[Cl^-]$ found in this work, $\partial U_{pit}/\partial \log[Cl^-] = -0.45$. The transfer coefficient of the reaction at the barrier/precipitated layer is calculated as

$$\alpha_{1/o} = -\frac{2.303RT}{F} \times \frac{\partial \log[Cl^-]}{\partial U_{pit}} = -\frac{0.06}{-0.45} = 0.13 \tag{4-20}$$

The value of a small transfer coefficient indicates that the potential drop across the interface is not very sensitive to the applied potential. This result may be caused by the shortage of experimental data and, hence, the error during the fitting of the linear slope.

4.5.2 Chloride ion concentration dependence of pitting initiation

Comparing the current and potential recordings in the absence and presence of chloride ions (Figs. 4-3 and 4-5), it is obvious that the addition of Cl^- results in the

90

degradation of passive film and the initiation of pits. When Cl⁻ concentration increases, the frequency of Cl⁻ attack on the passive film increases, which is reflected by the increasing number of the current transients (Fig. 4-20). So it is reasonable to assume that one of the main roles of Cl⁻ in pitting is to increase the chance of breakdown of the passive film.

Fig. 4-25 shows the effect of Cl⁻ on pit initiation of A516-70 carbon steel. The pit initiation rate (λ) is calculated by the total number of current transients during a certain time period divided by the time. It is seen that λ increases at first, and then decreases with the immersion time. The time dependence of the pit initiation rate follows the law:

$$\lambda(t) = \lambda(0)\exp(at) \qquad 0 \leq t < \tau$$

$$\lambda(t) = \lambda(\tau)\exp[-b(t-\tau)] \qquad t \geq \tau \qquad (4-21)$$

where $\lambda(0)$ and $\lambda(\tau)$ are the pit initiation rates at $t = 0$ and $t = \tau$, respectively. The variables of a and b are the rising and decaying parameters (s^{-1}). In the case of 0.05 M Cl⁻, $\lambda(0)$ and $\lambda(\tau)$ are equal to 5.06×10^{-4} s^{-1} and 3.11×10^{-2} s^{-1}, and a and b are 2.55×10^{-3} s^{-1} and 5.14×10^{-3} s^{-1}, respectively. When Cl⁻ concentration is 0.1 M, $\lambda(0)$ and $\lambda(\tau)$ are 4.49×10^{-3} s^{-1} and 9.31×10^{-2} s^{-1}, and a and b are 1.39×10^{-2} s^{-1} and 9.75×10^{-3} s^{-1}, respectively. The increase in pit initiation rate with time in the first stage is mainly due to the attack by Cl⁻ on the passive film to initiate pits. After a maximum value, the pit initiation rate decreases with time. The decrease should be attributed to the decreasing number of active sites because there is indeed a upper limit of potential pitting sites for a given system. Although some authors[9] believed that this decrease in pit initiation rate was caused by the passive film growth, it seems that the passive film could not develop continuously in Cl⁻-containing solutions in the present system. The solution containing a higher Cl⁻ concentration will be more aggressive; therefore, there is a larger pit initiation rate and the transition of metastable pits to stable pits is easier.

The attack of chloride ions on the passive film and the initiation of pitting mainly occurs in the first stage, that is, $t < \tau$. Figs. 4-26 and 4-27 show the effects of Cl⁻ concentration on $\lambda(0)$ and a, respectively. The average value of $\lambda(0)$ was approximately
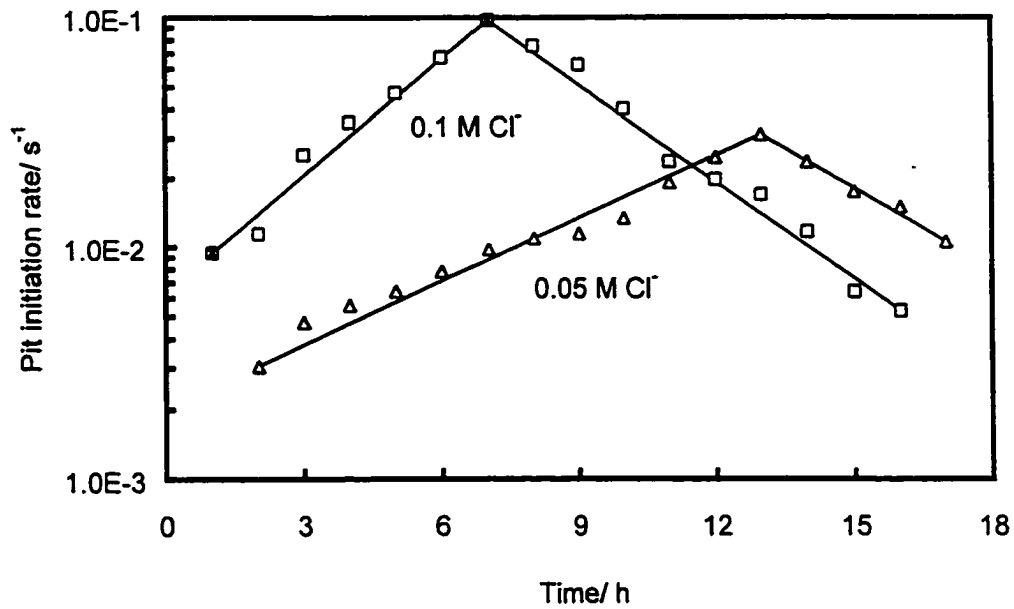
Fig. 4-25 Time dependence of the pit initiation rate of A516-70 carbon steel in 0.5 M NaHCO$_3$ solution containing 0.05 M and 0.1 M Cl$^-$.
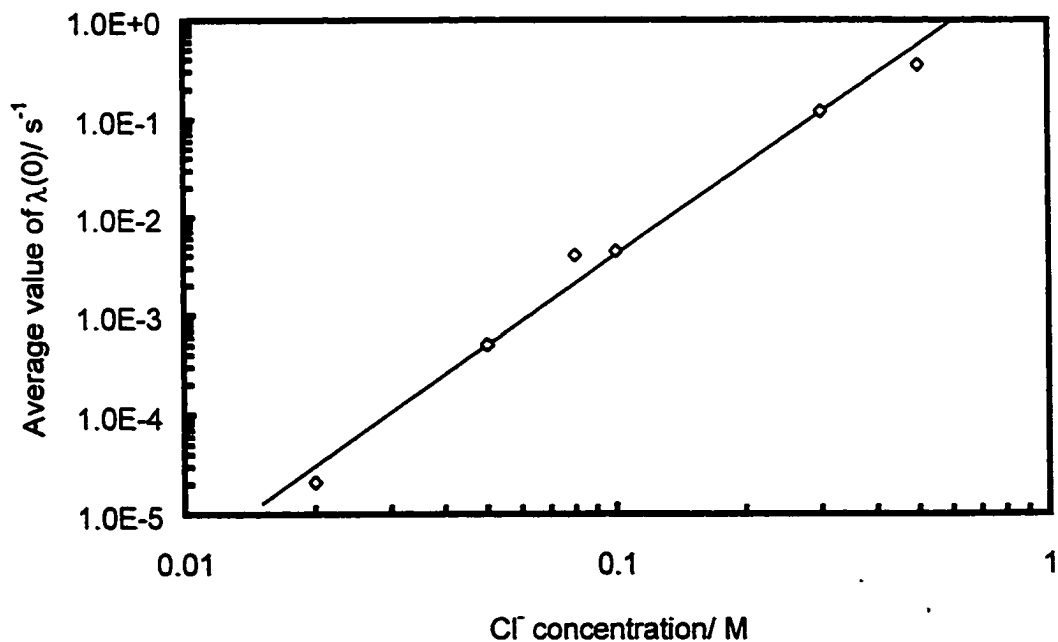
Fig. 4-26 Effect of Cl$^-$ concentration on the pit initiation rate at t = 0, λ(0).

92

proportional to the third power of the concentration of chloride ions. From Fig. 4-27, it is found that despite the large scatter of a, there is no obvious relationship between a and Cl⁻ concentration. The following equation can be used to summarize these results:

$$\lambda(t) = k[Cl^-]^3 \exp(at) \qquad (4\text{-}22)$$

where k and a are independent of Cl⁻ concentration and immersion time. This equation suggests that the reaction order between chloride ions and passive film is approximately 3. This result is consistent with Baroux's work.[80] He studied the kinetics of pit generation on stainless steel and determined that the pit generation rate was proportional to the third power of the Cl⁻ concentration. However, Hashimoto's results[9] on pit initiation showed that the reaction order of chloride ions was 2. The different test methods and test materials may cause this difference.

4.5.3 Chloride ion concentration dependence of pit growth

The quick rise in current and drop in potential indicate the breakdown of passive film and the initiation of metastable pits. The amplitudes of current and potential transient peaks are related to the concentration of Cl⁻. Fig. 4-28 shows the chloride ion concentration dependence of the pitting growth current, which is defined as the average amplitude of (I_{peak} - I_{org}) over 1,000 points, where I_{peak} is the peak current and I_{org} is the original passive current before the current transient. It is seen that I_{pit} continuously increases with Cl⁻ concentration. If the critical condition for pit stabilization is not reached, a higher Cl⁻ concentration will lead to a more aggressive solution and a larger pitting current.

During pit growth, the peak potential also depends on Cl⁻ concentration. In Fig. 4-29, the average peak potential ($<U_{peak}>$, mV) of A516-70 carbon steel over 1,000 points is plotted against the logarithm of Cl⁻ concentration. It can be seen that $<U_{peak}>$ changed in the negative direction when Cl⁻ concentration increased:

$$\langle U_{peak} \rangle = -308 - 93 \log[Cl^-] \qquad (4\text{-}23)$$
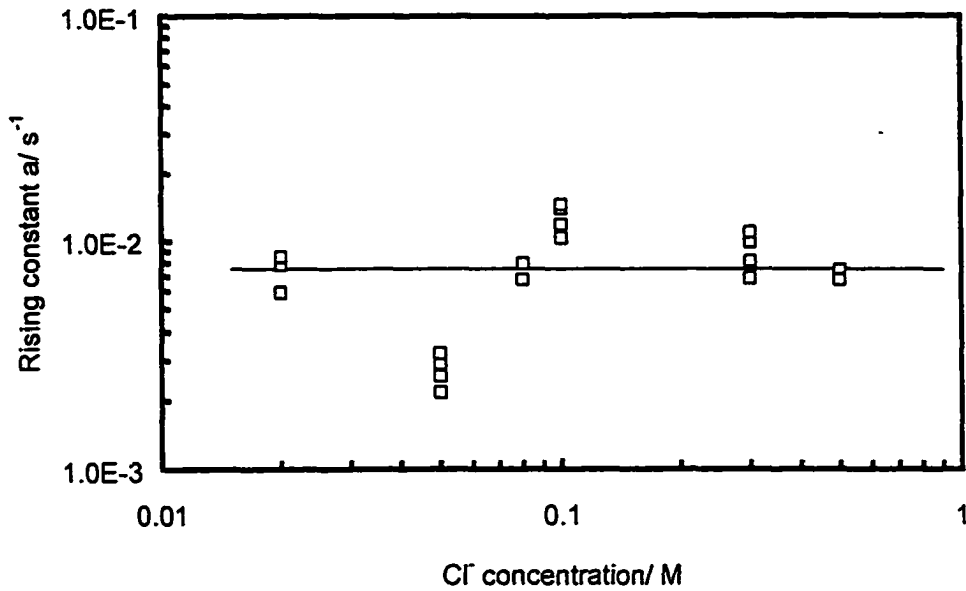
Fig. 4-27 Effect of Cl⁻ concentration on the current rise constant, a.
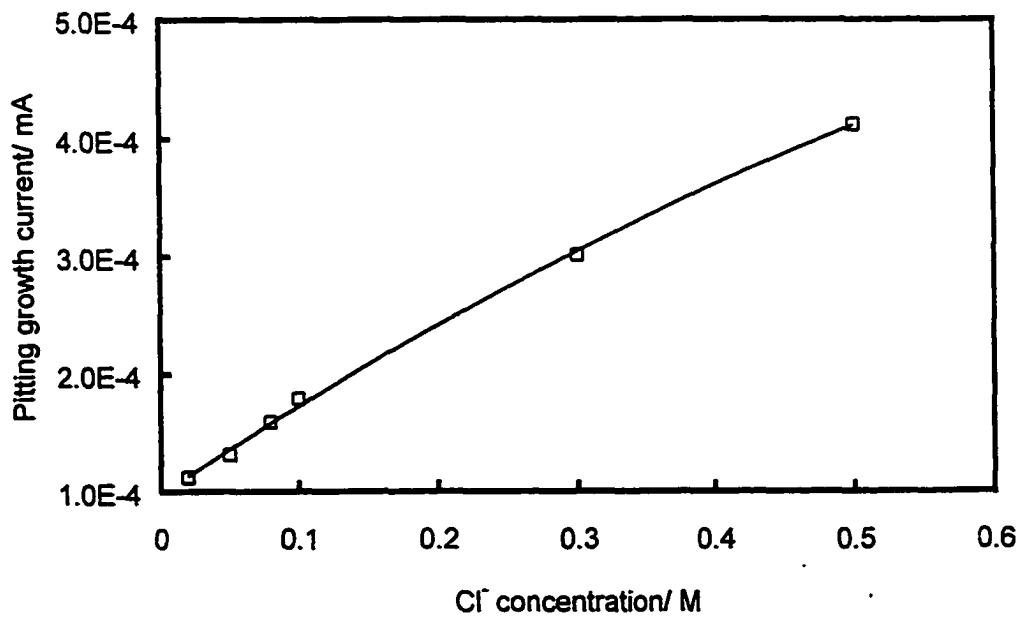
Fig. 4-28 Effect of Cl⁻ concentration on the average amplitude of pit growth current.

94
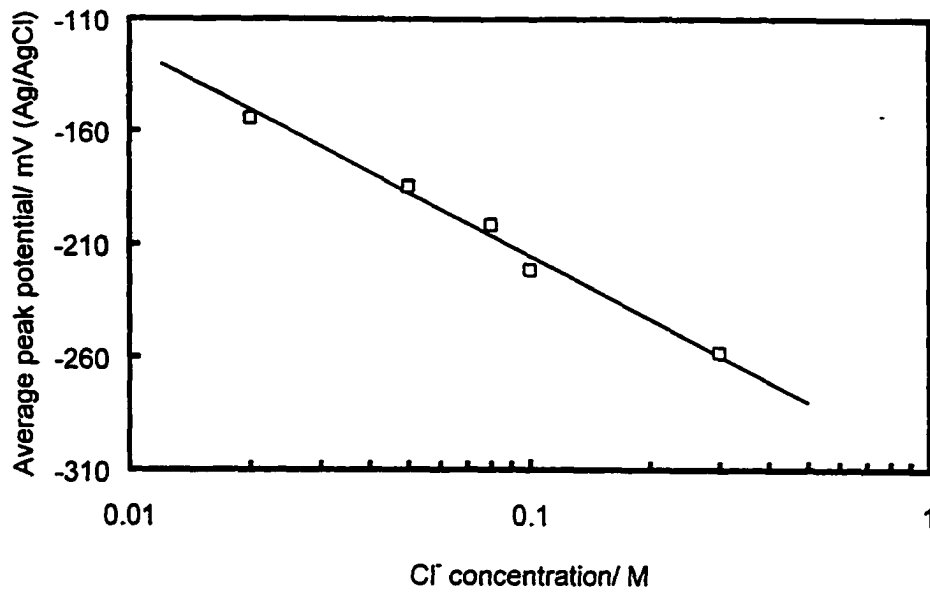
Fig. 4-29 Effect of Cl⁻ concentration on the average peak potential.
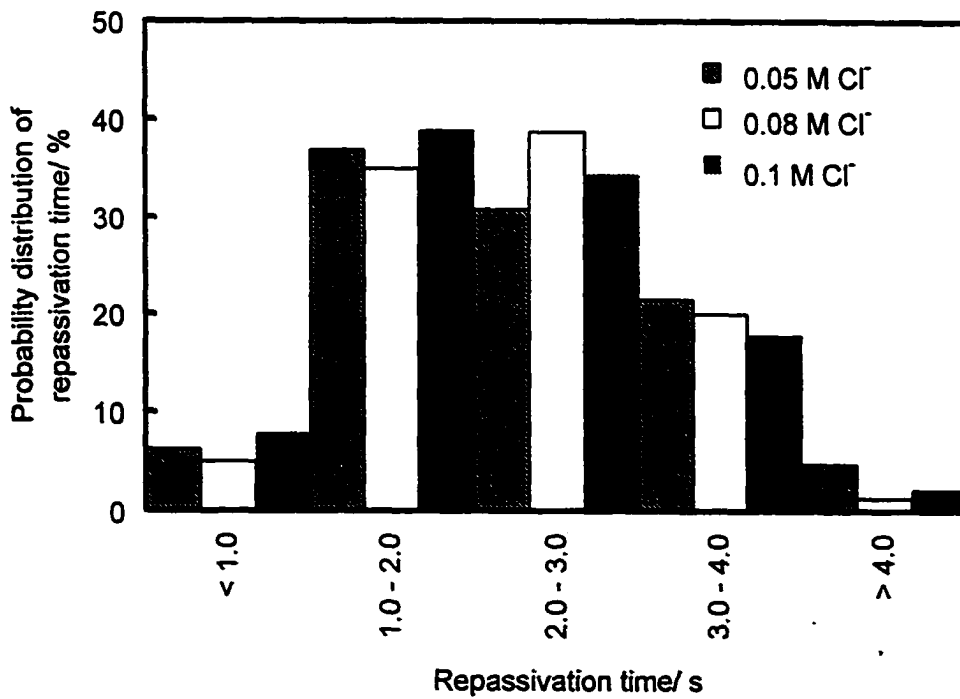
Fig. 4-30 Probability distribution of the repassivation time of metastable pits on A516-70 carbon steel in 0.5 M NaHCO₃ solution containing different amount of chloride ions.

It has been analyzed[9] that potential is a controlling factor for pit growth termination and then repassivation. If the potential shifts to a more negative value as the pit grows, the driving force for pit growth will decrease, and pit growth terminates finally. In the present work, the potential drops very quickly to a low value after a pit is initiated. The driving force of pit growth decreases quickly, so only metastable pitting phenomena are observed. In the case of a stable pitting, the potential is always observed as a slow drop. In addition, the average peak potential depends upon Cl⁻ concentration in a logarithmic fashion, which is identical to the chloride ion concentration dependence of the pitting potential derived in Eq. 4-15. This suggests that the average peak potential is somehow related to the pitting potential. Although Hashimoto's result[9] showed that the maximum peak potential approximately corresponded to pitting potential, the quantitative relationship between them was still lacking.

4.5.4 Chloride ion concentration dependence of pit repassivation

It has been analyzed that electrode capacitance plays a major role in potential fluctuations, and the discharging process of electrode capacitance is responsible for the slow recovery of potential. Only the current recovery directly reflects the repassivation process of metastable pits. In order to clarify the effect of chloride ions on the repassivation process, current transients have been investigated and the repassivation times statistically analyzed. Fig. 4-30 shows the probability distribution of the repassivation time of metastable pits for A516-70 carbon steel immersed in the Cl⁻-containing solutions. It can be seen that there is little change of the probability distribution of the repassivation time of metastable pits when Cl⁻ concentration is changed. More than 90% of the repassivation times lay in 1 ~ 4 seconds in the solutions containing different concentrations of Cl⁻. Therefore, it can be concluded that there is little effect of chloride ions on the repassivation process of the metastable pitting of carbon steel.

4.6 A statistical analysis of the distribution law of metastable pitting events on carbon steel

Statistical analysis of the EN during pitting corrosion of metals is an effective method to extract the basic information.[1,81,82,83,84,85,86] Two processes related to the generation of EN during metastable pitting are the breakdown of the passive film and the repassivation of pitted areas.[6,9,29,87]

The statistical approach to pitting studies has always been attractive. Williams et al.[81,82,83,88] considered a global stochastic model involving a pre-pitting stage and a stable pitting stage. They concluded that a simple local acidification model is valid to describe pitting initiation. The birth and death events of pits are controlled by fluctuations in the thickness of the solution boundary layer. Of all the statistical models describing pitting, the Poisson distribution of pitting events is the most popular. A Poisson random process describes a time signal, either current or potential, with discrete excursion from a base state.[89] Each event can be associated with the formation of a metastable pit.[90] For example, Hashimoto et al.[9] analyzed the potential fluctuations during passive film breakdown and repair on iron and concluded that a pit nucleation event can be approximated to a Poisson process and pit nucleation rate can completely describe this step.

The mutual effect among pitting events is possible if the following facts are considered: local variations in electrochemical potential fields[89] and chemical concentration gradients[90] around the pit sites, alteration of oxide film properties adjacent to pit sites[91] and over newly repassivated pits,[43] etc. These local alterations of conditions caused by previous pits may be expected to die out more slowly than the pit repassivation process, and thus affect the behavior of subsequent newly formed pits. Bertocci et al.[88] analyzed the stochastic current fluctuations of Fe-Cr alloys in a chloride solution and found that a homogeneous Poisson process cannot model the breakdown of the passive film. The clustering of current transients and the mutual dependence between the interval times are clearly observed. When rigorous analyses are applied to the experimental data, the interval times are generally neither independent nor identically distributed. Shibata[92] also pointed out that the mutual interaction of pitting results in a deviation of pit

97

occurrence distribution from the ideal Poisson distribution. Recently Scully and coworkers[89,85]developed a cooperative model describing the transition from low-activity pitting, where individual pitting events are independent and follow a Poisson distribution, to a high-activity state, where correlation exists among the pitting events and a large deviation from Poisson distribution statistics.

The present section is aimed at determining the conditions where the metastable pitting events generated on A516-70 carbon steel are independent of each other and follow the Poisson distribution, and where the distributions are non-Poissonian and the metastable pitting events influence subsequent events. The susceptibility of carbon steel to pitting is altered through controlling immersion time, applied potential, and chloride ion concentration. The current noise data were recorded from two kinds of experiments: two galvanically coupled carbon steel working electrodes and one electrode under potentiostatic control.

4.6.1 Analysis methods

The autocorrelation function of a stochastic process describes the general dependence of values at any instant on previous values. A plot of the autocorrelation function vs. lag time indicates the degree of memory of the process. If I_t, for $t = 1, 2... n$, denotes the sequence of measured current, the value of the autocorrelation function (ACF) at the data points I_t and I_{t+k} can be calculated according to the formula

$$ACF = \frac{\sum_{t=1}^{n}(I_t - I_{mean})(I_{t+k} - I_{mean})}{\sum_{t=1}^{n}(I_t - I_{mean})^2} \tag{4-24}$$

where

$$I_{mean} = \sum_{t=1}^{n}\frac{I_t}{n} \tag{4-25}$$

The autocorrelation plot is a graph of the ACF values vs. the lag time, for k = 1, 2... n. There is a lower correlation for the curves with smaller autocorrelation values. As the interaction among events is strengthened, the autocorrelation degree increases.

Another method to determine if the individual events are dependent on each other is to compare this process to a Poisson distribution, in which there is no cooperation among events. For a Poisson distribution

$$\frac{\sigma}{N_{mean}} = \frac{1}{\sqrt{N_{mean}}}$$ (4-26)

where N_{mean} is the average number of metastable pitting events (N) which occur in a given time interval and σ is the standard deviation of N. In a $\dfrac{\sigma}{N_{mean}}$ vs. $\dfrac{1}{\sqrt{N_{mean}}}$ plot, all points should lie on the diagonal for a Poisson distribution. The larger the deviation of the points from the diagonal, that is, the Poisson distribution, the stronger the cooperation of pitting events.

4.6.2 Results

4.6.2.1 Galvanically coupled A516-70 carbon steel

The current noise of A516-70 carbon steel after 1, 5 and 10 hours of immersion in 0.5 M $NaHCO_3$ + 0.1 M NaCl solution is shown in Fig. 4-31. The common feature of current transients is a quick current rise followed by a slow recovery. Each transient indicates a metastable pitting event.[86] Compared with the current noise recorded after 1 hour of immersion, the amplitude and occurrence frequency of current transients increased after 5 hours of immersion. When the electrodes were immersed in the solution for 10 hours, there was little change of the amplitude of current transients; however, the transient number decreased. The pit initiation rate as a function of the immersion time is shown in Fig. 4-25. In both solutions the pit initiation rate increased with time in the beginning, then decreased during immersion. Therefore, the pitting activity, indicated by the pit

99
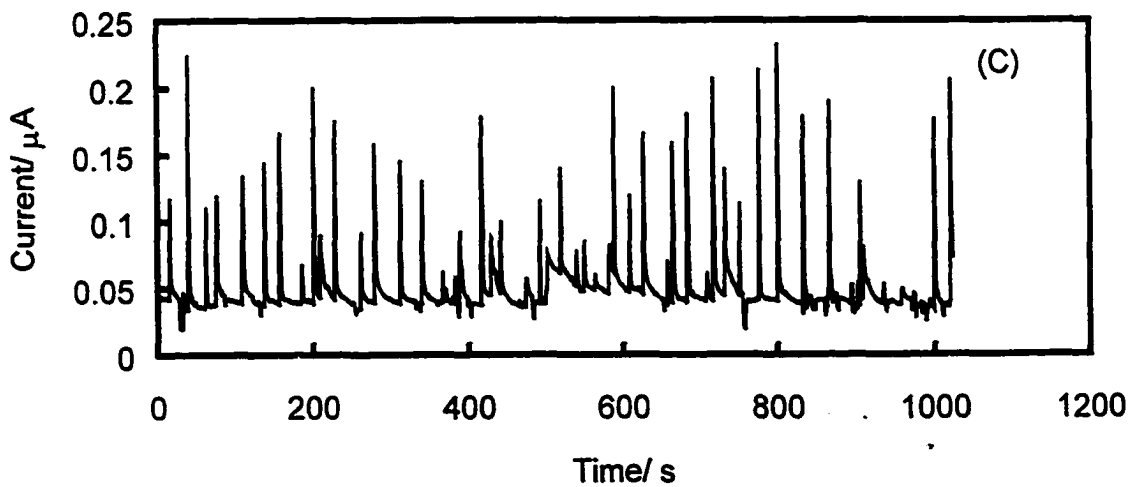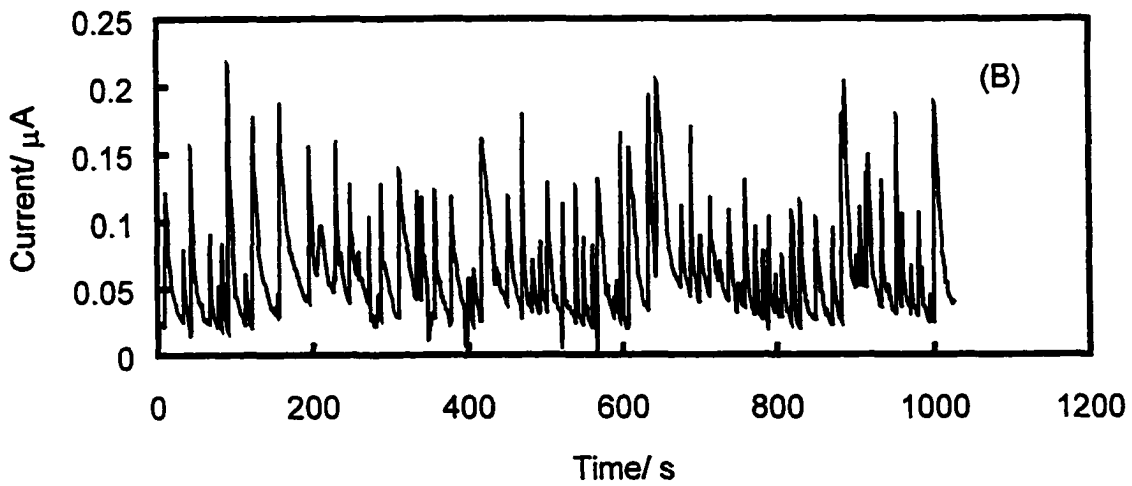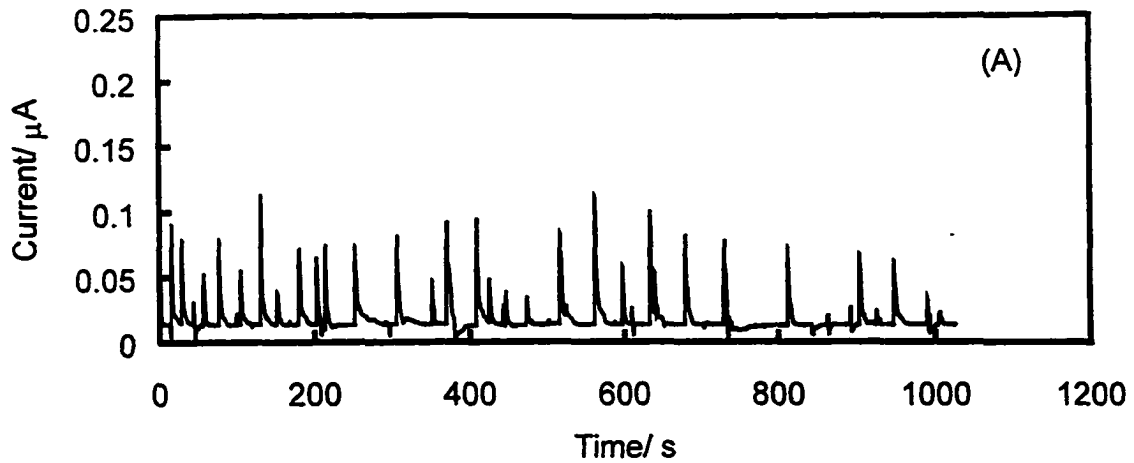
Fig. 4-31 Current noise recordings of A516-70 carbon steel after 1 hour (A), 5 hours (B) and 10 hours (C) of immersion in 0.5 M NaHCO₃ + 0.1 M NaCl solution.

initiation rate, increases with immersion time at the first stage, then decreases after the maximum pitting activity is reached.

It has been discussed that the increase in pitting activity, that is, pit initiation rate, with time in the first stage is mainly caused by the attack of Cl^- on the passive film and the initiation of metastable pits. However, there is indeed a maximum number of potential pit sites on the electrode surface for a given Cl^- concentration. Once a metastable pit grows and repassivates at a given site, that site is no longer available.[37] Therefore, there is a maximum value of pit initiation rate with immersion time. In addition, metastable pits will change towards stable pits when the corrosivity of the solution increases. In general, the higher the Cl^- concentration, the more aggressive the solution, then the higher the pit initiation rate and the easier the transition to stable pits.

The comparison of the Poisson distribution at three immersion times is shown in Fig. 4-32. The data calculated from 1 hour of immersion fell only slightly above the diagonal, indicating that the distribution of pitting events is almost Poissonian. After 5 hours of immersion, the curve was far away from the diagonal and the degree of Poisson distribution dropped. When the immersion time increased to 10 hours, the curve shifted towards the diagonal again. This result clearly indicates that metastable pitting events are non-Poisson in behavior at a higher pitting activity (5 hours of immersion). In the case of lower pitting activity, such as 1 hour and 10 hours of immersion, the pitting events approximately follow a Poisson distribution.

Finally, the autocorrelation for the different immersion stages is calculated and the results are shown in Fig. 4-33. The curve obtained from the data after 1 hour of immersion fell off the fastest in about 2 seconds. This behavior further verifies that there is little correlation among the pitting events after 1 hour of immersion and pitting occurrence is almost Poissonian under this condition. For 5 hours of immersion, the autocorrelation curve fell off more slowly. This is the evidence that the pitting events are interrelated at this stage. After 10 hours, the autocorrelation dropped again and lay between two curves obtained after 5 hours and 1 hour of immersion. These results show that the pitting activity and the cooperative degree of pitting events decrease after the maximum pitting activity is reached. The results from autocorrelation analysis confirm the conclusions obtained from the Poisson analysis.

.

101
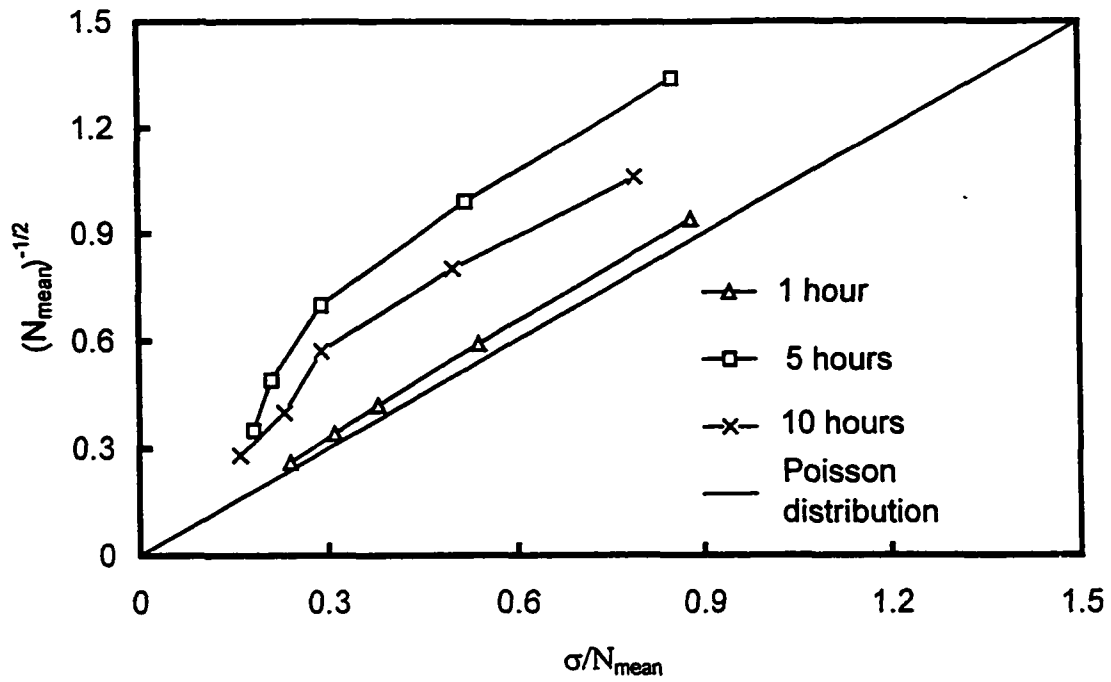
Fig. 4-32 Test for Poisson distribution on the galvanic coupling current of A516-70 carbon steel using the noise data in Fig. 4-34.
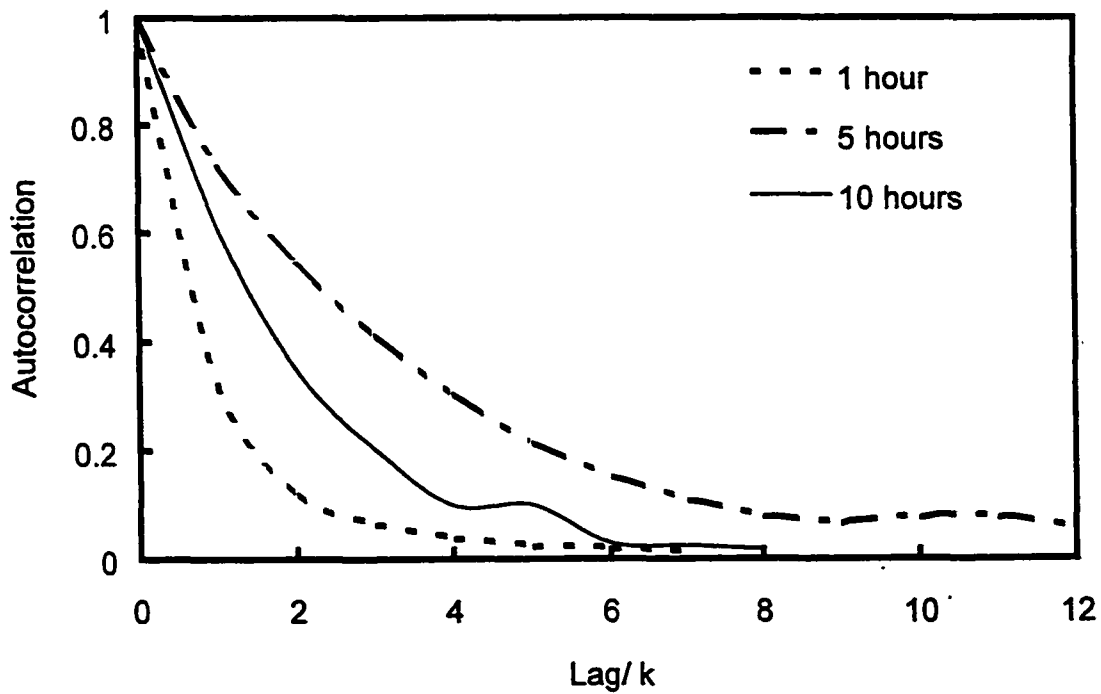
Fig. 4-33 Autocorrelation for the three immersion times on galvanically coupled A516-70 carbon steel using 1,000 points for each curve.

102

Therefore, the metastable pitting activity, qualitatively determined from the current noise recordings in the time domain and the pit initiation rate, increases with the immersion time firstly, and then decreases after a maximum is reached. From the comparison of Poisson distribution and the calculation of the autocorrelation function, it is clear that there is a correlation among the pitting events at a high pitting activity. When the pitting activity decreases, the correlation decreases and the pitting events are close to a Poisson distribution.

4.6.2.2 Carbon steel under potentiostatic control —effect of applied potential

It is believed[6] that increasing potential of the electrode can activate more "susceptible" sites on the electrode surface to initiate pits and lead to an increase in pit initiation rate until the pitting potential is reached. Time series of current noise of A516-70 carbon steel at -150, -50 and 50 mV are presented in Fig. 4-34. The pitting potential is about 80 mV in this system. When the applied potential exceeds the pitting potential, stable pits will develop, and no typical current transient is observed. Therefore, three potentials below U_{pit} were chosen. The feature of the current transients is identical to that measured from the galvanic coupled samples, that is, a quick current rise followed by a slow recovery. The amplitude and the number of current transients increased when the applied potential was increased.

The results of the Poisson analysis at three potentials are shown in Fig. 4-35. When the potential was -150 mV, there was a lower pitting activity and the curve fell almost on the diagonal, where the pitting events follow the Poisson distribution and are independent each other. When the potential increased, the curves displaced from the diagonal, denoting the deviation from the Possion behavior and the greater interaction among pitting events.

The calculated autocorrelation functions for three potentials are shown in Fig. 4-36. For the lowest pitting activity at the lowest potential (-150 mV), the curve fell off the fastest, indicating the smallest correlation of the pitting events. The curves obtained from

103
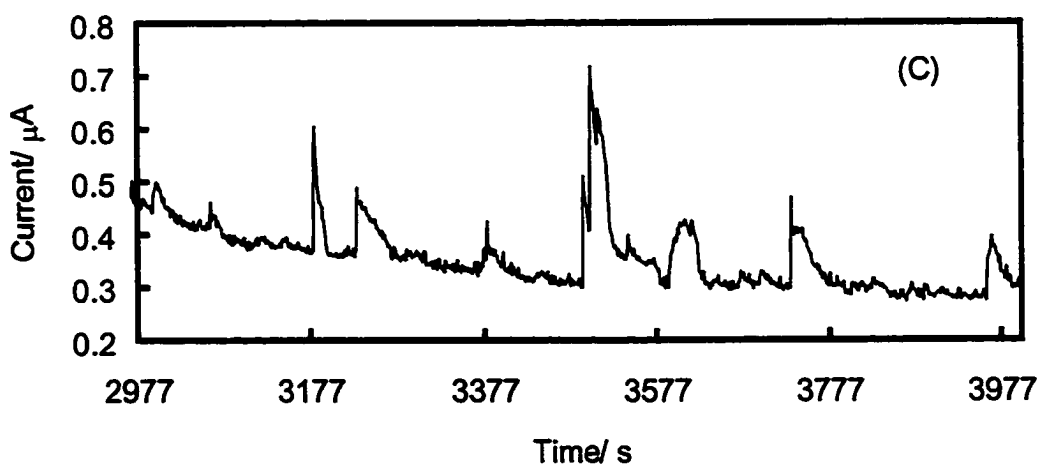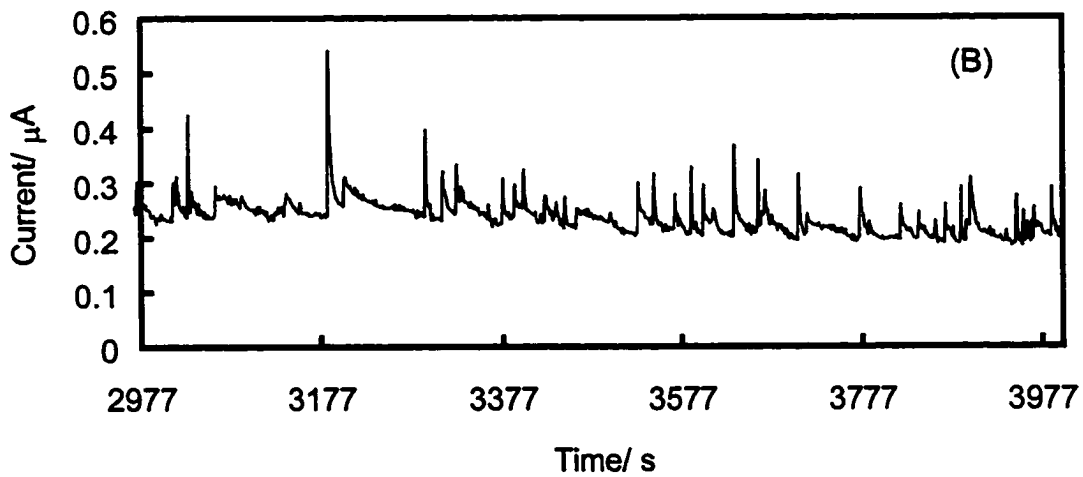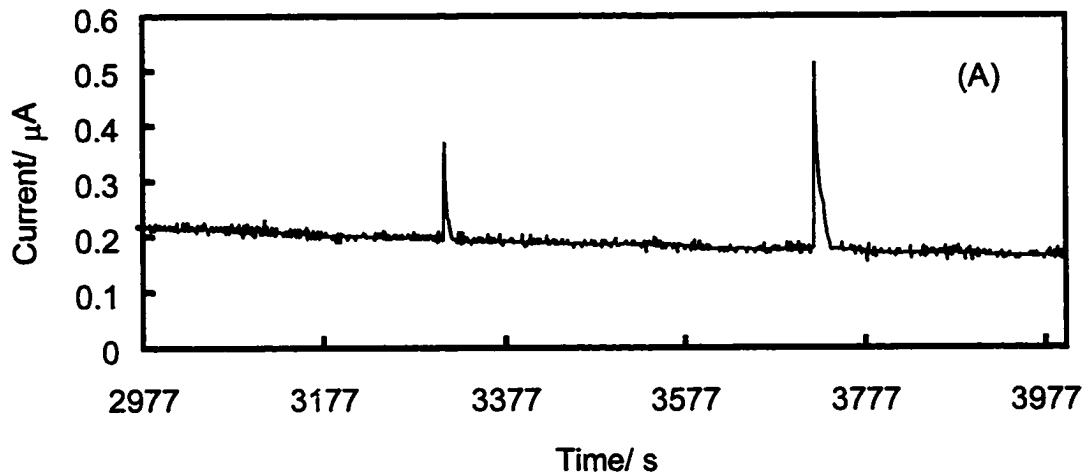
Fig. 4-34 Current fluctuations of A516-70 carbon steel at -150 mV (A), -50 mV (B) and 50 mV (C) after 4000 seconds of immersion in 0.5 M NaHCO₃ + 0.01 M NaCl solution.
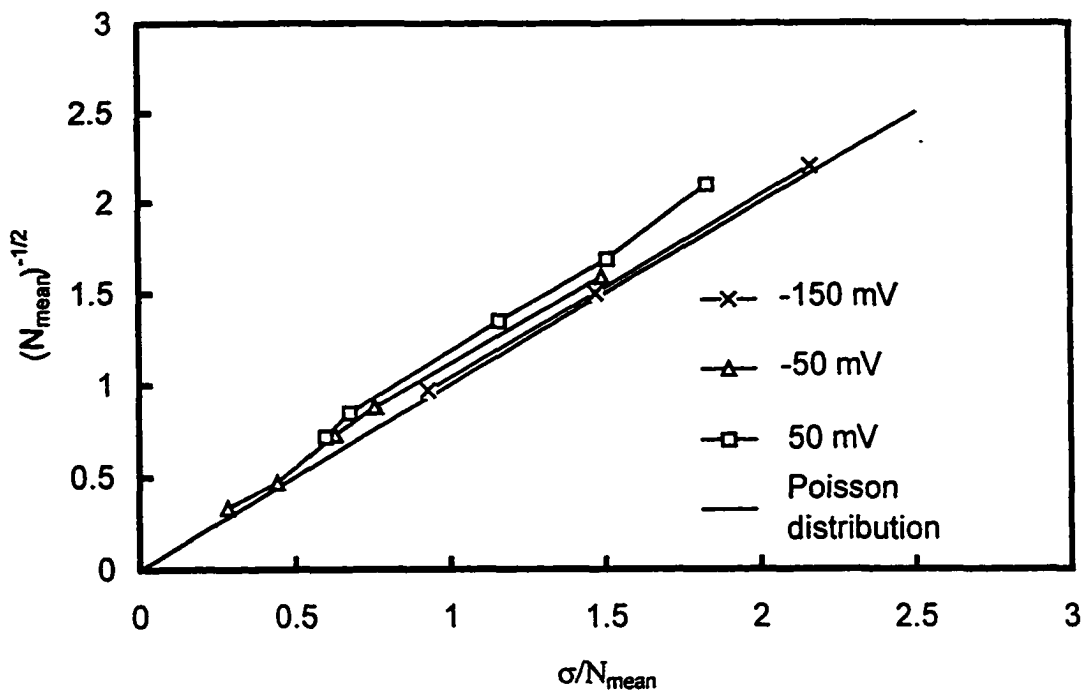
Fig. 4-35 Test for the Poisson distribution for potentiostatic A516-70 carbon steel at -150 mV, -50 mV and 50 mV using the noise data shown in Fig. 4-34.
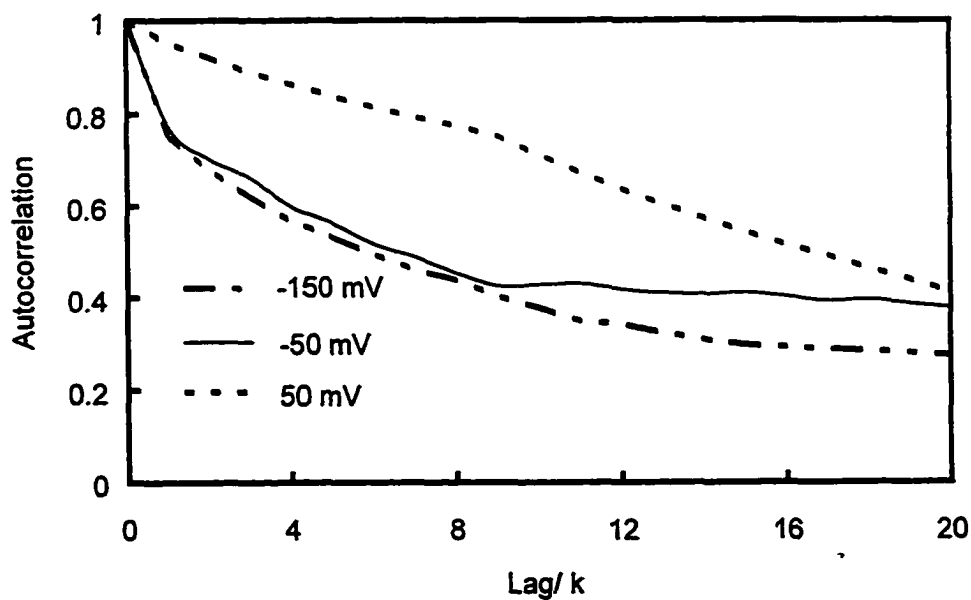
Fig. 4-36 Autocorrelation for the three applied potentials on potentiostatically controlled A516-70 carbon steel using 1,000 points for each curve.

105

the higher potentials fell off more slowly. This is the corroborating evidence that there is certain correlation among pitting events at higher potentials.

4.6.2.3 Carbon steel under potentiostatic control —effect of chloride ion concentration

The concentration of chloride ions is a vital factor affecting the pitting processes. It has been acknowledged[36,93] that the initiation rate of metastable pits and the pitting activity increased with the chloride ion concentration until a critical value, above which the stable pits were induced.

Fig. 4-37 shows the current noise of A516-70 carbon steel immersed in 0.5 M $NaHCO_3$ solution containing 0.01 M, 0.05 M and 0.1 M NaCl. The electrode was potentiostatically controlled at -150 mV considering the fact that the combination of a more positive potential and a higher Cl⁻ concentration will lead to stable pitting, where no typical current transients can be observed. It can be seen that the amplitude of current transients and the pitting initiation rate increases when the concentration of chloride ions increases. Therefore, the pitting activity increases with increasing Cl⁻ concentration.

The comparison of the Poisson distribution at three different concentrations of chloride ions is shown in Fig. 4-38. It is seen that the points calculated from the solution containing 0.01 M Cl⁻ almost lie on the diagonal, indicating a strong Poisson behavior and independent pitting events. Non-Poisson behavior, that is, the deviation of data points from the diagonal, increases with increasing chloride ion concentrations. So the cooperation of pitting events increases when the pitting activity rises due to increasing chloride ion concentration.

In order to confirm the above results, the autocorrelation functions were calculated from the data obtained in the solution containing three Cl⁻ concentrations. The results are shown in Fig. 4-39. The higher the concentration of chloride ions, the more correlated the pitting events. Thus, both the methods of Poisson distribution and autocorrelation function appear to be valid to analyze the cooperation of pitting.
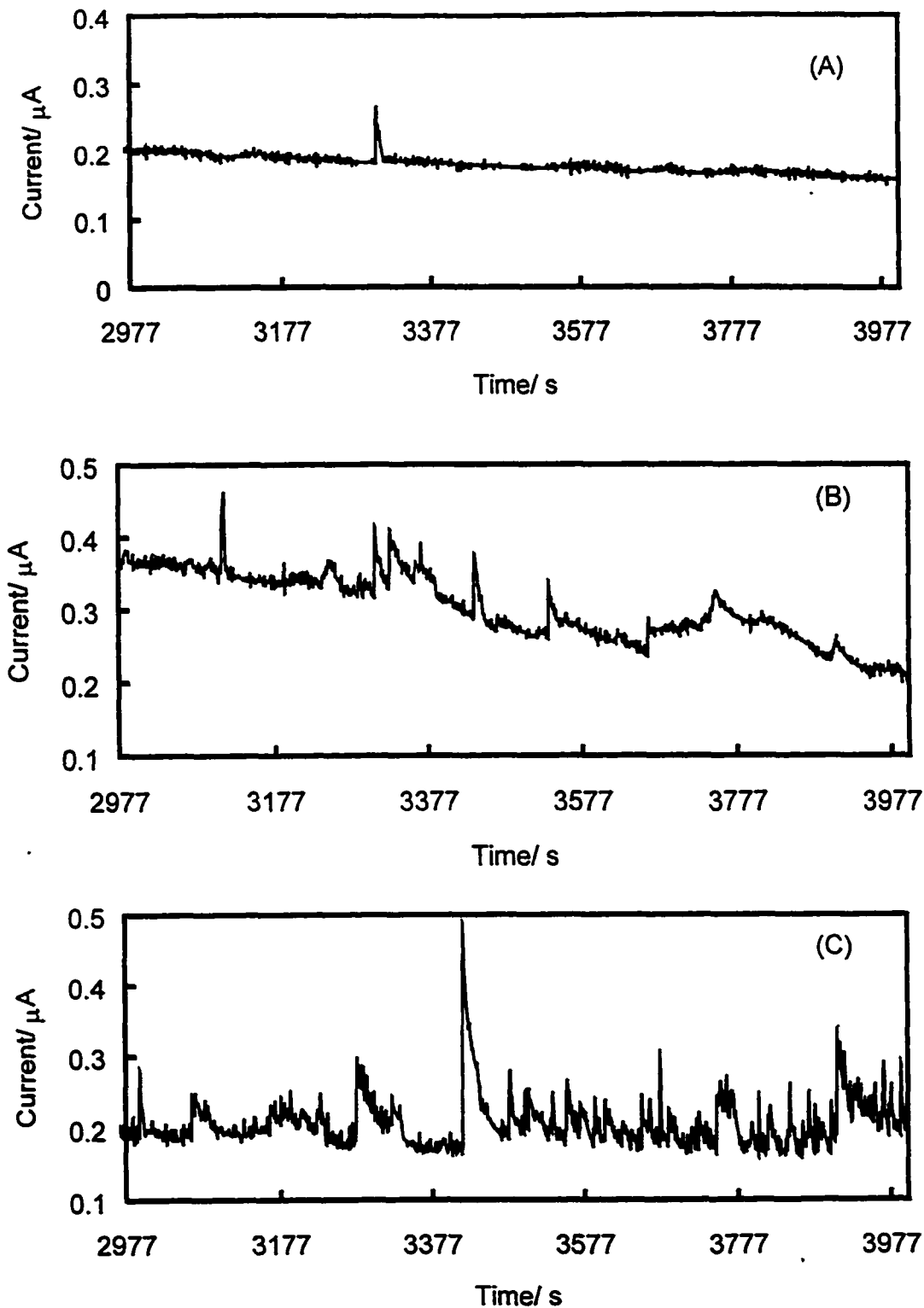
Fig. 4-37 Current fluctuations of A516-70 carbon steel at -150 mV immersed in 0.5 M NaHCO$_3$ solution containing 0.01 M (A), 0.05 M (B) and 0.1 M Cl$^-$ (C).
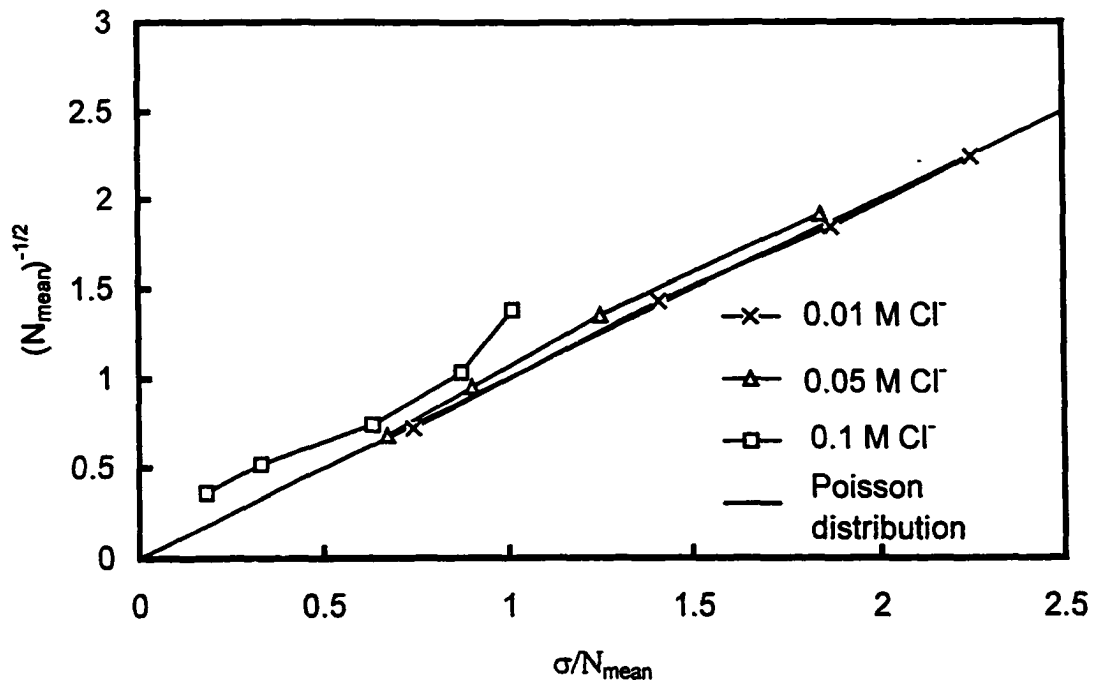
Fig. 4-38 Test for the Poisson distribution on the potentiostatic A516-70 carbon steel at -150mV with different Cl⁻ concentrations using the noise data shown in Fig. 4-37.
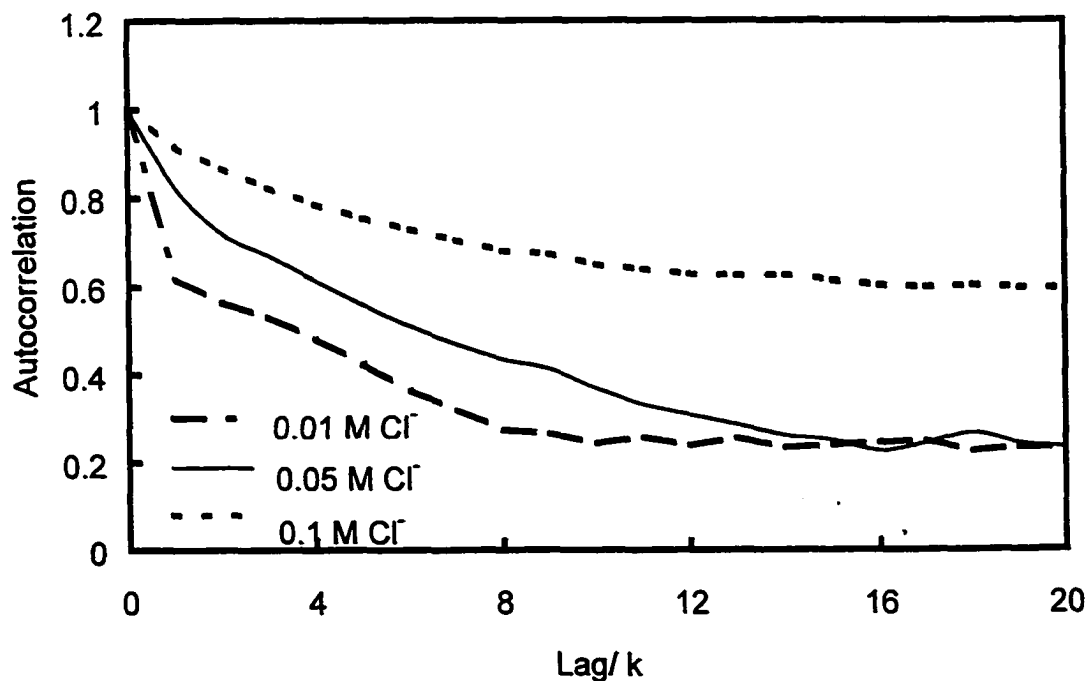
Fig. 4-39 Autocorrelation for the three concentrations of chloride ions on A516-70 carbon steel using 1,000 points for each curve.

4.6.3 Discussion

The experimental results and analysis presented above suggest a complicated picture of the pitting process: the initiation of a metastable pit can have a certain influence on the following pitting events under the condition of a high pitting activity. In such a case a simple Poisson distribution, which has often been assumed to describe pitting,[9,87] is not always suitable to model metastable pitting events. The correlation among pitting events must be assessed before a perfect pitting model is given.

It has been shown that the correlation degree of pitting events reflects the pitting activity. After a carbon steel specimen is immersed in the chloride-containing solution, the pitting activity and the correlation of pitting events increase with the immersion time due to the attack of chloride ions on the passive film. Because of the facts that the potential pitting sites become unavailable after the repassivation of metastable pits and some metastable pits change towards stable pits, a maximum value of the pitting activity will be inevitable. At the stage of higher pitting activity, metastable pits are continually initiated at closely spaced sites. This will allow the acidification of the local pit electrolyte due to hydrolysis of metal cations and the migration of chloride ions until the critical depassivating conditions are achieved. In addition, the aggressive local pit solution will also become more concentrated so as to attain the supersaturated conditions necessary for salt film precipitation.[85] Either of these results is reasonable since the close spatial proximity of two or more metastable pits that form soon after one another can lower the occurrence chance for subsequent pits. Moreover, continual pitting at the connected sites will allow the pit depth to gradually increase, thereby increasing the ohmic voltage drop that can aid pit stabilization.[94] Therefore, after the pitting activity reaches a maximum value, the increase of the total current to a threshold value for the case of multiple interacting pits causes the transition from metastable to stable pitting, which leads to the decrease in metastable pitting activity and correlation among pitting events.

The main role of potential in metastable pitting is to increase the dissolution rate (current density) inside the pit sites and to activate more susceptible sites. The increase in

chloride ion concentration facilitates the pitting initiation by maintaining sufficient transport of chloride ions from the bulk electrolyte to the pits and sustaining the propagation of metastable pits, or by increasing the number of susceptible sites, or decreasing pitting potential. So it is easy to understand the increase in pitting activity and correlation of pitting events when the potential and the concentration of chloride ions increase.

4.7 Design factors affecting the measurements and analysis of electrochemical noise during carbon steel corrosion

The measurements of EN contain the monitoring of current fluctuations under potentiostatic control, and of potential and current fluctuations without external polarization.[2,7,29,75,95] Considering the facts that the mechanisms of initiation and propagation of localized corrosion under potentiostatic control are different from those of a freely corroded electrode,[96] and potentiostatic control will introduce external noise into the measurement system,[97] it is insufficient to use potentiostatic control alone to investigate localized corrosion despite its ability to examine the behavior of the electrode as a function of applied potential. The EN measurements without applied polarization require two nominally identical working electrodes (WE) connected through a zero resistance ammeter (ZRA). Current noise is measured as the current passing between these two electrodes that are exposed to the same environment. Potential noise refers to measurement of the open-circuit potential of two coupled electrodes versus a reference electrode.

The advantages of EN measurements over other electrochemical techniques are apparent. The EN technique can study many semimacroscopic phenomena related to corrosion, which are random in nature, with simple instrumentation and no external polarization. The classic deterministic techniques (steady-state techniques for polarization curves or sine wave techniques for impedance measurement) cannot be performed to understand this special property.

110

Despite the simple configuration of electrodes and instruments in EN measurements, the effects of some design factors are still worthy of clarification. One important question for optimization of the experimental setup is that of the electrode size, since many of the causes of fluctuations do not scale with the geometric surface area.[98] During the evaluation of the effects of electrode size on EN measurements during general corrosion of carbon steel in Na_2SO_4 and H_2SO_4 solutions, Pistorius[99] found that the varied dependence of the standard deviation of current (σI) on the electrode area complicates the attempt to establish a quantitative relationship between σI and corrosion rate. Therefore, it is difficult to normalize noise measurements with respect to the electrode area. The electrode size of an EN probe must be kept constant for comparison of results. Bertocci and Huet[105] also confirmed by computer simulations that there are certain relationships between the electrode area and the magnitude of the standard deviations of current and potential.

Another important factor involving the measurements of EN is the sampling rate. Clearly, sampling rate must exceed a certain minimum value to capture the events that constitute the noise. This minimum value may depend on the rate at which anodic and cathodic areas fluctuate (for general corrosion) or the growth time of metastable pits (for pitting). There are certain critical sampling rates for different systems. Pistorius' work[106] indicated the typically used value of 1 Hz is probably inappropriate to study carbon steel corrosion in sulfuric acid and the sampling rate of 1,000 Hz is sufficient. However, others[9,74] used a sampling rate of 1 Hz to capture various noise features.

During metastable pitting, the current noise recorded by the ZRA reflects the pitting that has occurred on two WEs. It is inevitable that current transients superimpose on each other and negative current transients may appear in some cases. Indeed, the current noise during pitting is more difficult to interpret than the individual anodic process that occurs on each separate electrode. If it is possible to measure the pitting behavior of single electrode, analysis will be easier. This is practicable under potentiostatic control, but the introduction of a potentiostat will eliminate some advantages of EN measurements. Pistorius[106] tried to use two WEs with comparatively different sizes in acid during noise measurements and thought that the measured current noise mainly reflects the anodic

behavior occurring on the smaller electrode with reduced interference from the larger electrode.

The present section is aimed at statistically analyzing the influences of certain design factors, including electrode size, sampling rate and area ratio of two WEs, on the measurements of current and potential noise during A516-70 carbon steel corrosion. The noise analysis results in passivity and general corrosion systems are compared with those obtained in a pitting system.

4.7.1 Selection of corrosion systems

The polarization curves of A516-70 carbon steel in the solutions involving inhibitive HCO_3^- and aggressive Cl^- are shown in Fig. 4-40. It can be seen that A516-70 carbon steel was passivated in 0.5 M HCO_3^- solution. Chloride ions had a dramatically negative effect on carbon steel passivity. When the inhibitive solution contained 0.1 M Cl^-, the passive potential range decreased to about 150 mV and the passive current density also increased. The testing solution of 0.1 M NaCl showed an active dissolution of the carbon steel electrode. Therefore, the electrochemical behavior of A516-70 carbon steel in HCO_3^-, Cl^- and HCO_3^-/Cl^- solutions will reflect passivity, general corrosion and pitting systems, respectively.

4.7.2 Effects of electrode size on noise measurements

Statistical analysis of noise data represents the simplest form of analysis. It can reduce the large number of measurements in a noise recording to a single figure. Various statistical measures have been proposed to identify certain features of the corrosion process,[100,101,102,103] including the standard deviation of current and potential and the noise resistance, which has been taken as a direct measure of the changes of corrosion rate.

Fig. 4-41 shows the relationships between the standard deviation of current and the electrode size for A516-70 carbon steel immersed in 0.5 M HCO_3^-, 0.1 M·Cl^- and 0.5 M HCO_3^- + 0.1 M Cl^- solutions, which reflect passivity, general corrosion, and pitting systems, respectively. It is seen that σ_I increases with increasing electrode area, but with different slopes for different corrosion types. In the cases of passivity and general

112
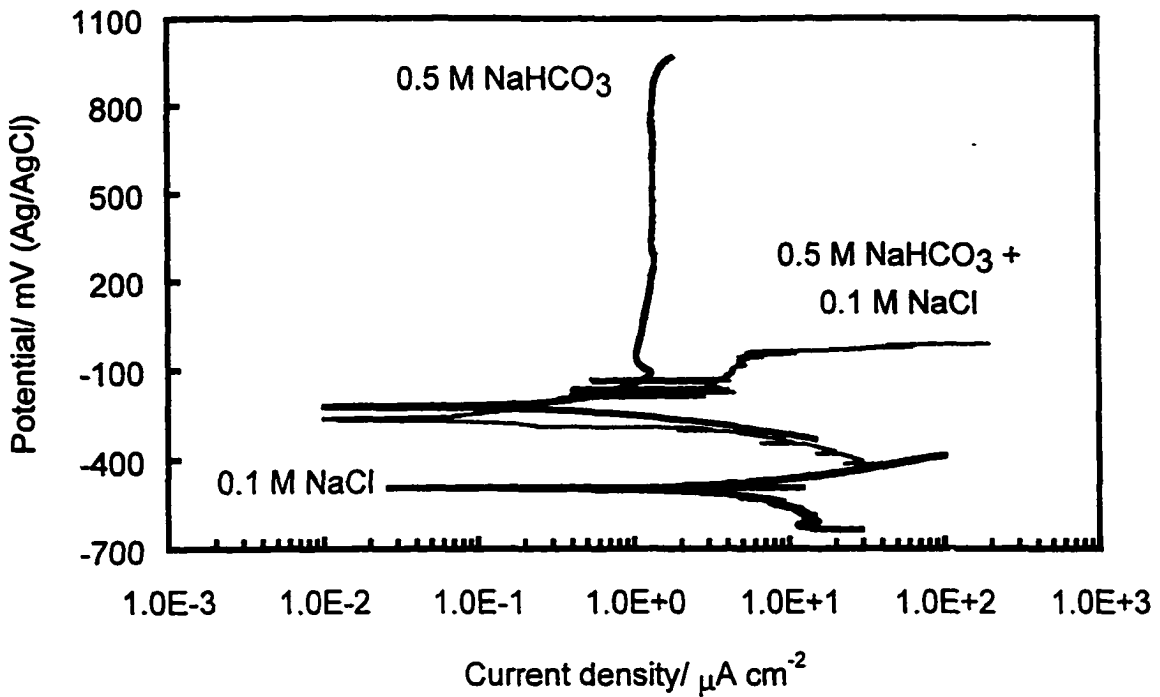
Fig. 4-40 Polarization curves of A516-70 carbon steel in three solutions.
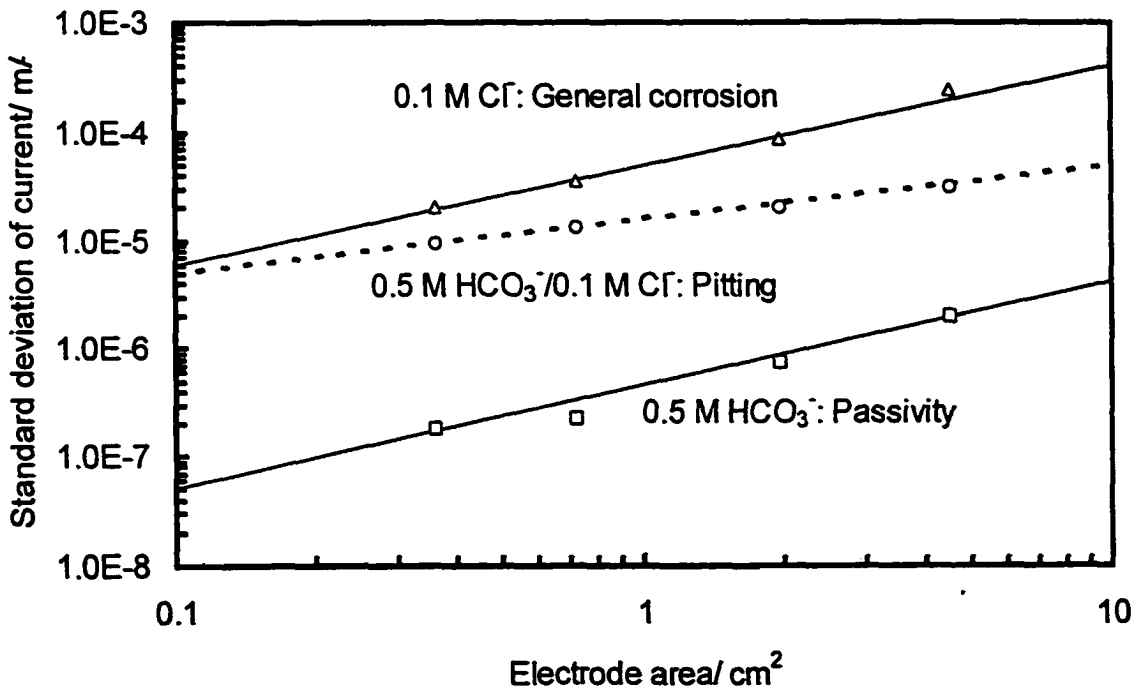
Fig. 4-41 Dependence of the standard deviation of current on electrode area in different corrosion systems.

113

corrosion, σI is proportional to the electrode area; while for pitting, the slope of the linear relation between σI and electrode area is smaller.

Other's work[106] showed that σI is proportional either to the corrosion current density (i_{corr}) or to the square root of the current density (i_{corr})$^{1/2}$, depending on whether the current transients are superimposed or temporally separated. Considering a corrosion system generating one current transient giving a standard deviation of 1 unit, if the corrosion rate is doubled, two transients occur (on average) in the measured time period. The two transients may be separated in time or be superimposed on one another. It is simple to show that, neglecting changes in the average current, the separated case has a standard deviation of $(2)^{1/2}$ units, while the standard deviation of the superimposed case is 2 units.

The same type of relationship is expected between σI and the electrode area. An increase in electrode area should cause an increase in the number of transients in the same way as does an increase in corrosion rate. This effect has been confirmed by simulated noise data.[106] Therefore, for localized corrosion processes where the duration of transients generally is short compared with the average inter-transient time, the square-root relationship is more likely. Proportionality is expected for general corrosion due to the superimposed transients, which fluctuate with a high frequency.

The results presented here show that the proportional relationship between σI and electrode area in passivity is identical to that in general corrosion systems, while the square root relationship is found for pitting. The different values of slope are caused by the current transients, superimposed (in passivity and general corrosion) or separated (in pitting). The noise features in different corrosion systems are apparently identified in their time recordings (Figs. 4-3, 4-5 and 4-42). The transient feature is not apparent in the case of general corrosion due to the large amplitude of the current combined with the large scale of the axis.

The varying dependence of σI on electrode area in different corrosion systems makes it impossible to establish a quantitative relationship between corrosion rate and

114
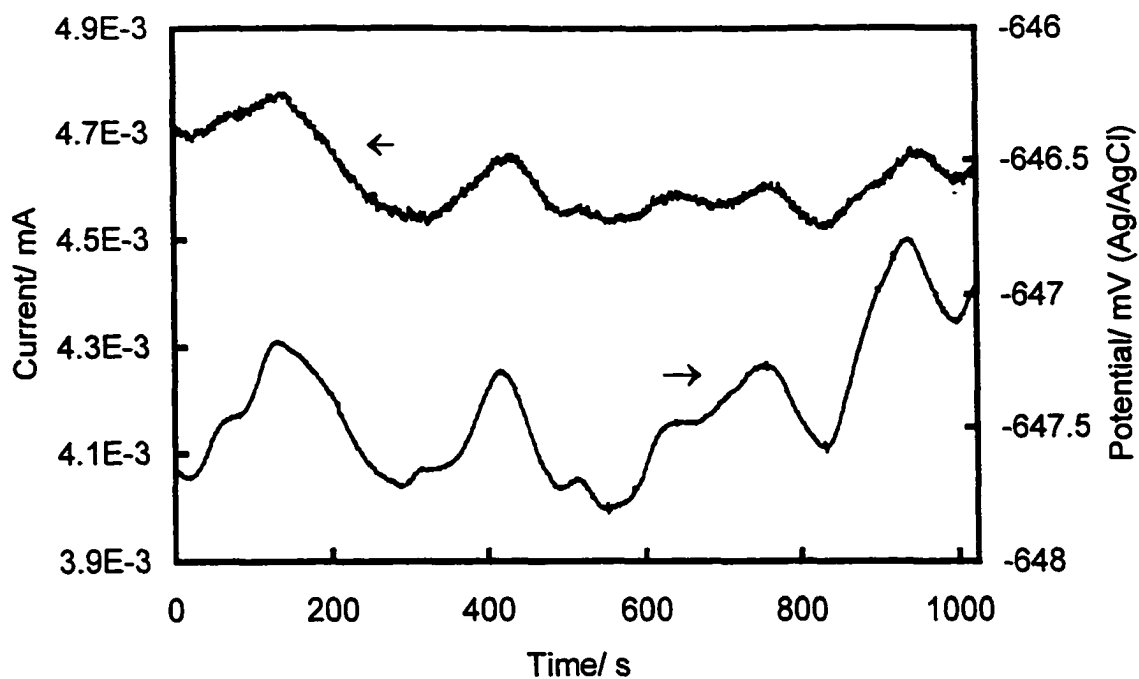
Fig. 4-42 Potential and current noise recorded in 0.1 M NaCl solution.
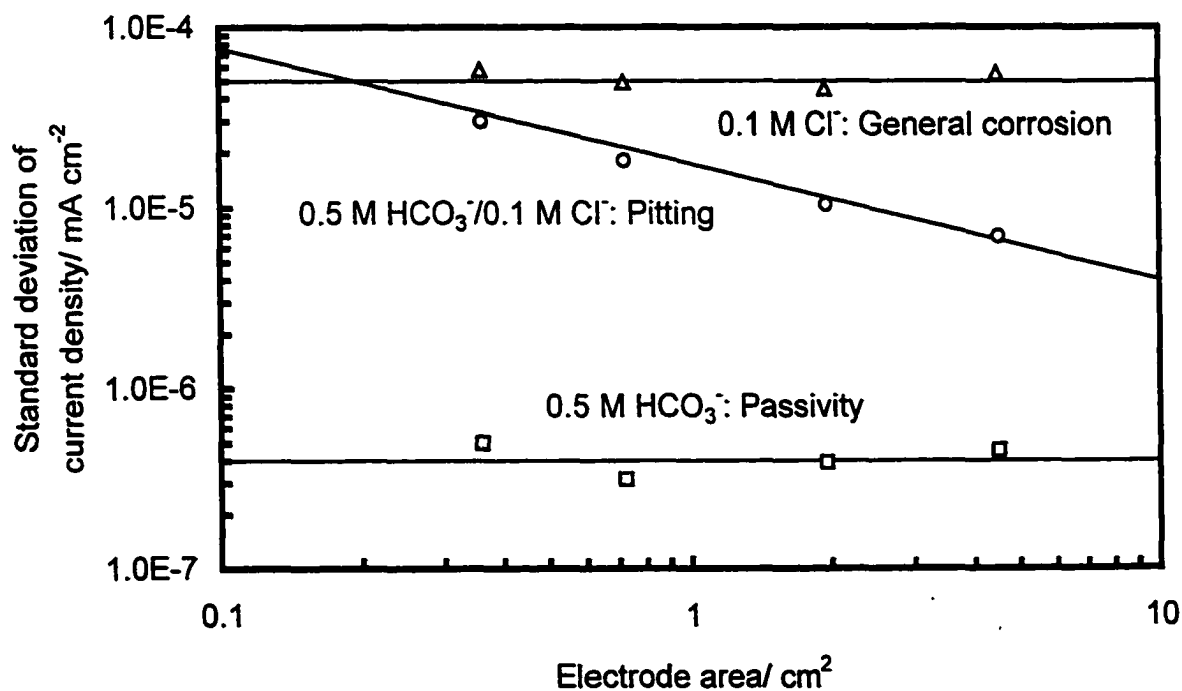
Fig. 4-43 Dependence of the standard deviation of current density on electrode area in different corrosion systems.

115

electrode area. For example, the corrosion rate is normally expressed as a current density, which is independent of the electrode size. No such simple relationship is available for pitting corrosion, since, if σI increase with the square root of the area, $\sigma I/S$ is inversely proportional to the square root of the electrode area. Therefore, the quantitative relationship between corrosion rate and electrode size depends on the corrosion type.

From Fig. 4-43, it is clear that the corrosion rate (current density) is independent of the electrode area for general corrosion and passivity systems. It is not true for pitting corrosion. In such a case, the current density is inversely proportional to the square root of electrode area. Therefore, the choice of electrode size in an EN probe is very important and must be kept constant for a comparison of the corrosion rate based on noise data during pitting.

Although the dependence of the standard deviation of potential (σU) on the electrode area also follows similar situations relating to superposition or separation of noise transients, the potential transients are usually superimposed even during pitting corrosion due to the damping effects of the electrode capacitance on potential.[106] Another point worth considering is that, with increasing electrode area, both the electrode capacitance and the area for cathodic reactions increase. Hence, the amplitude of the potential fluctuations in response to the current fluctuations is inversely proportional to electrode size. Fig. 4-44 shows the effects of electrode area on σE for A516-70 carbon steel in different corrosion systems.

Because the noise resistance (R_n) is equal to the ratio of σU to σI, its area dependence follows from those of the potential and current noise. Fig. 4-45 shows the area dependence of R_n of A516-70 carbon steel in different solutions. It is seen that R_n decreases with increasing electrode area. There is the largest R_n when the specimen is in passivity. Compared with the area dependence of R_n in general corrosion, R_n in pitting decreases more quickly, indicating stronger pitting aggressivity for the larger electrode. Therefore, R_n is a qualitative measure of the changes of corrosion activity.
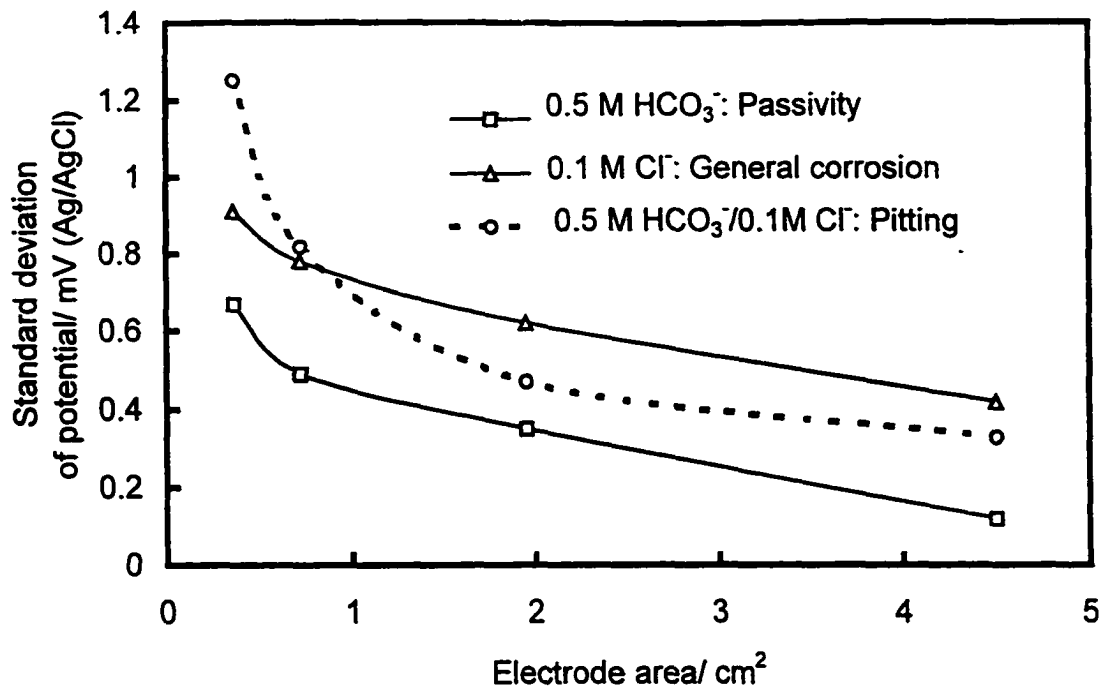
Fig. 4-44 Dependence of the standard deviation of potential on the electrode area in different corrosion systems.
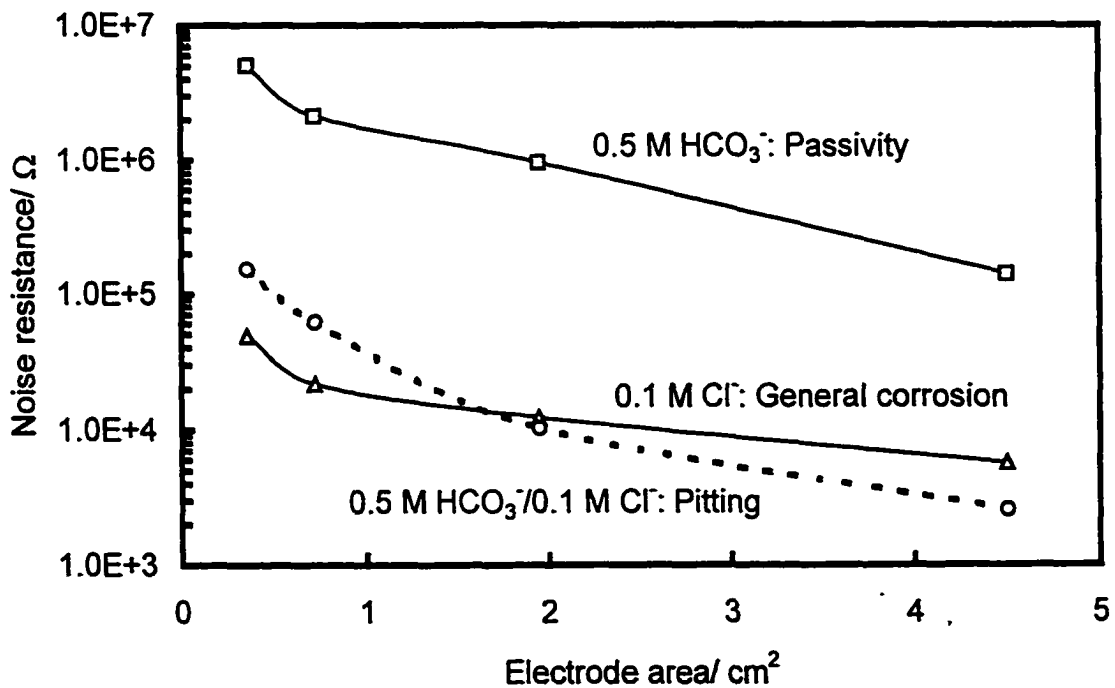
Fig. 4-45 Dependence of the noise resistance on the electrode area in different corrosion systems.

117

4.7.3 Effects of sampling rate on noise measurements

The appropriate sampling rate during EN measurements is not immediately apparent although many researchers chose and standardized on a rate of 1 Hz. A basic requirement for an appropriate sampling rate is that it must reach the minimum value to reflect the events that constitute the recorded noise, i.e., the fundamental information can be extracted by time-domain analysis of noise transients.

Considering the inherently damped nature of potential noise, basic information involving the sampling rate is probably most conveniently extracted from the current noise. Fig. 4-46 shows the measured noise signals for A516-70 carbon steel in HCO_3^-/Cl^- solution, which is a pitting system, at four sampling rates. The noise transients measured at an appropriate sampling rate must reflect the unit of the pitting process, that is, initiation, propagation and repassivation of metastable pits. Clearly, the nature of the noise signal is lost when the sampling rate is 0.5 Hz. For the sampling rates of 1 Hz, 2 Hz, and 20 Hz, the typical current transients characterizing the metastable pitting processes of carbon steel are apparent. These transients have a common feature: a quick current rise followed by a slow drop. With an increase in sampling rate, the number of current transients per unit time increases. Although it might be possible to miss some pitting transients at a small sampling rate, the sampling rate of 1 Hz is appropriate enough to reflect the features of metastable pitting of carbon steel in this work.

4.7.4 Effects of the area ratio of two coupled electrodes on noise measurements

In considering an EN probe containing two nominally identical electrodes, it is assumed that the measured noise is the result of the fluctuations of anodic activity on the electrodes, and that the cathodic activity is the same on the two electrodes. It is further assumed that, at a given moment, the anodic current densities on the two electrodes (i_1 and i_2) vary with time, leading to the measured electrochemical current noise, while cathodic current (i_c) is the same on both electrodes, fluctuating to balance the anodic current. Under this assumption, the cathodic current density is given by:
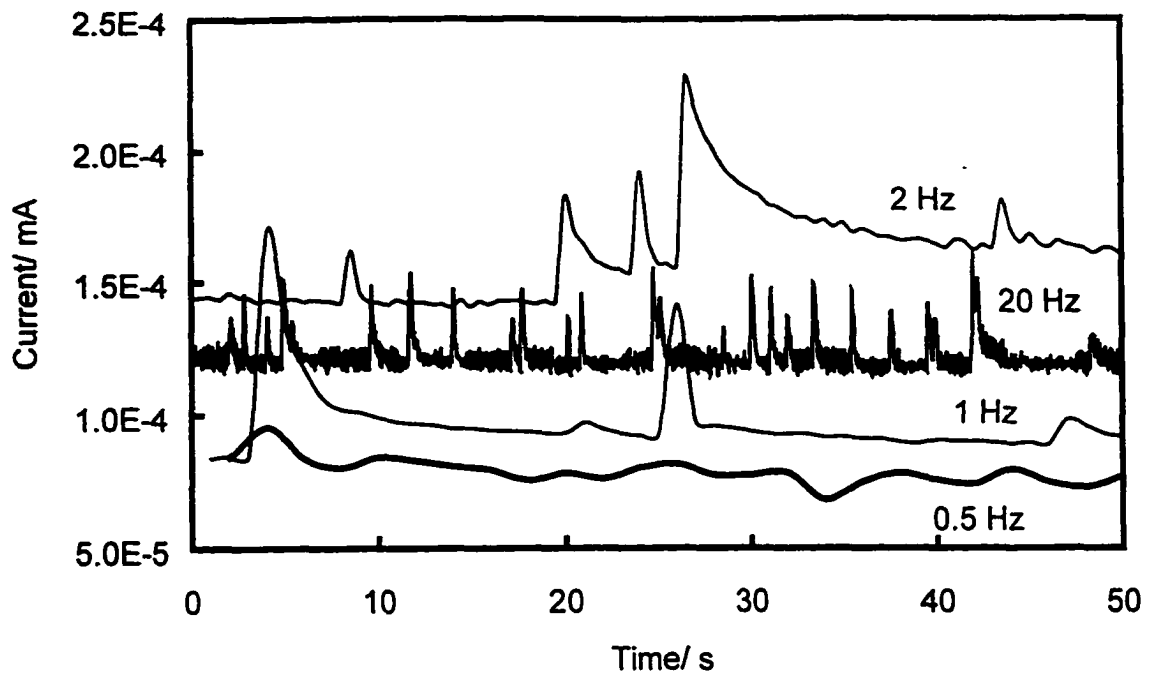
Fig. 4-46 Effect of the sampling rate on noise measurements.
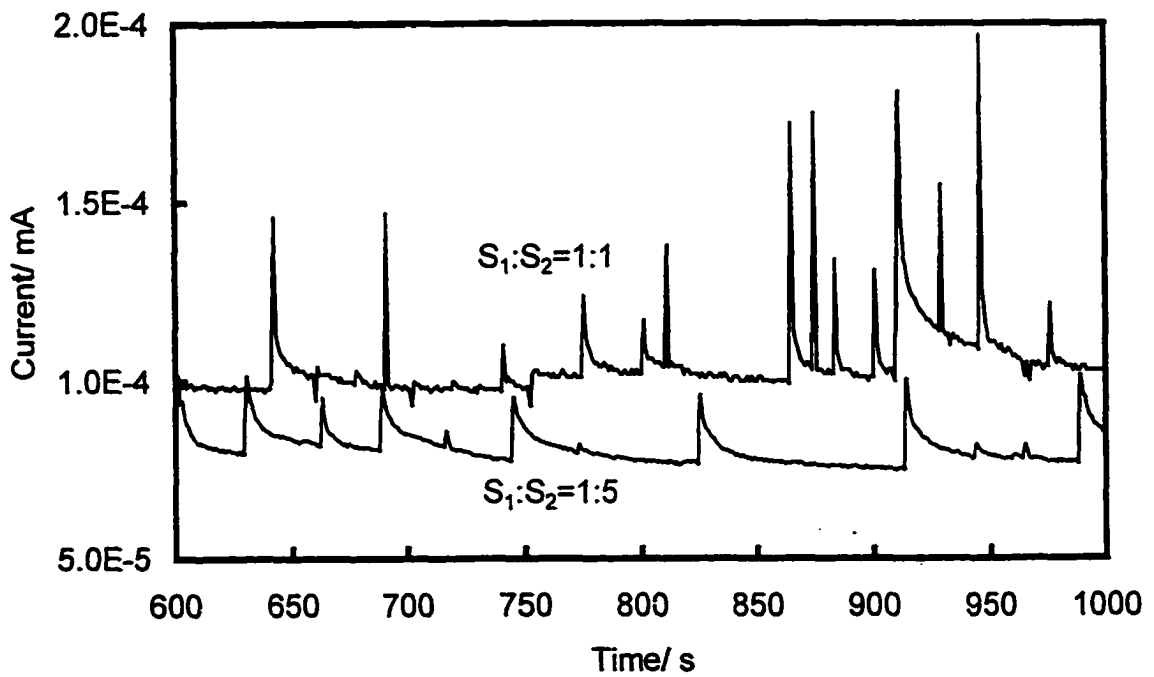
Fig. 4-47 Current noise recordings of A516-70 carbon steel electrode with different area ratio in HCO_3^-/Cl^- solution.

119

$$i_c = \frac{i_1 S_1 + i_2 S_2}{S_1 + S_2}$$

(4-27)

where S_1 and S_2 are the area of the two electrodes. The noise current (I) between two electrodes, through the ZRA, is equal to the amount by which the anodic current on each of the electrodes is not balanced by the cathodic current on that electrode. If the charge balance is performed at electrode 1, and if conventional current in the external circuit from electrode 2 to electrode 1 through the ammeter is taken to be positive, the noise current is given by:

$$I = i_1 S_1 + i_c S_1$$

(4-28)

The expression of the noise current can be achieved by substituting the expression of i_c in Eq. 4-24 by Eq. 4-23:

$$I = (i_1 - i_2)\frac{S_1 S_2}{S_1 + S_2} = (i_1 - i_2)\frac{S_1}{\frac{S_1}{S_2} + 1}$$

(4-29)

If the EN probe consists of two electrodes with very different areas, the current flowing through the ammeter due to the larger electrode will be smoother than that due to the smaller electrode. If the areas of two electrodes are much different (for example, $S_1 << S_2$), the instantaneous anodic current density on the larger electrode (i_2) is approximately constant with time, and the current measured by the ammeter, $I = S_1(i_1 - i_2)$, is simply the instantaneous current on the smaller electrode ($S_1 i_1$), offset by a constant value. So this approach allows the electrochemical behavior of one electrode in a noise couple to be measured.

Fig. 4-47 shows a comparison of the current noise for A516-70 carbon steel couples with area ratios of 1:1 and 1:5 in 0.05 M HCO_3^- + 0.1 M Cl^- solution. The current

120

transients measured in both cases are characterized by a quick current rise followed by a slow recovery, reflecting the metastable pitting of carbon steel. For the coupled electrodes with the same size, the stochastic current transients have quiet different values of the noise amplitude and the repassivation time. Some negative current transients are also observed. The current transients recorded in a couple with the area ratio of 1:5 are more regular. The approximately identical noise amplitudes approaching 50 nA and a repassivation time of about 15 seconds might be caused by the pitting occurring on the smaller electrode alone. This result shows how a comparatively different area ratio of two coupled electrodes clarifies the time-domain interpretation of the noise transients.

4.8   Conclusions

*   During the incubation period of pitting on carbon steel, the fluctuations of potential trace the current fluctuations and the faradaic current plays a major role in the electrode process. The initiation of metastable pits is indicated by the typical potential and current transients in the shape of a quick drop in potential and rise in current followed by a slow recovery.

*   Electrode capacitance plays a major role in the fluctuations of the potential. Only the current fluctuations reflect the initiation, growth and repassivation of metastable pits.

*   During metastable pitting of carbon steel under potentiostatic control, the deposited cover over the pit mouth plays an important role in sustaining pit growth and causing repassivation, and, consequently, in producing the typical current transients.

*   The pitting initiation rate increases with the applied potential, and then decreases after a maximum is reached. The potential dependence of the pit initiation rate is well illustrated by a point defect model. Pit growth kinetics are controlled by the ohmic potential drop across the cover over the pits. The potential dependence of the repassivation time mainly comes from the effect of applied potential on the pit cover. The increase of potential promotes the rupture of the pit cover, and leads to a decrease of repassivation time.

121

* A stabilization criterion of the metastable pits, the ratio of the peak pit current to the pit radius, must exceed 2×10^{-2} A cm^{-1} at all times during pit growth to avoid repassivation. The pit stabilization criterion indicates the critical condition to maintain pit growth. Below this value the pit anolyte is not aggressive enough to maintain pit growth and repassivation is inevitable.

* Chloride ions are responsible for the degradation of carbon steel passivation in 0.5 M bicarbonate solution. The main role of Cl$^-$ in pitting is to increase the chance of the breakdown of the passive film, rather than to inhibit the surface repassivation.

* Metastable pitting of carbon steel is non-Poisson behavior and the initiation of a metastable pit will have a certain influence on subsequent pitting events in the case of a high pitting activity, such as a critical immersion stage, a higher applied potential (not exceeding the pitting potential) and a higher Cl$^-$ concentration. When the pitting activity decreases, the metastable pitting events will follow a Poisson distribution.

* The corrosion rate (current density) of A516-70 carbon steel is independent of the electrode size for general corrosion and passivity systems, while the corrosion rate is inversely proportional to the square root of the electrode area for pitting. The quantitative relationship between corrosion rate and electrode size depends on the corrosion type. The sampling rate of 1 Hz is appropriate to reflect the features of metastable pitting on carbon steel in this work. A comparatively different area ratio of two coupled electrodes can allow the instantaneous anodic current on the smaller electrode to be measured with reduced interference from processes on the larger electrode, and thus clarify the time-domain interpretation of the noise transients.

References

1. C. Gabrielli, F. Huet, M. Keddam and R. Oltra, *Corrosion* 46, 266 (1990).

2. J.L. Dawson, in *Electrochemical Noise Measurement for Corrosion Applications*, J.R. Kearns, J.R. Scully, P.R. Roberge, D.L. Reichert and J.L. Dawson, Editors, p. 3, ASTM STP 1277, West Conshohocken, PA (1996).

122

3. C. Gabrielli, F. Huet and M. Keddam, in *Electrochemical and Optical Techniques for the Study and Monitoring of Metallic Corrosion*, M.G.S. Ferreira and C.A. Melendres, Editors, p. 135, Kluwer Academic Publishers, Netherlands (1991).

4. J.B. Lumsden, M.W. Kendig and S. Jeanjaquet, in *Corrosion '92*, paper no. 224, NACE, Houston, TX (1992).

5. C. Gabrielli, F. Huet, M. Keddam, R. Oltra and C. Pallotta, in *Passivity of Metals and Semiconductors*, M. Froment, Editor, p. 293, Elsevier, Amsterdam, Netherlands (1983).

6. P.C. Pistorius and G.T. Burstein, *Phil. Trans. Royal Soc. Lond.* A341, 531 (1992).

7. S.T. Pride, J.R. Scully and J.L. Hudson, *J. Electrochem. Soc.* 141, 3028 (1994).

8. G.S. Frenkel, L. Stockert, F. Hunkeler and H. Bohni, *Corrosion* 43, 429 (1987).

9. M. Hashimoto, S. Miyajima and T. Murata, *Corros. Sci.* 33, 885 (1992).

10. S. Magaino, A. Kawaguchi, A. Hirata and T. Osaka, *J. Electrochem. Soc.* 134, 2993 (1987).

11. P.R. Roberge, S. Wang and R. Roberge, *Corrosion* 52, 733 (1996).

12. C. Bataillon and C. Fiaud, *Materials Science Forum* 8, 141 (1986).

13. J. Stewart and D.E. Williams, *Corros. Sci.* 33, 457 (1992).

14. C. Monticelli, G. Brunoro, A. Frignanai and G. Trabanelli, *J. Electrochem. Soc.* 139, 693 (1992).

15. P.C. Pistorius, in *Electrochemical Noise Measurement for Corrosion Applications*, J.R. Kearns, J.R. Scully, P.R. Roberge, D.L. Reichert and J.L. Dawson, Editors, p. 343, ASTM STP 1277, West Conshohocken, PA (1996).

16. H.S. Isaacs and Y. Ishikawa, *J. Electrochem. Soc.* 132, 1288 (1985).

17. S.T. Pride, J.R. Scully and J.L. Hudson, in *Electrochemical Noise Measurement for Corrosion Applications*, J.R. Kearns, J.R. Scully, P.R. Roberge, D.L. Reichert and J.L. Dawson, Editors, p. 307, ASTM STP 1277, West Conshohocken, PA (1996).

18. D.H. Davies and G.T. Burstein, *Corrosion* 36, 416 (1980).

19. C.R. Valentini, C.A. Moina, J.R. Vilche and A.J. Arvia, *Corros. Sci.* 25, 985 (1985).

20. E.B. Castro, C.R. Valentini, C.A. Moina and J.R. Vilche, *Corros. Sci.* 26, 781 (1986).

21. J.O. Zerbino, J.R. Vilche and A.J. Arvia, *J. Appl. Electrochem.* 11, 703 (1981).

22. E.B. Castro, J.R. Vilche and A.J. Arvia, *Corros. Sci.* 32, 37 (1991).

23. D.D. MacDonald, *J. Electrochem. Soc.* 139, 3434 (1992).

24. T. Shibata, *Corrosion* 52, 813 (1996).

25. G. Daufin, J. Pagetti, J.P. Labbel and F. Michel, *Corrosion* 41, 533 (1985).

26. B.D. Cahan and C.T. Chen, *J. Electrochem. Soc.* **129**, 921 (1982).

27. R.D. Armstrong and K. Edmondons, *Electrochim. Acta* **18**, 937 (1973).

28. H. Bohni, *Materials Science Forum* **111-112**, 401 (1992).

29. L.Stockert and H. Bohni, *Materials Science Forum* **44 & 45**, 313 (1989).

30. N. Sato, *J. Electrochem. Soc.*, **129** 255 (1982).

31. P. C. Pistorius and G. T. Burstein, *Corros. Sci.* **33**, 1885 (1992).

32. D. E. Williams, C. Westcott and M. Fleischmann, *J. Electrochem. Soc.* **132**, 1804 (1985).

33. H. S. Isaacs, *Corros. Sci.* **29**, 313 (1989).

34. D. E. Williams, J. Stewart and P. H. Balkwill, in *Critical Factors in Localized Corrosion*, G. S. Frankel and R. C. Newman, Editors, **PV 92-9**, p. 36, The Electrochemical Society Proceedings Series, Pennington, NJ (1992).

35. G. T. Burstein, P.C. Pistorius and S. P. Mattin, *Corros. Sci.* **35**, 57 (1993).

36. P. C. Pistorius and G. T. Burstein, *Corros. Sci.* **36**, 525 (1994).

37. P. C. Pistorius and G. T. Burstein, *Materials Science Forum* **111-112**, 429 (1992).

38. L. Stockert and H. Bohni, in *Proc. 8th Europ. Corr. Cong.*, p. 22, Centre Francaise de la Corrosion, Paris (1985).

39. F. Hunkeler and H. Bohni, *Corrosion* **37**, 645 (1981).

40. Y.F. Cheng, J.L. Luo and M. Wilmott, in *Corrosion'98*, paper no. 389, NACE, San Diego (1998).

41. Y.F. Cheng, M. Wilmott and J.L. Luo, *Corros. Sci.* **41**, 1245 (1999).

42. H. S. Isaacs, in *Localized Corrosion*, B. F. Brown, J. Kruger and R. W. Staehle, Editors, p. 158, NACE, Houston, Texas (1974).

43. R. Holliger and H. Bohni, in *Proceedings of the Symposium on Computer Aided Acquisition and Analysis of Corrosion Data*, M. W. Kendig, U. Bertocci, and J. E. Strutt, Editors, **PV 85-3**, p. 200, The Electrochemical Society Proceedings Series, Pennington, NJ (1985).

44. D.D. Macdonald, S. Biaggio and H. Song, *J. Electrochem. Soc.* **139**, 171 (1992).

45. A. Goossens, M. Vazquez and D.D. Macdonald, *Electrochimica Acta* **41**, 35 (1996).

46. E. Sikora, J. Sikora and D.D. Macdonald, *Electrochimica Acta* **41**, 783 (1996).

47. C.B. Breslin, D.D. Macdonald, J. Sikora and E. Sikora, *Electrochimica Acta* **42**, 127 (1997).

48. L.F. Lin, C.Y. Chao and D.D. Macdonald, *J. Electrochem. Soc.* **128**, 1194 (1981).

49. M. Hashimoto, S. Miyajima and T. Murata, *Corros. Sci.* **33**, 905 (1992).

50. H. Ezuber, A. J. Betts and R. C. Newman, *Materials Science Forum* **44&45**, 247 (1989).

51. K. J. Vetter and H. H. Strehblow, in *Localized Corrosion*, R. W. Staehle, B. F. Brown, J. Kruger, A. Agrawal, Editors, p. 240, NACE, Houston, Texas (1974).

52. C. Gabrielli, F. Huet, M. Keddam and R. Oltra, *Corrosion* **46**, 266 (1990).

53. T. Hakkarainen, in *Advances in Localized Corrosion*, H.S. Isaacs, U. Bertocci, J. Kruger and S. Smialowska, Editors, p. 277, NACE, Houston, TX (1990).

54. H.C. Kuo and D. Landolt, *Electrochim. Acta* **20**, 393 (1975).

55. J.R. Galvele, *J. Electrochem. Soc.* **123**, 464 (1976).

56. A.N. Rothwell and A.N. Eden, in *Corrosion '92*, paper no. 223, NACE, Nashville (1992).

57. U.R. Evans, *Corrosion* **7**, 238 (1951).

58. Z. Szklarska-Smialowska, in *Pitting Corrosion of Metals*, p. 136, NACE, Houston, TX (1986).

59. M.G.S. Ferreira and A.M.P. Simoes, in *Electrochemical and Optical Techniques for the Study and Monitoring of Metallic Corrosion*, M.G.S. Ferreira and C.A. Melendres, Editors, p. 485, Kluwer Academic Publishers, Netherlands (1991).

60. J.R. Galvele, J.B. Lumsden and R.W. Staehle, *J. Electrochem. Soc.* **125**, 1204 (1978).

61. J.A. Richardson and G.C. Wood, *Corros. Sci.* **10**, 313 (1970).

62. J.L. Dawson and M.G.S. Ferreira, *Corros. Sci.* **26**, 1009 (1986).

63. T.P. Hoar and W.R. Jacob, *Nature* **216**, 1209 (1967).

64. C.Y. Chao, F.L. Lin and D.D. Macdonald, *J. Electrochem. Soc.* **128**, 1187 (1981).

65. M. Urquidi and D.D. Macdonald, *J. Electrochem. Soc.* **132**, 555 (1985).

66. T. P. Hoar, *Corros. Sci.* **7**, 335 (1967).

67. N. Sato, *Electrochim. Acta* **16**, 1683 (1971).

68. I.L. Rozenfeld and I.K. Marshakov, *Corrosion* **20**, 115 (1964).

69. M.A. Heine, D.S. Keir and M.S. Pryor, *J. Electrochem. Soc.* **112**, 24 (1965).

70. G. Okamoto, *Corros. Sci.* **13**, 471 (1973).

71. R.C. Newman, in *Corrosion Chemistry within Pits, Crevices and Cracks*, A. Turnbull, Editor, p. 14, HMSO, London (1987).

72. H.P. Leckie and H.H. Uhlig, *J. Electrochem. Soc.* **113**, 1262 (1966).

73. Z. Szklarska-Smialowska, in *Pitting Corrosion of Metals*, p. 201, NACE, Houston, Texas (1986).

74. U. Bertocci and Y.X. Ye, *J. Electrochem. Soc.* **131**, 1011 (1984).

75. J.C. Uruchurtu and J.L. Dawson, *Corrosion* **43**, 19 (1987).

125

76. K. Videm and A.M. Koren, *Corrosion* **49**, 746 (1993).

77. B. Delanty and J. O'Beirne, *Oil Gas J.* **6**, 39 (1992).

78. R.N. Parkins and P.M. Singh, *Corrosion* **46**, 485 (1990).

79. R.W. Revie and R.R. Ramsingh, *Can. Metall. Q.* **22**, 235 (1983).

80. B. Baroux, *Corros. Sci.* **28**, 969 (1988).

81. D.E. Williams, C. Westcott and M. Fleischmann, *J. Electroanal. Chem.* **180**, 549 (1984).

82. D.E. Williams, C. Westcott and M. Fleischmann, *J. Electrochem. Soc.* **132**, 1796 (1985).

83. D.E. Williams, C. Westcott and M. Fleischmann, *J. Electrochem. Soc.* **132**, 1804 (1985).

84. U. Bertocci, M. Koike, S. Leigh, F. Qiu and G. Yang, *J. Electrochem. Soc.* **133**, 1782 (1986).

85. B. Wu, J.R. Scully and J.L. Hudson, *J. Electrochem. Soc.* **144**, 1614 (1997).

86. T.T. Lunt, S.T. Pride, J.R. Scully and J.L. Hudson, *J. Electrochem. Soc.* **144**, 1620 (1997).

87. C. Gabrielli and M. Keddam, *Corrosion* **48**, 794 (1992).

88. P.H. Balkwill, C. Westcott and D.E. Williams, *Materials Science Forum* **44 & 45**, 293 (1989).

89. J. Newman, D.N. Hanson and K. Vetter, *Electrochim Acta* **22**, 829 (1977).

90. K. Sugimoto, S. Matsuda, Y. Ogiwara and K. Kitanwra, *J. Electrochem. Soc.* **132**, 1791 (1985).

91. G. Butler, H.C.K. Ison and A.D. Mercer, *Br. Corros. J.* **16**, 31 (1985).

92. T. Shibata, *Corros. Sci.* **31**, 413 (1990).

93. H. Bohni and L. Stockert, *Werkst. Korros.* **40**, 63 (1989).

94. Y. Xu, M. Wang and H.W. Pickering, *J. Electrochem. Soc.* **140**, 3448 (1993).

95. P.R. Roberge, R. Beaudoin and V.S. Sastri, *Corros. Sci.* **29**, 1231 (1989).

96. W.D. France and N.D. Greene, *Corrosion* **26**, 1 (1970).

97. I. Epelboin, C. Gabrielli, M. Keddam and L. Raillon, *J. Electroanal. Chem.* **93**, 155 (1978).

98. U. Bertocci and F. Huet, *Corrosion* **51**, 131 (1995).

99. P.C. Pistorius, *Corrosion* **53**, 273 (1997).

100. D.A. Eden and A.N. Rothwell, in *Corrosion '92*, paper no. 292, NACE, Houston (1992).

101. F. Mansfeld and H. Shih, *J. Electrochem. Soc.* **135**, 171 (1988).

102. F. Mansfeld, Y. Wang, H. Xiao and H. Shih, in *Proc. Symp. on Critical Factors in Localized Corrosion*, p. 469, ASTM STP 1134 (1992).

103. D.L. Reichert, in *Electrochemical Noise Measurement for Corrosion Applications*, J.R. Kearns, J.R. Scully, P.R. Roberge, D.L. Reichert and J.L. Dawson, Editors, p. 79, ASTM STP 1277, West Conshohocken, PA (1996).

Chapter 5 Spectral Analysis of Electrochemical Noise in the Frequency Domain

5.1 Introduction

Analysis of the EN can provide fundamental understanding about the pitting processes. Statistical analysis in the time domain and spectral analysis in the frequency domain are two main methods to extract information from the noise data.[1,2,3,4,5,6,7,8,9,10,11]

The statistical analysis of noise data recorded in the time series has been discussed in Chapter 4. The spectral analysis of EN will be presented in this chapter.

The calculations of power spectral density (PSD) of the noise data by the fast Fourier transform (FFT)[12] or the maximum entropy method (MEM)[13] are standard methods to study EN in the frequency domain. It has been shown that analysis of the noise spectrum and the spectral parameters, roll-off slope and roll-off frequency, can provide fundamental information about the corrosion mechanism and the corrosion kinetics processes.[14,15] For example, during pitting, "white" noise and $1/f^{\alpha}$ noise are generally observed in the regions of low frequency and high frequency, respectively. The values of the roll-off slope of PSD plots, that is, the slope in the $1/f^{\alpha}$ noise region, correspond to the different corrosion types.[16] The roll-off frequency (f_c), the frequency at the cross-point between the "white" noise region and the $1/f^{\alpha}$ noise region, is related to the repassivation kinetics of metastable pits.[17] Therefore, the analysis of the noise spectrum is a useful tool for interpretation of noise data.

In this chapter, the physical significance of the noise spectrum and some spectral parameters will be determined based on mathematical treatment and theoretical analysis.

128

This is an attempt to establish a reasonable relationship between noise transients and the noise spectrum.

5.2   Theoretical analysis of noise spectrum and spectral parameters

A PSD plot in the frequency domain is the Fourier transform of noise data collected in the time domain. The noise signals are generated due to the initiation, propagation and repassivation of metastable pits and, thus, directly related to the pitting process. It is reasonable to assume that there exists a certain relationship between noise transient variables and PSD parameters. Undoubtedly, analysis of this relation is essential to the understanding of the physical significance of the noise spectrum and PSD parameters and the pitting process.

In this section, a mathematical treatment is performed to establish the relationship between PSD parameters and pitting transient variables based on a pitting model. The physical significance of some spectral parameters is discussed.

5.2.1 Pitting model and theoretical analysis of the noise spectrum

For a given passive system containing aggressive ions such as Cl⁻, it is believed that every current transient represents the initiation of a single metastable pit.[11,18] The comparison of the probability distributions of pit size calculated from current noise data and that measured under the optical microscopy in Chapter 4 also shows the correspondence of current transients to metastable pits. During metastable pitting of carbon steel, the current transient is characterized by a quick current rise followed by a slow recovery (Fig. 4-6). It is assumed that the noise current increases linearly with time during pit growth and the following equation can describe the time dependence of noise current in this stage:

$$I(t) = at, \ 0 \le t \le t_c \tag{5-1}$$

where a is a stochastic variable reflecting the rate of current rise with the unit of amperes • second^{-1} (A s^{-1}), and t_c is the pit growth time (s). After t_c, pits growth terminates due to the repassivation process. During repassivation of metastable pits, the noise current decreases exponentially:

$$I(t) = (at_c)\exp[-b(t - t_c)], \ t \ge t_c \tag{5-2}$$

where b, with the unit of frequency (s^{-1}), is also a stochastic variable and reflects the rate of repassivation.

The Fourier transform of current noise data during one transient process, representing the passive film breakdown and repassivation, can be expressed as:

$$
\begin{aligned}
F(\omega) &= \int_{-\infty}^{\infty} I(t)\exp(-j\omega t)dt \\
&= \int_0^{t_c} (at)\exp(-j\omega t)dt + \int_{t_c}^{\infty} (at_c)\exp[-b(t - t_c)]\exp(-j\omega t)dt \\
&= a\left\{ \left[\frac{b^2 t_c \sin(\omega t_c)}{\omega(b^2 + \omega^2)} + \frac{b\omega^2 t_c + b^2 + \omega^2}{\omega^2(b^2 + \omega^2)}\cos(\omega t_c) - \frac{1}{\omega^2} \right] \right. \\
&\quad \left. + j\left[\frac{b^2 t_c}{\omega(b^2 + \omega^2)}\cos(\omega t_c) - \frac{b\omega^2 t_c + b^2 + \omega^2}{\omega^2(b^2 + \omega^2)}\sin(\omega t_c) \right] \right\}
\end{aligned}
\tag{5-3}
$$

The PSD of current noise during the period of time, T, is:

$$PSD = 2\lim_{T \to \infty} \frac{N(T)|F(\omega)|^2}{T} \tag{5-4}$$

130

where $N(T)$ is the number of current transients which correspond to the initiation of metastable pits during the time T. This PSD is defined for frequencies ($\omega = 2\pi f$) between 0 and $+\infty$; that is, only positive frequencies are considered. Therefore, the right side of Eq. 5-4 has to be multiplied by a factor of 2 in order to define the PSD in the frequency range of 0 to $+\infty$.

If it is further assumed that the initiation of metastable pits is a stochastic process and there is a linear relationship between the number of metastable pits and the area of the passive film, then

$$N(T) = \lambda \times S \times T \tag{5-5}$$

where λ is the average initiation rate of metastable pits per unit area and S is the area of the specimen. Then

$$PSD = 2S\lambda \times |F(\omega)|^2$$

$$= 2S\lambda \times a^2 \left[\frac{b^4 t_c^2}{\omega^2(b^2+\omega^2)^2} + \frac{1}{\omega^4} + \frac{b\omega^2 t_c + b^2 + \omega^2}{\omega^4(b^2+\omega^2)} \left(\frac{b\omega^2 t_c}{b^2+\omega^2} + 1 - 2\cos(\omega t_c) \right) \right.$$

$$\left. - \frac{2b^2 t_c \sin(\omega t_c)}{\omega^3(b^2+\omega^2)} \right] \tag{5-6}$$

$$= 2S\lambda \times a^2 \left[\frac{b^2 t_c^2}{\omega^2(b^2+\omega^2)} - \frac{2b^2 t_c \sin(\omega t_c)}{\omega^3(b^2+\omega^2)} + \frac{2(1-\cos(\omega t_c))}{\omega^2} \left(\frac{bt_c}{b^2+\omega^2} + \frac{1}{\omega^2} \right) \right]$$

When the frequency f is very low, the PSD takes the form of

$$PSD = \frac{2S\lambda \times a^2 t_c^2}{b^2} (1 + \frac{bt_c}{2})^2 \tag{5-7}$$

Therefore, the PSD is independent of frequency and the noise spectrum is "white" noise over the whole frequency range.

131

When the frequency is large enough to meet the condition of $2\pi f >> b$, then

$$PSD = \frac{S\lambda \times a^2}{2\pi^4}[\frac{b^2 t_c^2}{4} + (1 + bt_c)\sin^2(f\pi t_c)]f^{-4} \qquad (5\text{-}8)$$

There is a certain frequency dependence of PSD in the range of high frequency. The PSD decreases with increasing frequency and shows the $1/f^\alpha$ behavior.

5.2.2 Relationship between spectral parameters and transient variables

5.2.2.1 Current rise rate — variable a

The effect of a specific transient variable on the noise spectrum can be understood from Eq. 5-6 by keeping other variables unchanged. Fig. 5-1 shows the dependence of PSD plots on variable a, the rate of current rise during the pit growth stage (dI/dt). It is seen that the increase in variable a does not alter the noise spectrum but increases the PSD level. The spectral parameters, roll-off frequency and roll-off slope, are not altered by the variation of a. The rising rate of noise current corresponds to the growth rate of metastable pits. Therefore, the increase in pit growth rate will lead to an increasing noise spectrum level. The presence of lobes in the PSD plots in the high frequency region is caused by the sine function contained in the PSD formula.

5.2.2.2 Pit initiation rate — variable λ

Fig. 5-2 shows the PSD plots calculated at different pit initiation rates, λ. It is obvious that the higher the pit initiation rate, i.e., the more the current transients in a unit time, the higher the PSD level. The other PSD parameters remain unchanged. Therefore, the increase in pit initiation rate will also cause an increase in noise spectrum level.
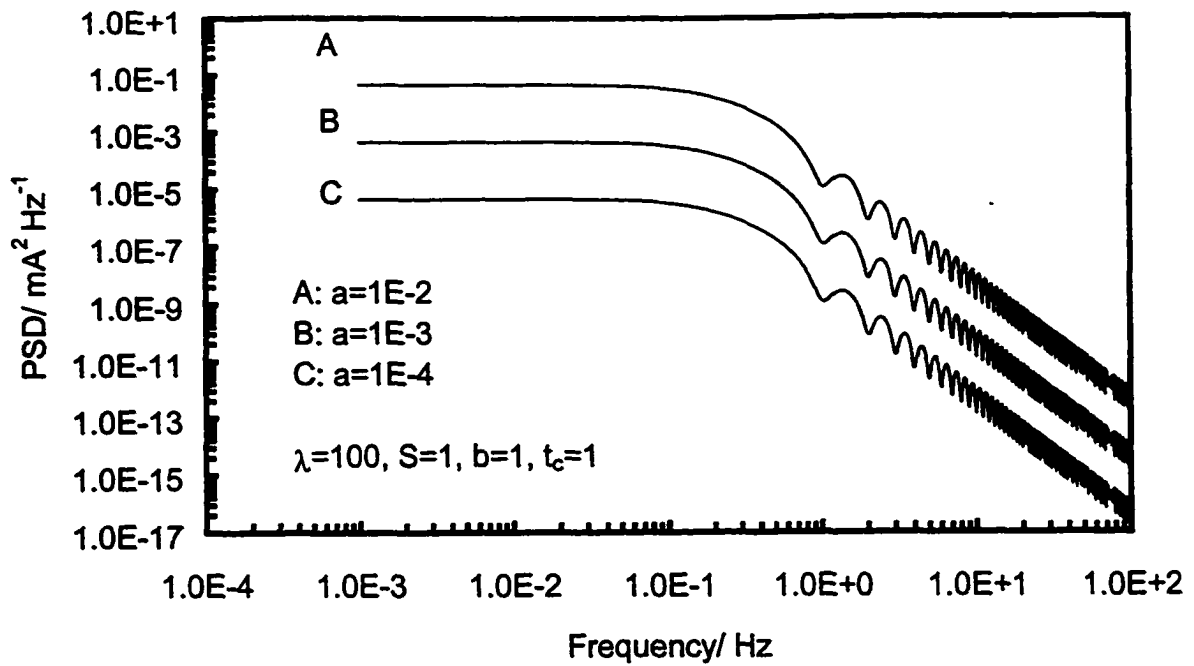
Fig. 5-1 Current PSD as a function of variable *a*, the rise rate of current.
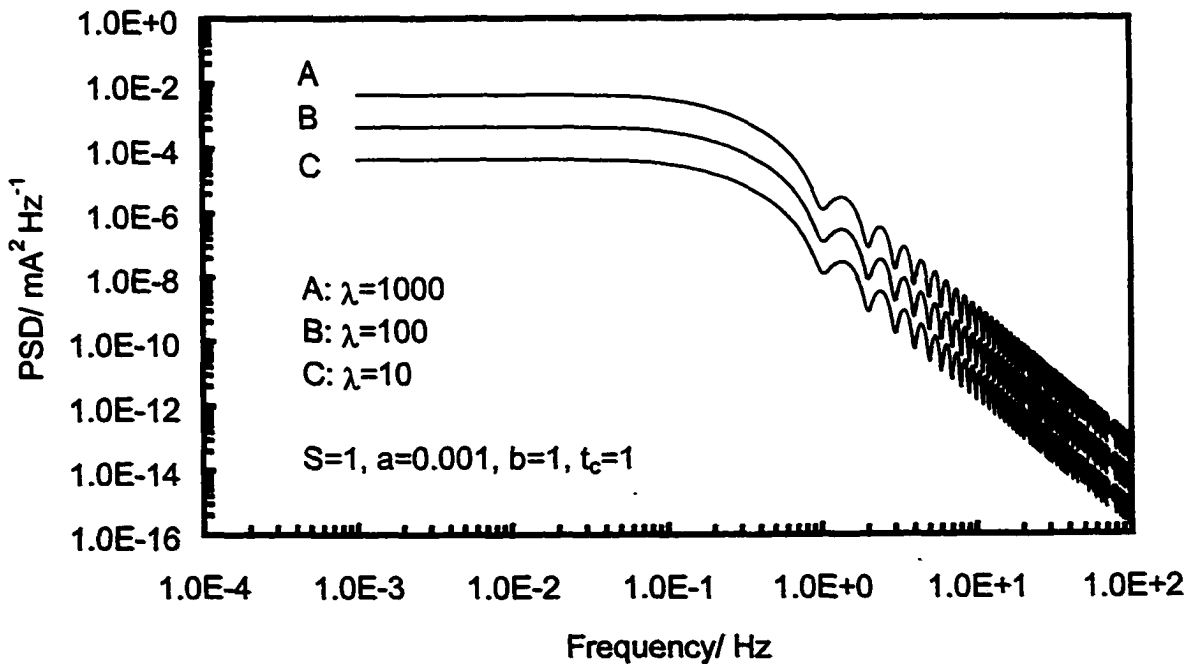
Fig. 5-2 Current PSD as a function of variable λ, the pit initiation rate.

133

Comparing Fig. 5-1 and 5-2, it can be seen that it is impossible to tell which one of the noise transient variables, current rise rate or pit initiation rate, plays the major role when the PSD level changes.

5.2.2.3 Pit growth time — variable t_c

The PSD plots corresponding to the different pit growth times, t_c, are shown in Fig. 5-3. It can be seen that the effect of variable t_c on the noise spectrum is mainly reflected by a change of the roll-off slope. The increase in variable t_c causes the increasing roll-off slope. In addition, the PSD level in the region of low frequency also increased with t_c.

It has been found[7,10] that PSD plots transformed from the noise data collected in passivity and general corrosion systems are generally a straight line with the roll-off slope approaching zero. The potential and current noise recordings generated during passivity and general corrosion contain stochastic fluctuations with a higher frequency. The noise transients occur quickly and superimpose on each other, with a very small value of variable t_c. Therefore, a smaller t_c in noise recordings will lead to a flatter PSD plot and a smaller roll-off slope. In pitting systems, the potential and current transients are generally separated with a larger variable t_c, so the roll-off slope of PSD plots for a pitting system is definitely larger than zero. Some authors have tried to relate the different values of roll-off slope to specific corrosion types.[4] Actually, the roll-off slope of a noise spectrum depends not only on the variable t_c for a specific shape of noise transient, but also on the transient pattern, which will be discussed in the next section. Therefore, there is no certain relationship between roll-off slope and corrosion type.

5.2.2.4 Pit repassivation rate — variable b

The PSD plots calculated with different values of variable b are shown in Fig. 5-4. It is seen that the main effect of altering b values is to change the roll-off frequency of

134
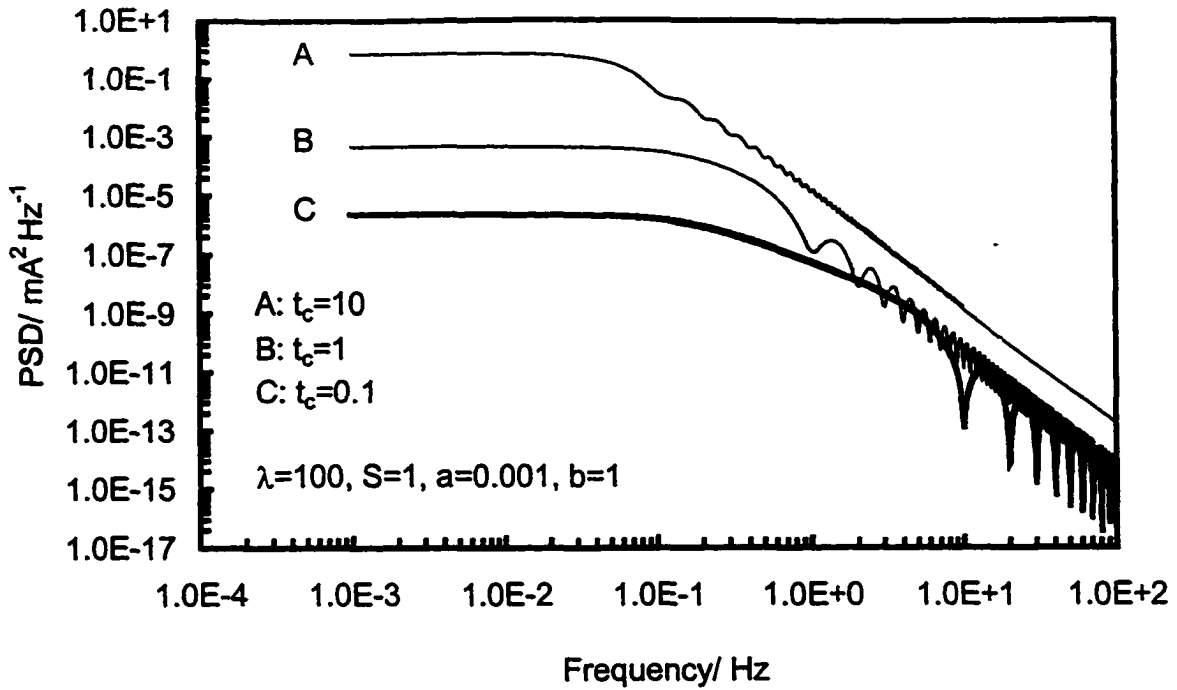
Fig. 5-3 Current PSD as a function of variable t_c, the pit growth time.
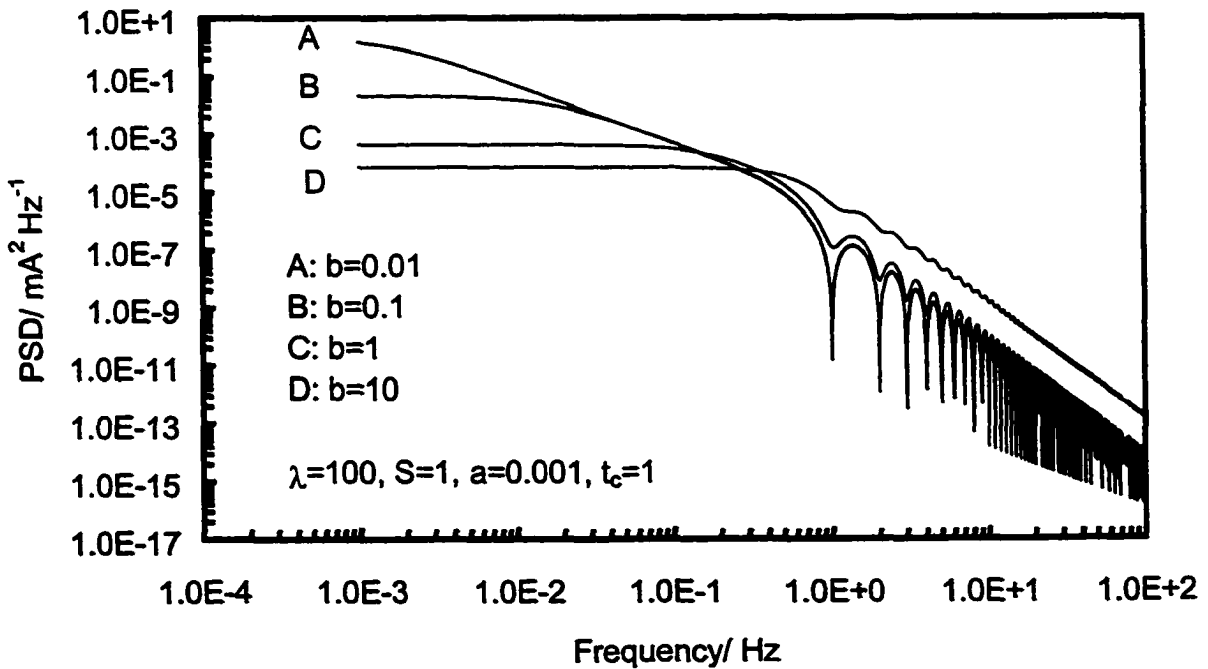
Fig. 5-4 Current PSD as a function of variable b, the pit repassivation rate.

135

PSD plots. The f_c decreased with decreasing b, that is, the repassivation rate of metastable pits. The f_c values are equal to 0.6, 0.2 and 0.04 Hz when the values of b are 10, 1, 0.1 s^{-1}, respectively. When b is reduced to 0.01 s^{-1}, there is no apparent roll-off frequency.

It has been pointed[17] that the roll-off frequency is directly related to the repassivation process of metastable pits by the following law:

$$f_c \propto b \qquad\qquad\qquad (5\text{-}9)$$

where b refers to the pit repassivation rate defined in Eq. 5-2. The amplitude of the pit repassivation rate reflects the aggressive degree of the local pit environment. As shown in Fig. 5-4, a greater value of b, that is, a larger pit repassivation rate corresponding to a less aggressive environment inside the pit, leads to a larger f_c. On the other hand, a smaller f_c represents a more aggressive pit environment. The repassivation process is thus slower, so a smaller b causes a smaller f_c. When the repassivation rate is so small that it is very difficult to repassivate the pitted area, f_c cannot be observed in the PSD plots. In addition, compared with the initiation of metastable pits, the repassivation of pits is a slower process. The features of the repassivation process are mainly reflected in the low frequency region of PSD plots. Therefore, the increase in variable b, that is, pit repassivation rate, causes an increasing PSD level mainly in the low frequency region.

5.3 Spectral analysis of electrochemical noise with different transient shapes

It has been shown in the previous section that the spectral parameters are related to the noise transient variables, and thus, to the corrosion process. However, there still exist some arguments on how the shapes of PSD plots and the spectral parameters are related to the corrosion process. For example, Uruchurtu and Dawson[16] thought that shallow roll-off slopes of -20 dB/decade or less are indicative of pitting corrosion, whereas a roll-off slope of more than -20 dB/decade represents general corrosion or a passive state. However, Legat et al.[7,19] found that the PSD for uniform corrosion is "white" and

constant over the whole frequency domain, while the PSD values during localized corrosion can be interpolated on a logarithm vs. logarithm scale by a $1/f^{\alpha}$ function. Monticelli et al.[20] evaluated some inhibitors on aluminum alloys by EN analysis and found that the noise spectrum exhibits a $1/f^{\alpha}$ trend with α close to 20 dB/decade under conditions of uniform attack. When steady growth of pits is reached, the spectra can be described by two straight lines with slopes of about 10 dB/decade in the low frequency portion (stationary pit growth) and 20 dB/decade in the high frequency portion (hydrogen gas evolution). Fukuda and Mizuno[14] studied the current transients for pure iron and showed that at a passive state, the roll-off slope is zero, which means "white" noise in both low and high frequency ranges, while the slope decreases and stays around -0.5 during the pit induction period and then steeply decreases to below -1 before pit generation.

The roll-off frequency also bears some controversy of opinions. Bertocci et al.[3] believed that the roll-off frequency of PSD is related to the time constant of repassivation and reflects the degree of aggressiveness of the local environment inside the pits. Bertocci and Huet[21] further pointed out that the roll-off frequency of PSD provides information on the time constant for the repassivation process, which is connected to the duration of the transient. Oltra et al.[17] studied the mechanical breakdown of a passive layer by spectral analyses. Two plateaus followed by an approximate $1/f^{2}$ PSD part were observed, so there are two roll-off frequencies. The higher roll-off frequency gives the average time constant of the current transient, which is not related to the repassivation rate, but to the $R_{e}C_{d}$ time constant (R_{e}: electrolyte resistance, C_{d}: double-layer capacitance) of the cell. The lower roll-off frequency is related to the film breakdown/repair process and can give the mean value of the elementary charge involved in each transient.

From previous research results, it is found that there are many controversial viewpoints about the experimental results and explanations about the noise spectrum. The physical meaning of the roll-off frequency and the relationship between roll-off slope and corrosion types are not clear. Bertocci and Huet[21] tried to simulate time domain records, similar to data as recorded in a digital oscilloscope and then to apply an FFT algorithm to obtain the power spectra. Although the results show that it is possible to recover from the

137

spectrum all the information necessary to reconstruct the time record, including transient amplitude, decay constant and intensity of the random process, it is still not obvious whether the shape of the transient will leave a recognizable mark on the spectrum.

The further analyses performed by Gabrielli et al.[22] indicated that when the current transient showed a sudden birth or a sudden death the high frequency limit of the PSD varies like f^{-2} whatever the shape of the transient. A slow birth followed by a slow death gives rise to an f^{-4} trend. Therefore, it seems probable a definite relationship can be established between the noise transient and the noise spectrum.

In the present work, the noise spectra are calculated under some transients with typical shapes found in the corrosion areas. The relationship between spectral parameters and transient variables in the time domain are analyzed. The influences of corrosion types on noise spectrum are also considered.

5.3.1 Mathematical background

During corrosion of metals, sequences of elementary current transients, $I(t)$, can be observed. If $F(\omega)$ is the Fourier transfer of the current transient, which is assumed to follow the Possian distribution, then

$$F(\omega) = \int_{-\infty}^{+\infty} I(t) \exp(-j\omega t) dt \tag{5-10}$$

The power spectral density (PSD) can be calculated as follows:[6]

$$PSD = 2 \lim_{T \to \infty} \frac{N(T)|F(\omega)|^2}{T}$$

$$= 2 \lim_{T \to \infty} \frac{\lambda \cdot S \cdot T|F(\omega)|^2}{T} \tag{5-11}$$

$$= 2\lambda \cdot S|F(\omega)|^2$$

where $N(T)$ is the number of current transients during a certain time T, λ is the average

138

occurrence rate of current transients per unit area, S is the area of the specimen and ω is the angle frequency which is equal to $2\pi f$. It is obvious, from Eq. 5-11, that the noise spectrum contains the information of the occurrence rate of events and the relevant transient variables included in transient equation $I(t)$. Therefore, it is reasonable to expect that some useful information can be extracted through spectral analysis.

For the calculation of PSD plots, all values of the variables contained in current transients recorded in the time domain were chosen based on the work presented in Chapter 4. The electrode area (S) is 0.5 cm^2, the pit initiation rate per unit area (λ) is approximately 65 s^{-1} cm^{-2}, the time constant of the exponential function of current transient (τ) ranged from 0.6 to 1.4 seconds and the average magnitude of the current signal (A) is about 10^{-3} mA. To simplify the calculation, these relevant parameters are assumed to be the integral values.

5.3.2   Spectral analysis

5.3.2.1 Current transients during metastable pitting

* Transient I: sudden birth followed by an exponential decay

The current transients, characterized by a quick current rise followed by an exponential decay as shown in Fig. 5-5, are often found to be characteristic of the metastable pitting of carbon steel[23,24,25] and pure iron.[26] As indicated by the current transients, the metastable pitting processes contain pit initiation, quick growth and slow repassivation. Some non-chemical initiation of the corrosion reactions such as laser illumination,[1] abrasion[17] and scratching,[27] also generate this kind of transient. The exponentially decaying current transients with a time constant τ can be expressed by:

$$I(t) = 0, \qquad\qquad t < 0$$

$$I(t) = A\exp(-\frac{t}{\tau}), \qquad t \geq 0 \qquad\qquad\qquad\qquad (5\text{-}12)$$

where A is a stochastic variable reflecting the magnitude of the current transient. When

139

$I(t) = A\exp(-t/\tau)$

$t = 0$
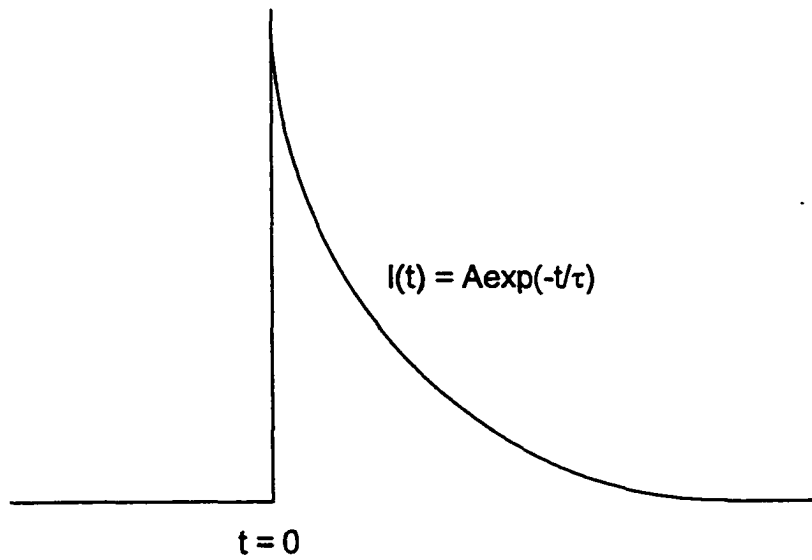
Fig. 5-5 Current transient with the shape of a sudden birth followed by an exponential decaying.

$S=1$ cm^2, $\lambda=100$ s^{-1}cm^{-2},

$\tau=1$ s, $A=0.001$ mA

$f_c = 1/(2\pi\tau)$

$= 0.16$ Hz

$PSD \propto f^{-2}$

PSD / mA^2 Hz^{-1}
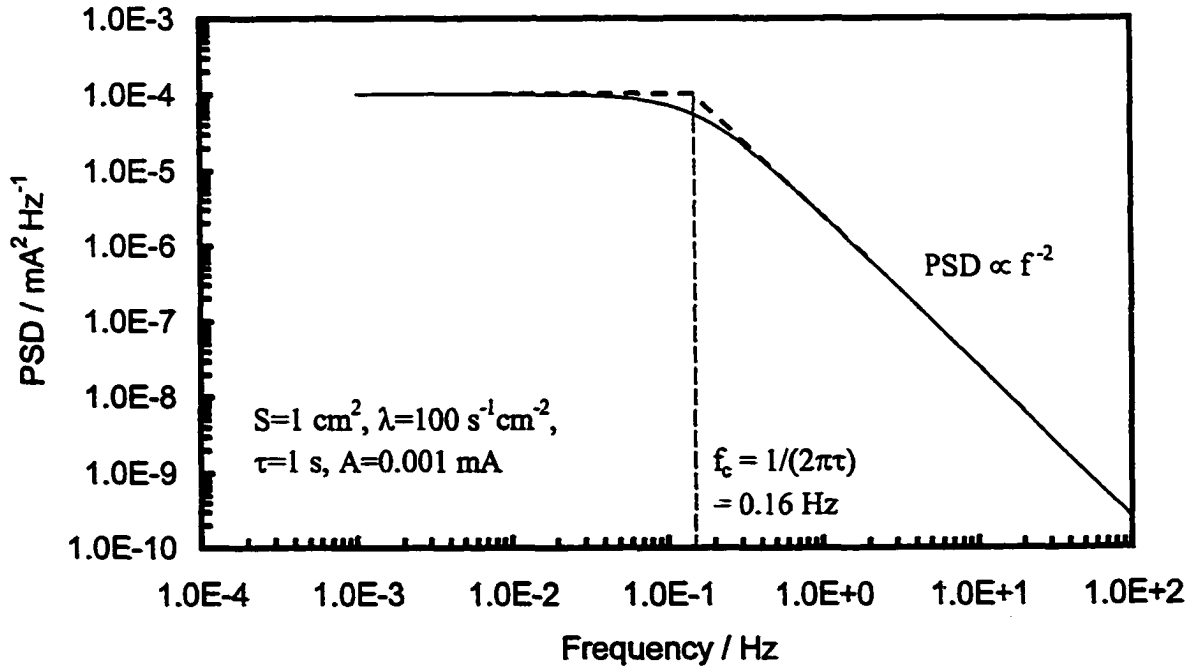
Frequency / Hz

Fig. 5-6 Noise spectrum derived from the transient shown in Fig. 5-5.

$I(t)$ in Eq. 5-10 takes the form of Eq. 5-12, the PSD, calculated from Eq. 5-11, becomes:

$$PSD = \frac{2S \bullet \lambda \bullet A^2 \bullet \tau^2}{1 + 4\pi^2 f^2 \tau^2}$$

(5-13)

When frequency $f << \dfrac{1}{2\pi\tau}$, Eq. 5-13 takes the form:

$$PSD = 2S \bullet \lambda \bullet A^2 \bullet \tau^2$$

(5-14)

the PSD is independent of the frequency and the spectra indicate the "white" noise. When the frequency is large enough to meet the condition of $2\pi f\tau >> 1$,

$$PSD = \frac{S \bullet \lambda \bullet A^2}{2\pi^2} \bullet f^{-2}$$

(5-15)

the noise spectrum shows the features of f^{-2} noise. Therefore, the noise spectrum has a "white" noise plateau in the low frequency range and decreases with f^{-2} in the high frequency range with the roll-off frequency of $\dfrac{1}{2\pi\tau}$, which is the frequency at the crossing point between "white" noise and f^{-2} noise.

The noise spectrum calculated based on Eq. 5-13 is shown in Fig. 5-6. It can be seen that the "white" noise and the f^{-2} noise cross at the roll-off frequency of $\dfrac{1}{2\pi\tau}$ of 0.16 Hz under the assumed conditions.

* Transient II: exponential birth followed by a sudden decay

The current transients with the feature of an exponential rise followed by a sudden decaying (Fig. 5-7) are very common during metastable pitting of various stainless steels,[28,29,30,31] which are quiet different from that for carbon steel. After initiation, the

141

I(t) = Aexp(t/τ)

t = 0
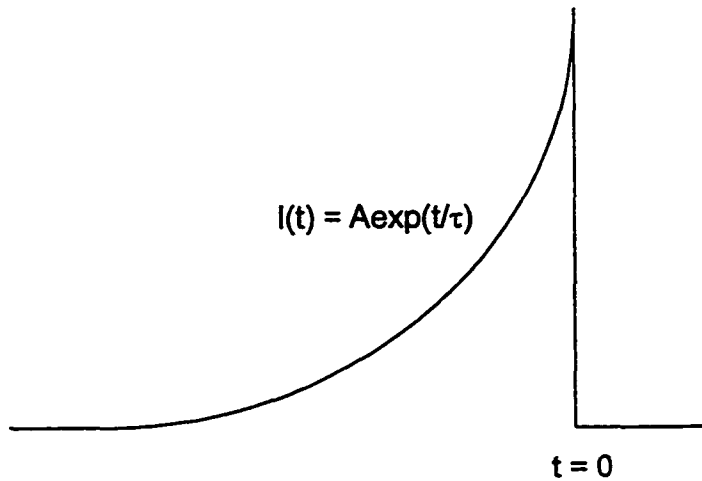
Fig. 5-7 The current transient with the shape of an exponential birth followed by a sudden death.

metastable pits grow slowly, and then repassivate very rapidly.

The exponentially rising current transient with a time constant τ is expressed by:

$$I(t) = A\exp(\frac{t}{\tau}), \qquad t < 0$$

$$I(t) = 0, \qquad t \geq 0 \qquad\qquad (5\text{-}16)$$

Following the same procedure as described above, the PSD is calculated as

$$PSD = \frac{2S \bullet \lambda \bullet A^2 \bullet \tau^2}{1 + 4\pi^2 f^2 \tau^2} \qquad\qquad (5\text{-}17)$$

It is obvious that the PSD calculated for transient II is exactly the same as that for transient I. The noise spectrum is also "white" in the low frequency range and has the

142

form of f^{-2} in the high frequency range with the roll-off frequency of $\dfrac{1}{2\pi\tau}$. Therefore, the PSD curve cannot tell the difference in features between two transients represented by Eq. 5-12 and 5-16. These two transients are symmetrical in the time domain.

* Transient III: exponential birth followed by an exponential death

For the case of the current transients both rising and decaying exponentially, the transients can be approximately processed as a double exponential wave with two time constants of τ_1 and τ_2 (Fig. 5-8).

$I(t) = A\exp(-t/\tau_2)$

t = 0
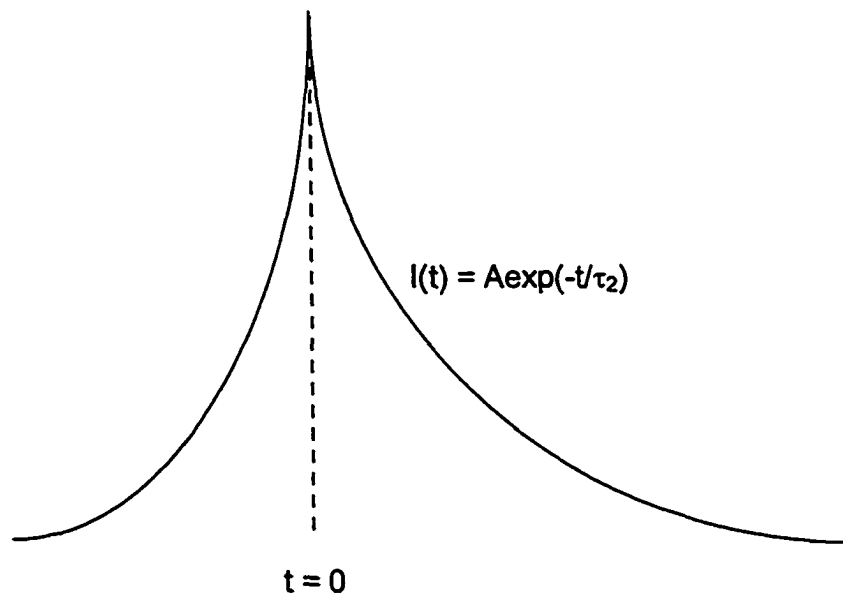
Fig. 5-8 Current transient with the shape of an exponential birth followed by an exponential death.

$$I(t) = A\exp(\frac{t}{\tau_1}), \qquad t < 0$$

$$I(t) = A\exp(-\frac{t}{\tau_2}), \qquad t > 0 \qquad\qquad (5\text{-}18)$$

143

Following the same calculation procedure as above, the PSD is calculated as

$$PSD = \frac{2S \cdot \lambda \cdot A^2 (\tau_1 + \tau_2)^2}{(1 + 4\pi^2 f^2 \tau_1^2)(1 + 4\pi^2 f^2 \tau_2^2)} \qquad (5\text{-}19)$$

When $f \ll \dfrac{1}{2\pi\tau_1}$ and $f \ll \dfrac{1}{2\pi\tau_2}$, the noise spectrum is "white" and independent of the frequency:

$$PSD = 2S \cdot \lambda \cdot A^2 (\tau_1 + \tau_2)^2 \qquad (5\text{-}20)$$

If $\tau_1 = \tau_2 = \tau$, then Eq. 5-19 becomes

$$PSD = \frac{8S \cdot \lambda \cdot A^2 \tau^2}{(1 + 4\pi^2 f^2 \tau^2)^2} \qquad (5\text{-}21)$$

In the high frequency range, i.e., when $f \gg \dfrac{1}{2\pi\tau}$, Eq. 5-21 becomes

$$PSD = \frac{S \cdot \lambda \cdot A^2}{2\pi^4 \tau^2} f^{-4} \qquad (5\text{-}22)$$

The PSD curve has only one slope with the feature of f^{-4} noise, as shown by the thick curve in Fig. 5-9 which was calculated based on Eq. 5-19 when $\tau_1 = \tau_2 = 1$.

If $\tau_1 \neq \tau_2$, assuming $\tau_1 < \tau_2$ and when the frequency $f \gg \dfrac{1}{2\pi\tau_1}$, Eq. 5-19 can be simplified as

$$PSD = \frac{S \cdot \lambda \cdot A^2 (\tau_1 + \tau_2)^2}{8\pi^4 \tau_1^2 \tau_2^2} f^{-4} \qquad (5\text{-}23)$$

144
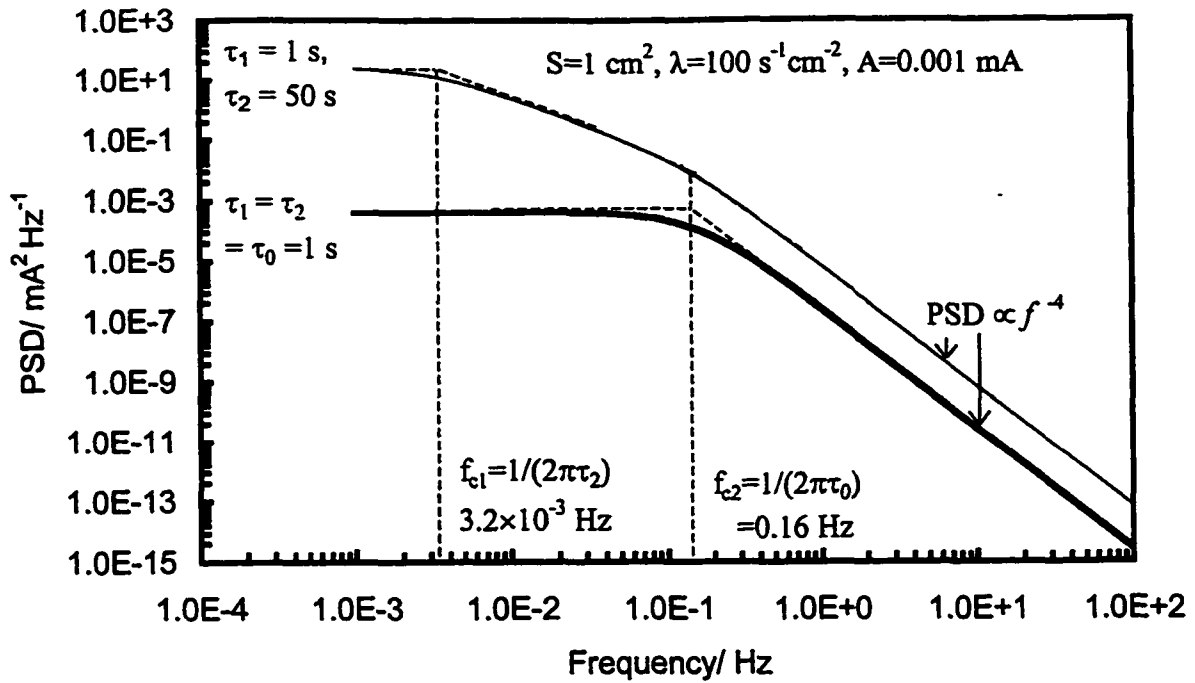
Fig. 5-9 Noise spectrum derived from the transient shown in Fig. 5-8.

It is clear that the noise spectrum is f^{-4} in nature. However, when the frequency is between

$\dfrac{1}{2\pi\tau_2}$ and $\dfrac{1}{2\pi\tau_1}$, the roll-off slope of PSD will be smaller than 4. As shown in Fig. 5-9,

two roll-off slopes appear in the PSD curve. It is also seen that the PSD curve has two

roll-off frequencies, $\dfrac{1}{2\pi\tau_2}$ and $\dfrac{1}{2\pi\tau_1}$ when $\tau_1 \neq \tau_2$.

From Eq. 5-19, it is very clear that PSD curves for the case of $\tau_1 > \tau_2$ will be the same

as those obtained when $\tau_1 < \tau_2$.

* Transient IV: linear birth followed by an exponential death

Similar to the case of transient I, when the pit growth time is considered, the transient

pattern has the form of a linear current rise during the pit growth time, t_c, and followed by

an exponential decaying (Fig. 5-10). The current is expressed as:

$$I(t) = at, \qquad\qquad 0 \leq t < t_c$$

145

$$I(t) = at_c \exp[-\frac{(t-t_c)}{\tau}], \qquad t \geq t_c \qquad\qquad (5\text{-}24)$$

where a is a stochastic variable reflecting the current rise rate, t_c is the pit growth time and τ is the time constant of the exponential function. The PSD is calculated as

I(t) = at   I(t) = at_c exp[-(t-t_c)/τ]

t = 0   t = t_c
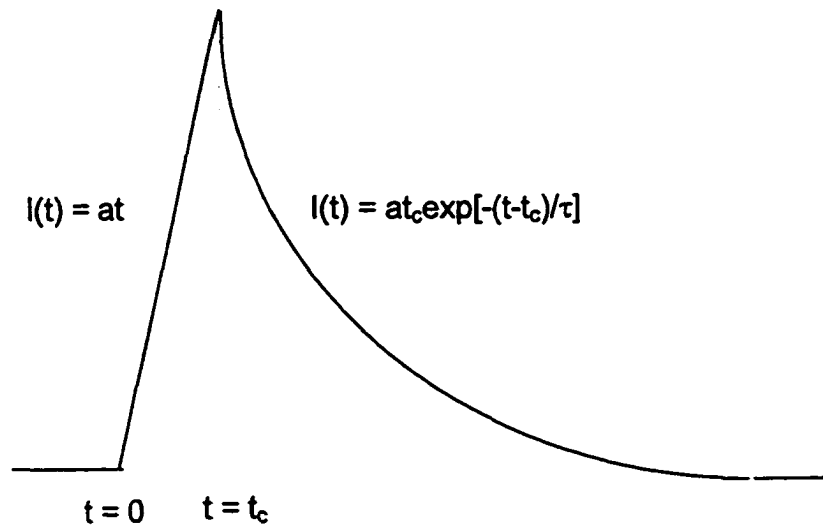
Fig. 5-10 Current transient with the shape of a linear birth followed by an exponential death.

$$PSD = 4S\lambda a^2 [\frac{t_c^2}{4\pi^2 f^2 (1+4\pi^2 f^2 \tau^2)} - \frac{t_c \sin 2\pi f t_c}{4\pi^3 f^3 (1+4\pi^2 f^2 \tau^2)}$$

$$+ \frac{(1-\cos 2\pi f t_c)}{2\pi^2 f^2} (\frac{t_c \tau}{1+4\pi^2 f^2 \tau^2} + \frac{1}{4\pi^2 f^2})] \qquad\qquad (5\text{-}25)$$

When the frequency $f \ll \frac{1}{2\pi\tau}$, then

146
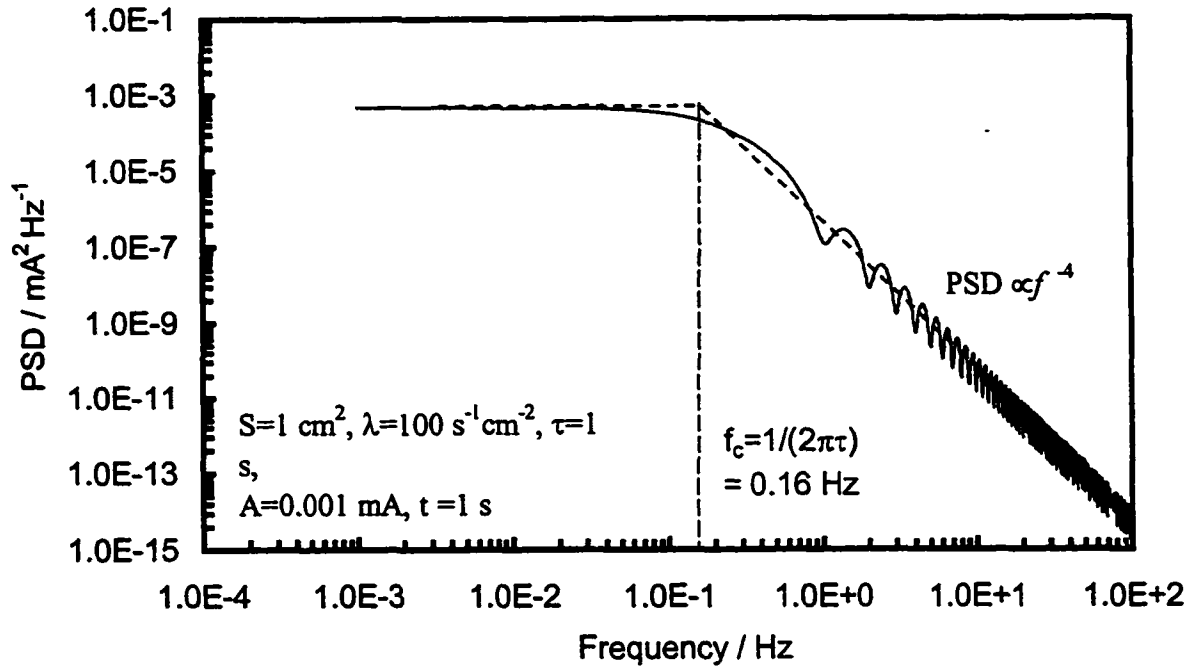
Fig. 5-11 Noise spectrum derived from the transient shown in Fig. 5-10.

$$PSD = 4S\lambda \bullet a^2 t_c^{\ 2}(\tau + \frac{t_c}{2})^2 \qquad\qquad (5\text{-}26)$$

The PSD is independent of the frequency and the noise spectrum is "white" noise in the low frequency range. In the frequency range of $f \gg \dfrac{1}{2\pi\tau}$, Eq. 5-25 takes the form:

$$PSD = \frac{S\lambda \bullet a^2}{\pi^4}[\frac{t_c^2}{4\tau^2} + (1 + \frac{t_c}{\tau})\sin^2(f\pi t_c)]f^{-4} \qquad\qquad (5\text{-}27)$$

Fig. 5-11 shows the PSD curve calculated based on Eq. 5-27. It is seen that f^{-4} behavior is displayed in the high frequency range with the roll-off frequency of $\dfrac{1}{2\pi\tau}$. The lobes presented are caused by the sine function.

147

Summarizing the spectral analysis about various current transients generated during metastable pitting, it can be seen that a "white" noise and a f^{-2} or f^{-4} noise are always present in the low and high frequency range, respectively. The transients having a sudden birth or a sudden death will result in f^{-2} noise, while the transients without sudden change show f^{-4} behavior. The roll-off frequency is directly related to the time constant of the exponential function, which indicates the growth rate or the repassivation rate of metastable pits. In addition, although the shapes of current transients recorded in the time domain can reflect the different metastable pitting processes, the noise spectra cannot show those differences in some cases.

5.3.3.2 Current transients during passivity and general corrosion

*** Transient V: triangular wave**

The current transients with the shape of a linear rise followed by a linear drop
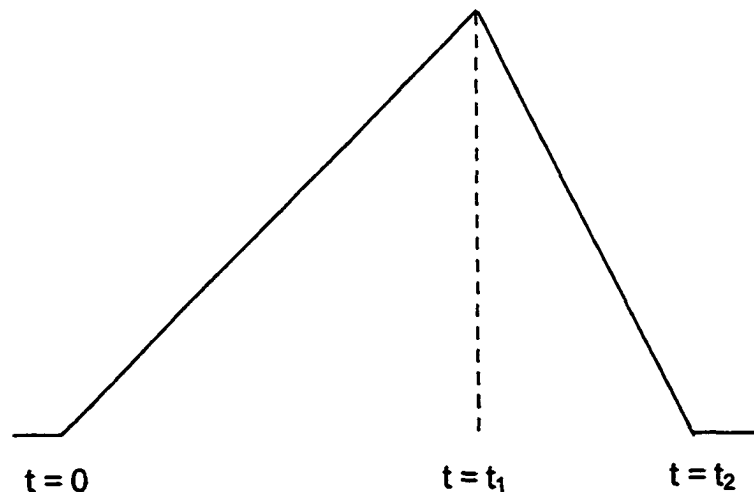
Fig. 5-12 Current transient with the shape of triangular wave: a linear rise followed by a linear drop.

(triangular wave) are always observed for metals in a passive state (Fig. 5-12). If t_1 and t_2 - t_1 represent the current rise time and drop time, which are generally in the order of 1 to 2

seconds, and a is a variable reflecting the current rise rate, the current transient can be expressed as:

$$I(t) = at, \qquad\qquad 0 \leq t < t_1$$

$$I(t) = \frac{-at_1(t-t_2)}{(t_2 - t_1)} \qquad t_1 \leq t < t_2 \qquad\qquad (5\text{-}28)$$

To simplify the equation of PSD, it is assumed that $t_2 - t_1 = t_1 = t_0$, and the PSD is calculated as:

$$PSD = 2S \bullet \lambda \bullet a^2 t_0{}^4 \frac{\sin^4(\pi f t_0)}{(\pi f t_0)^4} \qquad\qquad (5\text{-}29)$$

The PSD plot calculated from Eq. 5-29 is shown in Fig. 5-13. It is seen that if the frequency is so low that $(\pi f t_0)$ approaches zero, the PSD is independent of the frequency and will be equal to $2S\lambda a^2 t_0{}^4$. When the frequency is high enough to meet the criterion of $\pi f t_0 \gg 1$, many lobes related to the sine function are produced on the curve, but with the basic tendency of f^{-4} noise as shown by the broken line in Fig. 5-13. The roll-off frequency between the "white" noise part and the f^{-4} noise part, which is determined by the time interval of the current transient, that is, $\dfrac{1}{\pi t_0}$ is about 0.32 Hz determined from

Fig. 5-13. Therefore, the triangular wave-shaped current transient will generate f^{-4} noise in the high frequency range. The roll-off frequency is related to the time interval during the current rise or drop stage.

* Transient VI: Delta wave

The delta-waved transients, sudden birth lasting a time interval (t_0) and then sudden death (Fig. 5-14), are always observed when the metal is in a general corrosion state. The time interval is observed to be in the order of 1 second. The delta function of current transient can be expressed as:

149
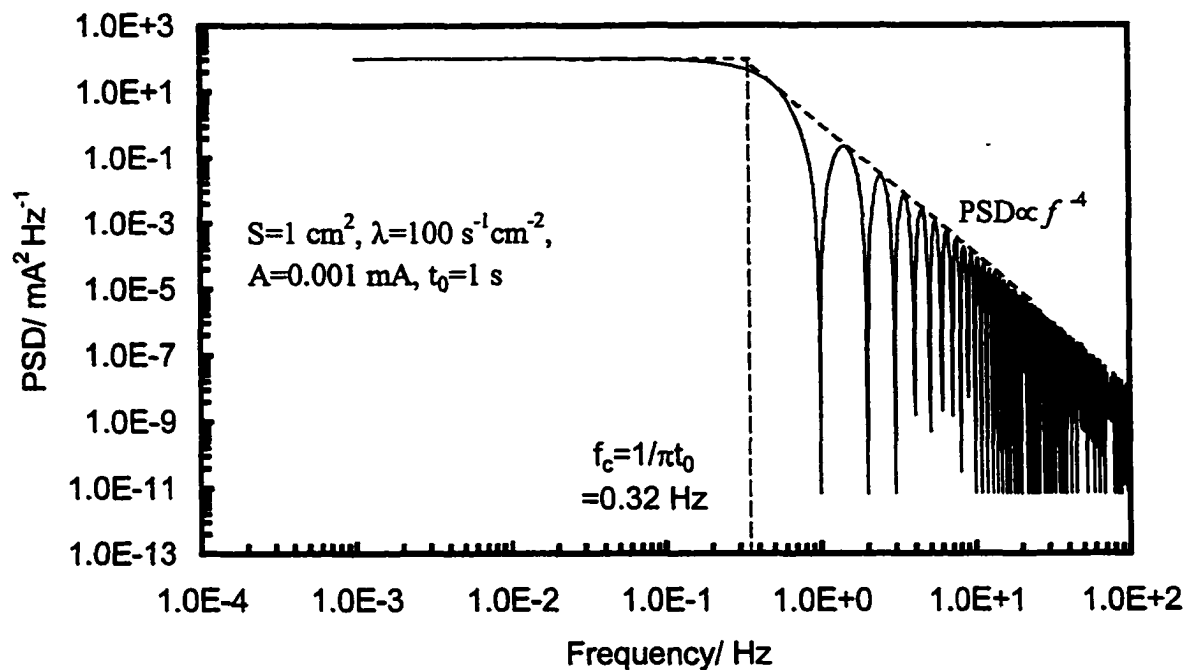
Fig. 5-13 Noise spectrum derived from the transient shown in Fig. 5-12.

$I(t) = 0$, $t < 0$ and $t \geq t_0$

$I(t) = A$, $0 \leq t < t_0$ (5-30)

where A is the amplitude of the delta function. The PSD is calculated as

$$PSD = 2S \cdot \lambda \cdot A^2 t_0{}^2 \frac{\sin^2(\pi f t_0)}{(\pi f t_0)^2}$$ (5-31)

When the frequency is low enough to meet the condition of $\pi f t_0 \approx 0$, the PSD is "white" and approximately equal to $2S\lambda A^2 t_0{}^2$. In the high frequency range of $\pi f t_0 \gg 1$, lobes appear and the basic tendency is f^{-2} noise, indicated in Fig. 5-15. Therefore, the noise

150

t = 0   t = t_0
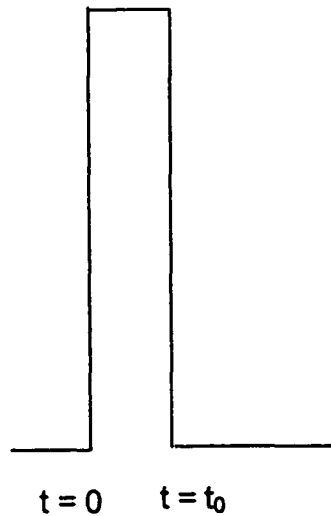
Fig. 5-14 Current transient with the shape of delta
wave lasting a time interval t_0.

spectrum for a delta function generated in a general corrosion system is also "white" in
the low frequency range for PSD analysis. Lots of lobes with the basic feature of f^{-2} noise
are observed with the roll-off frequency of approximate 0.32 Hz, which reflects the time

interval of delta current transient by $\dfrac{1}{\pi t_0}$.

According to the PSD analyses of the current transients generated in passivity and
general corrosion systems, it is concluded that "white" noise is always observed in the
low frequency range and f^{-2} and f^{-4} noise, corresponding to the current transients with
and without sudden change respectively, appear in the high frequency range. The roll-off
frequency of the PSD plot is directly related to the time interval of the current transient
during the rise or drop stage.

5.3.4   Experimental
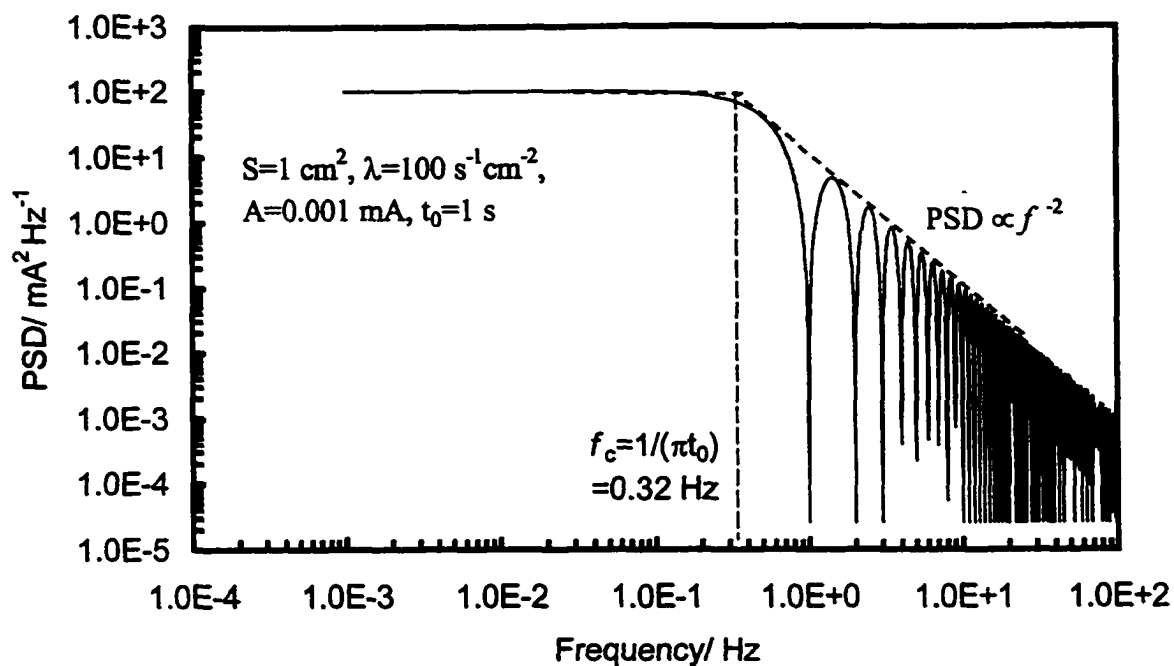
Fig. 5-15 Noise spectrum derived from the transient shown in Fig. 5-14.
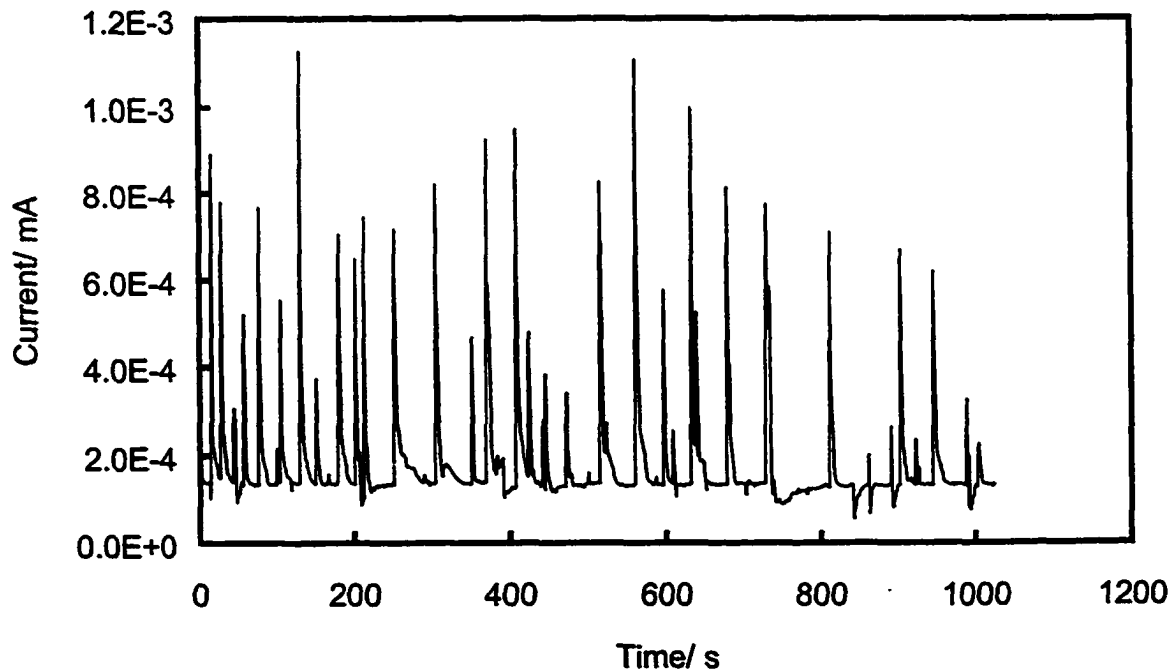
Fig. 5-16 Current noise of A516-70 carbon steel in 0.5 M
$NaHCO_3$ + 0.1 M NaCl solution.

In order to investigate the validity of the theoretical spectral analysis results, the measurements of EN signals in several corrosion systems were designed. To generate a pitting system, the specimens were prepassivated in 0.5 M NaHCO₃ solution for 2 hours. After the stable passive state was reached, NaCl based on a pre-designed volume was added such that the testing solution contained 0.5 M NaHCO₃ + 0.1 M NaCl..

5.3.5 Pitting system

The recordings of current noise of A516-70 carbon steel in HCO₃⁻/Cl⁻ solution are shown in Fig. 5-16. The typical current transients, characterized by a quick rise followed by a slow recovery, are believed to reflect the metastable pitting process: initiation, growth and repassivation of metastable pits. Therefore, the current transients generated in this work can be approximately expressed by transient I, i.e., a sudden current rise followed by an exponential decaying. The average time constant (τ) during the repassivation process is approximately 2.5 seconds.

The PSD plot calculated from the current noise data in Fig. 5-16 is shown in Fig. 5-17. It is seen that the "white" noise appears in the low frequency range and f^{-2} noise in the high frequency range with a roll-off slope of 2, which corresponds to the typical current transients generated during pitting. The roll-off frequency is 0.055 second from the figure, which is determined by the time constant of $\dfrac{1}{2\pi\tau}$ for the repassivation process.

5.3.6 Passive system

After a certain period of immersion of A516-70 carbon steel in 0.5 M NaHCO₃ solution, stable passivity is reached. The current noise generated during carbon steel passivity is shown in Fig. 4-3. The details of the shape of current transients during passivity is enlarged in Fig. 5-18. A triangular-shaped current transient with an average time interval of current rise or drop stage of approximately 3 seconds is apparent. The current PSD plot calculated from noise data in Fig. 5-18 is shown in Fig. 5-19. The
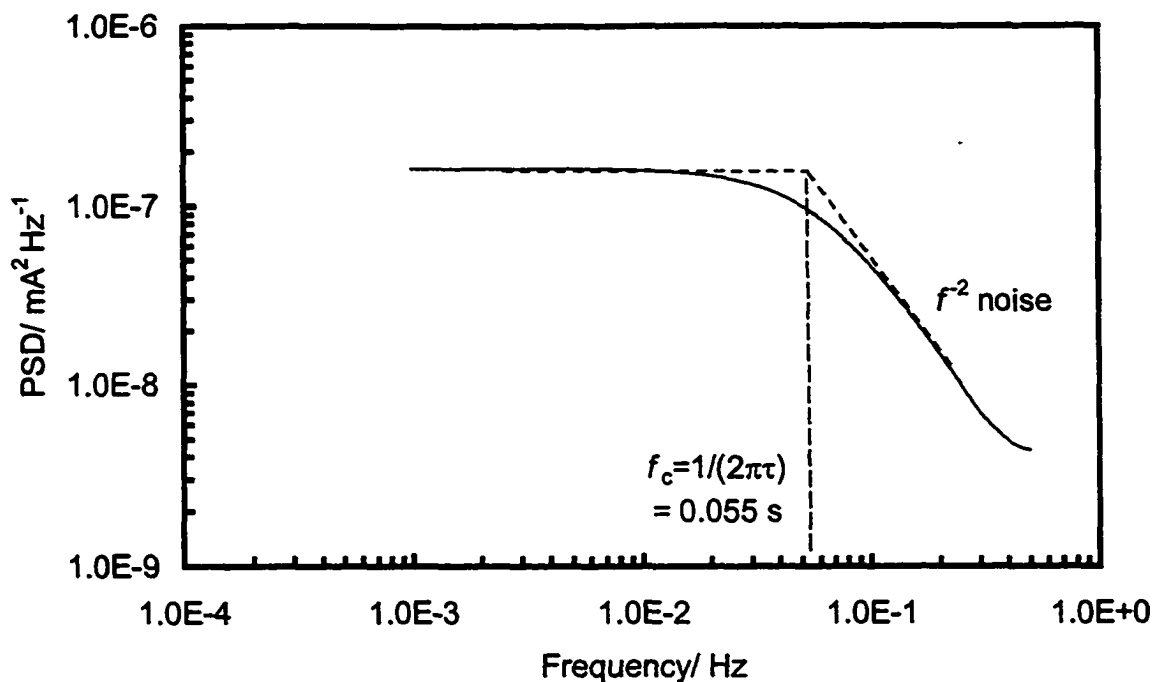
Fig. 5-17 PSD plot calculated from the current noise data in Fig. 5-16 generated during metastable pitting of carbon steel.
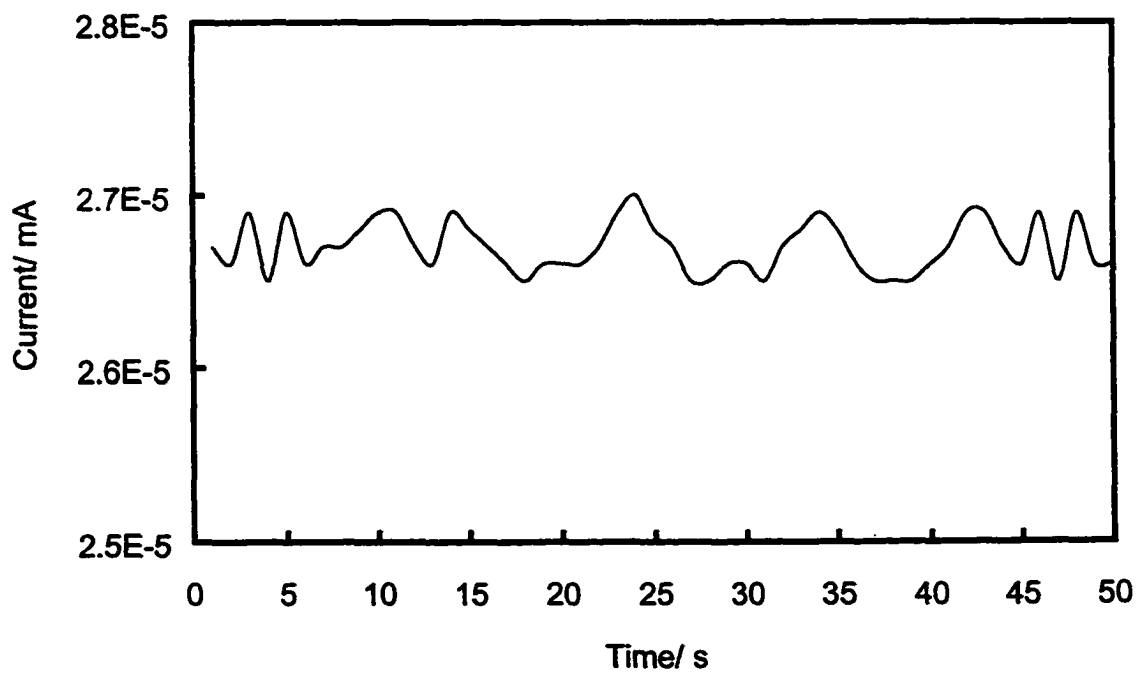
Fig. 5-18 The details of the current transients during passivity of carbon steel.

154
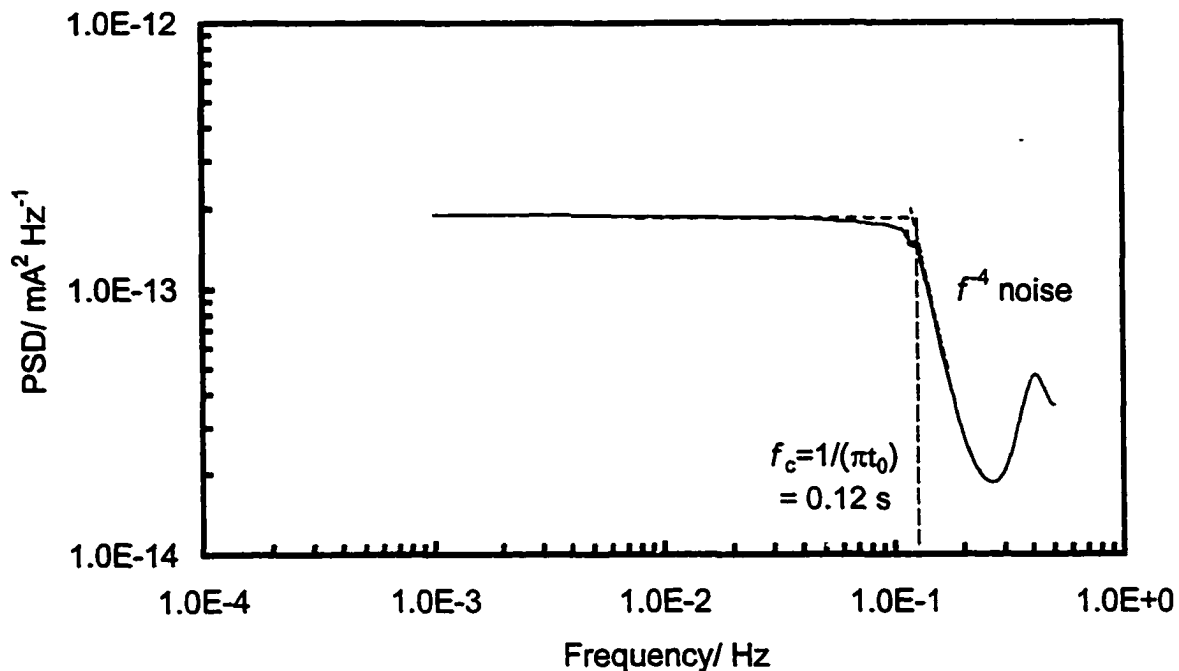
Fig. 5-19 PSD plot calculated fron the current noise data generated during passivity of carbon steel.

"white" noise part and the f^{-4} noise part are connected at the roll-off frequency of about

0.12 second, which is equal to $f_c = \dfrac{1}{\pi t_0} = 0.12 Hz.$

According to the PSD analysis of noise data generated during pitting and passivity of carbon steel, it is seen that the theoretical analysis results of the noise spectrum are quite consistent with the PSD values calculated from the measured noise data. Therefore, it is reasonable to predict the PSD plot and extract useful information from the recorded noise transient based on the analysis results in this work.

5.4 Conclusions

155

*   The relationship between spectral parameters and transient variables during pitting is established based on a pitting model. The PSD level reflects the pitting activity and increases with the current rise rate and the pit initiation rate. The roll-off slope increases with increasing pit growth time. The roll-off frequency represents the repassivation kinetics of metastable pits.

*   Any transient having a sudden birth or a sudden death generates f^{-2} noise in the high frequency range, while the transients without sudden change show f^{-4} behavior. The "white" noise spectrum appears in the low frequency range. This result is independent of the corrosion system (localized corrosion, general corrosion and passivity).

*   The roll-off frequencies of PSD corresponding to the transients with an exponential function in the time domain generated during pitting have a definite physical meaning, that is, the time constant of the exponential function. For the transients showing the features of triangular and delta waves generally generated in passivity and general corrosion systems, the roll-off frequency is directly related to the time interval of the current transient during the current rise or drop stage.

*   The PSD results calculated from the measured noise data are quite consistent with the theoretical analyses of the noise spectrum. It is reasonable to predict the PSD plots and extract useful information from the recorded noise transients based on the analysis results in this work.

References

1. C. Gabriell, F. Huet, M. Keddam and R. Oltra, *Corrosion* **46**, 266 (1990).

2. D.E. Williams, C. Westcott and M. Fleischmann, *J. Electrochem. Soc.* **132**, 1804 (1985).

3. U. Bertocci and Y.X. Ye, *J. Electrochem. Soc.* **131**, 1011 (1984).

4. P.C. Searson and J.L. Dawson, *J. Electrochem. Soc.* **135**, 1908 (1988).

5. P.C. Pistorius and G.T. Burstein, *Corros. Sci.* **36**, 525 (1994).

6. C. Gabrielli and M. Keddam, *Corrosion* **48**, 794 (1992).

7. A. Legat and V. Dolecek, *Corrosion* **51**, 295 (1995).

8. G.T. Burstein, P.C. Pistorius and S.P. Mattin, *Corros. Sci.* **35**, 57 (1993).

9. J.L. Dawson, in *Electrochemical Noise Measurement for Corrosion Application*, J.R. Scully, P.R. Roberge, D.L. Reichert and J.L. Dawson, Editors, p. 3, ASTM STP 1277, West Conshohocken, PA (1996).

10. P.R. Roberge, S. Wang and R. Roberge, *Corrosion* **52**, 733 (1996).

11. S.T. Pride, J.R. Scully and J.L. Hudson, *J. Electrochem. Soc.* **141**, 3028 (1994).

12. J.W. Cooly and J.W. Tukey, *Mathematics of Computation* **19**, 297 (1965).

13. J.P. Burg, Maximum Entropy Spectral Analysis, in *Proceedings of the 37th International Meeting of the Society of Exploration Geophysicists*, Oklahoma City, OK (1967).

14. T. Fukuda and T. Mizuno, *Corros. Sci.* **38**, 1085 (1996).

15. K. Hladky and J.L. Dawson, *Corros. Sci.* **22**, 231 (1982).

16. J.C. Uruchurtu and J.L. Dawson, *Corrosion* **43**, 19 (1987).

17. R. Oltra, C. Gabrielli, F. Huet and M. Keddam, *Electrochim. Acta* **31**, 1501 (1986).

18. G. S. Frankel, L. Stockert, F. Hunkeler and H. Bohni, *Corrosion* **43**, 429 (1987).

19. A. Legat and E. Govekar, in *Electrochemical Noise Measurement for Corrosion Applications*, J.R. Kearns, J.R. Scully, P.R. Roberge, D.L. Reichert and J.L. Dawson, Editors, p. 129, ASTM STP 1277, West Conshohocken, PA (1996).

20. C. Monticelli, G. Brunoro, A. Frignani and G. Trabanelli, *J. Electrochem. Soc.* **139**, 706 (1992).

21. U. Bertocci and F. Huet, *Corrosion* **51**, 131 (1995).

22. C. Gabrielli, F. Huet and M. Keddam, *Electrochim. Acta* **31**, 1025 (1986).

23. Y.F. Cheng, J.L. Luo and M. Wilmott, in *Corrosion '98*, paper no. 389, NACE, San Diego (1998).

24. Y.F. Cheng, M. Wilmott and J.L. Luo, *Corros. Sci.* **41**, 1245 (1999).

25. Y.F. Cheng and J.L. Luo, *J. Electrochem. Soc.* **146**, 970 (1999).

26. G. T. Burstein, P.C. Pistorius and S. P. Mattin, *Corros. Sci.* **35**, 57 (1993).

27. J. Pattinson and G.T. Burstein, in *Computer Aided Acquisition and Analysis of Corrosion Data*, M.W. Kendig, U. Bertocci and J.E. Strutt, Editors, PV 85-3, p. 108, The Electrochemical Society Proceeding Series, Pennington, NJ (1984).

28. P. C. Pistorius and G. T. Burstein, *Phil. Trans. R. Soc. Lond* A **341**, 531(1992).

157

29. P. C. Pistorius and G. T. Burstein, *Corros. Sci.* **33**, 1885 (1992).

30. H. Bohni, *Materials Science Forum* **111-112**, 401 (1992).

31. D. Gorse, C. Boulleret and B. Baroux, in *Electrochemical Noise Measurement for Corrosion Applications*, J.R. Kearns, J.R. Scully, P.R. Roberge, D.L. Reichert and J.L. Dawson, Editors, p. 332, ASTM STP 1277, West Conshohocken, PA (1996).

Chapter 6 Monitoring of Corrosion Rate by Electrochemical Noise Technique — Application of Noise Resistance

6.1 Introduction

The measurements and analyses of EN have become widespread in obtaining corrosion information.[1,2,3] Of various analysis methods of EN data, the application of noise resistance has recently attracted increasing interest.[4,5,6,7,8,9,10]

EN is generally measured as potential and current fluctuations in the time domain. The noise resistance (R_n) is calculated as the ratio of the standard deviation of potential (σ U) to the standard deviation of current (σI) over a fixed period of time.[5,6] Theoretical analysis proves that the potential and current noise are related by the impedance of the metal/solution interface. It is proposed that noise resistance can be interpreted in essentially the same way as conventional polarization resistance (R_p).[11,12] Obviously, the noise resistance is a function of the electrochemical behavior of the material under study. In addition, if the period of sampling time (the number of sample data times the sampling interval) used to statistically calculate the standard deviations of potential and current changes, the noise resistance will be different. Therefore, the noise resistance is a function of the period of sampling time.

The noise data can also be transformed from the time domain into the frequency domain to obtain power spectral density (PSD) by the fast Fourier transform (FFT)[13] or the maximum entropy method (MEM).[14] The transformed potential and current data at each frequency can be used to calculate the spectral noise impedance R_{sn} (f), the square root of the ratio of potential PSD to current PSD, at each frequency.[6] Similar to the relationship between noise resistance and polarization resistance, the spectral noise impedance should have some analogy with the magnitude of the electrochemical impedance.

159

Noise resistance has been used in many aspects of corrosion, such as coating performance and degradation,[5,6,15] corrosion rate determination,[5] and onset of localized corrosion. Others' results have shown[16] that noise resistance can qualitatively monitor the changes of corrosion resistance. However, there still exist arguments on the relationship between noise resistance and polarization resistance. For example, Dawson et al.[17] found that R_n correlates well with both polarization resistance and weight loss of carbon steel in acid, while the analysis for 410 stainless steel in chloride solutions performed by Kelly et al.[16] indicated that R_n generally overestimates the polarization resistance, leading to an underestimate of the corrosion rate. Although some attempts to justify the relationship between R_n and R_p on theoretical grounds have been published,[18] their validity is questioned.[19,20] Chen and Bogaert[21] proposed a mathematical derivation based on the kinetics of the interfacial processes. However, its applicability is restricted because the treatment assumes appropriate conditions such as activation-controlled anodic and cathodic reactions. Bertocci and Huet[3] described a model linking R_n and the magnitude of the electrode impedance by computer simulation. The model still needs experimental verification.

In order to clarify the physical meaning of noise resistance, Bertocci et al.[9] presented a model describing the current and potential fluctuations simultaneously occurring in an electrochemical cell based on either a current or potential noise source internal to the electrodes. This model allows the evaluation of R_n and $R_{sn}(f)$, and the development of the theoretical basis for the relationship between R_n and electrode impedance, considering the various measurement schemes and affecting parameters such as cell geometry, solution resistance and electrodes with different kinetics. It was shown that, over a quite large range of corrosion conditions (localized, uniform with or without hydrogen evolution), $R_{sn}(f)$ coincides with the impedance modules $|Z|$ of the electrode. R_n is equal to R_p only if certain conditions are satisfied. Further experimental results[11] proved that the above derivation does not depend on the corrosion kinetics and can be true for various corrosion situations.

In this chapter, the noise resistance and spectral noise impedance were calculated based on noise data recorded in different corrosion systems and then compared with the

160

polarization resistance and electrode impedance, respectively. The theoretical basis of the application of noise resistance to carbon steel corrosion in various systems is discussed.

6.2   Some basic terms

The noise resistance and spectral noise impedance were statistically calculated in the time and frequency domain, respectively, according to the following equations:[4,5,6,9,15]

$$R_n = \frac{\sigma U(t)}{\sigma I(t)} \tag{6-1}$$

$$R_{sn}(f) = \left| \frac{U_{PSD}(f)}{I_{PSD}(f)} \right|^{\frac{1}{2}} \tag{6-2}$$

where $U_{PSD}(f)$ and $I_{PSD}(f)$ are the PSD data of potential and current noise, respectively. The spectral noise resistance $R_{sn}{}^0$ is defined as the zero frequency limit of the spectral noise impedance:[4,5]

$$R_{sn}^0 = \lim_{f \to 0} R_{sn}(f) \tag{6-3}$$

6.3   Results

6.3.1   Carbon steel in bicarbonate solution

The polarization curves of A516-70 carbon steel in the solutions containing inhibitive HCO_3^- ions and aggressive Cl^- ions are shown in Fig. 4-40. It can be seen that the carbon steel electrode passivates in 0.5 M HCO_3^- solution with the passive range of -100mV to 950mV. The passivation mechanism of carbon steel in bicarbonate solution has been discussed in Chapter 4. A516-70 carbon steel in sodium bicarbonate solution is a passive system.

161

The electrochemical noise generated in a passive system mainly comes from the dissolution of passive film and the reduction of oxygen. The recorded potential and current noise, as shown in Fig. 4-3, consist of very frequent potential and current fluctuations with amplitudes of approximately 0.8 mV and 2 nA, respectively.

The recordings of potential and current noise versus time are analyzed statistically to calculate R_n and R_{sn}^0. The values of R_p are determined by impedance measurements. The variations of R_n, R_{sn}^0 and R_p with exposure time in 0.5 M NaHCO$_3$ solution are plotted in Fig. 6-1. The three parameters are found to have the same trend. After about six hours of immersion, all of the resistance fluctuate around 1.8×10^6 Ω, indicating that a stable passive state has been reached. In a passive system, there are very similar values of R_n, R_{sn}^0 and R_p although they are mathematically unrelated.

The spectral noise impedance $R_{sn}(f)$ is determined by transforming the noise data from the time domain into the frequency domain by FFT. The comparison of $R_{sn}(f)$ and the magnitude of electrode impedance $|Z|$ measured by the EIS technique is shown in Fig. 6-2. Excellent agreement between both curves obtained by different methods is observed at frequencies lower than 0.5 Hz. Spectral analysis at a higher frequency range is not possible because of the limitations in the sampling rate.

6.3.2 Carbon steel in chloride solution

Fig. 4-40 shows that a carbon steel electrode in 0.1 M NaCl solution displays an active dissolution behavior, which corresponds to a general corrosion. Fig. 4-42 shows the potential and current noise recorded in this system. It is seen that there is an apparent DC shift for both potential and current fluctuations. However, the magnitude of background current of about 10^{-3} mA is much larger than that measured in the passive system (about 10^{-5} mA), and the background potential of about -646 mV is more negative than that of approximate -172 mV in passivity. So the carbon steel electrode dissolves with a much higher rate in this system.

The comparison of R_n, R_{sn}^0 and R_p as a function of the exposure time is shown in Fig. 6-3. It is seen that these parameters decrease with the immersion time in the beginning.

Fig. 6-1 Time dependence of R_n, R_{sn}^0 and R_p in 0.5 M NaHCO$_3$ solution.
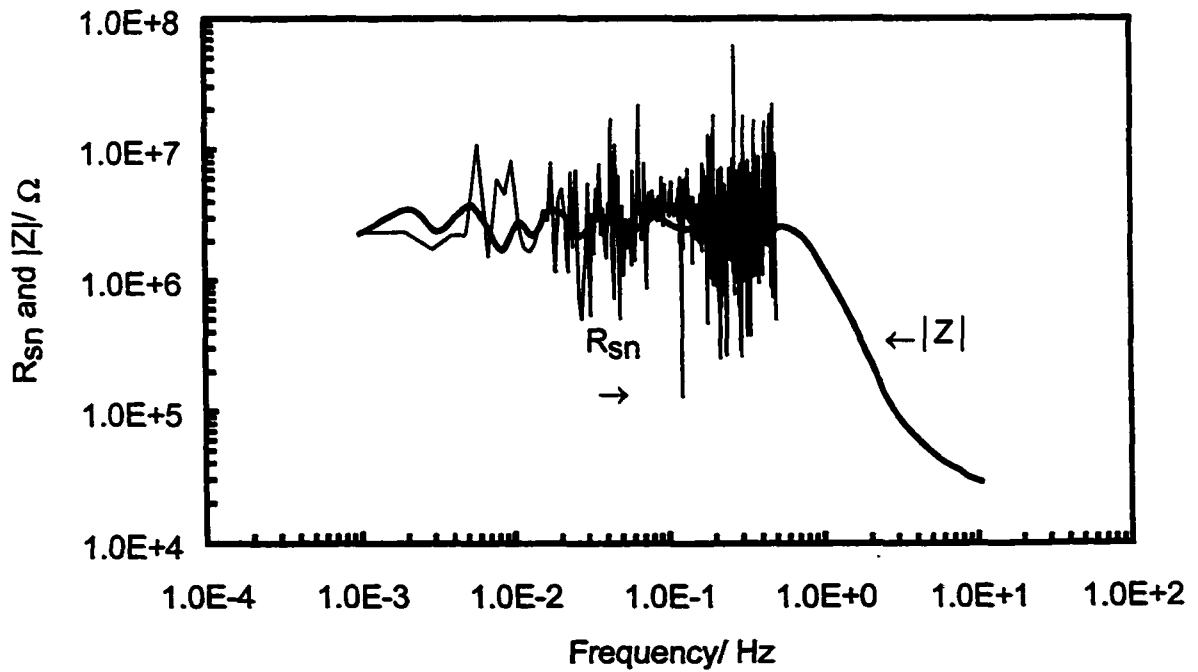
Fig. 6-2 Frequency dependence of $R_{sn}(f)$ and $|Z|$ for A516-70 carbon steel in 0.5 M NaHCO$_3$ solution.
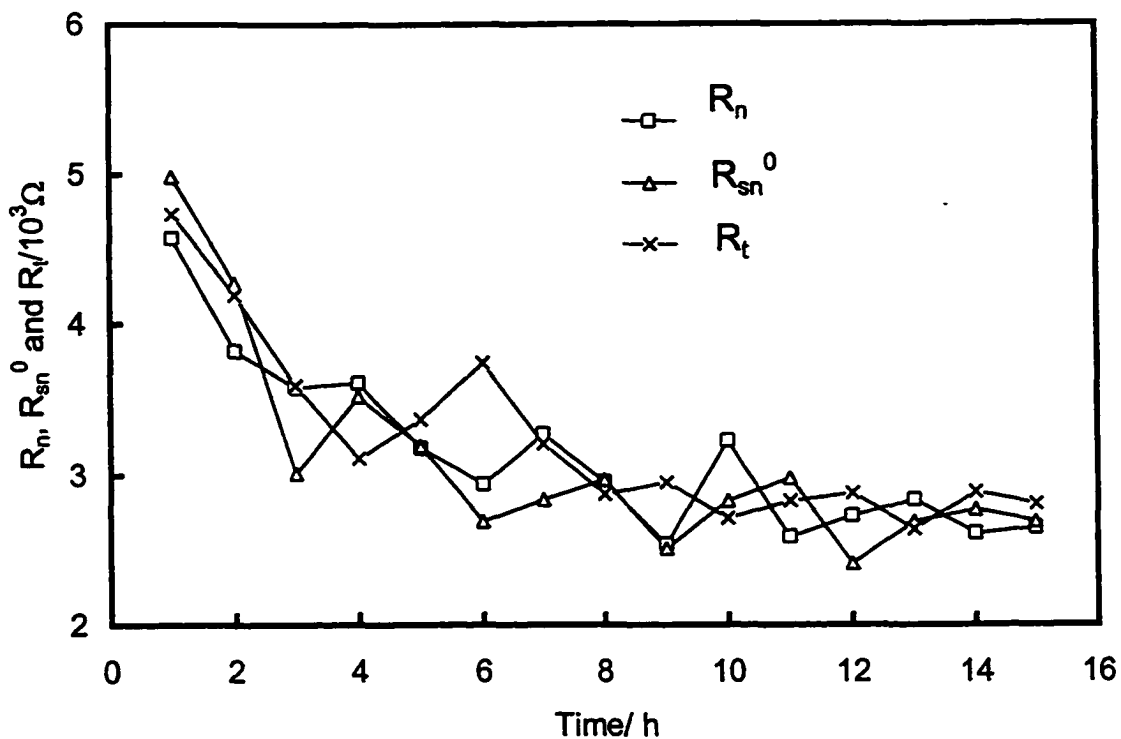
Fig. 6-3 Time dependence of R_n, R_{sn}^0 and R_p in 0.1 M NaCl solution.
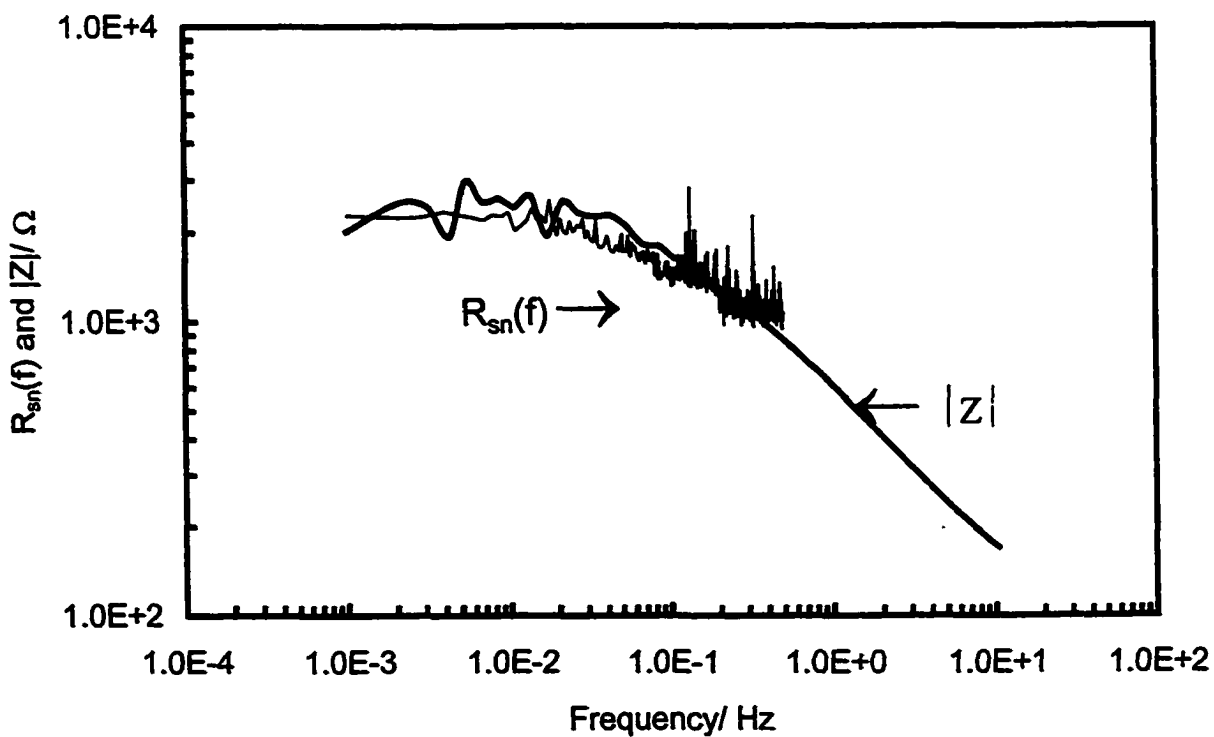
Fig. 6-4 Frequency dependence of $R_{sn}(f)$ and $|Z|$ in 0.1 M NaCl solution.

After about six hours of immersion, all of the three resistances become constant and fluctuated around 2.6×10^3 Ω, three orders of magnitude less than that measured in the passive system. When the stable state of general corrosion of carbon steel is reached, R_n, R_{sn}^0 and R_p have very similar values.

The comparison of the spectral noise impedance and the magnitude of electrode impedance as a function of frequency is shown in Fig. 6-4. The two curves almost copies each other at frequencies lower than 0.5 Hz, which is the lower frequency limitance for PSD analysis.

6.3.3 Carbon steel in bicarbonate and chloride solution

It has been analyzed in Chapter 4 that the addition of chloride ions to the inhibitive solution will degrade the passivity of carbon steel. As shown in Fig. 4-40, the passive potential range decreases to about 150 mV when 0.1 M Cl$^-$ is added to 0.5 M HCO$_3^-$ solution. The passive current density also increases. The potential and current noise recordings after 10 hours of immersion, as shown in Fig. 4-5, are characterized by typical transients, which consist of a quick current rise and a potential drop followed by a slow recovery. This kind of transients is believed to be an indication of the initiation of metastable pits.[22,23,24] Therefore, A516-70 carbon steel in 0.5 M HCO$_3^-$ + 0.1 M Cl$^-$ solution leads to a pitting system.

Fig. 6-5 shows R_n, R_{sn}^0 and R_p as a function of exposure time for A516-70 carbon steel in HCO$_3^-$/Cl$^-$ solution. It is found that the time dependence of the three resistences is similar, that is, slightly decreasing with the exposure time. However, the numerical values of R_n are much lower than R_{sn}^0 and R_p, while the values of R_{sn}^0 and R_p are close to each other.

Fig. 6-6 shows $R_{sn}(f)$ calculated from the potential and current PSD data, together with impedance magnitude obtained from EIS measurements. It is seen that $|Z|$ coincides with the $R_{sn}(f)$ curve over the whole experimental frequency range. In contract to the curves collected in the passive state shown in Fig. 6-2 and in the general corrosion system
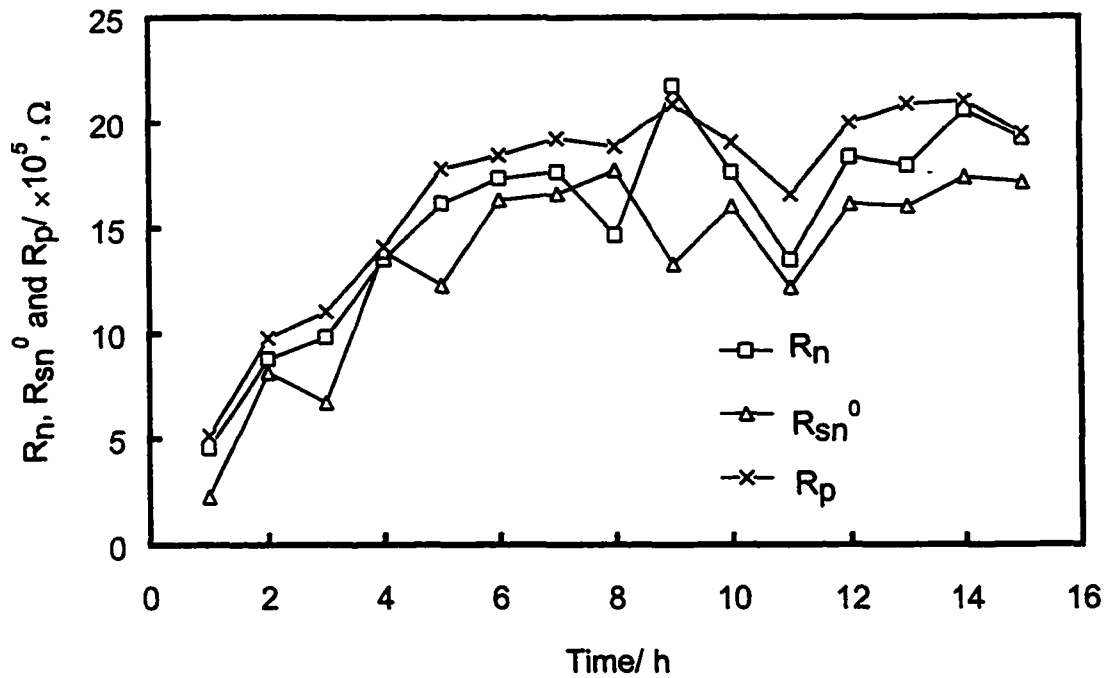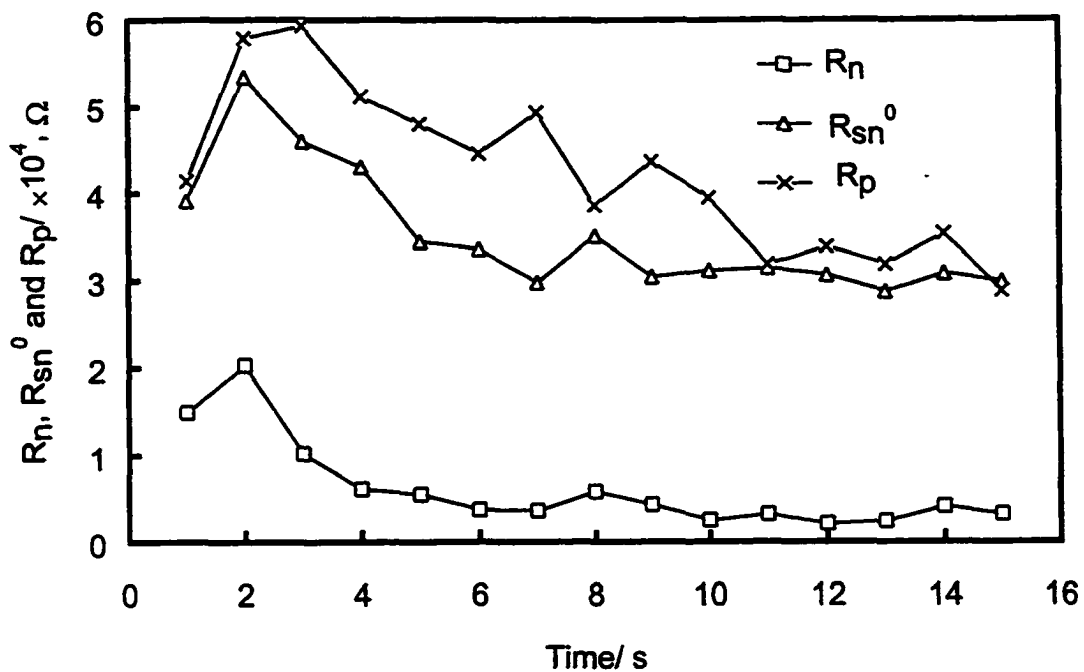
Fig. 6-5 Time dependence of R_n, R_{sn}^0 and R_p in 0.5 M $NaHCO_3$ + 0.1 M NaCl solution.
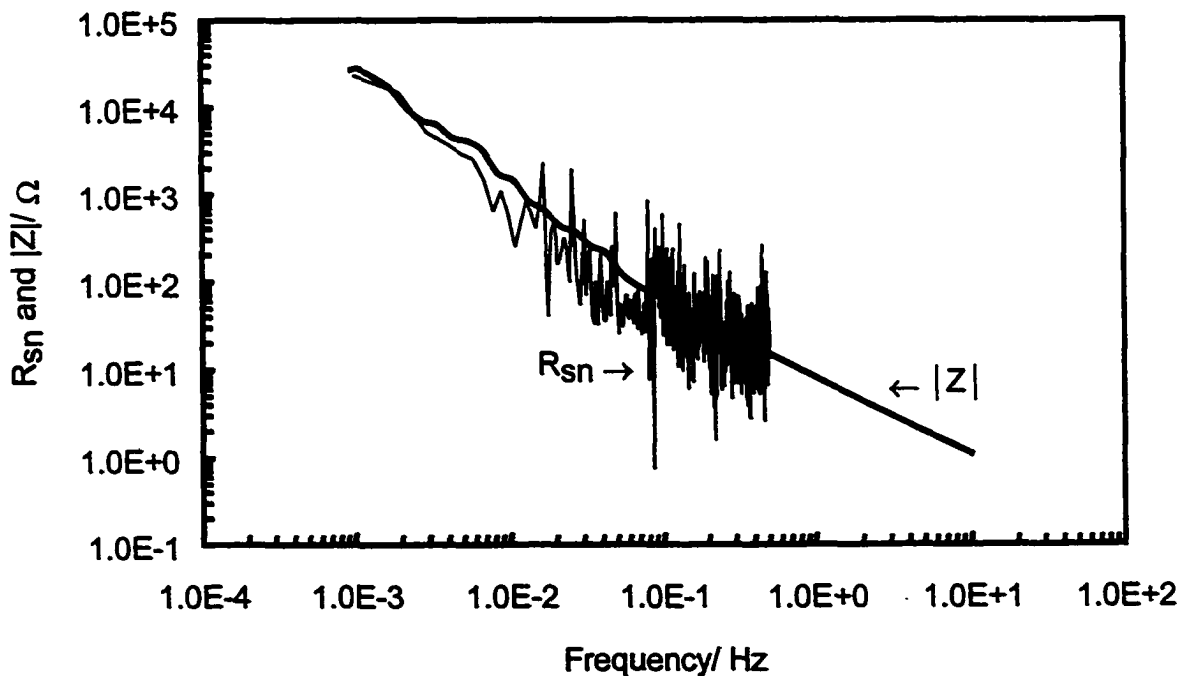
Fig. 6-6 Frequency dependence of $R_{sn}(f)$ and $|Z|$ for A516-70 carbon steel in 0.5 M $NaHCO_3$ + 0.1 M NaCl solution.

166

in Fig. 6-4, there is no low frequency plateau for either curve in Fig. 6-6, that is, the impedance continuously increased when the frequency decreased.

6.4 Discussion

The experimental results of EN measurements have confirmed that the spectral noise impedance $R_{sn}(f)$ is equal to the magnitude of the electrode impedance $|Z|$ in various corrosion situations. The results presented in this work were obtained from three systems with quite different noise sources. For passivated carbon steel in bicarbonate solution the principal source of EN is the slow dissolution of passive film. When the carbon steel specimen is in chloride solution, the EN mainly comes from the general corrosion of carbon steel. While for carbon steel in HCO_3^-/Cl^- solution, the noise source is pitting of carbon steel. Therefore, the agreement between $R_{sn}(f)$ and $|Z|$ is independent of the corrosion situation. The theoretical model developed by Bertocci et al.[10] predicted that the spectral noise impedance is proportional to the magnitude of the electrode impedance, and with the proportional factor having the value of 1 if a "noiseless" RE is used. The noise analysis performed on carbon steel in HCO_3^{2-} and/or Cl^- solutions confirm the theoretical predictions of their model.

Once it is established that $R_{sn}(f)$ is equivalent to $|Z|$, it is possible to discuss the significance of noise resistance obtained by EN measurements. The relationship between R_n and $R_{sn}(f)$ is[11]

$$R_n = \frac{\sigma U(t)}{\sigma I(t)} = \left[\frac{\int_0^{+\infty} U_{PSD}(f)df}{\int_0^{+\infty} I_{PSD}(f)df} \right]^{\frac{1}{2}} \qquad (6-4)$$

In practice, the PSD plots are measured in a limited frequency bandwidth (f_{min}, f_{max}). The low frequency limit is the inverse of the measurement time. The high frequency limit is one-half of the sampling time. Considering Eq. (6-2),

167

$$R_n = \left[\frac{\int_{f\,min}^{f\,max} I_{PSD}(f) R_{sn}(f)^2 \, df}{\int_{f\,min}^{f\,max} I_{PSD}(f) \, df} \right]^{\frac{1}{2}}$$

(6-5)

Therefore, each point on the R_n curves produced in the real time corresponds to the right side of Eq. (6-5). When the spectral noise impedance $R_{sn}(f)$ does not depend on the frequency in the range of (f_{min}, f_{max}), the noise resistance is equal to R_{sn}.

For the $R_{sn}(f)$ (or $|Z|$) vs. frequency curve with a long low frequency plateau, as those shown in Fig. 6-2 and Fig. 6-4, the right side of Eq. 6-5 gives a value corresponding to the zero frequency limit of the spectral noise impedance. Generally, the current noise spectra obtained in passivity and general corrosion systems are characterized by a "white" noise in the low frequency range and a $1/f^\alpha$ noise in the high frequency range, as shown in Fig. 5-13 and Fig. 5-15. The potential noise spectrum will have identical features to current spectrum because both potential and current fluctuations have the same pattern with time (Fig. 4-3). Therefore, the frequency dependence of spectral noise impedance is characterized by a plateau in the region of low frequency, and a zero frequency limit can thus be estimated. This conclusion can also be numerically verified. For example, in a passive system, the values of R_n obtained from the time records in Fig. 6-1 after 6 hours of immersion (with the system is in a stable state) range from 1.349×10^6 to 2.172×10^6 Ω, with a mean of 1.761×10^6 Ω, which is close to the zero frequency limit of the $R_{sn}(f)$ and $|Z|$ curves, which is close to 2×10^6 Ω, in Fig. 6-2. In such a case, both R_n and R_{sn}^0 coincide with R_p, as shown in Fig. 6-1. Therefore, noise resistance provides an indication of the corrosivity of material in stable passivity. For a general corrosion system, the average value of noise resistance is determined as about 2.835×10^3 Ω from Fig. 6-3. The zero frequency limit of the spectral noise impedance is approximately 2.5×10^3 Ω, as shown in Fig. 6-4. Therefore, noise resistance also provides an indication of material corrosivity in a general corrosion system.

However, there are some cases where R_n might differ substantially from the zero frequent limit of $|Z|$. This is well illustrated by the measurements in bicarbonate/chloride solution shown in Fig. 6-5 and 6-6. As analyzed in Chapter 4, carbon steel electrode where pitting occurs behave like leaky capacitors subjected to extremely short current bursts as shown in Fig. 4-5. The corresponding current PSD is very flat in the low frequency region. While the potential transients cannot follow the current transients because of the damping effect of the electrode capacitance on potential fluctuations,[25] the potential PSD does not show a low frequency plateau. As a consequence, $R_{sn}(f)$ in Fig. 6-6 is frequency dependent in the whole range and no plateau is observed in the low frequency range. R_n is not equal to the low frequency limit of the spectral noise impedance, R_{sn}^0. In fact, R_n is much lower than R_{sn}^0 and R_p as shown in Fig. 6-5. Therefore, noise resistance can not be used to track quantitatively the change of corrosion resistance of the electrode during pitting. Spectral noise resistance is consistent with polarization resistance and can be used to indicate the corrosivity of materials in the test solutions.

6.5 Conclusions

* The spectral noise impedance is equivalent to the magnitude of the electrode impedance. This relationship is independent of the corrosion situations (i.e., passivity, general corrosion and pitting).

* Noise resistance coincides with spectral noise resistance and polarization resistance only in a specific condition, such as passivity or general corrosion, where noise resistance provides an indication of the corrosion resistance of the material under study.

* In the case of pitting corrosion, noise resistance is much lower than spectral noise resistance and polarization resistance, and does not correspond quantitatively to the change of the corrosion resistance of system.

Reference

1. J.L. Dawson, in *Electrochemical Noise Measurement for Corrosion Applications*, J.R. Kearns, J.R. Scully, P.R. Roberge, D.L. Reichert and J.L. Dawson, Editors, p. 3, ASTM STP 1277, West Conshohocken, PA (1996).

2. C. Gabrielli, F. Huet and M. Keddam, in *Electrochemical and Optical Techniques for the Study and Monitoring of Metallic Corrosion*, M.G.S. Ferreira and C.A. Melendres, Editors, p. 135, Kluwer Academic Publishers, Netherlands (1991).

3. U. Bertocci and F. Huet, *Corrosion* **51**, 131 (1995).

4. F. Mansfeld and H. Shih, *J. Electrochem. Soc.* **135**, 1171 (1988).

5. F. Mansfeld and H. Xiao, *J. Electrochem. Soc.* **140**, 2205 (1993).

6. H. Xiao and F. Mansfeld, *J. Electrochem. Soc.* **141**, 2332 (1994).

7. A. Legat and C. Zevnik, *Corros. Sci.* **35**, 1661 (1993).

8. C.T. Chen and B.S. Skerry, *Corrosion* **47**, 598 (1991).

9. U. Bertocci, C. Gabrielli, F. Huet and M. Keddam, *J. Electrochem. Soc.* **144**, 31 (1997).

10. U. Bertocci, C. Gabrielli, F. Huet, M. Keddam and P. Rousseau, *J. Electrochem. Soc.* **144**, 37 (1997).

11. R.A. Cottis, S. Turgoose and J. Mendoza-Flores, in *Electrochemical Noise Measurement for Corrosion Applications*, J.R. Kearns, J.R. Scully, P.R. Roberge, D.L. Reichert and J.L. Dawson, Editors, p. 93, ASTM STP 1277, West Conshohocken, PA (1996).

12. R. A. Cottis and S. Turgoose, *Materials Science Forum* **192-4**, 663 (1995).

13. J.W. Cooly and J.W. Tukey, *Mathematics of Computation* **19**, 297 (1965).

14. W.H. Press, B.P. Flannery, S.A. Teukolsky and W.T. Vettering, in *Numerical Recipes in Pascal*, p. 217, Cambridge University Press, Cambridge, UK (1989).

15. F. Mansfeld and H. Xiao, in *Electrochemical Noise Measurement for Corrosion Applications*, J.R. Kearns, J.R. Scully, P.R. Roberge, D.L. Reichert and J.L. Dawson, Editors, p. 59, ASTM STP 1277, West Conshohocken, PA (1996).

16. R.G. Kelly, M.E. Inman and J.L. Hudson, in *Electrochemical Noise Measurement for Corrosion Applications*, J.R. Kearns, J.R. Scully, P.R. Roberge, D.L. Reichert and J.L. Dawson, Editors, p. 101, ASTM STP 1277, West Conshohocken, PA (1996).

17. J.L. Dawson, D.M. Farrel, P.J. Aylott and K. Hladky, in *Corrosion '89*, paper no. 31, NACE, Houston, TX (1989).

18. G.P. Bierwagen, *J. Electrochem. Soc.* **141**, L155 (1994).

19. F. Mansfeld and H. Xiao, *J. Electrochem. Soc.* **141**, 1403 (1994).

20. F. Huet, *J. Electrochem. Soc.* **142**, 2861 (1995).

21. J.F. Chen and W.F. Bogaerts, *Corros. Sci.* **37**, 1839 (1995).

22. S.T. Pride, J.R. Scully, J.L. Hudson, in *Electrochemical Noise Measurement for Corrosion Applications*, J.R. Kearns, J.R. Scully, P.R. Roberge, D.L. Reichert and J.L. Dawson, Editors, p. 307, ASTM STP 1277, West Conshohocken, PA (1996).

23. G.S. Frankel, L. Stockert, F. Hunkeler and H. Bohni, *Corrosion* **43**, 429 (1987).

24. S.T. Pride, J.R. Scully and J.L. Hudson, *J. Electrochem. Soc.* **141**, 3028 (1994).

25. P.C. Pistorius, *Corrosion* **53**, 273 (1997).

Chapter 7 Semiconducting Properties of the Passive Film on Carbon Steel and Relationship between the Electronic Structure and the Pitting Susceptibility

7.1 Introduction

The passivity of metals has been subjected to special attention since the last century.[1] Although a large number of models and theories[2,3,4,5,6,7,8] have been proposed to explain the kinetics, thermodynamic, structural and electronic properties, a satisfactory description of the phenomenon of passivity is still lacking. However, it is generally acknowledged[9] that oxygen ions must be transported from the film/solution interface to the metal/film interface, resulting in the penetration of the barrier layer into the substrate metal phase. On the other hand, metal ions are transported in the reverse direction, with the relative fluxes of these species depending on the energies of formation of the respective vacancies.

Compared with many theories qualitatively describing the passive state, the point defect model (PDM)[9,10] provides a microscopic description of the growth and breakdown of the passive film and an analytical expression for the flux and the concentration of vacancies within the passive film, and hence affords an opportunity for quantitative analysis. The PDM is based on the migration of point defects (oxygen and metal vacancies) under the influence of the electrostatic field in the film. Because the film is grown into the metal by the generation of oxygen vacancies at the metal/film interface, and by their annihilation at the film/solution interface, the transport properties and spatial distribution of oxygen vacancies within the film is of great interest. A key parameter in describing the transport of oxygen vacancies and hence the kinetics of film growth is the vacancy diffusivity (D). By using Mott-Schottky analysis in conjunction with the PDM for passive films, Macdonald and co-workers[11] determined the oxygen vacancy diffusion

172

coefficient in the WO_{3-x} passive film formed on tungsten in phosphoric acid (pH = 0.96) solution at ambient temperature to be in the range of 10^{-14} to 10^{-15} cm^2/s.

It is well known that the electrochemical behavior of passive films on metals can be interpreted in terms of the semiconducting properties of the films.[12,13] Capacitance measurements have often been employed to study the electronic properties of the passive films and to obtain donor or acceptor density (N_D or N_A) and flat-band potential (U_{fb}) by analysis of the Mott-Schottky plots.[14,15,16,17,18,19,20,21]

Electrochemical investigations of the passive film on iron suggested[14,15,16,20,22,23,24,25] that the passivated iron behaves like a metal electrode covered with an n-type semiconducting film with a high donor density of 10^{25} - 10^{27} m^{-3}. Stimming[15] and Searson[22] claimed that the amorphous nature of the passive film on iron plays a major role in the semiconducting properties, such as the strong frequency dependence of the electrode capacitance. Azumi et al.[20] evaluated the passive films on iron in neutral borate and phosphate solutions from Mott-Schottky analysis and concluded that the values of N_D and U_{fb} are affected by ionic species present in the solution. Phosphate ions, not borate ions, can penetrate into the passive film and produce a large number of structural and electronic defects.

Capacitance studies and photoelectrochemical techniques have also been performed on the passive films grown on various stainless steels.[19,21,26,27,28,29] The results suggested an n-type semiconductor behavior of the passive films on stainless steels. Capacitance measurements at different frequencies indicated that the passive films are amorphous or strongly disordered semiconductors with donor concentrations similar to the values obtained for passivated iron.

The corrosion resistance of passive films is often determined by their susceptibility to local breakdown. It has been indicated[30] that the electronic structure and properties of the passive films are responsible for film breakdown and pitting initiation. Bianchi et al.[13,31] found that higher pit density occurring on the metal surface is associated with an n-type oxide film, and attempted to relate the electronic properties of passive films on stainless steels to the pitting susceptibility. However, no fundamental studies were performed to

understand the correlation between the semiconducting properties and the pitting susceptibility of the passive film.

In this chapter, capacitance measurements and Mott-Schottky analyses are performed to study the electronic properties of the passive film formed on A516-70 carbon steel in bicarbonate solution with and without chloride ions. The influences of applied potential on pitting are analyzed by electrochemical noise measurements. The relationship between electronic properties and pitting susceptibility of the passive film on carbon steel is discussed. In addition, the oxygen vacancy diffusivity is calculated based on the consideration of PDM.

7.2   Mott-Schottky analysis

The charge distribution at the semiconductor/electrolyte interface is often determined by measurements of the capacitance of the space-charge layer (C_{sc}) as a function of the electrode potential (U). The Mott-Schottky relationship ($1/C_{sc}^2$ vs. U plot) expresses the potential dependence of C_{sc} of a semiconductor electrode under depletion conditions:[32,33,34]

$$\frac{1}{C_{sc}^2} = \frac{2}{\varepsilon \varepsilon_0 e N_D} (U - U_{fb} - \frac{kT}{e}) \qquad \text{for n-type semiconductors}$$

$$\frac{1}{C_{sc}^2} = -\frac{2}{\varepsilon \varepsilon_0 e N_A} (U - U_{fb} - \frac{kT}{e}) \qquad \text{for p-type semiconductors} \qquad (7\text{-}1)$$

where ε is the dielectric constant of the passive film, taken as 15.6,[19] ε_0 is the permittivity of free space (8.854×10^{-14} F m^{-1}), e is electron charge, N_D and N_A are donor and acceptor densities, respectively, U_{fb} is flat-band potential, k is the Boltzmann constant and T is the absolute temperature. N_D and N_A can be determined from the slopes of the experimental $1/C_{sc}^2$ vs. U plots, while U_{fb} comes from the extrapolation for $1/C_{sc}^2 = 0$. The thickness of the space charge layer (W_{sc}) can also be calculated (for an n-type semiconductor) by:[19]

$$W_{sc} = [\frac{2\varepsilon\varepsilon_0}{eN_D}(U - U_{fb} - \frac{kT}{e})]^{\frac{1}{2}}$$

(7-2)

The validity of the Mott-Schotky analysis is based on the assumption that the capacitance of the space charge layer is much less than that of the Helmholtz layer.[35] In such a case, the data points in $1/C_{sc}^2$ vs. U plots can describe the semiconducting properties of the depletion region. When the frequency for capacitance measurements is so high that the contribution coming from Helmholtz capacitance to the measured electrode capacitance is negligible, the capacitance of the semiconductor/electrolyte interface mainly expresses the capacitance of the space charge layer of the semiconductor.[36] In this work, 1000 Hz was used for capacitance measurements unless specified otherwise.

7.3   Results and Discussion

7.3.1   Frequency dependence of capacitance behavior

To investigate the electronic band structures and the crystallinity of passive films, the electrode capacitance of the passive film/electrolyte interface was measured as functions of both frequency and applied potential. Fig. 7-1 shows the capacitance-potential curves measured at 1000 Hz. The results obtained at other frequencies have very similar shapes, as shown in Fig. 7-2. It is seen that at low potentials the capacitance was rather high. With increasing potential the capacitance decreased first, then became nearly constant and finally increased again at higher potentials. A hysteresis of capacitance vs. potential was observed when changing the direction of the potential sweep. Similar capacitance behavior has also been observed for pure iron[26] and stainless steels.[21,26]

The band structure model proposed by Stimming and Schultze[37] is appropriate to illustrate the capacitance behavior of a semiconducting passive film observed in this work. In the low applied potential region, the decrease of the capacitance with potential
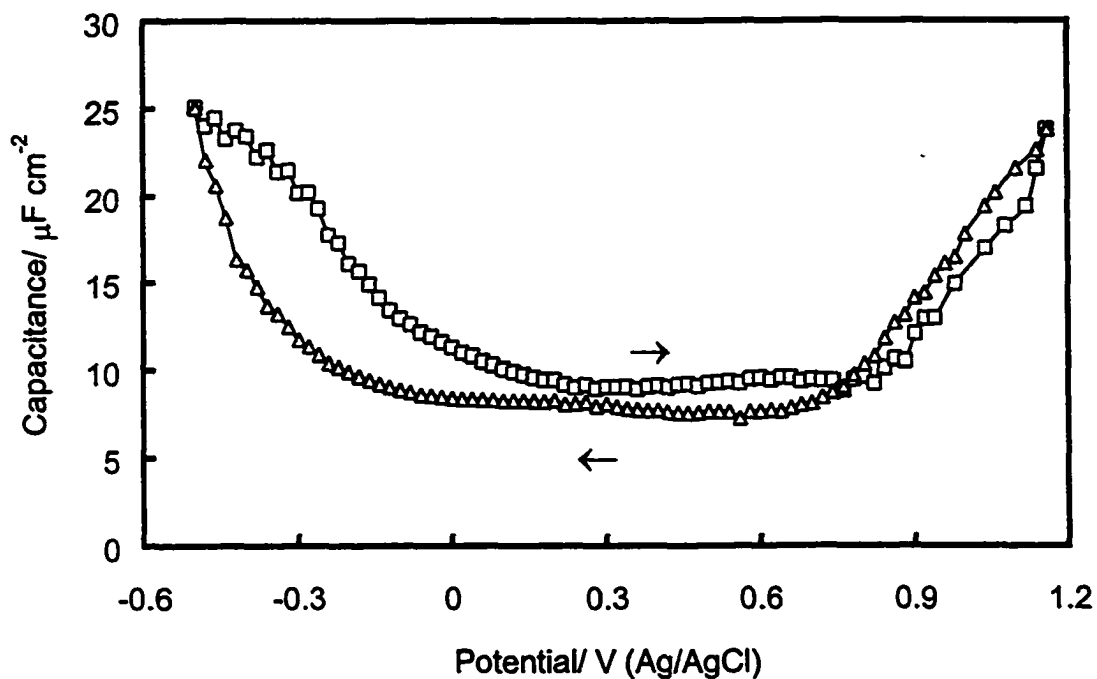
Fig. 7-1 The capacitance-potential behavior measured at 1000 Hz in 0.5 M NaHCO₃ solution.
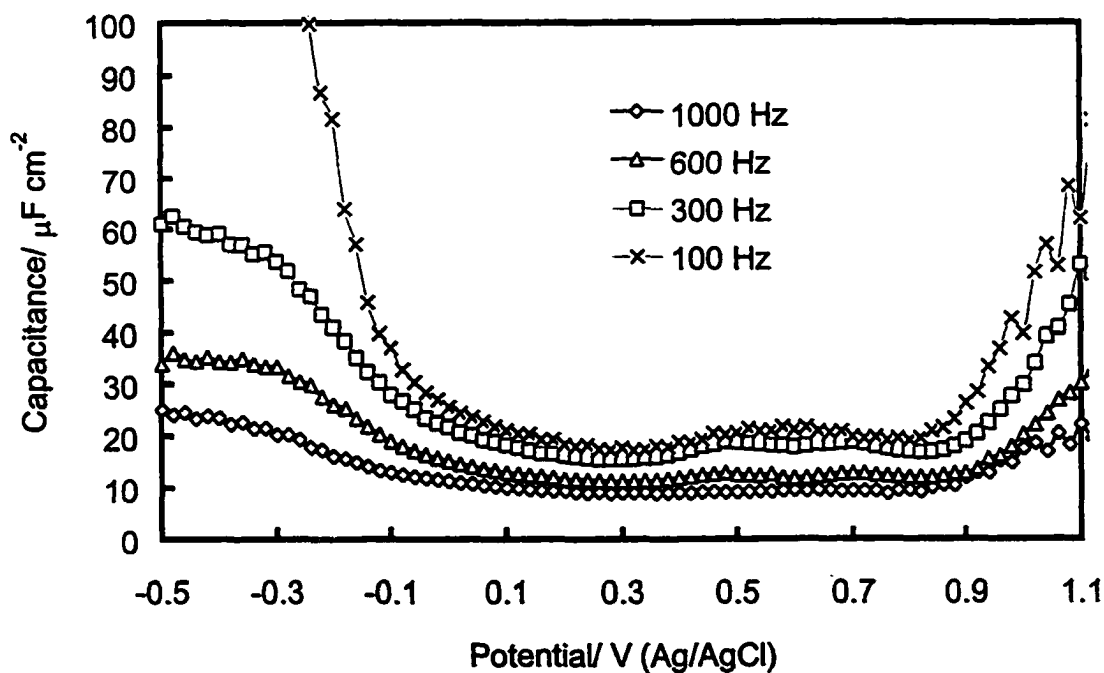
Fig. 7-2 The capacitance-potential behavior measured at different frequencies.

can be attributed to an increasing thickness of the depletion layer and a diminishing number of charge carriers (donor for an n-type semiconductor). The behavior in the range of approximately constant capacitance is due to the exhaustion of all donors in the passive film, which behaves like an insulator. At the higher potential range, the increase in capacitance can be associated with the participation of the valence band, i.e., an increasing hole concentration in the valence band, leading to their predominant accumulation and the formation of an inversion layer in the space charge layer.

The experimental results show that the capacitance values are also frequency dependent. As shown in Fig. 7-2, the curves shifted to lower values with increasing frequencies. Fig. 7-3 shows the Mott-Schottky plots obtained at different frequencies. There was also a strong frequency dispersion of Mott-Schottky plots and the straight lines obtained at low potentials were curved at high potential values.

According to Peterson and Parkinson,[38] a high density of states localized between the valence and the conduction bands characterizes a crystalline semiconductor with extensive existence of short-range disorder. Dean and Stimming[39,40,41] analyzed the influence of localized states on the capacitance as encountered in such kinds of semiconductors and suggested that a semiconductor with the existence of disorder status can show curved Mott-Schottky lines, a strong frequency dependence and a large hysteresis in the capacitance behavior. According to their analysis results, it is concluded that the presence of a hysteresis in the capacitance behavior (Fig. 7-1) and the strong frequency dependence of capacitance and Mott-Schottky plots (Fig. 7-2 and 7-3) observed in this work show that the passive film on carbon steel is a strongly disordered semiconductor with the presence of extensive short-range disorder.

The frequency dependence of capacitance is attributed to the ionic part of the space charge. Because of the low ionic mobility, these ionic charges give a contribution to the capacitance only at the lower frequencies.[26] Therefore, the capacitance decreases with increasing frequency. This frequency effect is apparent especially in heavily doped and disordered materials where the space charge layer is very thin. The passive films generally satisfy this requirement.

177
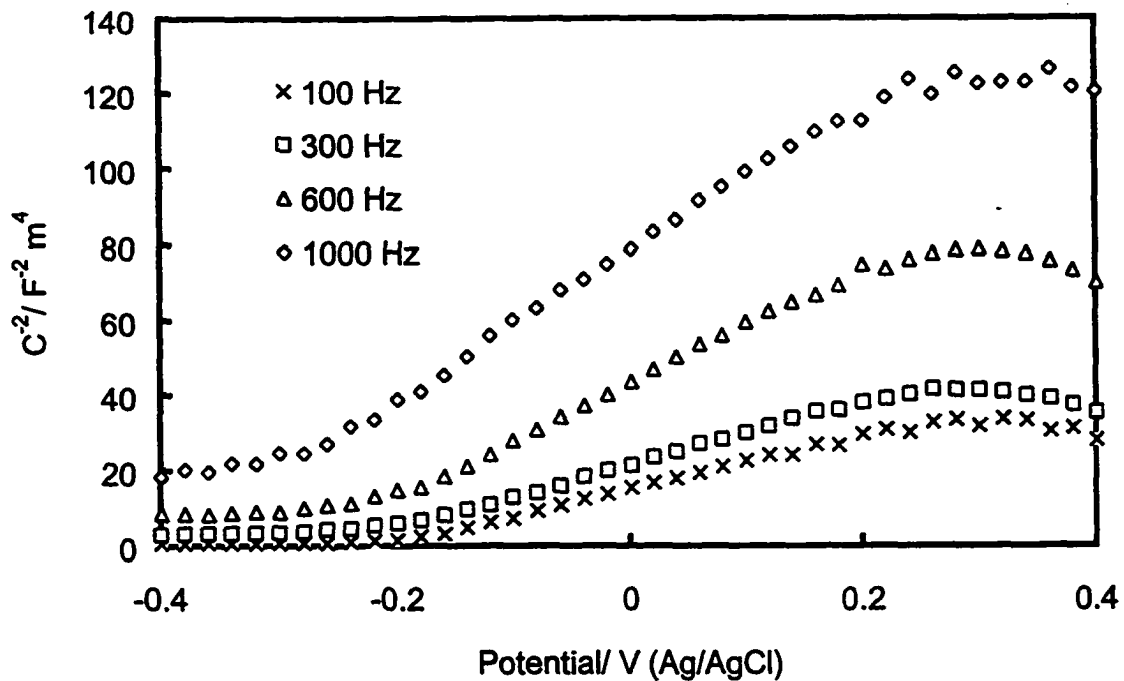
Fig. 7-3 The Mott-Schottky plots measured at different frequencies.

Based on the above-mentioned analysis, it is concluded that the model of a crystalline semiconductor with extensive short-range disorder structure is an appropriate one to describe the capacitance behavior of the passive film on carbon steel in this work.

7.3.2 Analysis of the electronic band structure of passive films

To study the influences of film formation potential on capacitance behavior, the specimens were pre-passivated at various potentials and the Mott-Schottky plots were then measured. The results for passive films formed at the corrosion potential (U_{corr}), -200 mV and 200 mV, respectively, are shown in Fig. 7-4. The shape of Mott-Schottky plots is an indicator of the conductivity type of semiconductor. From the positive slopes present in this work, it is concluded that the passive film formed on carbon steel is an n-type semiconductor.

For the passive films formed at U_{corr} and -200 mV, there is a break point at the potential of about -70 mV, which is determined from the fitting of the data with different

178

slopes, in the Mott-Schottky plots. The slopes of the Mott-Schottky lines above and below their break points are different. The potential at the break point in Mott-Schottky plots is defined as the critical potential (U_c). Similar behavior is observed on the passive films formed at potentials lower than -70 mV. For the film formed at 200 mV, the two-slope behavior was not observed and the Mott-Schottky plot showed one single straight linear section, which is the common case when the passive film is formed above -70 mV.

Non-linearity of Mott-Schottky plots has been reported in the literature. The explanations offered for such behavior are various, including surface roughness and non-uniform donor distribution,[42] the presence of surface states which alter the potential difference across the Helmholtz layer,[43,44] distribution of donor states over a broad range of energies[40] and the existence of a second donor level in the band gap that is not ionized at the flat-band potential.[19,45] In addition, Goossens et al.[46,47] reported that the non-linear Mott-Schottky plot is due to the change of the thickness of a passive film with the applied potential. So the following analysis of the band structure is based on the assumption that the thickness of the passive film does not change during the capacitance measurements.

The influence of a deep donor level on the potential dependence of capacitance and the space charge density can be used to explain the non-linearity of Mott-Schottky plots, as suggested by Dean and Stimming[40], and Myamlin and Oleskov.[45] At flat-band conditions, the positive charge of ionized donors at the shallow energy level (E_{D1}) is neutralized by an equal concentration of conduction band electrons (Fig. 7-5a). For small values of potential difference across the space charge layer ($\Delta\phi_{SC}$), the electrons are removed from the region near the electrode surface, resulting in the formation of a depletion layer with a net positive space charge due to uncompensated donors. The growth of a depletion layer shown in Fig. 7-5b indicates the situation of a single, shallow donor level in the potential range of $\Delta\phi_{SC} \leq (E_F - E_{D2})/e$, where E_F and E_{D2} are the Fermi energy and the energy of the deep donor level, respectively. The potential U_c, at which the break of the Mott-Schottky straight line takes place, is interpreted as the critical potential for the ionization of the deep level in the space charge layer. In such a case, a significant fraction of donor states at E_{D2} becomes ionized. With the values of $\Delta\phi_{SC}$ larger than the
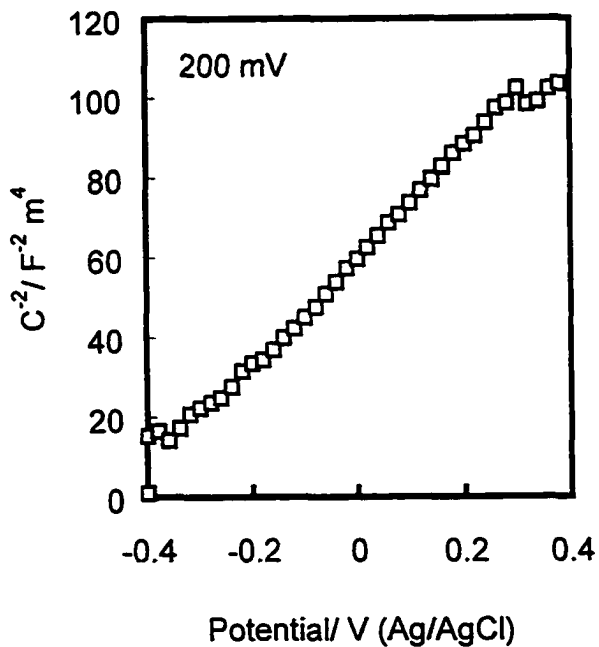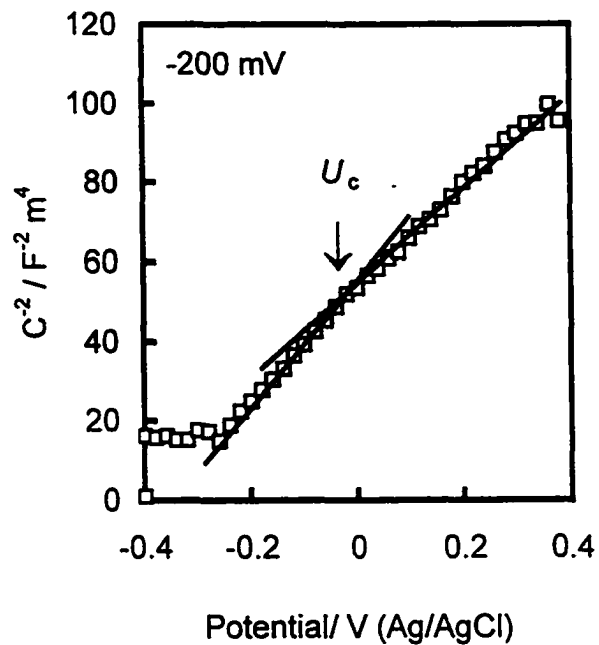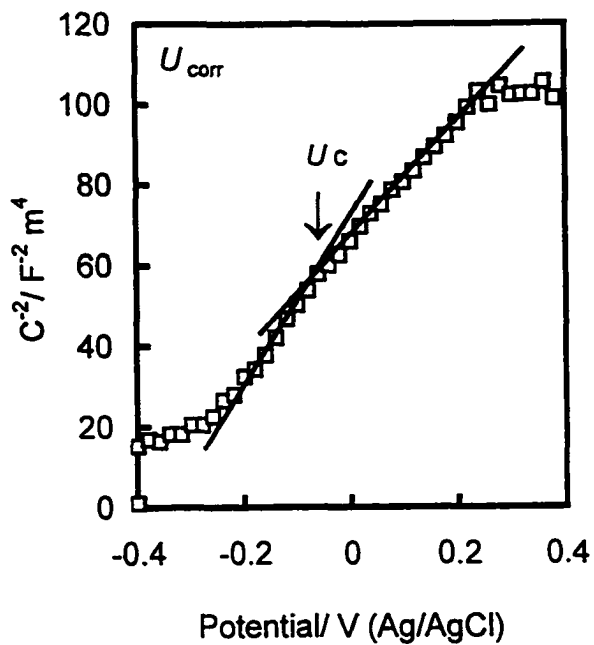
Fig. 7-4 Mott-Schottky plots for passive films on A516-70 carbon steel formed at corrosion potential, -200 mV and 200 mV at 1000 Hz in 0.5 M NaHCO₃ solution.
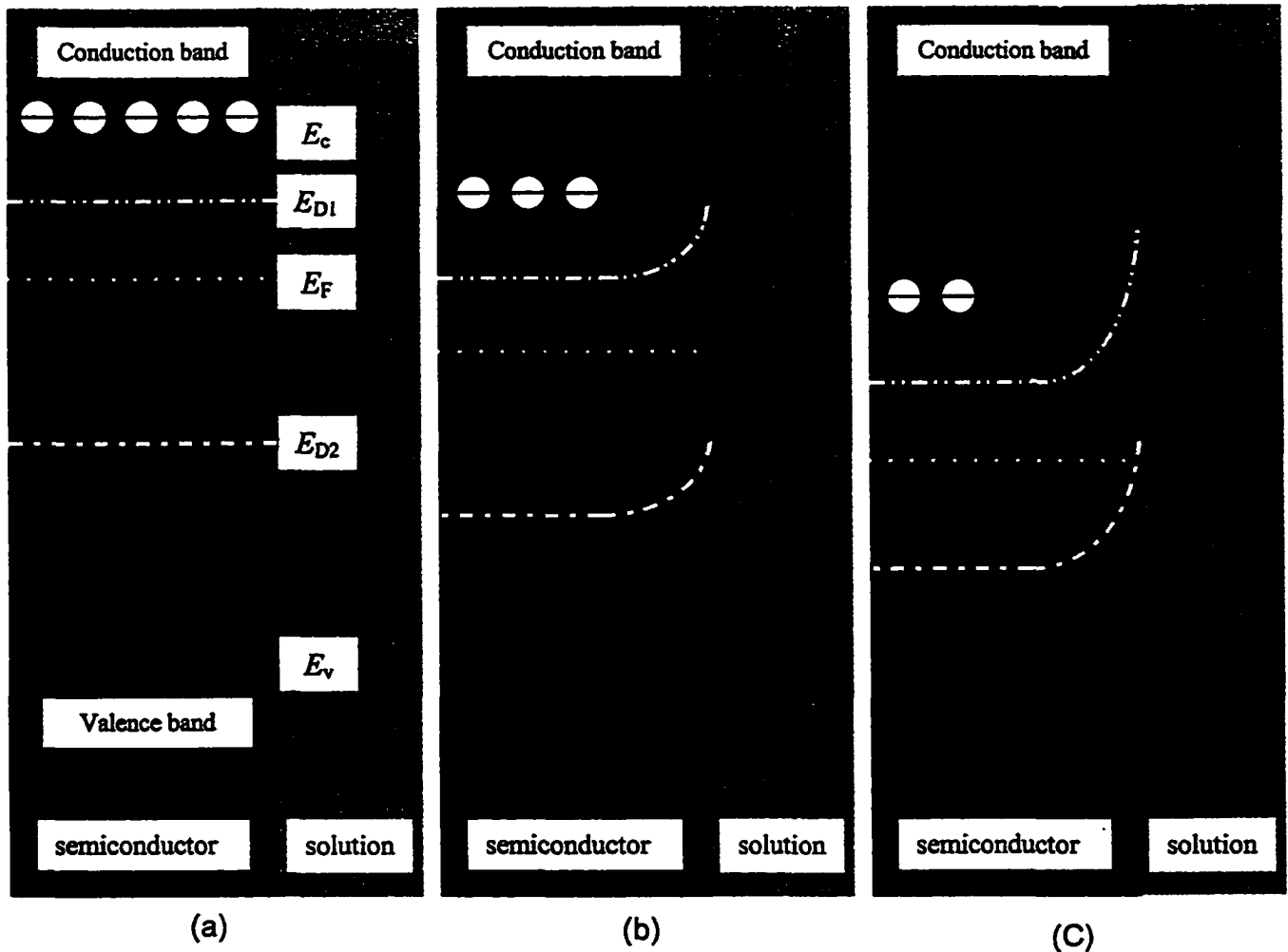
Fig. 7-5 Energy level diagram of a semiconductor with two discrete donors. (a) At flat-band conditions, the donor states at E_{D1} are completely ionized while those at E_{D2} are occupied. (b) When $e\Delta\phi_{sc} \leq E_F - E_{D2}$, the charge in the depletion layer is due to the ionized donors at E_{D1}. (c) When $e\Delta\phi_{sc} \geq E_F - E_{D2}$, donors at E_{D2} are also ionized and contribute to the space charge.

potential of (U_c-U_{fb}), the Fermi level falls below E_{D2}. Both the shallow and the deep levels of donor states contribute to the electrode capacitance. The concentrations of donors at shallow and deep levels can be determined from the two slopes S_1 and S_2, respectively, of Mott-Schottky plots by using the equation:

181

$$S_1 = \frac{2}{\varepsilon\varepsilon_0 e N_{D1}} \qquad \text{for } U < U_c \qquad (7\text{-}3a)$$

$$S_2 = \frac{2}{\varepsilon\varepsilon_0 e (N_{D1} + N_{D2})} \qquad \text{for } U > U_c \qquad (7\text{-}3b)$$

where N_{D1} and N_{D2} are the densities of the donors at shallow and deep donor levels, respectively.

Fig. 7-6 shows that for the passive films formed at potentials below -70 mV, the nonlinear Mott-Schottky plots reveal the presence of two donor levels. The total donor density of $N_{D1} + N_{D2}$ increased when the film formation potential became more negative. For a passive film formed at higher potentials, only the shallow donor was detected and N_{D1} values decreased when the formation potentials increased. The order of magnitude of N_{D1} is in the range of 10^{26} - 10^{27} m^{-3}, which are in the same order of donor densities of passive films formed on stainless steels[19,26] and iron.[23,25] Such high donor concentrations are also a corroborating indication of the highly disordered nature of the passive film on carbon steel.

7.3.3 Relationship between the semiconducting properties of passive film and the film formation potential

The influences of film formation potential on the thickness of the space charge layer and the flat-band potential in 0.5 M NaHCO$_3$ solution measured at 1000 Hz are shown in Fig. 7-7 and 7-8. It is seen that both the thicknesses of the space charge layer and the flat-band potential increase when the film formation potential becomes more positive.

The thickness of the space charge layer of the passive films on carbon steel ranges from 1 to 6 Å. The dependence of the thickness of the space charge layer on the film formation potential can be illustrated by Eq. 7-2.

Employment of the Mott-Schottky relationship for estimating the donor density has been justified by Schmuki et al.[48] They found a good agreement between the dopant concentrations determined from Mott-Schottky analysis on bulk oxides and thin passive
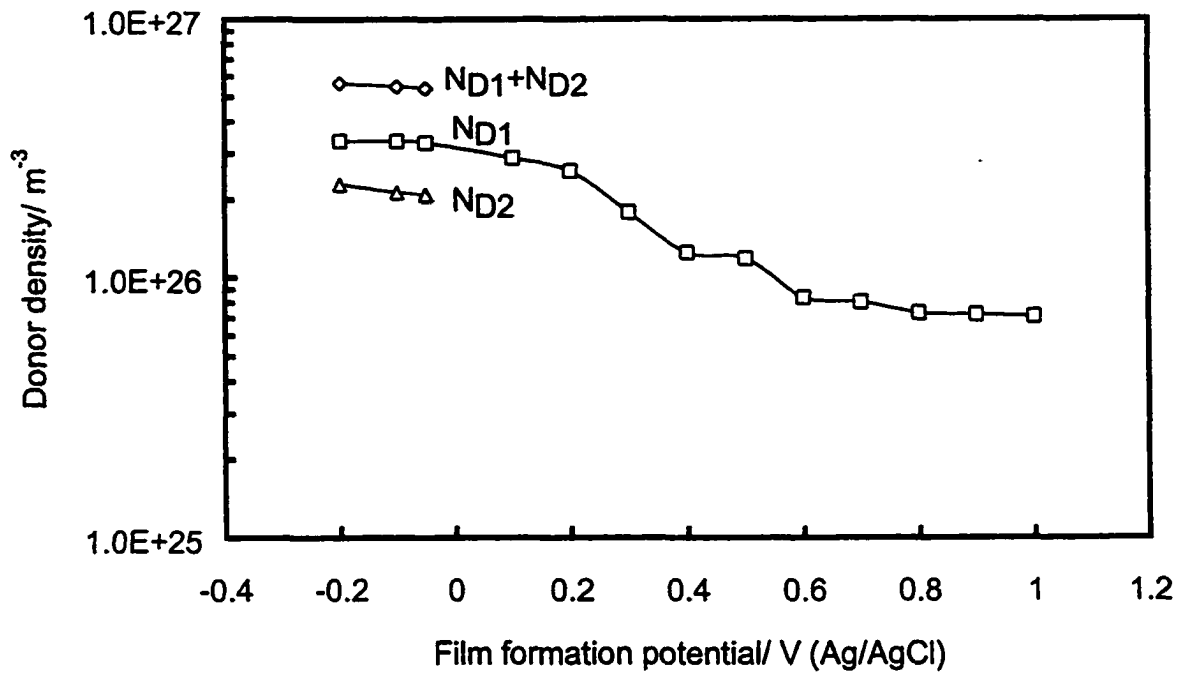
Fig. 7-6 Dependence of the donor densities at shallow level, deep level and both levels on the film formation potential.
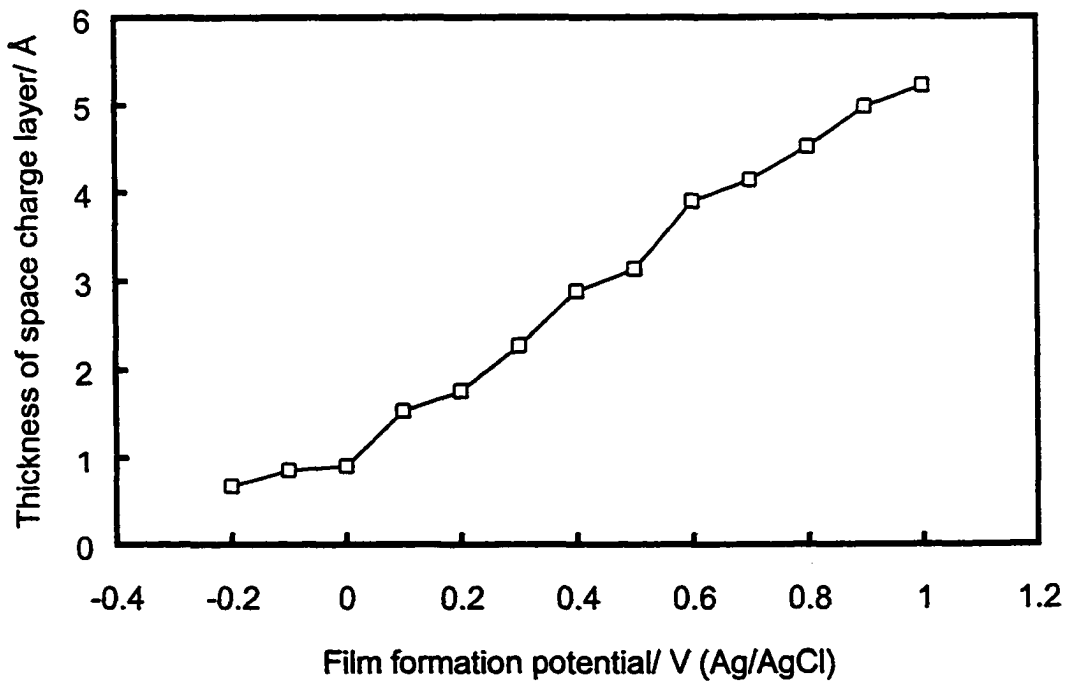
Fig. 7-7 Dependence of the thickness of the space charge layer of passive film on the film formation potential.

183

films on iron and chromium, and those measured by chemical analysis. The data in Fig. 7-6 show that the donor density decreases with increasing film formation potential. This result is consistent with that reported by Sikora et al.[49] The relationship between N_D and film formation potential established in this work is theoretically interpreted in terms of the point defect model (PDM),[9,50] assuming that oxygen vacancies are the electron donors for an n-type semiconductor. The Mott-Schottky data are consistent with that for an inhomogeneously doped film, such that the region close to the metal/film interface is a highly doped n-type semiconductor while that close to the film/solution interface is insulating in nature. Accordingly, the measured donor density is the oxygen vacancy concentration at the metal/film interface.

Flat-band potential is a critical parameter in determining the position of the semiconductor energy bands with respect to the redox potentials of electroactive ions in the electrolyte. These positions are in turn governed by the charge transfer across the semiconductor/electrolyte interface, the contact potential (band bending) between semiconductor and electrolyte, and the thermodynamic stability of a semiconductor. For the passive films formed at more positive potentials, there is a thicker space charge layer, smaller donor density and then a more stable structure. The Fermi level of the passive film will move negatively because U_{fb} depends on the concentration of impurities. Considering that flat-band potential is related to Fermi level by the relation of U_{fb} = -e•E_F, it is easy to know why E_{fb} shifts positively when the film formation potential increases.

7.3.4 Pitting susceptibility of the passive film in chloride solution

The pitting susceptibility of passivated carbon steel has been studied by monitoring the current noise in bicarbonate/chloride solutions. Polarization measurements shown in Fig. 4-1 show that A516-70 carbon steel was passivated over a large range of potential in a bicarbonate solution. The addition of chloride ions degraded the passivity of carbon steel. The initiation of metastable pits is indicted by typical current transients, i.e., a rapid current rise followed by slow recovery, as shown in Fig. 4-6. Fig. 7-9 shows the potential dependence of the pit initiation rate of A516-70 carbon steel during 4,000 seconds of

184
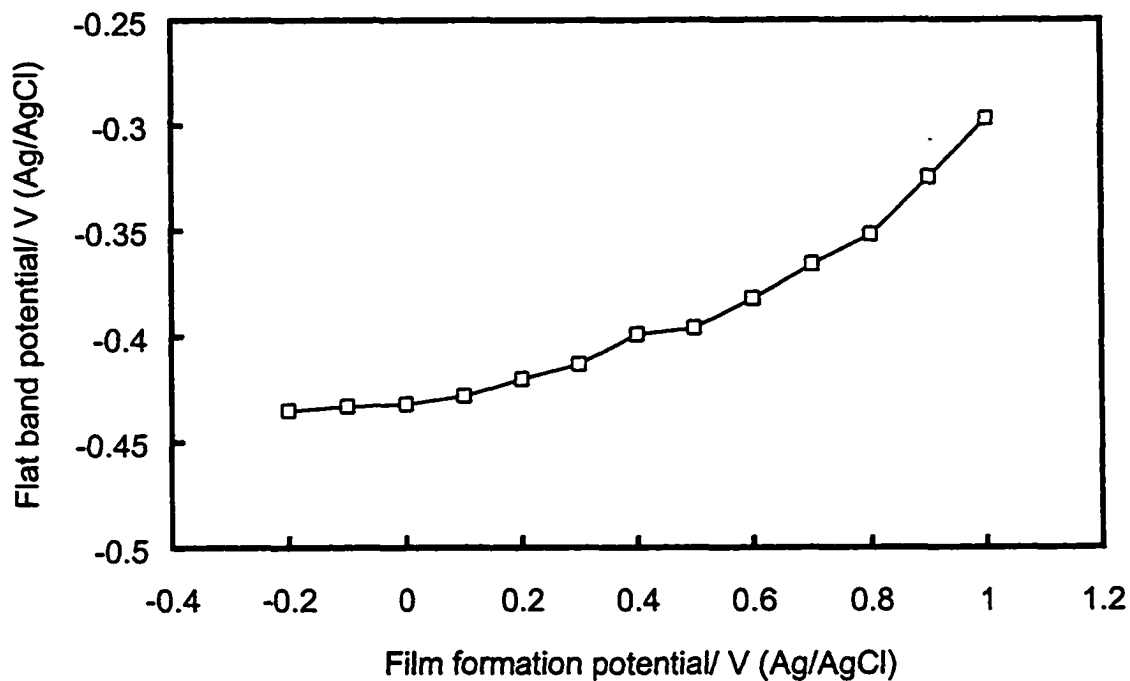
Fig. 7-8 Dependence of the flat-band potential on the film formation potential.
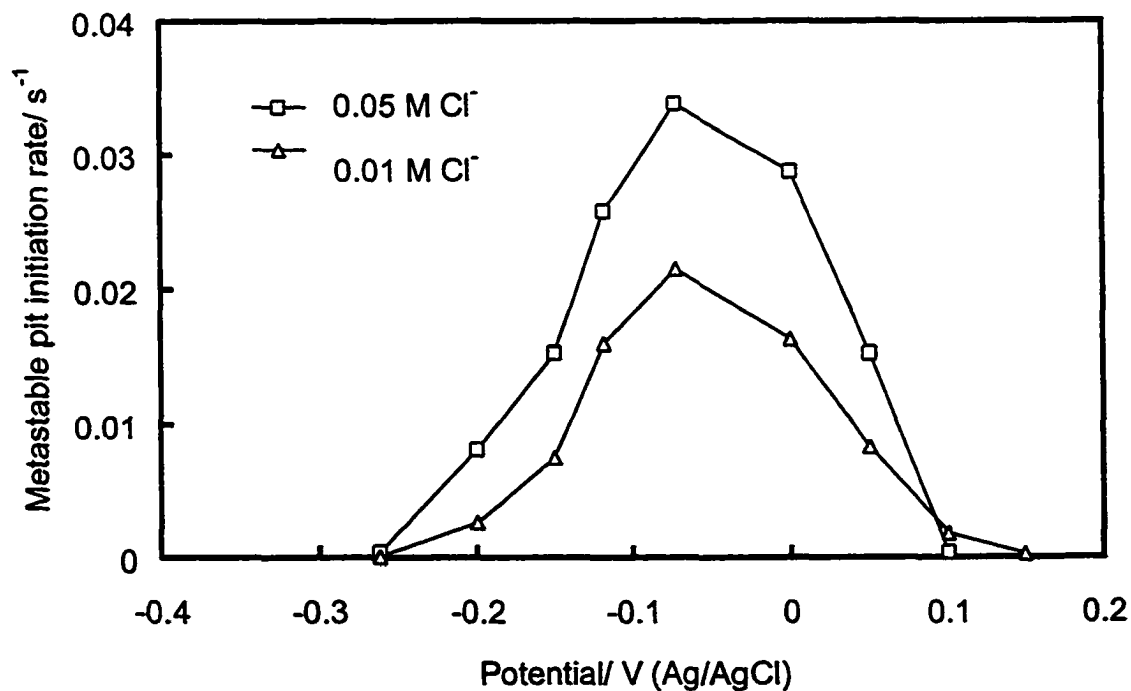
Fig. 7-9 Potential dependence of the pit initiation rate in 0.5 M NaHCO₃.solution containing 0.01 M and 0.05 M NaCl.

immersion in the testing solutions. It is seen that the onset of metastable pits occurred at a potential of -250 mV, and was followed by an increase in pit initiation rate up to a maximum at about -70 mV, and a subsequent decrease at more anodic potentials. The potential corresponding to the maximum pit initiation rate is defined as the transitional potential. From Fig. 7-9, it is also seen that neither the shape of the curve nor the characteristic values of pit onset potential and transitional potential were affected by the concentrations of chloride ions. This phenomenon was observed in the studies performed by Schmuki and Bohni[29] and Burstein et al.[51] They found that the potential dependence of the initiation rate of metastable pits is independent of the solution pH value, Cl^- concentration, the type of purging gas and H_2O_2 concentration. Therefore, the pit onset potential and the transitional potential can be considered as special features for certain steels.

As discussed in Chapter 4, the point defect model (PDM) can illustrate the breakdown of passive film and the pitting initiation.[9] Below the pit onset potential, the cation vacancy diffusivity in some "weak spots" is not high enough to nucleate pits. When the potential increases positively from the pit onset potential, more "weak spots" that are characterized by high cation vacancy diffusivity will be activated and become the potential pit nucleation sites. Therefore, the pit initiation rate increases with increasing potential. When the applied potential is increased to reach a critical value, i.e., the transitional potential in this work, the pit initiation rate is found to decrease with increasing potential. The exact mechanism, which is discussed in the following section, is based on the PDM and the relationship between pitting susceptibility and electronic band structure of the passive film. Once the applied potential reaches the pitting potential, the condensation of cation vacancies at the metal/film interface leads to a macroscopic de-cohesion of the film from the metal. When the breakdown of a passive film has occurred over a macroscopic scale, the high dissolution rate of the substrate will inhibit the re-formation of the film. Accordingly, the system does not passivate and the initiation rate of metastable pits drops to zero quickly.

186

7.3.5 Relationship between the pitting susceptibility and the electronic structure of passive film

The electronic properties of a passive film are acknowledged to play a major role in the corrosion resistance.[24,27] For example, Macdonald and co-workers[52,53] studied the influence of uv light on the passive behavior of stainless steels and explained the reason that illumination increases the resistance to pitting attack in terms of the semiconducting nature of the passive film and the point defect model for growth and breakdown of a passive film. It was proposed that generation of electron-hole pairs led to a quenching of the electric field strength and consequent modification of the vacancy structure, causing a decrease in the flux of cation vacancies across the barrier layer.

Fig. 7-10 shows the comparison of the Mott-Schottky plots for passive films formed at the corrosion potential in solutions with various Cl⁻ concentrations. The flat-band potentials were -305 mV and -280 mV for the passive films formed in 0.01 M and 0.05 M Cl⁻ solutions, respectively. Another important result obtained from Fig. 7-10 is that the potential at the break point of the Mott-Schottky straight line (-70 mV), that is, the critical potential for the ionization of both levels in the space charge layer, was not affected by the concentrations of chloride ions. This is a typical feature for the passive films formed below -70 mV. Comparing Fig. 7-9 and 7-10, it is found that the values of pit onset potential (-0.25 V) and flat-band potential (-0.305 V to -0.280 V) are close to each other. Furthermore, the values of transitional potential (-0.07 V) and the critical potential ionizing both levels of the space charge layer (-0.07 V) are the same. Therefore, it is reasonable to assume that there is a certain relationship between the pitting susceptibilities and the electronic structure and semiconducting properties of passive films. The existence of two donor levels has been suggested for the passive films formed on iron by Stimming and Schultze,[14] the deep and shallow levels being respectively ascribed to the oxygen vacancies combined with the Fe atoms in octahedral and tetrahedral positions in the unit cell of a spinel structure. As Simoes et al. stated,[19] when the film formation potential is below -70 mV, the corrosion product is dominated by Fe_3O_4, whereas for a higher film formation potential, the stable iron oxide is Fe_2O_3.
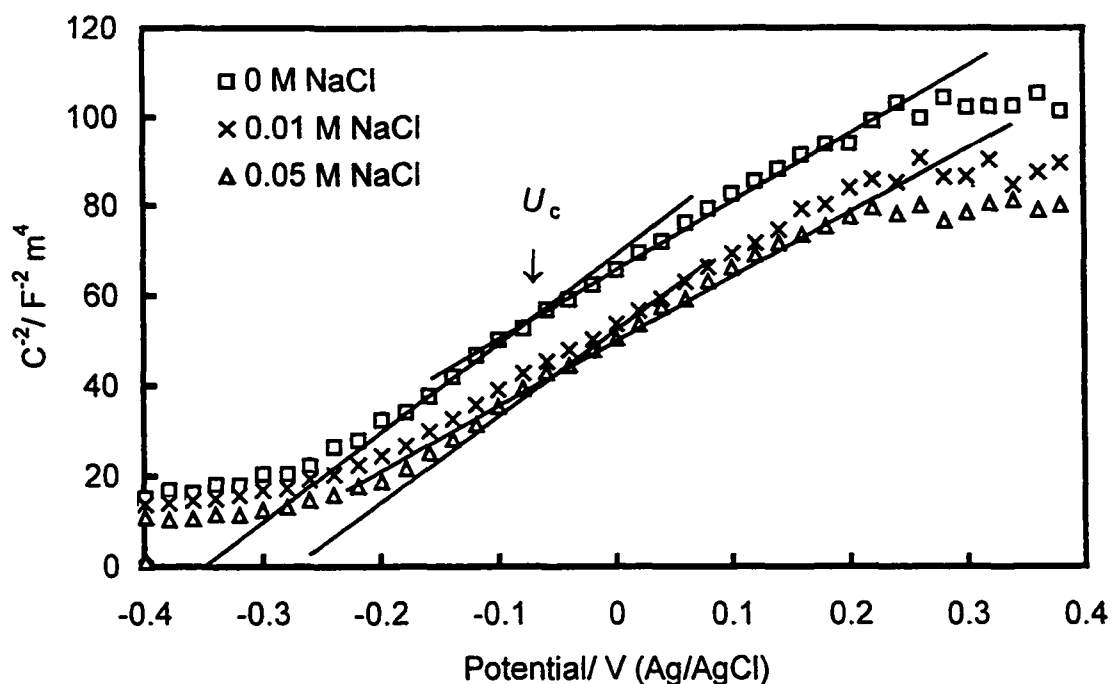
Fig. 7-10 The Mott-Schottky plots measured at corrosion potential of A516-70 carbon steel in 0.5 M $NaHCO_3$ solution with different amount of chloride ions.

Therefore, when the film is mainly composed by Fe_3O_4, an inverse spinel crystalline structure, the deep levels are occupied by oxygen vacancies combined with Fe atoms containing both 2 and 3 valence electrons, and tetrahedral sites correspond to the shallow levels occupied by oxygen vacancies combined with Fe atoms containing 3 valence electrons. When the applied potential is higher than the critical potential, Fe_2O_3 becomes the main barrier layer. According to Davenport et al.'s work,[54] the film is not composed only of octahedrally coordinated iron units. The structure may be a composite of γ-Fe_2O_3/Fe_3O_4 (with one-third tetrahedrally corrodination iron). Therefore, the deep donor levels are mainly occupied by oxygen vacancies combined with Fe atoms containing 3 valence electrons, while the shallow levels host about one-third oxygen vacancies with tetrahedral Fe atoms of 3 valence electrons.

When a passive film is formed at a potential below the transitional potential, i. e., the critical potential causing the non-linear Mott-Schottky behavior, both the shallow and the deep levels of donor states in the space charge layer will be ionized to contribute to the

188

space charge. According to the PDM, the oxygen vacancies combined with the Fe atoms containing 2 and 3 free electrons are ionized, giving out the electrons and becoming the divalent and trivalent iron cation. The combination of these Fe cation with chloride ions in the solution produces the divalent and trivalent Fe cation vacancies. These cation vacancies move towards the metal/film interface and form a cation vacancy condensate, which is responsible for the pitting events. For film formation potentials higher than the transitional potential, only the shallow donor level is ionized, which is detected by single linear Mott-Schottky plots. In such a case, only the trivalent iron cation vacancies generate, condensate at the metal/film interface, and lead to pit initiation. However, the pit initiation rate is found to decrease with the applied potential based on noise analysis. The main reason may be that at the higher film formation potentials the divalent iron cation vacancies are unavailable and only trivalent iron vacancies condense at the metal/film interface. Therefore, it seems that the divalent iron cation vacancies caused by the ionization of the deep donor levels in the space charge layer are mainly responsible for pitting corrosion.

7.3.6 Determination of the Diffusivity of Oxygen Vacancies in the Passive Film on Carbon Steel

The anodic polarization curve of A516-70 carbon steel in 0.5 M $NaHCO_3$ solution is shown in Fig. 4-1. It was seen that carbon steel electrode was passivated over a potential range of –0.1 V to 0.9 V (Ag/AgCl). The stable passive current density within 0 – 0.4 V is about 5×10^{-7} A cm^{-2}.

After stabilizing the passive film at various film formation potentials within the passive potential range for 2 hours, the capacitance-voltage relationship was recorded with a measuring frequency of 1000 Hz and the corresponding Mott-Schottky plot was then derived. Some typical examples of Mott-Schottky plots measured at different film formation potentials are shown in Fig. 7-11. It is seen that a linear part is distinguished for measuring potential greater than –0.25 V, where the measured capacitance is dominated by the space charge. The donor density can be estimated from Eq. 7-1.

189
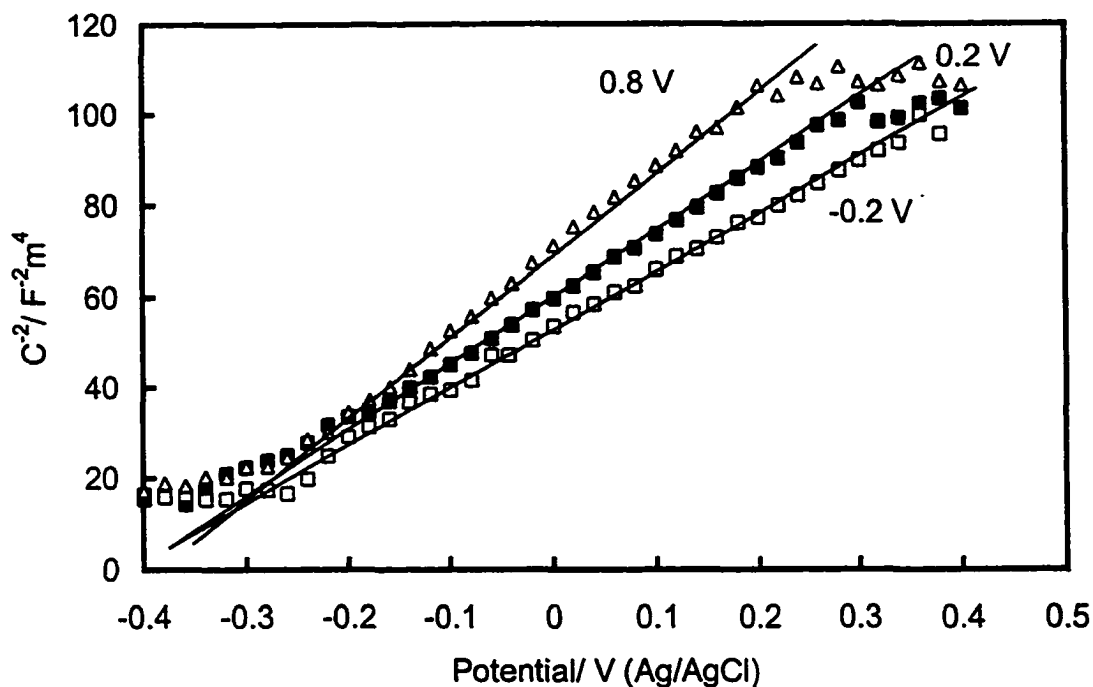
Fig. 7-11 Mott-schottky plot of C^{-2} as a function of measuring potential for a passive film on A516-70 carbon steel at some film formation potentials in bicarbonate solution.

$$N_D = [2.44 \exp(-1.60 \ U)+0.45]10^{26} \ m^{-3}$$
$$R^2 = 0.9513$$
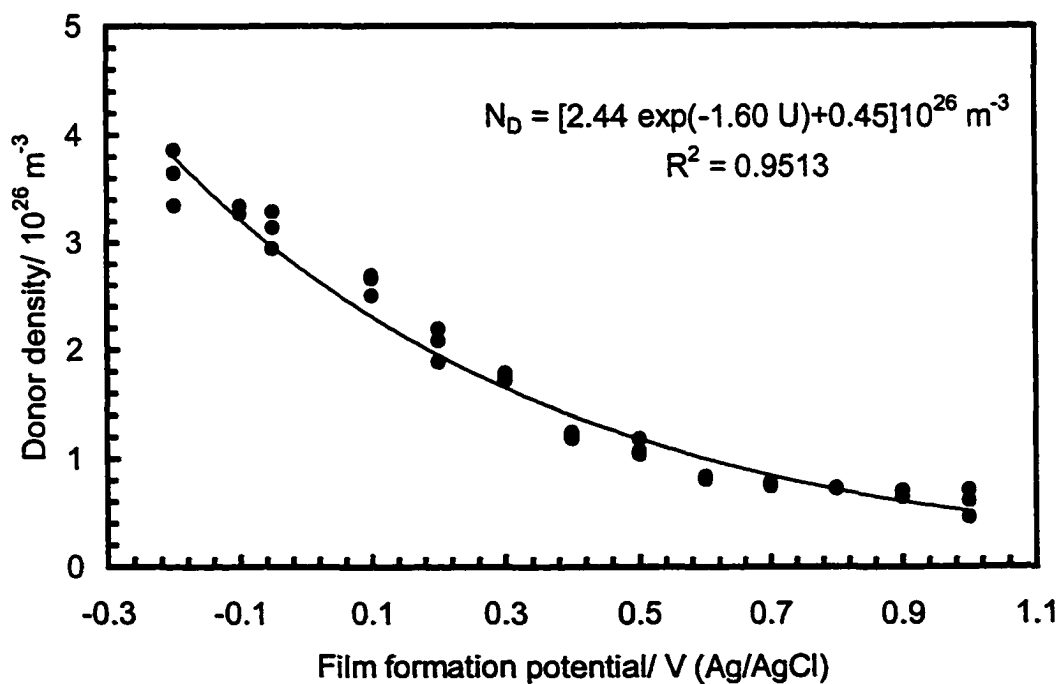
Fig. 7-12 Donor density of the passive films formed on carbon steel in bicarbonate solution as a function of film formation potential. The solid line is the functional dependence of N_D on film formation potential.

190

The data plotted in Fig. 7-12 show that the donor density decreases with increasing film formation potential. Based on the best fitting of the experimental data, the exponential relationship between the donor density (N_D) and the film formation potential (U) is derived as

$$N_D = [2.44\exp(-1.6U) + 0.45] \times 10^{26} \tag{7-4}$$

Macdonald et al.[11] have proven that the relationship between N_D and the film formation potential can be developed theoretically on the basis of the PDM, assuming that the oxygen vacancies are the electron donor. This theoretical relationship yields a good fit to the experimental results, and allows the diffusivity of the oxygen vacancies in the passive film to be calculated. According to the PDM, the flux of oxygen vacancies, J_O, through the passive film can be written as

$$J_O = -D_O(\frac{\partial C_O}{\partial x}) - 2KD_OC_O \tag{7-5}$$

where $K = \gamma\varepsilon_L$, ε_L is the electric field strength, $\gamma = F/RT$ and D_O is the diffusion coefficient of oxygen vacancies. The concentration profile for oxygen vacancies in the steady state is obtained by solving the Nernst-Planck equation to yield

$$C_O(x) = C_O(0)\exp(-2Kx) - \frac{J_O}{2KD_O}[1 - \exp(-2kx)] \tag{7-6}$$

where $C_O(0)$ is the concentration of the oxygen vacancies at the film/solution interface. It has been found[11] that the lower concentration of oxygen vacancies close to the film/solution interface results in the occurrence of an insulation layer. The almost constant concentration of oxygen vacancies close to the metal/film interface should result in a linear Mott-Schottky plot. Accordingly, it is concluded that the measured donor

191

density, N_D, is the oxygen vacancy concentration at the metal/film interface. Thus, for $x = L$, Eq. 7-6 gives

$$N_D = C_O(L) = C_O(0)\exp(-2kL) - \frac{J_o}{2KD_O}[1 - \exp(-2KL)]$$

(7-7)

Because the measured passive current is found to be independent of the film formation potential, then so is the flux J_O. The dependence of the concentration, $C_O(0)$, on the formation potential, U, is obtained by observing that in steady state the flux, J_O, at the film/solution interface must equal the rate of annililation of oxygen vacancies. Therefore,

$$-J_O = k_4 C_O(0)$$

(7-8)

where k_4 is the rate constant for reaction (4) in Fig. 2-4. The rate constant depends on the potential drop across the film/solution interface, $\phi_{f/s}$, as

$$k_4 = k_4^0 \exp(2\alpha_4\gamma\phi_{f/s})$$

(7-9)

where k_4^0 is the rate constant for $\phi_{f/s} = 0$, and α_4 is the transfer coefficient. According to the PDM,

$$\phi_{f/s} = \phi_{f/s}^0 + \alpha U + \beta pH$$

(7-10)

As the potential drop at the film/solution interface, $\phi_{f/s}$, grows with increasing formation potential, then the rate constant k_4 also increases. Thus, according to Eq. 7-8, the concentration $C_O(0)$ must decrease with increasing formation potential, so as to keep J_O constant.

192

The film thickness is estimated from capacitance measurements, where at frequencies higher than 1000 Hz, the electrochemical impedance displays an almost purely capacitive frequency response. Accordingly, we can use the well-known expression for the capacitance

$$C = \frac{\varepsilon_0 \varepsilon_r S}{L_{film}} \qquad (7\text{-}11)$$

to estimate the steady state thickness L_{film}, where S is the surface area, ε_0 is the permittivity of free space, and ε_r is the dielectric constant. A linear relationship exists between the steady state film thickness and the film formation potential. This relationship may be expressed as

$$L_{film} = \frac{1}{\varepsilon_L}(1-\alpha)U + B \qquad (7\text{-}12)$$

where ε_L is the electric field strength of the passive film, and B is a constant that depends on pH and on the rate constants for film formation at the metal/film interface and film dissolution at the film/solution interface.

Substituting $C_0(0)$ from Eq. 7-8 and k_4 from Eq. 7-9 into Eq. 7-7, we obtain

$$C_O(L_{film}) = -\frac{J_o}{k_4^0}\exp(-2\alpha_4\gamma\phi_{f/s}) \times \exp(-2KL_{film}) - \frac{J_o}{KD_O}[1-\exp(-2KL_{film})] \qquad (7\text{-}13)$$

Substituting $\phi_{f/s}$ from Eq. 7-10, L_{film} from Eq. 7-12 and noting that 1-exp(-2KL_{film}) ≈1, we find from Eq. 7-13 that

$$C_O(L_{film}) = N_D = \omega_1\exp(-bU) + \omega_2 \qquad (7\text{-}14)$$

where

193

$$\omega_2 = -\frac{J_o}{2KD_o} \tag{7-15}$$

and ω_1, ω_2 and b are unknown constants that are to be determined from the experimental data. The best exponential fit to the experimental data is shown in Fig. 7-12. The corresponding values of the parameters are calculated as $\omega_1 = 2.44 \times 10^{26}\ m^{-3}$, $\omega_2 = 0.45 \times 10^{26}\ m^{-3}$ and $b = -1.6\ V^{-1}$. The diffusivity can be calculated from Eq. 7-15 by

$$D_O = -\frac{J_o}{2K\omega_2} = -\frac{J_o RT}{2F\omega_2\varepsilon_L} \tag{7-16}$$

$$J_O = -\frac{i_{pass}}{2e} \tag{7-17}$$

where i_{pass} is the steady-state passive current density, which is determined from the polarization curve (Fig. 4-1) to be $1.5 \times 10^{-6}\ A\ cm^{-2}$. The ε_L is approximately determined to be $3.9 \times 10^6\ V\ cm^{-1}$ by Smialowska and Kozlowski[54] for the passive film grown on iron, while Haupt et al.[55] measured the field strength of passive film on iron in 1 M NaOH solution to be about $3.5 \times 10^6\ V\ cm^{-1}$. Therefore, it was assumed that the electric field strength of passive film on carbon steel in this system is approximately $4.0 \times 10^6\ V\ cm^{-1}$. Substitution of i_{pass}, e, ε_L, ω_2, R ($8.314\ J\ mol^{-1}\ K^{-1}$), T (298 K) and F (96500 C/mol) into Eqs. 7-16 and 7-17 yields $D_O = 3.42 \times 10^{-16}\ cm^2\ s^{-1}$. Taking into account the error caused by the assumption of ε_L in Eq. 7-16, the diffusivity of oxygen vacancies in the passive film formed on carbon steel in chromate solution is estimated to be in the range of $10^{-16} - 10^{-15}\ cm^2\ s^{-1}$.

There are few reports about the studies of the passivity of carbon steel. No exact values of the diffusivity of point defects in the passive film on carbon steel was found in the literature. Smialowska and Kozlowski[54] assumed that the film growth kinetics is controlled by a diffusion process of ions. Although the atomic nature of the ions was not exactly described, they calculated the apparent diffusion coefficient of ions to be in the

order of 10^{-15} cm^2 s^{-1}, which is very close to the diffusivity of oxygen vacancies in the passive film on carbon steel.

7.4 Conclusions

* The passive film on A516-70 carbon steel in bicarbonate solution shows characteristics of a highly disordered n-type crystalline semiconductor with the existence of extensive short-range disorder structure, which is indicated by the frequency dependence of capacitance behavior and Mott-Schottky plots: a positive Mott-Schottky slope, the curved Mott-Schottky lines at higher potentials and a large capacitance hysteresis.

* The donor concentration of passive films, which is in the range of 10^{26} - 10^{27} m^{-3}, decreases with increasing film formation potential. The thickness of the space charge layer of passive films ranges from 1 to 6 Å. Flat-band potential increases when the film formation potential moves positively.

* The non-linearity of Mott-Schottky plots, depending upon the film formation potential, indicates the existence of two donor levels in the space charge layer. When the film formation potential is below -70 mV, two slopes in Mott-Schottky plots reveal two levels. Above -70 mV, only the shallow donor level can be ionized, and single linear Mott-Schottky plots are observed.

* A point defect model can illustrate the passive film breakdown and metastable pitting events. The condensation of cation vacancies at the metal/film interface leads to film rupture and pitting initiation. The onset potential and the transitional potential for metastable pitting events on A516-70 carbon steel are approximately -250 mV and -70 mV, respectively, which are close to the flat-band potential and the critical potential ionizing both deep and shallow donor levels in the space charge layer.

* For a passive film formed below the transitional potential, a condensate at the metal/film interface of both divalent and trivalent iron cation vacancies, caused by the ionization of both shallow and deep levels of donor states in the space charge layer and the combination of the ionized iron cation with chloride ions, is responsible for

195

the pitting events. For the film formation potentials higher than the transitional potential, the decrease in pit initiation rate with potential is due to the facts that only the shallow donor level is ionized and no divalent iron cation vacancy generates in such a case. So it is the divalent iron cation vacancies caused by the ionization of the deep donor level of the space charge layer that are mainly responsible for carbon steel pitting.

* The experimental data are interpreted in terms of the point defect model for passivity of carbon steel, assuming that the donors are oxygen vacancies. The oxygen vacancy diffusivity is calculated to be $10^{-16} - 10^{-15}$ cm^2 s^{-1}.

References

1. M. Faraday, in *Experimental Research in Electricity*, Vol. II, University of London (1844).

2. C. Foley, J. Kruger and C. Bechtoldt, *J. Electrochem. Soc.* **114**, 994 (1967).

3. L. Young, in *Anodic Oxide Film*, Academic Press, New York (1961).

4. N. Sato and M. Cohen, *J. Electrochem. Soc.* **111**, 512 (1964).

5. C. Wagner, *Ber. Phys. Chem.* **77**, 1090 (1973).

6. B. MacDougall and M. Cohen, *J. Electrochem. Soc.* **121**, 1152 (1974).

7. K.J. Vetter, *Electrochim. Acta* **16**, 1923 (1971).

8. M. Sakashita and N. Sato, in *Passivation of Metals*, R.P. Frankental and J. Kruger, Editors, p. 479, The Electrochemical Society, Corrosion Monograph Series, Princeton (1978).

9. D.D. Macdonald, *J. Electrochem. Soc.* **139**, 3434 (1992).

10. D.D. Macdonald and M. Urquidi-Macdonald, *J. Electrochem. Soc.* **137**, 2395 (1990).

11. E. Sikora, J. Sikora and D.D. Macdonald, *Electrochim. Acta* **41**, 783 (1996).

12. U. Stimming, *Electrochim. Acta* **31**, 415 (1986).

13. G. Bianchi, A. Cerquetti, F. Mazza and S. Torchio, *Localized Corrosion* **3**, 339 (1974).

14. U. Stimming and J.W. Schultze, *Electrochim. Acta* **24**, 859 (1979).

15. U. Stimming, in *Passivity of Metals and Semiconductors*, M. Froment, Editor, p. 477, Elsevier Publishing Company, Amsterdam (1983).

16. F.M. Delnick and N. Hackerman, *J. Electrochem. Soc.* **126**, 732 (1979).

17. G. Cooper, J.A. Turner and A.J. Nozik, *J. Electrochem. Soc.* **129**, 1973 (1982).

18. R. Silva, M.A. Barbosa, B. Rondot and M. Cunha Belo, *Br. Corros. J.* **25**, 136 (1990).

19. A.M.P. Simoes, M.G.S. Ferreira, B. Rondot and M.Cunha Belo, *J. Electrochem. Soc.* **137**, 82 (1990).

20. K. Azumi, T. Ohtsuka and N. Sato, *J. Electrochem. Soc.* **134**, 1352 (1987).

21. A.D. Paola, D. Shukla and U. Stimming, *Electrochim. Acta* **36**, 345 (1991).

22. P.C. Searson, R.M. Latanision and U. Stimming, *J. Electrochem. Soc.* **135**, 1358 (1988).

23. P.C. Searson, U. Stimming and R.M. Latanision, in *Surface, Inhibition and Passivation*, E. McCafferty and R.J. Brodd, Editors, p. 175, The Electrochemical Society, New Jersey (1986).

24. S.M. Wilhelm and N. Hackerman, *J. Electrochem. Soc.* **128**, 1668 (1981).

25. L.M. Abrantes and L.M. Peter, *J. Electroanal. Chem.* **150**, 593 (1983).

26. A.D. Paola, *Electrochim. Acta* **34**, 203 (1989).

27. T.D. Burleigh and R.M. Latanision, *J. Electrochem. Soc.* **134**, 135 (1987).

28. J.A. Harrison and D.E. Williams, *Electrochim. Acta* **31**, 1063 (1986).

29. P. Schmuki and H. Bohni, *J. Electrochem. Soc.* **139**, 1908 (1992).

30. P. Schmuki and H. Bohni, *Werkst. Korros.* **42**, 203 (1991).

31. G. Bianchi, A. Cerquetti, F. Mazza and S. Torchio, *Corros. Sci.* **12**, 495 (1972).

32. J.F. Dewald, *J. Phys. Chem. Solid* **14**, 155 (1960).

33. R. Memming, in *Comprehensive Treatise of Electrochemistry*, B.E. Conway, J.O'M. Bockris, E. Yeager. S.U.M. Khan and R.E. White, Editors, p. 533, Vol. 7, Plenum Press, New York (1983).

34. H.W. Wilson, *J. Appl. Phys.* **48**, 4292 (1977).

35. R.De Gryse, W.P. Gomes, F. Cardon and J. Vennik, *J. Electrochem. Soc.* **122**, 711 (1975).

36. S.R. Morison, in *Electrochemistry at Semiconductor and Oxidized Metal Electrodes*, p. 26, Plenum Press, New York (1981).

37. U. Stimming and J.W. Schultze, *Ber. Bunsenges Phys. Chem.* **80**, 1297 (1976).

38. M.W. Peterson and B.A. Parkinson, *J. Electrochem. Soc.* **133**, 2538 (1986).

39. M.H. Dean and U. Stimming, *Corros. Sci.* **29**, 199 (1989).

40. M.H. Dean and U. Stimming, *J. Electroanal. Chem.* **228**, 135 (1987).

41. M.H. Dean and U. Stimming, *J. Phys. Chem.* **93**, 8053 (1989).

42. J. Schoonman, K. Vos and G. Blasse, *J. Electrochem. Soc.* **128**, 1154 (1981).

43. G. Nogami, *J. Electrochem. Soc.* **132**, 76 (1985).

44. G. Nogami, *J. Electrochem. Soc.* **133**, 525 (1986).

45. V.A. Myamlin and Y.V. Oleskov, in *Electrochemistry of Semiconductors*, Plenum Press, New York (1967).

46. A. Goossens, M. Vazquez and D.D. Macdonald, *Electrochim. Acta* **41**, 35 (1996).

47. A. Goossens, M. Vazquez and D.D. Macdonald, *Electrochim. Acta* **41**, 47 (1996).

48. P. Schmuki, M. Beuchler. H. Boehni, R. Miller and L.J. Gauckler, in *Oxide Films on Metals and Alloys VII*, 186th Meeting Electrochem. Soc., Miami Beach (1994).

49. E. Sikora, J. Sikora and D.D. Macdonald, *Electrochim. Acta* **41**, 783 (1996).

50. D.D. Macdonald, S. Biaggio and H. Song, *J. Electrochem. Soc.* **139**, 171 (1992).

51. G. T. Burstein, P.C. Pistorius and S. P. Mattin, *Corros. Sci.* **35**, 57 (1993).

52. C.B. Breslin, D.D. Macdonald, J. Sikora and E. Sikora, *Electrochim. Acta* **42**, 127 (1997).

53. C.B. Breslin, D.D. Macdonald, J. Sikora and E. Sikora, *Electrochim. Acta* **42**, 137 (1997).

54. A.j. Davenport and M. Sansone, J. Electrochem. Soc. 142, 725 (1995).

55. Z. Szklarska-Smialowska and W. Kozlowski, in *Passivity of Metals and Semiconductors*, M. Froment, Editor, p. 89, Elsevier, Netherlands (1983).

56. S. Haupt, C. Carinski, U. Collisi, H.W. Hoppe and H.H. Strehbolw, *Surf. Interf. Anal.* **9**, 357 (1986).

Chapter 8 Summaries and Recommendations

8.1 Main conclusions

Fluctuations of the potential or current from a corroding electrode are a well-known and easily observable phenomenon. Before the 1970s, electrochemical noise was regarded as a source of bias and error that compromised electrochemical measurements rather than a rich source of information. However, during the last twenty years, we have witnessed the active development of electrochemical measurements and analyses associated with the corrosion process, especially various localized corrosion processes. The integration of EN measurement parameters with other electrochemical measures of systems status demonstrates the optimum use of the EN technique. The unique advantages of the EN technique are rapidly expanding fundamental corrosion studies and in-situ corrosion monitoring by noise measurements and analyses.

The significance of this work lies in the fact that some fundamental results about the electrochemical noise analysis related to carbon steel pitting are obtained and the relationship between the electronic properties and the pitting susceptibility of the passive film is established at an atomic scale. In addition, the physical significance of the noise spectrum and some spectral parameters are interpreted and some controversial viewpoints involving EN analysis and application are clarified. The conclusions drawn from this research work undoubtedly constitute an important component in pitting and electrochemical noise studies in the field of corrosion science. Some important conclusions about the analysis of electrochemical noise related to carbon steel pitting are summarized here.

* During the incubation period of pitting, the fluctuations of potential are in phase with the current fluctuations, and the faradaic current plays a major role. The initiation of metastable pits is indicated by typical potential and current transients shaped as a quick drop in potential and rise in current followed by a slow

199

recovery. The potential fluctuations come from the response of electrode capacitance to pit growth charge.

* Potential dependence of the pit initiation rate is well illustrated by a point defect model. Pit growth is controlled by the ohmic potential drop across the cover deposited over the pits. Potential dependence of the repassivation time of metastable pits mainly comes from the effect of applied potential on the pit cover. A stabilization criterion of metastable pits, indicating the critical condition to maintain stable pitting, must exceed 2×10^{-2} A cm^{-1} at all times during pit growth to avoid repassivation.

* The main role of chloride ions in pitting is to increase the chance of the breakdown of the passive film, rather than to inhibit surface repassivation. Metastable pitting events on carbon steel show non-Poisson behavior, and the initiation of a metastable pit will have a certain influence on subsequent pitting events in the case of high pitting activity. When the pitting activity decreases, metastable pitting events follow the Poisson distribution.

* The current noise spectrum for carbon steel pitting is generally characterized by a "white" noise in the low frequency region and a $1/f^{\alpha}$ noise in the high frequency region. The spectral level reflects the pitting activity and is related to current rise rate and pit initiation rate. The roll-off slope increases with the pit growth time. The roll-off frequency represents the repassivation kinetics of metastable pits.

* Any transient having a sudden birth or a sudden death generates the f^{-2} noise in the high frequency range, while the transients without sudden change will show the f^{-4} behavior. This result is independent of the corrosion types (localized corrosion, general corrosion or passivity). The roll-off frequency of the noise spectrum for the exponential transients generated during pitting reflects the time constant of the exponential function. For the transients showing features of triangular and delta waves during passivity and general corrosion, the roll-off frequency is related to the time interval of the current rise or drop stage.

* The spectral noise impedance is equivalent to the magnitude of the electrode impedance, which is independent of the corrosion situations. Noise resistance coincides with polarization resistance during passivity and general corrosion, and

200

indicates the corrosion resistance of the material under study. In the case of pitting, noise resistance can not track quantitatively the change of corrosion resistance of a system.

* The passive film on carbon steel in a bicarbonate solution shows characteristics of a highly disordered n-type semiconductor with the existence of extensive short-range disorder structure. The non-linearity of the Mott-Schottky plot indicates the existence of two donor levels in the space charge layer of the passive film. It is the divalent iron cation vacancies caused by the ionization of the deep donor level that are mainly responsible for carbon steel pitting.

* The diffusivity of oxygen vacancies, serving as the donors in the semiconducting passive film, is estimated to be in the range of $10^{-16} - 10^{-15}$ $cm^2 s^{-1}$.

8.2 Current State and Future Direction

The reliable interpretation of EN data is the major challenge to the advance of the technology in corrosion research, materials testing and industrial monitoring. At this time, it has been established that EN measurement systems are capable of detecting subtle changes in the material or environment or both under a wide variety of plant processes and laboratory test conditions. With strong corroborating information from other sources, EN data can be related with confidence to changes in corrosion behavior and environmental conditions. However, until a theoretical framework for interpreting corrosion events from noise data are established and standard testing practices are widely accepted, one must still be skeptical about detailed physical interpretations of EN data in the absence of strong corroboration.

In addition to the reliable interpretation of data, other exciting developments are also anticipated. No doubt there will continue to be more unique applications for EN measurements in corrosion monitoring and even process control. The challenges encountered in the field will set the pace for much laboratory experimentation and research. Besides successful industrial applications, the next major step towards validating EN measurements is anticipated to be in regard to its use in elucidating various forms of localized corrosion, such as SCC and pitting. In addition to comparisons of

parameters common to EN measurements and more established electrochemical techniques, such as linear polarization resistance (LPR) and EIS, one can also look forward to the analysis of EN data by computer-intensive tools associated with artificial neural networks and nonlinear dynamics.

Measurement is the final area for future work. There is a need, in both the lab and plant, for techniques/instruments that can handle the large amounts of data that are acquired during real-time monitoring without losing valuable information. Especially, more work is needed to define the best methods for electronic filtering, trend subtraction, and localized event recognition of EN signals. It is very important to consider just how electrochemical signals are processed into EN data to avoid mis- and over-interpretation of data. With this caution in mind, it is essential that calibration procedures for instrumentation and reference corroding systems be established along with diagnostic tests for the validity of data so that measurements can be compared with confidence.

202

Curriculum Vitae

Part I Personal Information

Family Name: **Cheng**   First Names: **Yufeng**

Date of Birth: May 29, 1969

Status: Canada permanent resident

Part II   Previous Academic Record

Name of institution	From	To	Major	Degree
1.Hunan University, China	Sept. 1986	July, 1990	Corrosion	Bachelor
2.Institute of Corrosion & Protection of Metals, Chinese Academy of Sciences	Sept. 1990	July, 1993	Corrosion and Electrochemistry	Master
3.University of Alberta	Sept. 1996	Nov. 1999	Materials Engineering	Ph. D.

Part III   Previous Working Record

Name of institution	From	To	Occupation (Title)
Institute of Corrosion & Protection of Metals, Chinese Academy of Sciences	July 1993	August 1996	Engineer Research Associate

Part IV   Awards

Name of scholarship or award	Date	Name of institution
1. Mr. Lisheng Pan Scholarship	July, 1989	Hunan University, China
2. Director Scholarship	July, 1993	Inst. of Corrosion & Protection of Metal, Chinese Academy of Sciences

203

3. The 2nd-Prize of Research Paper	Oct. 1993	Chinese Society of Corrosion Science
4. The 1st-Prize of Research Paper	Nov. 1994	Chinese Society of Corrosion Science
5. W. Johns Graduate Tuition Scholarship	Sept. 1996	University of Alberta, Canada
6. W. Johns Graduate Tuition Scholarship	Sept. 1997	University of Alberta, Canada
7. Greenhalgh Graduate Memorial Scholarship	Sept. 1998	University of Alberta, Canada
8. Student Presentation Award	Aug. 1999	The 38th conference of the MetSoc of CIM, Quebec City, Canada

PART V Publications in referred journals (related to Ph. D. research project)

1. Y.F. Cheng and J.L. Luo, Metastable Pitting of Carbon Steel Under Potentiostatic Control, *J. Electrochem. Soc.* 146, **1999**: 970-976.

2. Y.F. Cheng and J.L. Luo, Electronic Structure and Pitting Susceptibility of Passive Films on Carbon Steel, *Electrochimica Acta* 44, **1999**: 2947-2957.

3. Y.F. Cheng and J.L. Luo, Passivity and pitting of carbon steel in chromate solutions, *Electrochimica Acta* 44, **1999**: 4795-4804.

4. Y.F. Cheng, M. Wilmott and J.L. Luo, Analysis of the Role of Electrode Capacitance of A516-70 Carbon Steel on the Initiation of Pits by Electrochemical Noise Measurements, *Corrosion Science*, 41, **1999**: 1245-1256.

5. Y.F. Cheng and J.L. Luo, Spectral Analysis of Electrochemical Noise with Different Transit Shapes, accepted by *Electrochimica Acta* on October 20, **1999**.

6. Y.F. Cheng and J.L. Luo, Role of chloride ions in pitting of carbon steel in chloride solutions, accepted by *Applied Surface Science* on June 18, **1999**, proof received.

7. Y.F. Cheng, M. Wilmott and J.L. Luo, The Transition Criterion of Metastable Pitting towards Stability for Carbon Steel in Chloride Solutions, accepted by *Br. Corros. J.* on April 8, **1999**, proof received.

8. Y.F. Cheng, B.R. Rairdan and J.L. Luo, Features of electrochemical noise generated during pitting of inhibited A516-70 carbon steel in chloride solutions, *J. Applied Electrochemistry*, 28 (12), **1998**: 1371-1375.

204

9. Y.F. Cheng and J.L. Luo, Analysis of Noise Features at the Different Stages during Carbon Steel Pitting in Chloride Solutions, accepted by *Bulletin of Electrochemistry* on June 10, 1999.

10. Y.F. Cheng and J.L. Luo, Factors Affecting the Measurements and Analysis of Electrochemical Noise during Carbon Steel Corrosion, accepted by *Bulletin of Electrochemistry* on May 1999.